MATRIX ISOLATION AND CHARACTERIZATION OF 1,1-DIAZENES

Thesis by

Alan Paul Sylwester

In Partial Fulfillment of the Requirements

for the Degree of

Doctor of Philosophy

California Institute of Technology

Pasadena, California

1986

(Submitted July 22, 1985)

To My Parents

and to Laura

ACKNOWLEDGMENTS

I would like to thank my research advisor, Peter Dervan, for his advice, encouragement, and enthusiastic support of this work. I also want to thank the members of the Dervan group, past and present, for providing a diverse and stimulating environment in which to grow and learn. Special thanks go to Dan Duan, Pete Schultz, and Dan McIntyre for help in the early years, Burt Leland for his help and friendship and Jim Hanson for picking up the torch. Helpful discussions of matrix isolation with Mary Mandrich and members of the Chapman group at UCLA are much appreciated. I would like to thank Mark Thompson for the Toepler pump analyses and Mattson Instruments for a great FT-IR. Thanks go to Sig and Eric of the glass shop, Tony and Bill of the mechanical shop, and Tom in the electronics shop, for their frequent assistance in turning ideas into working reality. I am indebted to Dot Lloyd for typing this thesis during a busy time. Financial support of the National Science Foundation and a W. R. Grace graduate fellowship are gratefully acknowledged. Final thanks go to Laura for her love and support and for "talking science" at 2 a.m.

ABSTRACT

CHAPTER 1

The photochemical generation, matrix isolation and direct spectroscopic characterization of H_2NN **3** is reported. UV (VIS filtered) photolysis of carbamoyl azide **15** in a rigid glass (2-MTHF, 80°K) generates blue-violet **3**. The electronic absorption spectrum of **3** reveals a structured absorption curve λ_{max} = 636 nm, $\lambda_{0,0}$ = 695 nm for the n-π^* transition of **3**. This transition is blue shifted in a more polar glass (2-MTHF:nPrCN, 1:1, 80°K) to λ_{max} = 624 nm, $\lambda_{0,0}$ = 681 nm. The argon matrix FT-IR spectrum of **3** shows bands at 2865.55, 2807.20, 1863.20, 1574.16, and 1003.07 cm^{-1} (1:2000, Ar, 10°K). The characteristic N=N stretch for **3** at 1574.16 demonstrates the considerable double bond character in the 1,1-diazene. Incorporation of a terminal ^{15}N label into H_2N-^{15}N **3**-^{15}**N** shifts the N=N stretch to 1547.64 cm^{-1}. The argon matrix infrared spectra of **3**, **3**-^{15}**N**, **3**-d_2, and **3**-d_2-^{15}**N** are reported. Thermal decomposition of **3** (2-MTHF, 90°K) affords 2-tetrazene (λ_{max} = 260 nm), <u>trans</u> HNNH **1** (λ_{max} = 386 nm) and an unidentified species (λ_{max} = 480 nm). Subsequent thermolysis (>100 K) affords NH_3, N_2H_4, $NH_4^+\bar{N}_3$, H_2 and N_2 products. Direct irradiation of **3** in a glass (2-MTHF, 77°K) with visible light affords H_2, N_2, and <u>trans</u>-HNNH **1**. Photodecomposition of matrix isolated **3** (Ar, 10°K) with visible light in the presence of CO affords formaldehyde (H_2CO), <u>trans</u>-HNNH **1**, H_2, and N_2. This represents the first direct observation of thermal and photochemical interconversion of H_2N_2 isomers.

CHAPTER 2

Preliminary studies of the low temperature matrix isolation and spectroscopic characterization of 1,1-dimethyldiazene **7** and 1,1-diisopropyldiazene **18** are reported. The UV (VIS filtered) photolysis of carbamoyl azides **13** and **17** in a rigid medium (organic glass, 80°K or Ar matrix, 10°K) provides a new general method for the photochemical generation of reactive 1,1-diazenes. This photochemical route is considered to proceed <u>via</u> the photo-Curtius rearrangement of a carbamoyl azide to an aminoisocyanate followed by photodecarbonylation to a 1,1-diazene and carbon monoxide. Electronic absorption spectroscopy (2-MTHF, 80°K) reveals structured absorption curves ($n-\pi^*$) λ_{max} = 556 nm, $\lambda_{0,0}$ = 643 nm for **7** and λ_{max} = 504 nm, $\lambda_{0,0}$ = 620 nm for **18**. 1,1-Dimethyldiazene **7** was independently generated by UV (VIS filtered) photolysis of (Z)-3,3-dimethyl-1-phenyltriazene-1-oxide **16** to afford **7** and nitrosobenzene. Matrix isolation FT-IR spectroscopy (Ar, 10°K) reveals the characteristic N=N stretch for **7** at 1600.96 cm^{-1}. Incorporation of a terminal ^{15}N label shifts this stretch to 1581.83 cm^{-1}. The N=N stretch for **18** at 1600.92 cm^{-1} is ^{15}N shifted to 1579.46 cm^{-1}. Photochemical decomposition of **7** (Ar, 10°K) yields the infrared bands of ethane and an unidentified species (U) which is subsequently photolyzed to ethane. The effects of substitution on the electronic transitions and $R_2N=N$ stretches of 1,1-diazenes correlates with the trends of the isoelectronic carbonyl compounds. Thermolysis of **7** and **18** (2-MTHF, 90°K) yields red-orange **9** (λ_{max} = 464 n, $\varepsilon \simeq 3000\ M^{-1}\ cm^{-1}$) and **30** ($\lambda_{max}$ = 474 nm, $\varepsilon \simeq 3000\ M^{-1}\ cm^{-1}$), respectively. These species are tentatively

identified as the azomethinimine tautomers of the 1,1-diazenes with α-hydrogens. Irradiation of **7** and **18** at their n-π* transitions in the visible (2-MTHF, 80°K) also initially yields **9** and **30**, respectively, in addition to the hydrocarbon products expected from nitrogen extrusion. Subsequent bimolecular decomposition of **9** (E_a = 8.2 ± 0.5 kcal/mol, $\log_{10}$ A = 1.8 ± 0.6) yields tetramethyl-2-tetrazene **19**. Bimolecular decomposition of **9-d$_6$** (E_a = 8.6 ± 0.5 kcal/mol, $\log_{10}$ A = 1.4 ± 0.6) reveals a deuterium isotope effect k_H/k_D = 6.7 at 190°K for loss of **9**. Thermal decomposition of **30** affords hydrocarbon products **32**, **33**, and **34** expected for nitrogen extrusion from 1,1-diazene **18**. The activation parameters for unimolecular decomposition of **30** are E_a = 16.8 ± 0.5 kcal/mol, $\log_{10}$ A = 11.8 ± 0.3.

CHAPTER 3

The low-temperature ^{15}N NMR spectrum of the 1,1-diazene, N-(2,2,6,6-tetramethylpiperidyl)nitrene (**1**) is reported. The ^{15}N double- and mono-labeled 1,1-diazenes **1a** and **1b** were synthesized. The nitrene and amino nitrogens of **1** have resonances in dimethyl ether at -90°C at 917.0 and 321.4 ppm, respectively, downfield from anhydrous $^{15}NH_3$, affording a chemical-shift difference of 595 ppm for the directly bonded nitrogen nuclei. The chemical shift of the ring nitrogen is consistent with an amino nitrogen whose lone pair is largely delocalized. The large downfield shift of the nitrene nitrogen is consistent with a large paramagnetic term due to a low-lying n-π* transition.

TABLE OF CONTENTS

TABLE OF CONTENTS (continued) Page

INTRODUCTION

The isomers of H_2N_2 **1**, **2**, and **3** have been implicated as reactive intermediates in a number of chemical systems such as diimide reduction, hydrazine oxidation and nitrogen fixation. Much of our understanding of the structures and energetics of the H_2N_2 isomers comes from theoretical efforts[1] due to the limited experimental[2] characterization of these reactive species.

1 **2** **3a** **3b**

"Diimide" generated <u>in situ</u> has been widely used as a reagent for the stereospecific reduction of multiple bonds.[3a] The accepted mechanism for this transformation requires the <u>cis</u> HNNH isomer **2**. Prior to this work, only the <u>trans</u> HNNH isomer **1** had been spectroscopically characterized.[4]

Hydrazine (H_2NNH_2) is used in hundred million pound quantities annually as a fuel and as a corrosion inhibitor. The H_2N_2 isomers represent the formal oxidative intermediates in these hydrazine oxidations.

Transition metal dinitrogen complexes and metal complexes of each of the H_2N_2 isomers have been prepared. These complexes have received considerable attention as possible models for the discrete steps in the fixation and reduction of dinitrogen to hydrazine and ammonia in the active site of nitrogenase enzymes.[5]

Spectroscopic characterization of each of the isomers of H_2N_2 is essential for direct studies probing their role as reactive intermediates in these and other chemical systems.

Until 1978, 1,1-diazenes[6] **3a** or aminonitrenes **3b** unlike their more stable 1,2-diazene[7] isomers (azo compounds) **1** and **2**, were not usually isolated or characterized, but were assumed intermediates based on a substantial body of chemical evidence. The recent preparation of kinetically persistent 1,1-diazenes **4**, **5**, and **6** by Dervan and coworkers have made possible the direct experimental characterization of the 1,1-diazene functional group.[8] These

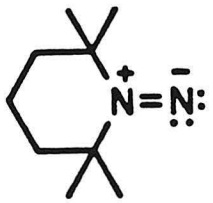

4

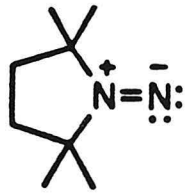

5

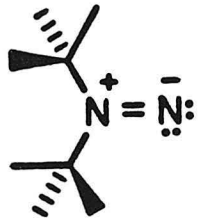

6

studies have provided much information concerning the electronic structure, the kinetics of thermal reactions and the photochemistry of 1,1-diazenes with tertiary alkyl substituents.

Aided by the studies of kinetically persistent 1,1-diazenes, the method of low temperature matrix isolation[9] is utilized for spectroscopic characterization of the parent 1,1-diazene, H_2NN **3** (providing entry to the H_2N_2 energy surface), and other simple dialkyl 1,1-diazenes lacking kinetic persistence. These studies are described herein.

Theoretical Studies

Theorists have devoted considerable effort to the H_2N_2 energy surface with regard to the electronic structures, relative energies and mechanisms for interconversion of the H_2N_2 isomers.[1] The most important question concerning the electronic structure of H_2NN **3** is the nature of its ground electronic state. Unlike simple nitrenes (R-$\dot{N}$·) the chemical behavior of aminonitrenes or 1,1-diazenes suggests a singlet ground electronic state. Early ab initio calculations found a triplet nitrene-like ground state **3b** for H_2NN as found experimentally for simple alkyl nitrenes. However, more recent calculations employing larger basis sets and configuration interaction found the singlet form **3a** to be the ground electronic state.

Table I. Singlet-Triplet Energy Gap in H_2N-N.

Calculational Method	Ground State	S-T Gap[a]	Reference
STO-3G	Triplet	26.3	Baird, 1973[1b]
4-31G	Triplet	11.7	Pople, 1978[1p]
HF	Triplet	5.2	Ahlrichs, 1976[1h]
SCF	Triplet	2.1	Wagniere, 1973[1d]
4-31G-CI	Singlet	1.6	Baird, 1977[1j]
GVB-CI	Singlet	13.8	Goddard, 1977[1n]

[a]kcal/mol^{-1}, both states at equilibrium geometries.

From the recent calculations of Davis and Goddard (GVB-CI), the following picture for the three lowest electronic states of H_2NN emerges. The ground state is calculated to be a singlet ($^1A_1$) of planar C_{2v} geometry

with a low lying triplet excited state ($^3A_2$) at 0.6 eV (13.8 kcal). The ground state singlet structure (S_0) results from stabilization due to delocalization of the amino nitrogen lone pair to the terminal nitrene nitrogen giving rise to substantial NN double bond character ($H_2\overset{+}{N}=\overset{-}{N}:$). This NN double bond character is reflected in the calculated NN bond length Re(NN) = 1.25 Å (for comparison the experimental Re(NN) for trans HNNH 1 is 1.25 Å),[2i] the large dipole moment (μ = 4.036 D), and the calculated planar C_{2V} geometry. To

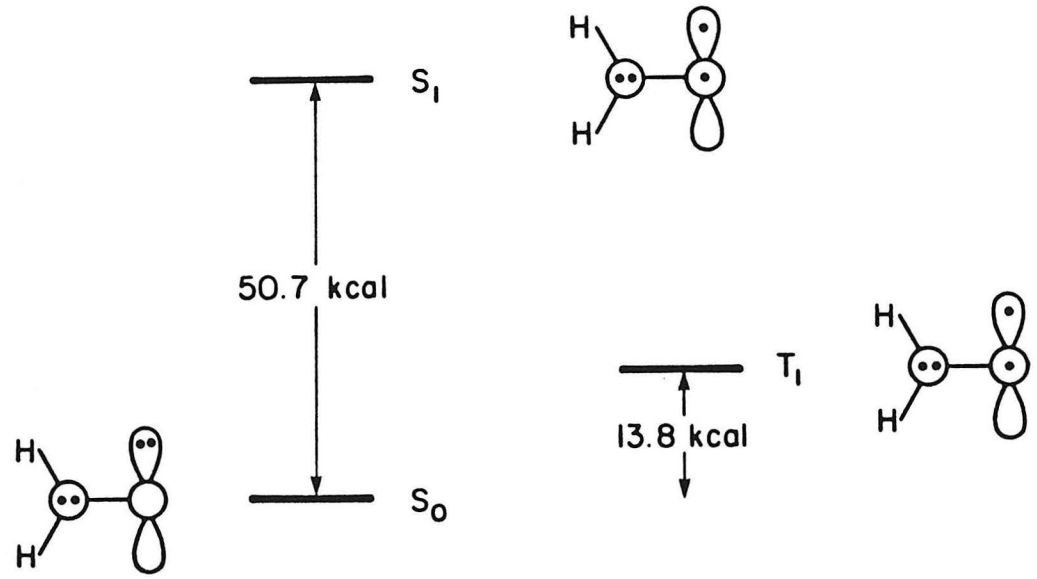

Figure 1. GVB-CI Calculations for H_2NN.

the experimentalist, the calculations suggest that H_2NN should show an NN double bond stretch near the 1500 to 1600 cm^{-1} region of the infrared ($\nu_{N=N}$ for trans HNNH 1 is 1529 cm^{-1} in the Raman).[2f] The first excited

singlet state (S_1) is calculated to lie 2.2 eV (50.7 kcal/mol) above the ground state. This gap corresponds to an n-π^* electronic transition. Important to the experimentalist, the calculations predict that H_2NN should be a colored species detectable by electronic spectroscopy with an n-π^* transition in the visible region near 560 nm.

The S_1 and T_1 excited states have electronic configurations similar to the lowest singlet and triplet states of nitrene (H-$\dot{N}$·). Interaction of the amino lone pair with the nitrene π electrons is equivalent in both spin states so the 37 kcal/mol separation between T_1 and S_1 corresponds to the triplet-singlet gap in nitrene. In the T_1 and S_1 excited state there are two opposing forces: pyramidalization which reduces antibonding interactions and planarization which gives rise to a favorable two-center three-electron bond. These two effects are calculated to be comparable leading to an optimal pyramidal geometry (21° angle between the H_2N plane and the N-N bond axis) with a calculated barrier of less than 1 kcal/mol (for comparison, the experimental inversion barrier for NH_3 is 6 kcal/mol).[10] The calculated NN bond length (1.37 Å) for S_1 and T_1 (Re(NN) for hydrazine is 1.45 Å) and the calculated dipole moment of 2.35 D are indicative of some two-center three-electron bonding.

The H_2N_2 energy surface has also been investigated theoretically.[1q,r,s,t,u] The recent <u>ab initio</u> calculations of Casewit and Goddard (GVB-CI)[1t] are summarized in Figure 2. The <u>trans</u> HNNH isomer 1 is found to be lowest in energy with a calculated heat of formation $\Delta H_{f(298)}$ = 56.9 kcal/mol in good agreement with the latest experimental

value for the heat of formation of **1**, $\Delta H_{f(298)} = 50.7 \pm 2$ kcal/mol.[2m] The cis isomer **2** is calculated to lie 4.7 kcal/mol higher than **1** and the 1,1-diazene isomer **3** is calculated to lie 29.4 kcal/mol higher than **1**. The N-H bond strengths were also calculated affording N-H bond strengths of 42

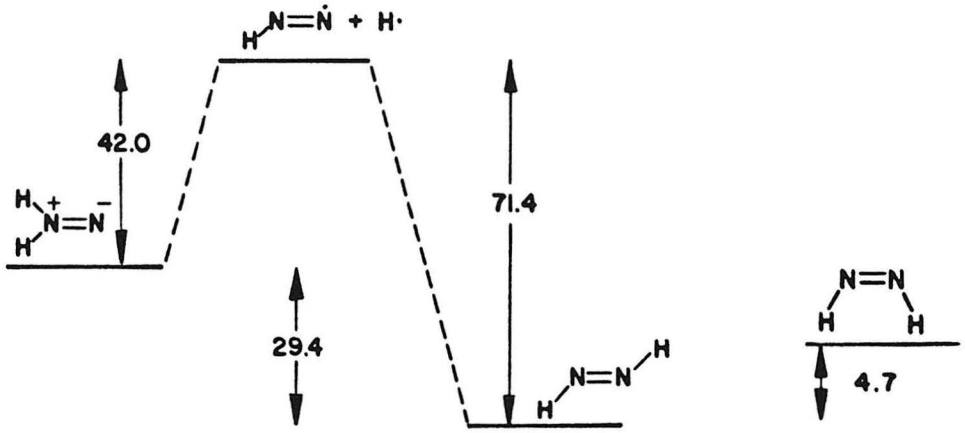

Figure 2. GVB-CI calculations for the H_2N_2 energy surface and the diazenyl radical.

kcal/mol for H_2NN **3**, 71.5 kcal/mol for **1**, and 66.7 kcal/mol for **2**. These calculations suggest that unimolecular interconversion of the H_2N_2 isomers through bond homolysis requires surmounting substantial barriers. Various other theoretical treatments for unimolecular cis to trans HNNH isomerization find inversion barriers[1a,c,f,h,i,k,m,q,r] of 45-51 kcal/mol and rotational barriers[1a,c,h,m] of 55-84 kcal/mol. None of these calculated barriers is consistent with experimental 4.2 kcal/mol activation energy for gas phase

Scheme I

trans-HNNH + trans-HNNH	→ $H\cdot + N_2 + H_2\dot{N}NH$	ΔH = -15 kcal	(1)
trans-HNNH + $H\cdot$	→ $H_2\dot{N}NH$	ΔH = -62.3 kcal	(2)
$H_2\dot{N}NH$ + trans-HNNH	↗ cis-HNNH + $H_2\dot{N}NH$	ΔH = 4.7 kcal	(3)
	↘ $H\dot{N}N + H_2NNH_2$	ΔH = -4.6 kcal	(4)
$H\dot{N}N$ + trans-HNNH	→ $N_2 + H_2\dot{N}NH$	ΔH = -86 kcal	(5)
$H\dot{N}N$	→ $N_2 + H\cdot$	ΔH = -24.1 kcal	(6)

decomposition of **1** found by Willis and coworkers.[12] Casewit and Goddard[11] have proposed a radical-chain decomposition mechanism for **1** (Scheme I) which finds the experimental barrier to be consistent with the calculated energy gap of 4.7 kcal/mol between cis and trans HNNH. However, a radical chain mechanism, for the reduction of olefins by "diimide" in the gas phase has been ruled out.[12]

Correcting Casewit and Goddard's calculated N-H bond strength of H_2NN for the difference between an N-H and N-CH_3 bond strength [D(HMeN-H) - D(HMeN-CH_3) = 18.5 kcal/mol][13] provides an estimate for the N-CH_3 bond energy in 1,1-dimethyl diazene **7** of 23.5 kcal/mol. Application of this correction to the calculated N-H bond strength for trans HNNH **1** results in an estimate for the N-C bond strength in trans-1,2-dimethyl

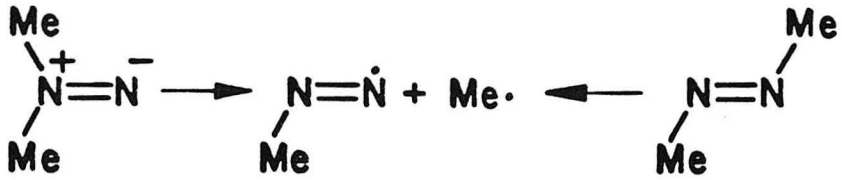

7 8

diazene **8** of 52.9 kcal/mol. This estimate is in excellent agreement with the experimental value of 52.5 kcal/mol[14] for the thermal decomposition of **8** in the gas phase. Hartree-Fock (HF) calculations of Pasto and Chipman[1r] result in a 40 kcal/mol N-H bond strength for H_2NN **3** and a 26 kcal/mol C-N bond strength for 1,1-dimethyldiazene **7** in good agreement with Casewit and Goddard.[1t] One must be cautious in applying GVB-CI results to 1,1-diazene thermochemical estimates as the 18.5 kcal/mol correction may not be

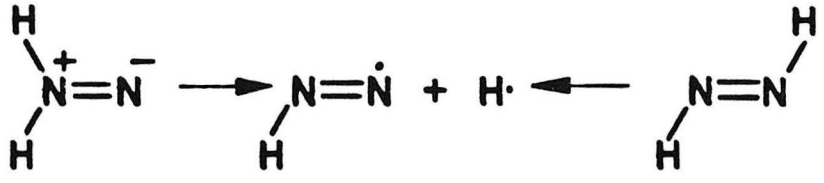

3 1

directly applicable to 1,1-dialkyl diazenes. Qualitatively, the N-H bond energy is $H_2\overset{+}{N}=\overset{-}{N}$ is lower than the N-H bond energy in trans HN=NH because α cleavage in $H_2\overset{+}{N}=\overset{-}{N}$ results in the formation of a full N=N double bond (HN=N·) without the need for charge separation. Although an N-H bond is broken, substantial π-bonding is gained. However, in HN=NH, a full N=N double bond already exists so only two-center three-electron bonding is gained upon breaking an N-H bond.

Generation and Chemistry of 1,1-Diazenes

In the last several decades, the chemistry of presumed 1,1-diazene intermediates has been extensively investigated.[6] There are numerous methods reported for generating the presumed 1,1-diazene intermediate (Figure 3). The most versatile method is oxidation of 1,1-disubstituted hydrazines with oxidants such as tert-butyl hypochlorite[15] and nickel peroxide.[16] Other methods include the reduction of N-nitrosamines,[17] base induced thermolysis of 1,1-disubstituted sulfonyl hydrazines[18] and difluoramine addition to secondary amines.[19] Other attractive routes involve the thermal or photochemical cleavage of N-amino sulfoximines.[20] The intermediacy of 1,1-diazenes in these reactions is supported from the resulting products of their thermal decomposition. The thermal reactions of 1,1-diazenes can be divided into three general classes: (a) fragmentations, (b) isomerizations, and (c) bimolecular reactions (Figure 4). The actual reaction pathway is dependent upon the mode of generation, structure, degree of substitution, and reaction conditions. In general, the fragmentation of 1,1-

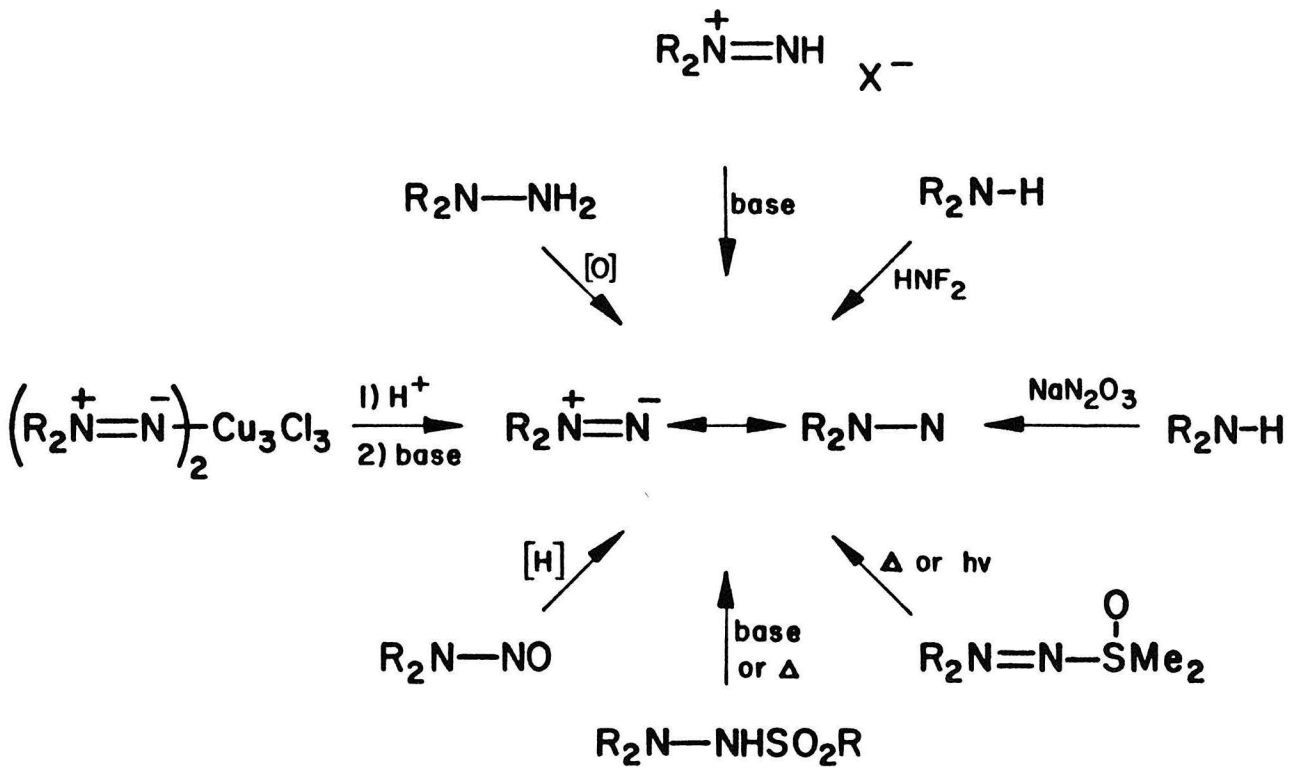

Figure 3. Methods for generation of 1,1-diazenes.

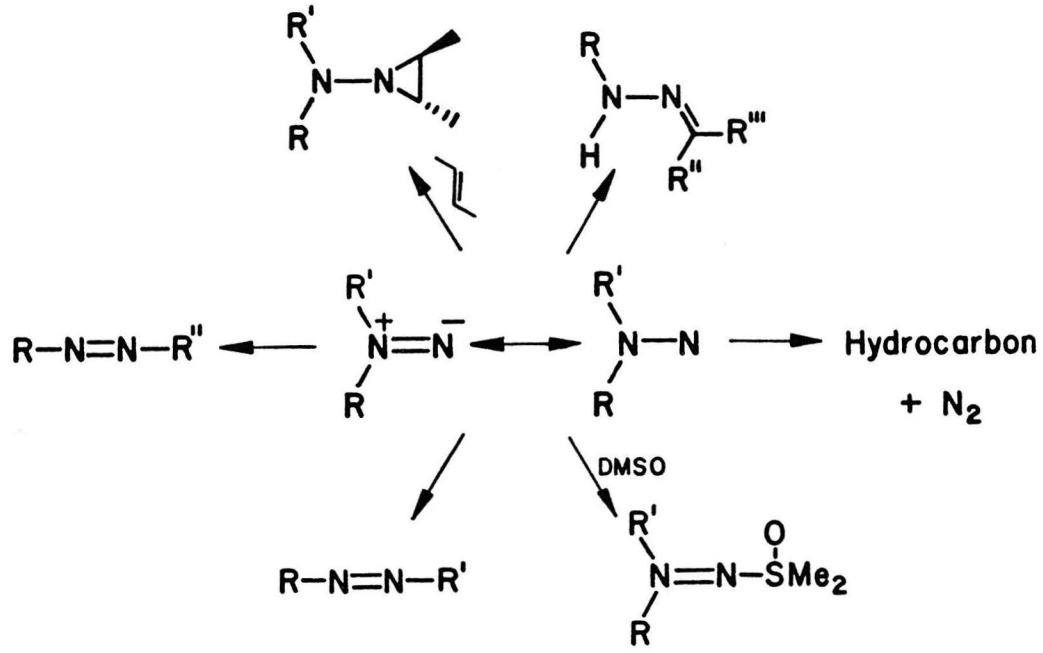

Figure 4. Reactions of 1,1-diazenes.

diazenes is in accord with a mechanism involving radical or biradical formation with loss of nitrogen. The presence of radical stabilizing substituents may favor fragmentation. Pyrolysis of N-sulfonyl-2,5-dimethylpyrrolidylhydrazine[18c] at 400°C yields 1,2-dimethyl cyclo-

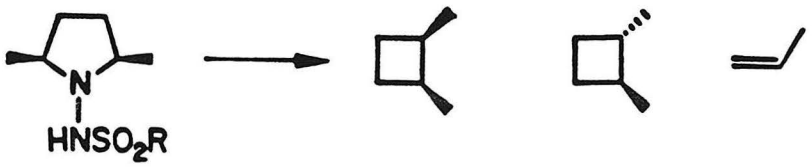

butanes, propene and nitrogen. Oxidation of 1,1-dibenzyl hydrazine with mercuric oxide at 25°C yields dibenzyl and nitrogen.[21] The question of whether symmetrical 1,1-diazenes decompose by sequential one bond or simultaneous two bond cleavage remains unanswered.[22]

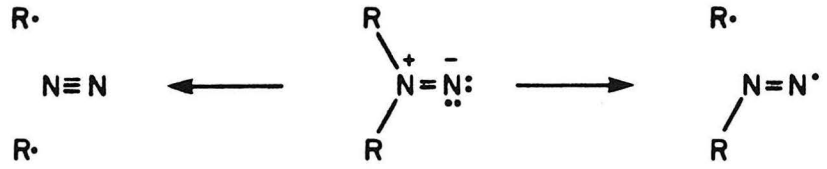

Concerted fragmentation of 1,1-diazenes may occur in a number of cases. For example, treatment of cis and trans 2,3-dimethylaziridines with difluoramine results in apparent stereospecific extrusion of nitrogen from the

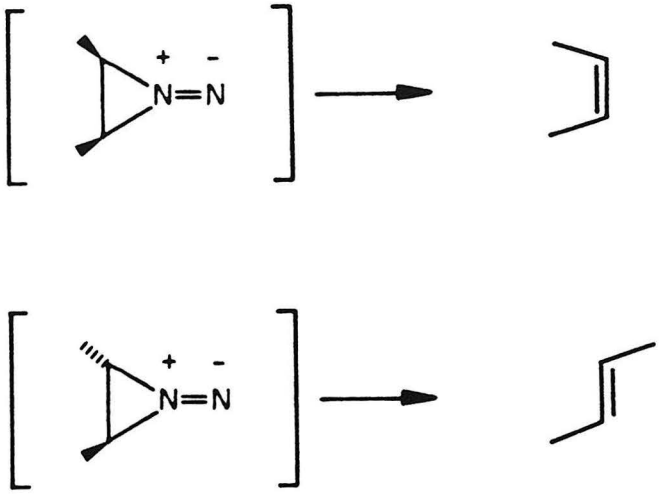

proposed 1,1-diazene intermediates.[23] Recently Duan and Dervan have demonstrated a stereospecific 2,3-elimination pathway for 1,1-diazenes with β-hydrogens.[24]

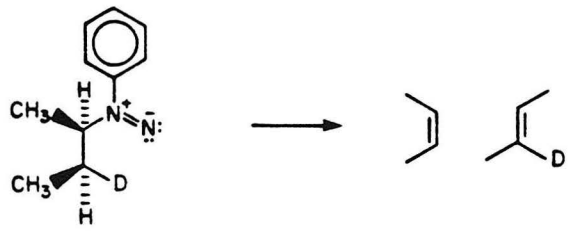

Isomerization of 1,1-diazenes consist mainly of two reaction types: (a) rearrangement to hydrazones and (b) isomerization to 1,2-diazenes.

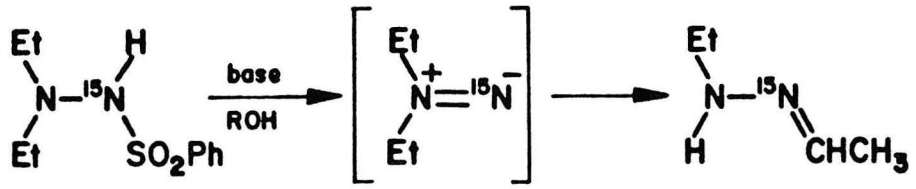

Hydrazone formation is a general reaction for 1,1-diazenes with α-hydrogens generated by several different methods.[6] A protic solvent is generally necessary for hydrazone formation. Labeling studies have demonstrated that the nitrene nitrogen ends up as the doubly bonded nitrogen in the product hydrazone.[25] Cyclic 1,1-diazenes have also been shown to ring expand to isomeric hydrazones. Although this rearrangement has been the

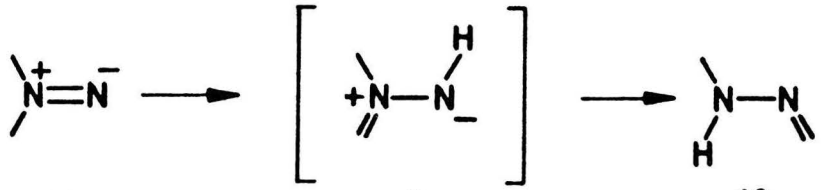

7 9 10

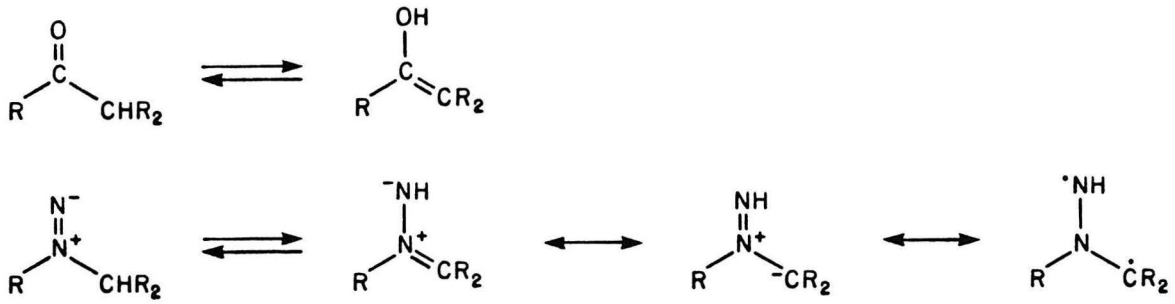

subject of extensive research, the mechanism remains uncertain. Diaziridines and 1,2-diazenes have been ruled out as possible intermediates.[26] Both of these species have been shown to survive the reaction conditions necessary to generate hydrazones. To date the reaction is considered to proceed through the intermediacy of an azomethinimine[6] 9 (analogous to the enol form of a ketone). The function of the protic solvent may be to facilitate the tautomerization of the 1,1-diazene.

Rearrangement of 1,1-diazenes to 1,2-diazenes has been shown to occur when the product 1,2-diazene N=N functionality is incorporated into an aromatic system.[27] 1,1-Diazene precursors have also been proposed to give rise to 1,2-diazenes as the result of a concerted 2,3-sigmatropic rearrangement of the intermediate 1,1-diazenes.[28]

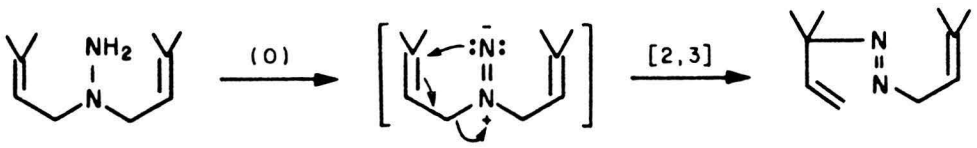

Dimerization of 1,1-diazenes results in the formation of 2-tetrazenes. The formation of tetrazenes is a general reaction for 1,1-diazenes.[6] However, the mechanism may vary depending on the reaction conditions and mode of generation of the 1,1-diazene. In only a few cases is the mechanism

known.[6,8] Neutralization of solutions of 1,1-dialkyl diazenium ions leads to the formation of a colored species with the ultimate reaction product being the corresponding 2-tetrazene.[29] The tetrazene product probably results, at least in part, from the reaction of a 1,1-dialkyl diazene with a diazenium ion giving a protonated tetrazene which then deprotonates. Rees and coworkers[30]

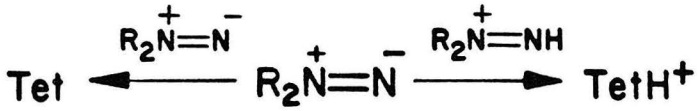

Tet = $R_2N-N=N-NR_2$

isolated a tetrazane **11** from the lead tetraacetate oxidation of N-aminophthalimide, which upon further oxidation yielded the corresponding tetrazene **12**. Direct bimolecular dimerization of kinetically persistent 1,1-diazenes to form tetrazenes has been demonstrated.[8]

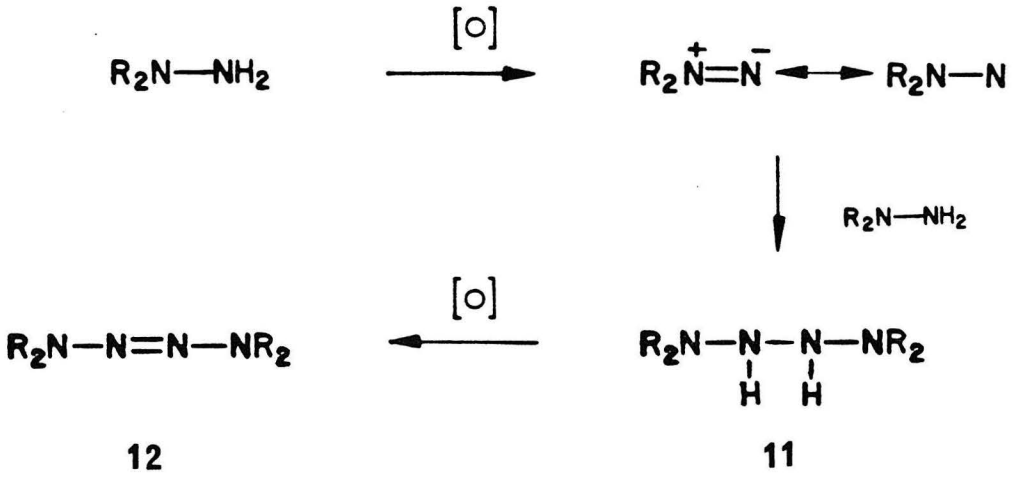

1,1-Diazenes substituted with electron withdrawing groups have been shown to add to π-bonds and to sulfoxides,[6] suggesting that these additions are electrophilic in nature. Addition of diacyl 1,1-diazenes to olefins is greater than 95% stereospecific even at low alkene concentrations.[31] By analogy to carbene chemistry, this has been taken as evidence for a singlet 1,1-diazene ground state. Simple dialkyl 1,1-diazenes have not been shown to be trapped by alkenes or sulfoxides.

Kinetically Persistent 1,1-Diazenes

Recently, direct studies of the 1,1-diazene functional group became available with the preparation of kinetically persistent 1,1-diazenes **4** and **5** by Hinsberg, Schultz, and Dervan.[8f] Additionally, the acyclic 1,1-diazene **6** was prepared by MacIntyre and Dervan.[8g] All three persistent 1,1-diazenes are prepared from the corresponding 1,1-disubstituted hydrazines by oxidation

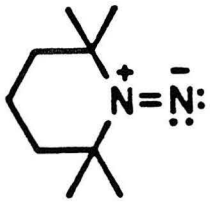

4

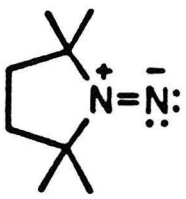

5

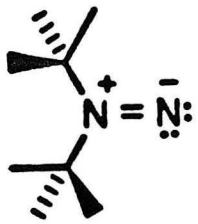

6

with tert-butyl hypochlorite in low temperature solution (-78 to -120°C) in the presence of triethylamine. The kinetic persistence of these diazenes is due to the tetramethyl steric blockade which slows dimerization to the corresponding tetrazenes, the absence of α hydrogens which precludes any tautomerization/hydrazone rearrangement chemistry and their preparation at low temperatures, where nitrogen extrusion is prevented.

As predicted from theoretical studies, these persistent 1,1-diazenes are colored species, giving purple (**4**) and red (**5** and **6**) solutions. Absorption and emission spectra are shown in Figures 5, 6, and 7. The absorptions are n-π* transitions, which show an expected blue shift in the more polar solvent isopropanol. The extinction coefficients are 20 ± 3. The vibrational structure in the absorption curves correspond to the N-N vibrational

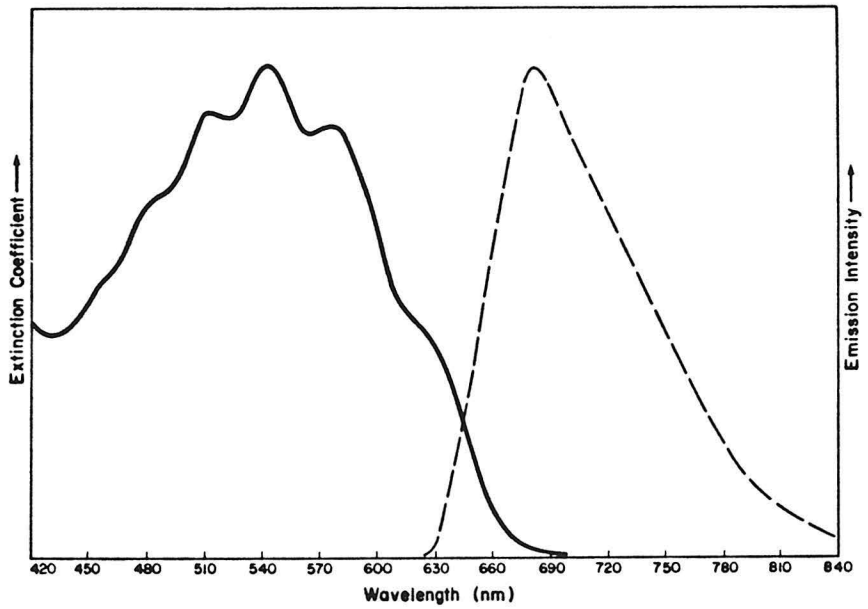

Figure 5. Absorption (——) and fluorescence (---) spectra of **4** in $CFCl_3$ at -78°C and -196°C, respectively.

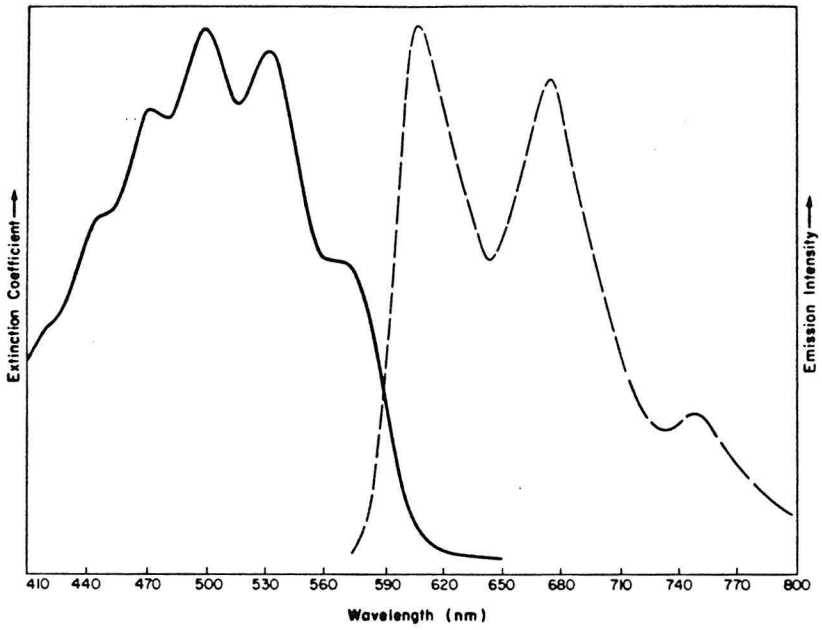

Figure 6. Absorption (——) and fluorescence (---) spectrum of **5** in $CFCl_3$ at -78°C and -196°C, respectively.

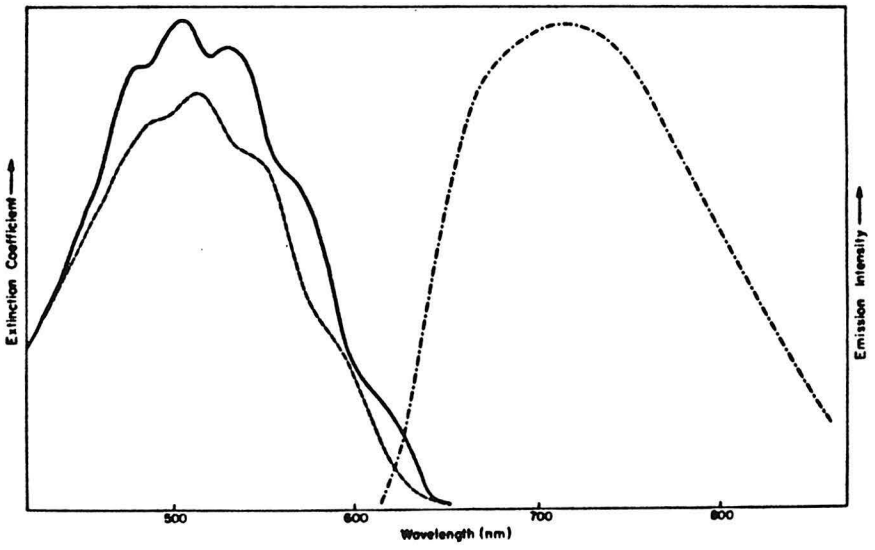

Figure 7. Absorption spectrum of **6** at -125°C in Me_2O (——) and $nPrOH/Me_2O$ (---). Fluorescence spectrum of **6** at -196°C in Me_2O/CD_2Cl_2 (-·-·-).

frequencies of the respective excited S_1 states. The average vibrational spacings from these absorption curves are 1040 to 1250 cm^{-1}. Weak emission occurs from S_1 with a fluorescence quantum yield of 7×10^{-3} for **5**.[8h] The lifetime of the excited state S_1 is about 20 nanoseconds with internal conversion being the primary decay mode.[8h] No other electronic transitions ($\varepsilon > 50$ M^{-1} cm^{-1}) were detected for **5**.

Infrared absorptions are observed at 1595 cm^{-1} for the 6-membered ring diazene and at 1638 cm^{-1} for the 5-membered ring diazene in dichloromethane solution.[8f] In order to characterize these infrared bands as the respective N-N double bond stretches, the diazenes were prepared with a terminal ^{15}N label. As expected, the infrared bands were found to shift to

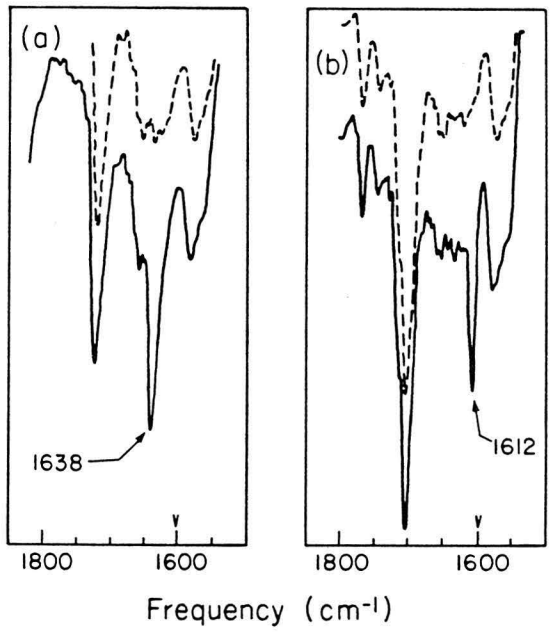

Figure 8. Infrared spectra of **5** (a) $R_2{}^{14}N{=}{}^{14}N$ and (b) $R_2{}^{14}N{=}{}^{15}N$ at -78°C (—— and at -78°C after warming to 25°C (---).

lower energy as calculated from Hooke's law (Figure 8). The similarity of these infrared transitions to the 1576 cm^{-1} Raman active N=N double bond stretch for trans-1,2-diazenes is indicative of substantial N=N double bond character in the 1,1-diazenes.

	electronic (nm)		infrared (cm^{-1})	
	$\lambda_{max}(CH_2Cl_2)$	λ_{max}(iPrOH)	$^{14}N=^{14}N$	$^{14}N=^{15}N$
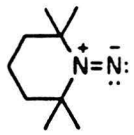	543	526	1595	1568
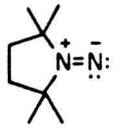	497	487	1638	1612

Warming the purple-red 1,1-diazene solutions results in decolorization and formation of decomposition products shown in Figures 9 and 10. Bimolecular decomposition (k_2) is a low activation energy process (E_a = 6.4 ± 0.9 kcal/mol, log A = 3.8 ± 0.7 for **4**), which predominates at low temperatures (< -30°C for **4** and **5**). At warmer temperatures the unimolecular nitrogen extrusion pathway (k_1) dominates. The Arrhenius parameters determined for k_1 in ether solution are E_a = 20.0 ± 0.4 kcal/mol and log A = 13.7 ± 0.3 for diazene **4**,[8f] E_a = 19.0 ± 0.6 and log A = 12.4 ± 0.4 for diazene **5**,[8f] and $E_a \simeq$ 13 kcal/mol for an assumed log A = 13 for diazene **6**.[8g]

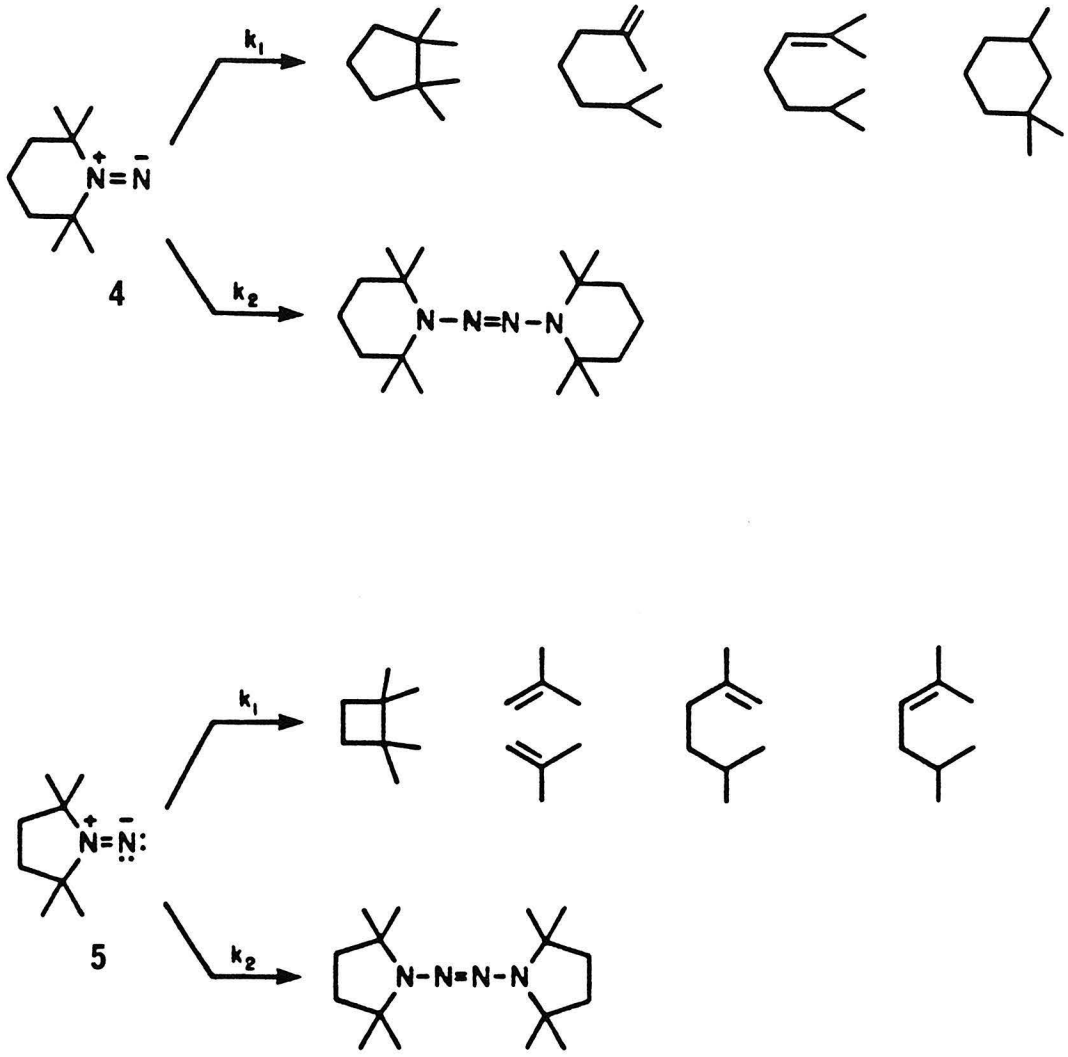

Figure 9. Unimolecular and bimolecular decompositions for 1,1-diazenes **4** and **5**.

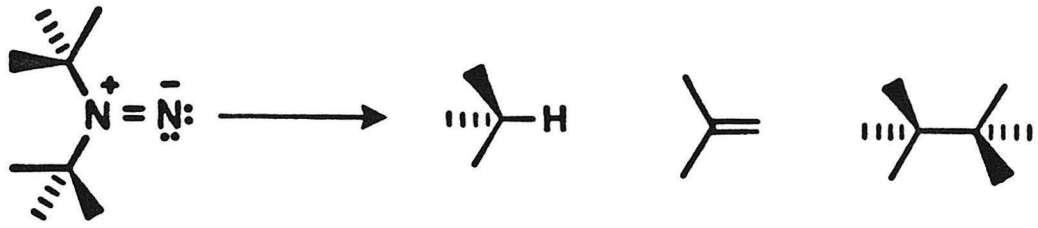

6

Figure 10. Unimolecular decomposition products for 1,1-diazene **6.**

The direct and triplet sensitized photolyses of 1,1-diazene **5** with visible light yield the tetrazene and hydrocarbon products in 4:1 and 9:1 ratios, respectively.[8h] The high yields of tetrazene from photolysis have been shown to be the result of bimolecular reaction of the nitrene-like excited state S_1,T_1 with the ground state 1,1-diazene S_0. A spin correlation effect has been demonstrated in the products resulting from direct and triplet sensitized photolysis of d,ℓ-**14**.[8h] To date attempts to locate or directly observe T_1 of a 1,1-diazene have been unsuccessful. Figure 11 summarizes the excited state parameters for 1,1-diazene **5**.[8h]

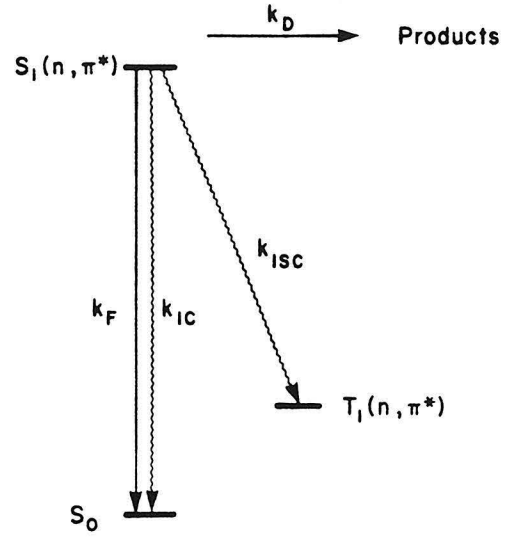

$E(S_1)$	=	47-50 kcal (CH_2Cl_2)
$E(T_1)$	<	31 kcal
k_F	=	3×10^5 sec^{-1}
k_{IC}	=	2×10^8 sec^{-1} (-78°C)
k_D	=	$k_{DIM} + k_{N_2}$
k_{N_2}	=	3×10^5 sec^{-1} (-78C)
k_{DIM}	=	8×10^7 mol^{-1} sec^{-1} (-78C)
k_{ISC}	<<	k_{N_2} or $\sim 10^4$ sec^{-1}

Figure 11. Excited state parameters for kinetically persistent 1,1-diazene **5.**

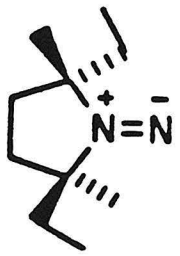

14

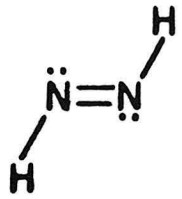

1

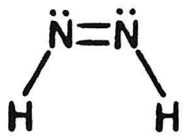

2

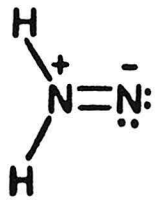

3

H_2N_2 Spectroscopic Characterization

Numerous methods have been employed to generate H_2N_2 as a reducing agent for organic synthesis or for spectroscopic characterization and study.[2] Among the more useful modes of generation for spectroscopic study are (a) microwave (or Tesla coil) discharge of hydrazine vapor,[2f] (b)

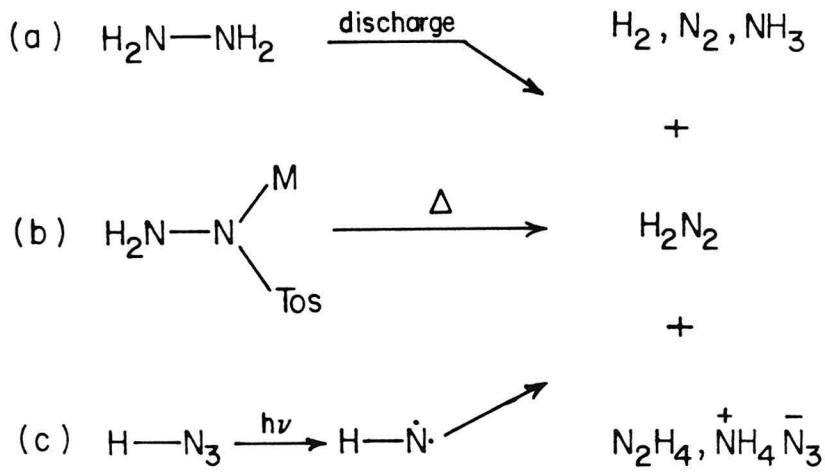

pyrolysis of metal tosyl hydrazide salts[2g] and (c) dimerization of nitrene (H-$\dot{N}$·) produced from photolysis of hydrazoic acid.[2c] H_2N_2 has been demonstrated to be extremely reactive with a lifetime of several minutes at room temperature (gas phase).[2e] Thermal decomposition of H_2N_2 occurs rapidly near liquid nitrogen temperatures (neat).[2g] H_2N_2 is also efficiently decomposed photochemically either in condensed phase or as a vapor.[2d,32] All of the above methods for generation of H_2N_2 might be expected to initially produce a mixture of isomers **1**, **2**, and **3**. However, due to the high reactivity of these species and the presence of substantial amounts of hydrogen bonding side products (e.g., NH_3, N_2H_4) in these modes of generation, firm experimental characterization is available only for the trans

Table II. Spectral Characteristics H_2N_2 Isomers.

	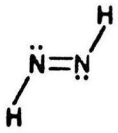	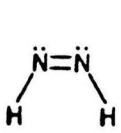	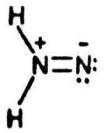	Reference
electronic (UV/VIS) λ_{max} (nm)	386	--	--	2j
infrared (IR) (cm^{-1})	3131	(3074)[a]	--	2c,2f
	1286	(1279)[a]	--	
Raman (cm^{-1})	3128	--	--	2f
	1583	--	--	
($\nu_{N=N}$)	1529	--	--	

[a]Tentative assignments.

HNNH isomer **1** (Table II).[2,33] Various other ambiguous assignments have been claimed for the other H_2N_2 isomers under non-matrix isolation conditions only to be later reinterpreted as hydrogen bonded complexes of **1** and side products.[2] Conclusive assignments have resulted from careful matrix isolation studies, the use of heavy isotopes (D, ^{15}N)[2c,2f] to aid in the assignment of vibrational transitions, and observations of thermal and photochemical reactivity.

Trans HNNH **1** has been characterized as a yellow species showing a non-structured absorption, λ_{max} = 386 nm (neat, 77°K).[2j] In contrast, a structured absorption, λ 320-440 nm ($\epsilon \simeq 4$ at 365 nm), is observed for a mixture of **1** (15%) in a large excess of ammonia in the gas phase.[34]

In 1964, Rosengren and Pimentel[2c] identified two infrared transitions for trans HNNH at 3131 cm^{-1} (weak, NH asymmetric stretch) and 1286 cm^{-1} (very strong, NNH asymmetric bend), produced from photolysis of hydrazoic acid in a nitrogen matrix at 20 K. In addition, heavy isotopes (D, ^{15}N) were incorporated to verify these assignments. Tentative assignments were made for two cis HNNH bands at 3074 cm^{-1} (weak, NH stretch) and 1279 cm^{-1} (strong). In 1973, Bondybey and Nibler[2f] reported the infrared and Raman spectra of isotopically labeled **1** produced from the microwave or Tesla coil discharge of hydrazine, followed by deposition in a nitrogen matrix at 12 K. Their infrared assignments were consistent with those of Rosengren and Pimentel, resulting in a conclusive vibrational characterization of **1**. None of the tentative cis HNNH infrared bands were located. The characteristic N=N double bond stretch for **1** was located in the Raman at 1529 cm^{-1}. However,

the ^{15}N shifted multiple for this mode was not located. Additional Raman bands for **1** were found at 3128 cm^{-1} (weak, NH symmetric stretch) and 1583 cm^{-1} (very weak, NNH symmetric bend).

Analysis of the gas phase rotational structure of the high resolution infrared spectrum[2i] of **1** has provided the following geometrical parameters: $R_e(NN) = 1.25$ Å, $R_e(NH) = 1.03$ Å, $\angle HNN = 106.9°$. These parameters are consistent with the established singlet ground state of planar geometry for trans HNNH.[2i]

Trans HNNH **1** has also been characterized by photoelectron spectroscopy,[2k] vacuum UV spectroscopy,[2o] and by mass spectroscopy.[2n] Foner and Hudson[2m] have recently reported an experimental value for the heat of formation of **1** ($\Delta H_{f(298)} = 50.7 \pm 2$ kcal/mol) from a combination of ionization potential and appearance potential measurements. All of these studies indicate that H_2N_2 exists predominantly as the trans isomer **1**.

Wiberg has reported[2g] that pyrolysis of solid metal tosyl hydrazide salts followed by trapping of the less volatile side products (NH_3, N_2H_4, -78°C) as means of preparing clean **1** by condensation onto a cold finger at 77° K. According to Wiberg, a mixture of **1**, **2**, and possibly **3**, is obtained from pyrolysis of metal tosyl hydrazides (M = Li, Na, K, Rb) followed by condensation of the products. When M = Cs, however, Wiberg reports[2j] that an isomer "isodiazene" (**3**) is obtained. This "isomer" is reported to be 13 kcal/mol higher in energy than **1** by appearance potential measurement in the gas phase. In addition, this "isomer" is reported to be a colorless species, $\lambda_{max} = 260$ nm (77°K). A yellow addition product ($\lambda_{max} = 398$ nm) forms

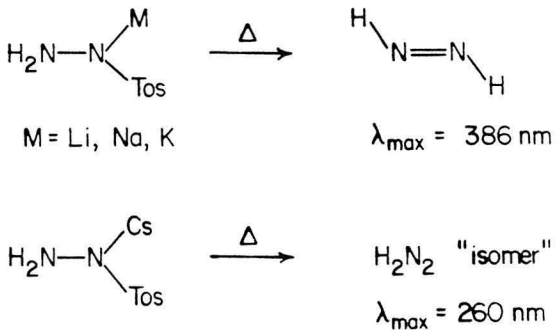

quickly with ammonia (77°K). The same yellow addition product is formed slowly with **1** at 110°K. No further characterization for this "isomer" has been reported. Wiberg's assignment for "isodiazene" seems suspect and not in accord with ab initio (GVB-CI) calculations[1t] for the H_2N_2 energy surface which predict 1,1-diazene **3** to be 29 kcal/mol higher in energy than **1**. The UV transition (λ_{max} = 260 nm) observed by Wiberg, is also inconsistent with the theoretical (GVB-CI) prediction[1n] of an n-π* transition for **3** near 560 nm in the visible region and the observed n-π* (λ_{max} = 500-540 nm) for kinetically persistent 1,1-dialkyl diazenes.[8] The parent 2-tetrazene **25** H_4N_4, which would be expected to result from dimerization of 1,1-diazene **3** has been reported as a meta-stable species (λ_{max} = 263 nm).[35]

H_2N_2 Chemistry

The gas phase thermal and photochemical decompositions of HNNH **1** in the presence and absence of unsaturated compounds (e.g., alkenes, dienes) have been studied by Willis et al.[2e,h,32,34,36] Thermal and photochemical decompositions of neat and matrix isolated **1** have been noted by others.[2]

The result of gas phase kinetic studies of the thermal decomposition of **1** (generated by microwave decomposition of hydrazine) as a dilute gas mixture (approximately 10-15% H_2N_2 in excess ammonia) with alkenes has been interpreted in terms of the following complex reaction (Scheme II).[34,36] The thermal decomposition of **1** (monitored spectrophotometrically), for the most part, follows first order decay kinetics, excluding a fast initial non-exponential decay which is presumably due to self heating and surface effects. The rate determining step is assumed to be the unimolecular isomerization of trans **1** to cis **2** (eq. 1), although theory predicts the barrier for this unimolecular transformation to be quite high.[1] Cis **2** is then assumed to be the species responsible for further reduction by the accepted concerted

Scheme II

$$\text{trans-}H_2N_2 \longrightarrow \text{cis-}H_2N_2 \text{ (slow, rate controlling)} \qquad (1)$$

$$\text{cis-}H_2N_2 + \text{trans-}H_2N_2 \longrightarrow N_2H_4 + N_2 \qquad (2a)$$

$$\text{cis-}H_2N_2 + \text{trans-}H_2N_2 \longrightarrow N_2 + H_2 + \text{trans-}H_2N_2 \qquad (2b)$$

$$\text{cis-}H_2N_2 + \text{olefin} \longrightarrow N_2 + \text{product} \qquad (3)$$

$$\text{cis-}H_2N_2 + \text{olefin} \longrightarrow \text{adduct} \qquad (4)$$

$$\text{adduct} + \text{trans-}H_2N_2 \longrightarrow N_2 + N_2H_4 + \text{olefin} \qquad (5)$$

$$\text{adduct} + \text{olefin} \longrightarrow \text{product} + \text{olefin} + N_2 \qquad (6)$$

$$\text{adduct} \longrightarrow \text{olefin} + \text{trans-}H_2N_2 \qquad (7)$$

Woodward-Hoffman allowed cyclic transition state to give hydrazine (disproportionation) (eq. 2a) or reduction of added alkene (eq. 3). Pasto and Chipman[1r] have calculated (4-31G) $\Delta H^{\ddagger}$ for this concerted reaction (eq. 3) to be 26.7 kcal/mol. In addition, Pasto[1s] calculates (4-31G) $\Delta H^{\ddagger}$ for the disproportionation step (eq. 2a) to be 23.8 kcal/mol. Thus, both the unimolecular isomerization of **1** to **2** and reduction of alkenes by **2** are predicted by theory to have rather substantial barriers which are apparently not found experimentally. However, the measured first order decay of **1** is observed to be faster in the presence of added hydrazine or water and is dependent upon the structure of added alkene.[34,36] The self reactions of H_2N_2 (disproportionation) are some 4-8 times faster than alkene addition (reduction) at 100°C in the gas phase. The first order decay of **1** as a function of temperature in the presence of added 1,3-butadiene gives Arrhenius activation parameters (log A = 0.255, E_a = 5.70 kcal/mol)[36] which are different from the activation parameters for the decay of **1** in the absence of added alkene (log A = 0.477, E_a = 4.20 kcal/mol).[34,36] In addition, the measured first order decay shows a deuterium kinetic isotope effect. Thermal decomposition of D_2N_2 **1-d$_2$** in the absence of alkene gives Arrhenius activation parameters log A = 0.301 and E_a = 4.40 kcal/mol.[34,38] The gas phase thermal decomposition of **1** is not affected by added O_2 and no conclusive evidence for a radical chain mechanism for the thermal decomposition of **1** has been noted. The stereospecificity (syn reduction) of alkenes by N_2D_2 was <u>not</u> demonstrated in this work.[34,36]

Willis[2e,34,36] finds only H_2, N_2, and hydrazine as thermal products of

1 with no evidence for formation of ammonia or ammonium azide. Wiberg[2g,37] reports that in addition to H_2, N_2, and hydrazine, ammonia and ammonium azide are also produced from thermal decomposition of neat 1 prepared from the pyrolysis of metal tosyl hydrazides. Wiberg has also noted a very rapid reaction of 1 with O_2 yielding HOOH and N_2.[2g]

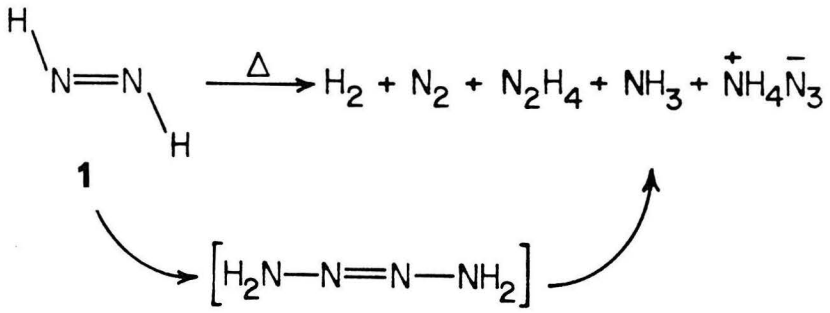

The photochemical decomposition of 1 in the presence and absence of added alkenes has also been reported by Willis.[32] Photochemically, 1 yields H_2 and N_2 as products (>97%). The quantum yield for loss of 1 in the gas phase ranges from 13-20. Apparent quantum yields for alkene reduction are approximately 7. The presence of O_2 suppresses alkene reduction supporting the interpretation of a radical chain mechanism for the photochemical decomposition of 1 and resulting alkene reduction. The parent diazenyl radical ($\cdot N_2H$) is implicated as a chain carrier. The rate constant for homolysis of diazenyl radical is estimated to be 3×10^3 sec^{-1} at room temperature. Assuming a pre-exponential factor of 10^{13}, the activation barrier for diazenyl radical homolysis is estimated to be approximately 13 kcal/mol. The lifetime of the n-π^* excited state of 1 is estimated to be 5 x

10^{-12} sec. No evidence for photochemical trans **1** to cis **2** isomerization has been reported.[2,32] No evidence for collisional deactivation of the excited state of **1** is noted and dissociation of the excited state of **1** to $\cdot N_2H + H\cdot$ or $N_2 + 2H\cdot$ is concluded to have a quantum yield near unity, although dissociation directly to $N_2 + H_2$ cannot be excluded.[32] Primary photodissociation of **1** may occurs from high vibrational levels of the ground state reached by rapid internal conversion or intersystem crossing from the excited state.[32]

$$N_2H_2^{\ddagger} \longrightarrow \cdot N_2H + H\cdot \qquad \Delta H = 71.5 \text{ kcal/mol}$$

$$N_2H_2^{\ddagger} \longrightarrow N_2 + 2H\cdot \qquad \Delta H = 47 \text{ kcal/mol}$$

$$N_2H_2^{\ddagger} \longrightarrow N_2 + H_2 \qquad \Delta H = -57 \text{ kcal/mol}$$

‡ = Vibrationally hot H_2N_2

Experimental Strategy

From the direct studies of kinetically persistent 1,1-dialkyl diazenes[8] several factors are apparent concerning the generation and direct spectroscopic characterization of the parent 1,1-diazene H_2NN and its simple alkyl derivatives (e.g., R = CH_3, C_2H_6, etc.). Due to the lack of a steric blockade to dimerization, H_2NN **3** and its simple dialkyl derivatives are likely to dimerize to their corresponding 2-tetrazenes at near diffusion controlled rates. Although **3** and its simple dialkyl derivatives should be more stable to unimolecular nitrogen extrusion than the tertiary substituted

persistent 1,1-diazenes, the use of very low temperatures may be necessary to prevent other possible decomposition pathways (e.g., tautomerization, isomerization). Direct spectroscopic characterization is likely to require the use of low temperature matrix isolation techniques.

The generation of highly reactive species (carbenes, nitrenes, radicals, etc.) isolated in a non-reactive material (noble gases, organic glasses, polymers, etc.) has been a successful method for the spectroscopic characterization (UV-VIS, IR, Raman, ESR) of reactive intermediates.[9] Low temperature matrix isolation in a solid inert gas matrix is generally the method of choice for preventing diffusion and resulting intermolecular chemistry of reactive species. As a result of the low temperatures (10-30°K) necessary to prepare a rigid inert gas matrix (Ar, Kr, Xe, N_2) the activation energy for thermal reactions is not available to the isolated species. The spectroscopic transparency of these inert host gases facilitates extensive characterization of reactive intermediates using routine spectroscopic probes.

Among the techniques commonly used for the generation and matrix isolation of reactive intermediates are (a) photolysis of a matrix isolated photochemical precursor, (b) pyrolysis or microwave discharge decomposition of a thermal precursor in the gas phase followed by co-deposition with matrix host gas, and (c) gas phase chemical reaction (crossed beam) of two volatile species followed by co-deposition with host matrix gas onto a cold spectroscopic window. Photolysis of a suitable matrix isolated photochemical precursor is probably the most widely utilized technique. A common feature

of the photochemical routes is the loss of a small stable molecule (e.g., N_2, CO, CO_2) which can diffuse away and become a part of the matrix, leaving a reactive nitrene, carbene, radical or highly strained molecule as an isolated species. The chemically inert noble gases (Ar, Kr, Xe) are considered to form rigid matrices at temperatures below 30% of their melting points (Tm). In the temperature regime of 10° to 25°K, even small molecules (two to three atoms) can be effectively trapped in an argon matrix.

Prior to this work no general method for the photochemical generation of 1,1-diazenes had been reported. However, a number of potential photochemical precursors to **3** and its simple dialkyl derivatives suitable for matrix isolation studies were given consideration. These are briefly described below.

Photoextrusion of nitrogen from an aminoazide might provide a general means of generating 1,1-diazenes in a low temperature matrix. However, the only successful synthesis of an aminoazide reported is the

$$R_2N{-}N_3 \xrightarrow{h\nu} R_2N{-}N \quad N_2$$

preparation of dimethylaminoazide.[39] Dimethylaminoazide has been found to be very unstable thermally.

Oxidation of 1,1-dialkyl hydrazines with nitroso benzene yields (Z)-3,3-

dimethyl-1-phenyltriazene-1-oxide adducts.[40] 1-Phenyl-2-phthalimido-diazene-1-oxide has been shown to photochemically cleave in solution to products consistent with initial formation of N-phthalimidonitrene (phthalimido-1,1-diazene) and nitroso benzene.[40] The N-phthalimido nitrene so generated has been trapped as an adduct with olefins, dimethylsulfoxide and as its dimer the 2-tetrazene. Ultraviolet photolysis of a matrix isolated (Z)-3,3-dimethyl-1-phenyltriazene-1-oxide **16** (yellow, λ_{max} = 326 nm, ε = 8700, λ = 227 nm, ε = 8200) might be expected to produce a 1,1-dialkyl diazene (purple, λ_{max} = 500-600 nm, ε = 20) and nitroso benzene (blue, λ_{max} = 780 nm, ε = 45). With the use of appropriate visible light filters to prevent the anticipated photochemical decomposition of the colored products, the extinction coefficient of a 1,1-dialkyl diazene product could be determined by comparison with the visible absorption of the nitroso benzene co-product.

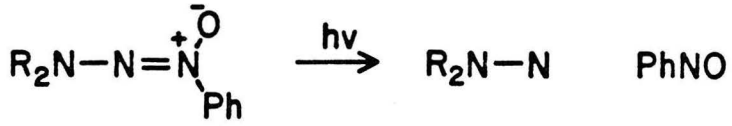

R = CH_3 **16**

Thermolysis of some N-amino aziridines yields products consistent with the formation of an olefin and 1,1-diazene.[41] Vacuum-UV irradiation (124 nm, 147 nm) of the parent aziridine, ethylenimine, in the gas phase produces ethylene and nitrene with a quantum yield of 0.2 to 0.3.[42] The reverse thermal reaction has been demonstrated in an argon matrix.[43] Aromatic substituents on the aziridine ring might provide a chromophore

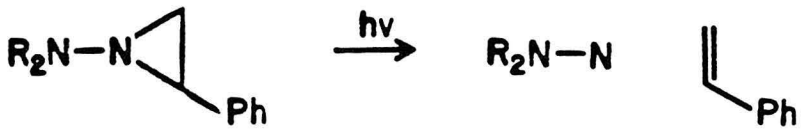

suitable for effecting this transformation with ultraviolet light. In order to generate a 1,1-diazene by this method, the rate of nitrene like S_1 relaxation to the ground state S_0 (1,1-diazene) via fluorescence or internal conversion must exceed the rate of S_1 addition to the olefinic fragment produced. Results from this laboratory with N-(2,2,5,5-tetramethylpyrolidyl) nitrene 5 in solution have shown that addition to activated olefins is not a significant pathway upon direct irradiation of 1,1-diazenes.[8g]

In solution, photolysis of carbamoyl azides yields products consistent with the intermediacy of aminoisocyanates,[44] which readily dimerize or are trapped with alcohols.[45] The resulting dimers of aminoisocyanates can be

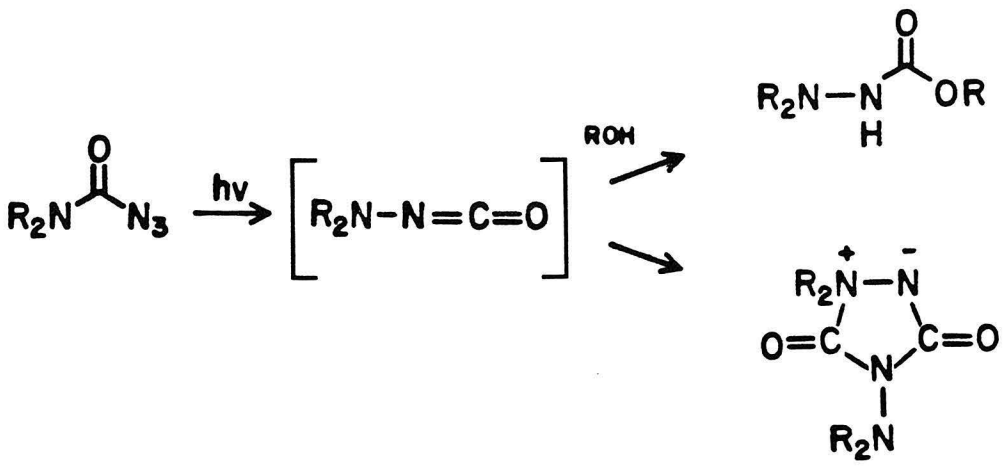

photolyzed in alcohol solution to products consistent with the intermediacy of the aminoisocyanate monomer.[46] The photo-Curtius rearrangement of carbamoyl azides has been shown to be sufficiently facile to occur under matrix isolation conditions at low temperatures (6°K, neon).[47] The intermediacy of aminoisocyanates is supported by matrix isolation infrared spectroscopy with a characteristic infrared absorption at 2230 cm^{-1} attributed to the aminoisocyanate.[47] Ultraviolet (UV) photolysis of a matrix

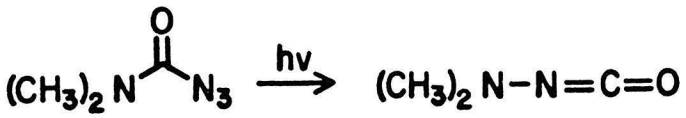

13 I.R. 2230 cm^{-1}

isolated aminoisocyanate, produced by the photo-Curtius rearrangement of a carbamoyl azide, might be expected to produce an aminonitrene (1,1-diazene) and carbon monoxide (CO) just as photolysis of aryl and alkyl isocyanates produces nitrenes and carbon monoxide.[6a,48]

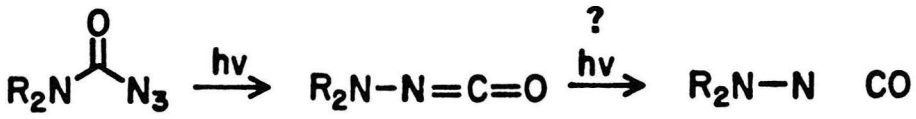

H_2NN and its simple dialkyl derivatives are expected to be colored species with n-π^* transitions in the visible region. Photochemical generation of 1,1-diazenes in a rigid matrix is likely to require the use of visible light filters to prevent subsequent photochemical decomposition of the 1,1-diazene product. The generation of H_2NN and simple dialkyl derivatives by the photo-Curtius rearrangement/photodecarbonylation of carbamoyl azides is described.

RESULTS AND DISCUSSION

CHAPTER 1

Low Temperature Matrix Isolation and Characterization of H_2NN

Synthesis of Carbomoyl Azides (15)

Carbomoyl azide **15** was prepared by treatment of semicarbazide hydrochloride with sodium nitrite.[49] The resulting stable crystalline solid was purified by recrystallization and sublimation. Deuterated

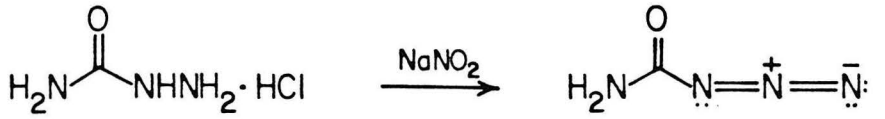

15

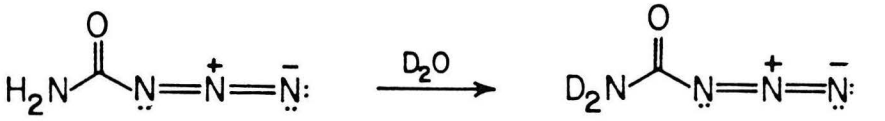

15 **15-d_2**

15 (**15**-d_2) was prepared by exhaustive H,D exchange in excess D_2O.

Electronic Absorption Spectrum of H_2NN 3 and D_2NN 3-d_2

For electronic absorption spectroscopy of H_2NN **3**, a solution of carbomoyl azide **15** in dry, degassed 2-methyltetrahydrofuran (2-MTHF) was loaded into a 1.0 cm path length low temperature spectroscopic cell[50] attached to the low temperature matrix isolation apparatus. The solution was loaded under a positive pressure of argon through Teflon tubing with syringe suction. Cooling the solution to 80°K results in the formation of a rigid optically transparent glass. Irradiation of **15** in a 2-MTHF glass at 80°K

with ultraviolet (UV) light from a 1000 watt xenon lamp[51] through two Corning filters CS-7-54 (UV transmitting, visible (VIS) λ = 400-680 nm cut-out filters) results in the loss of the UV transition due to **15** and formation of a blue-violet glass. Electronic absorption spectroscopy of this blue violet glass (80°K) reveals a structured absorbance curve (Figure 12) in the visible λ_{max} =

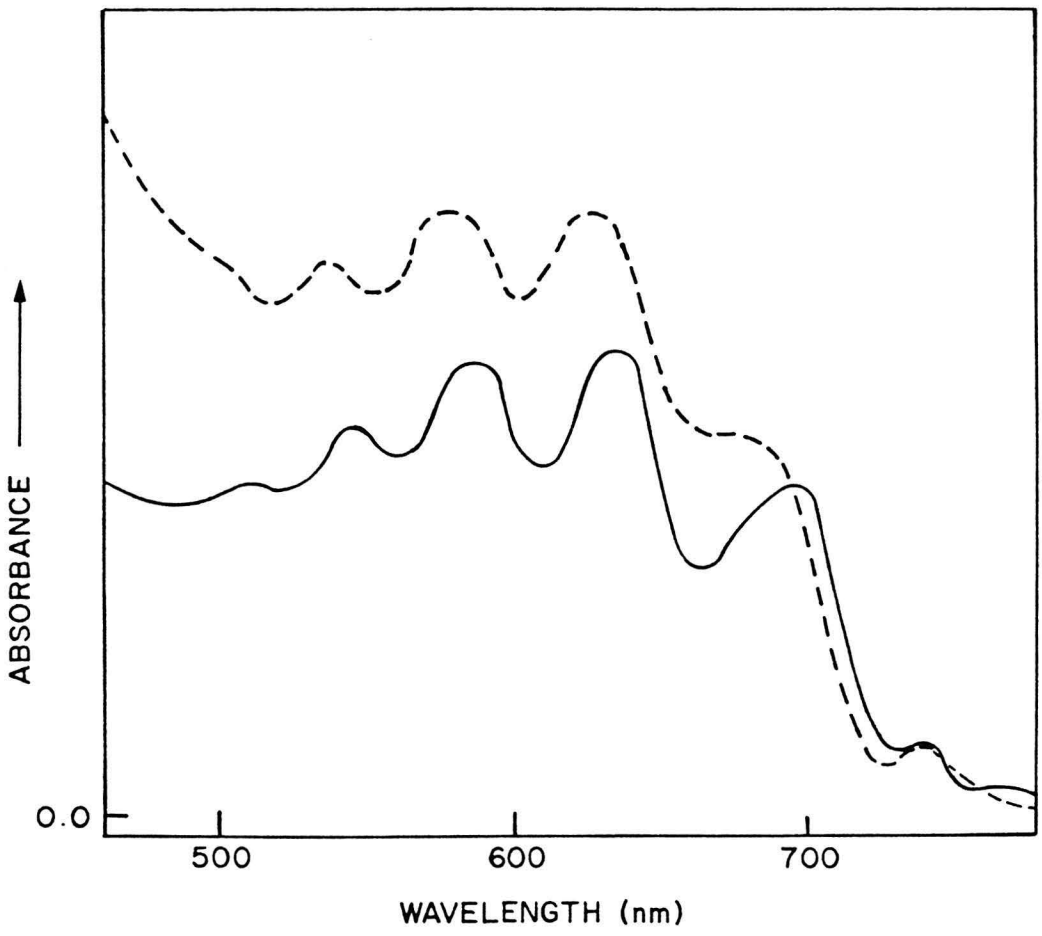

Figure 12. Electronic absorption spectrum of H_2NN **3** in 2-MTHF glass 80°K (——) and 1:1 2-MTHF/nPrCN glass 80°K (---).

636 nm. The spectrum reveals fairly well resolved bands at 695, 636, 587, 545, and 509 nm. The maximum absorption at 636 nm (45 kcal/mol) corresponds to the vertical transition for H_2NN **3.** This is close to the n-π* electronic transition of 560 nm (50.7 kcal/mol) calculated by Davis and Goddard[1n] for H_2NN **3.** The first absorbance band at 695 nm (41 kcal/mol) is tentatively assigned to the adiabatic transition λ 0,0.[52a] This structured transition (λ_{max} = 636 nm) is comparable to the structured transitions (λ_{max} = 497 to 543 nm) observed[8] for kinetically persistent 1,1-diazenes **4, 5,** and **6.** The average vibrational spacing between absorbance maxima in Figure 12 of 1315 cm^{-1} corresponds to the average vibrational spacing of the N-N stretch in the excited S_1 state of **3.** The prominence of the N-N stretching mode is indicative of a substantial change in the Re (N-N) on excitation from S_0 to S_1. Using the ratio of force constants predicted by Davis and Goddard[1n] for the N-N stretches of S_0 and S_1 of H_2NN **3,** ν(N-N) in S_1 should be 1357 cm^{-1}.[52b] The smaller experimental average vibrational spacing of 1315 cm^{-1} possibly suggests that pyramidalization may be more important than 2-center three electron bonding in stabilizing S_1 of **3.** However, the separation of the first two absorbance maxima in the spectrum of **3** at 695 and 636 nm corresponds to a vibrational frequency for ν(NN) of S_1 of 1335 cm^{-1} closer to the calculated stretching frequency. For comparison, the average vibrational spacing observed for kinetically persistent 1,1-diazenes **4, 5,** and **6** are 1040 to 1250 cm^{-1}.[8]

The position of an n-π* transition involving non-bonding electrons is

Table III. Comparison 1,1-Diazene Electronic Transitions.

1,1-Diazene		λ_{max} (nm)	$\lambda_{0,0}$ (nm)	$\bar{\nu}$ (cm^{-1})	$E(S_0-S_1)$ (max) (kcal/mol)
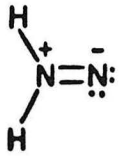	a	636	695	1315	45.1
(Theory, GVB-CI)c		560	--	1357d	50.7
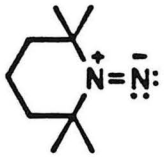	b	543	610	1040	52.7
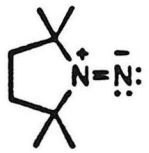	b	506	620	1200	56.6
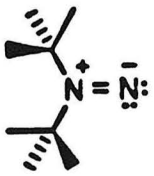	b	497	572	1238	57.6

a2-MTHF glass, 80°K. bMe_2O solution. Refs. 8f,g. cRef. 1n. dRef. 52b.

sensitive to solvent polarity and hydrogen bonding effects.[53] Using a more polar glass forming solvent would be expected to shift the structured absorbance curve of **3** to higher energy. Irradiation of **15** in a rigid optically transparent glass consisting of a 1:1 mixture of 2-MTHF and n-butyronitrile (nPrCN) shifts the structured absorbance curve to higher energy affording λ_{max} = 624 nm and λ 0,0 = 681 nm (Figure 12). This blue shift of λ 0,0 14 nm to higher energy suggests that thermally equilibrated ground and excited states must be differentially solvated, consistent with differing degrees of electron delocalization of S_0 and S_1. For comparison, the n-π^* transition of persistent 1,1-diazene **5** shifts from λ 0,0 = 565 nm in Me_2O to λ 0,0 = 552 nm in isopropyl alcohol solution.[8e] Irradiation of **15-d_2** in a 2-MTHF glass at 80°K affords a structured absorbance curve for D_2NN **3-d_2** similar to that obtained for **3** (Figure 13). The average vibrational spacing for **3-d_2** of 1305 cm^{-1} is slightly smaller than the average vibrational spacing observed for **3**.

Table IV. 1,1-Diazene **3** Electronic Transitions.

1,1-Diazene	Solvent[a]	λ_{max} (nm)	λ 0,0 (nm)	E (0,0) (kcal/mol)	(S_1)
3	2-MTHF	636	695	41.2	1315
3	2-MTHF/nPrCN	624	681	42.0	1315
3-d_2	2-MTHF	636	695	41.2	1305

[a] 80°K, glass.

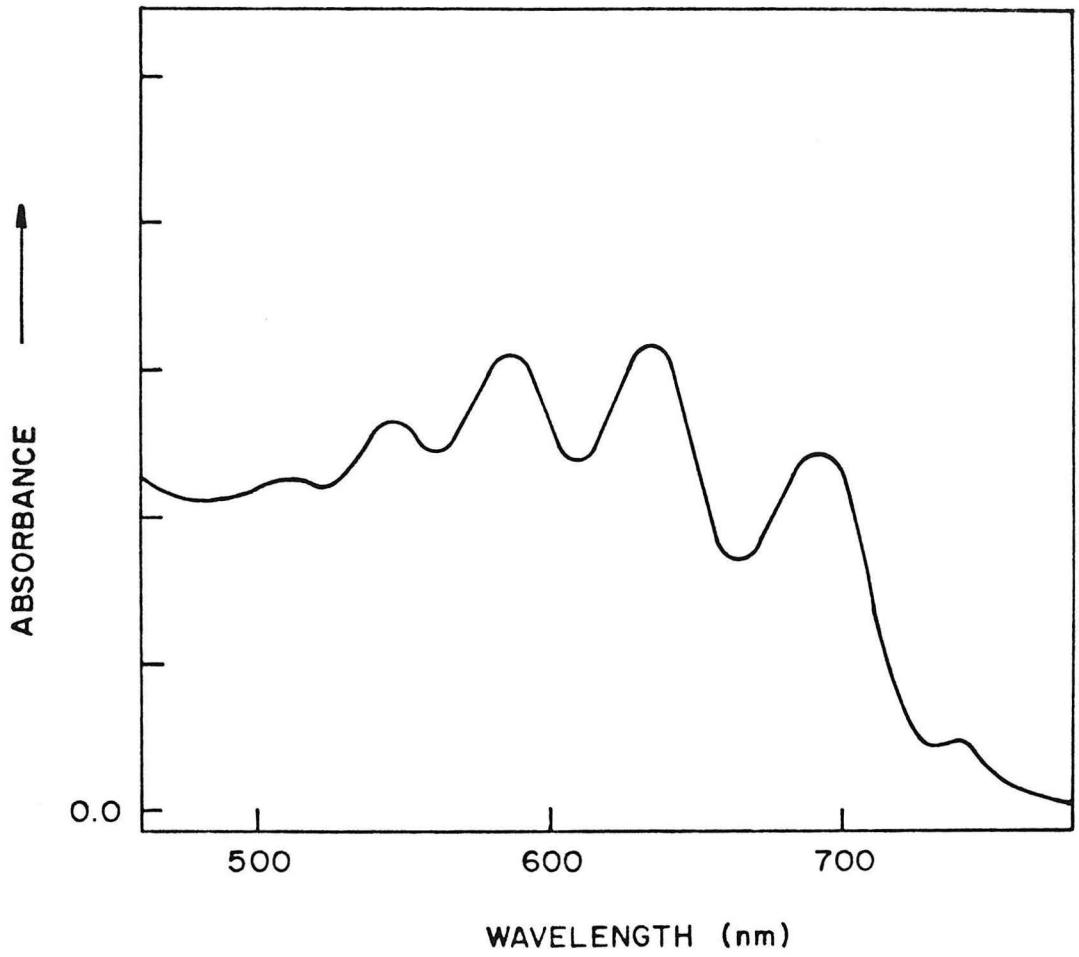

Figure 13. Electronic spectrum of D_2NN 3-d_2 (2-MTHF, 80°K).

Thermal Decomposition of H_2NN

Warming the 2-MTHF glass of **3** from 80°K to the point at which the 2-MTHF glass softens (~90°K) results in loss of the structured absorbance curve and the blue-violet color due to **3**. As the structured absorbance due to **3** diminishes, three new absorbances are observed to grow in at λ_{max} = 260 nm, λ_{max} = 386 nm, and λ_{max} ≈480 nm (Figure 14). The softened glass appears yellow-orange. The very intense band at 260 nm appears to have a very large extinction coefficient as it very rapidly exceeds

the measurable range. By spectral comparison the 260 nm transition is assigned to the known[35] λ_{max} = 263 nm transition for the parent trans-2-tetrazene **25** the expected dimerization product of H_2NN **3**. The extinction coefficient for the λ_{max} = 263 nm transition of this unstable species is unknown. For comparison tetramethyl-2-tetrazene **19** has a rather large extinction coefficient λ_{max} = 280, $\varepsilon \simeq 14{,}000$.[58] The λ_{max} = 386 nm transition is assigned by spectral comparison to the known[2j] λ_{max} = 386 nm transition for trans HNNH **1**. The identity of the $\lambda_{max} \simeq 480$ nm transition is uncertain at this point. Warming the softened glass further to 95-100°K results in loss of the λ_{max} 386 and λ_{max} 480 nm transitions. Warming the now colorless solution to approximately 220°K results in vigorous gas evolution and formation of ammonium azide as an insoluble white precipitate. The parent tetrazene **25** has been shown to decompose to give hydrazine, ammonia, and ammonium azide as products.[35] These products together with N_2, H_2, and CO are obtained overall from photolysis of **15** to form **3** followed by thermolysis as described. Full product analysis from thermal decomposition of **3** will be reported in a later section. Similar thermal behavior is found for **3-d_2**. Other glass forming solvents gave similar results in the same temperature regimes (see Experimental).

Photochemical Decomposition of H_2NN

1,1-Diazenes have been reported to photodecompose when irradiated at their n-π* transition in the visible.[8g] Irradiation of a blue-violet glass of **3** in 2-MTHF at 80°K with visible light (VIS) using Corning CS-1-75 and

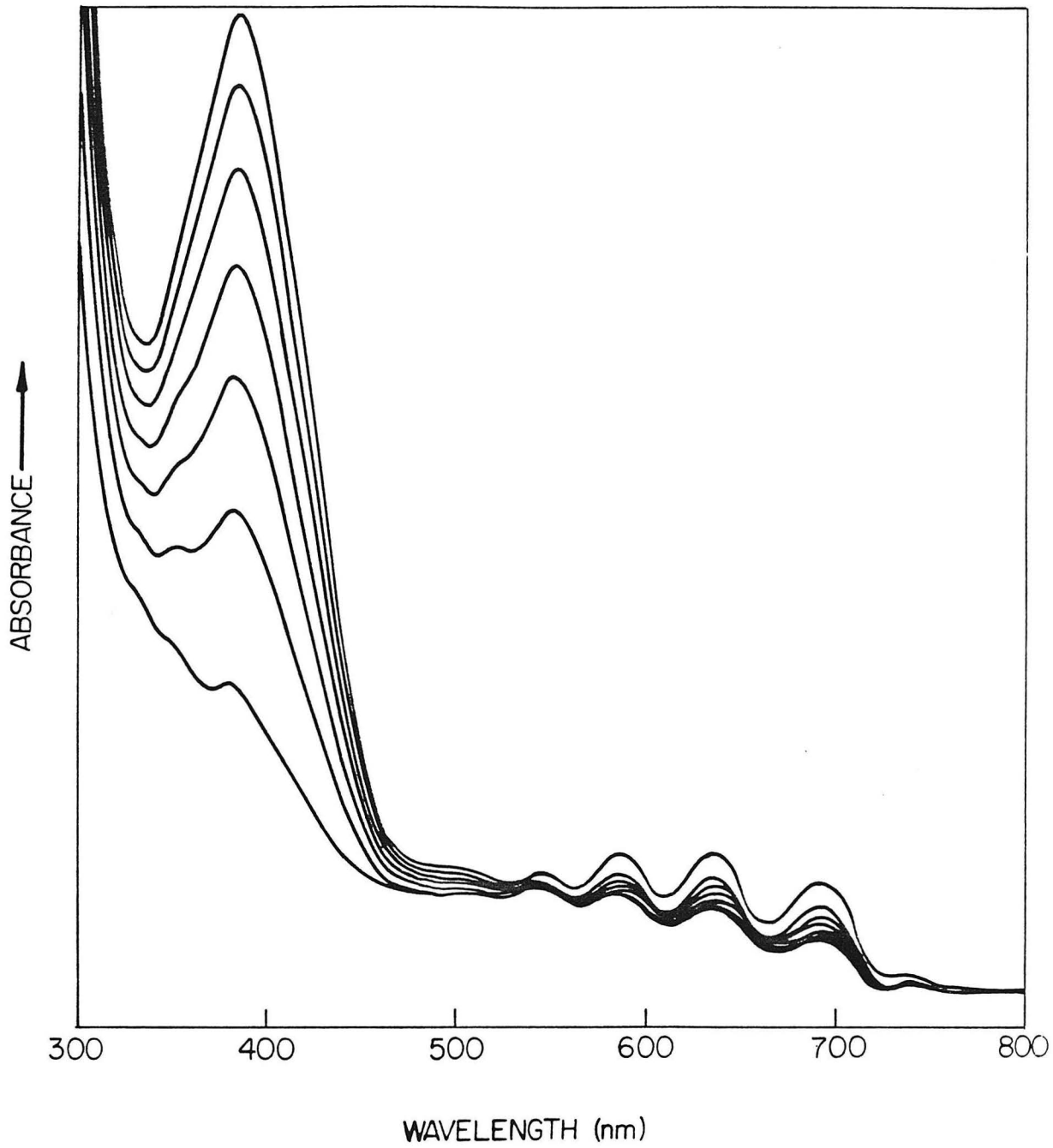

Figure 14. 2-MTHF glass of **3** warmed to 90°K. Spectra taken at 10 min intervals.

two CS-3-70 filters (λ >500 nm) results in loss of the blue-violet color and the structured absorbance curve of **3**, together with growth of the λ_{max} = 386 nm transition due to **1**. Likewise, irradiation of the λ_{max} = 386 nm and λ_{max} = 480 nm transitions obtained from thermolysis of **3** in softened 2-MTHF at 90°K, after recooling to 80°K with visible light from Corning filter CS-1-75 (λ >340 nm) results in the loss of these two transitions and the associated yellow-orange color. The major products from

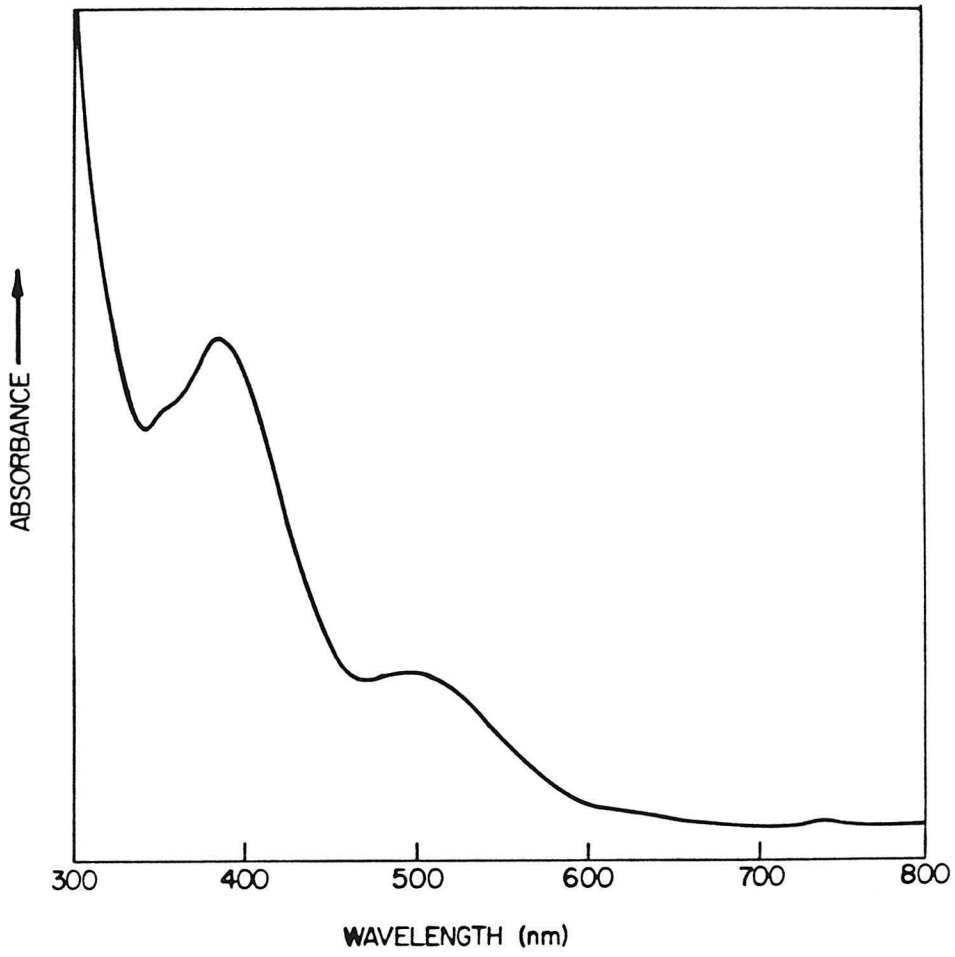

Figure 15. Absorption curve after warming 2-MTHF glass of **3** to 90°K for 2 h and recooling to 80°K showing λ_{max} = 386 and λ_{max} = 480 nm transitions.

photo-decomposition of **3** in a 2-MTHF glass at 80°K are H_2 and N_2. Similarly photolysis of the λ_{max} = 386 and 480 nm transitions affords H_2 and N_2 products. Full product analysis for photochemical and thermal decomposition of **3** will be reported in a later section.

One possible assignment for the λ_{max} = 480 nm transition may be the as yet uncharacterized cis HNNH isomer **2**. In general cis 1,2-diazenes are found to have longer wavelength, lower energy n-π* transitions than their trans 1,2-diazene isomers due to destabilizing lone pair-lone pair interactions.[7] Calculations (GTO-CI) of the electronic states of **1** and **2** suggest an energy difference of 0.56 eV (12.8 kcal/mol) for the n-π* transitions with the cis **2** n-π* at lower energy.[67] This energy difference would place the n-π* transition for **2** at 467 nm relative to 386 nm for trans

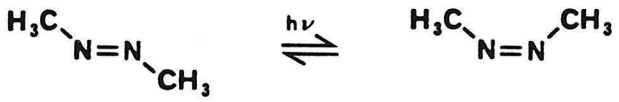

8t **8c**

λ_{max} (nm)	352	368
ΔE (kcal/mol)	81.4	77.8
ε	25	250

1. The molar extinction coefficient (ε) for a cis 1,2-diazene is typically an order of magnitude greater than in the trans isomer. Irradiation of 1,2-diazene n-π* transitions results in photointerconversion of cis and trans with quantum yields of 0.3 to 0.5. Higher pressures and longer wavelengths

generally decrease competitive decomposition pathways and increase isomerization yields. Direct irradiation of either isomer is considered to produce a common singlet excited state (S_1) which populates vibrationally excited cis and trans ground states ($S_0^{\ddagger}$) with nearly equal probabilities.[7] The hot ground states may then decompose or are deactivated by collision. Consistent with this interpretation, the use of shorter wavelength excitation would produce hot ground states with greater excess vibrational energy which would be expected to result in greater decomposition yields. This has been observed previously in some cases.[7]

Attempts to verify the assignment of the λ_{max} = 480 nm transition to **2** by photointerconverison of the λ_{max} = 386 nm transition of **1** and the λ_{max} = 480 nm transition are shown in Figure 16. The solid curve is that obtained after thermally decomposing **3** in softened 2-MTHF at 90°K followed by recooling to 80°K where 2-MTHF is again rigid (Figure 15). Irradiation of the λ_{max} = 480 nm transition with monochromatic light (470 ± 10 nm) for 3 h or broad-band irradiation (λ >470 nm) for 1 h results in decrease of the λ_{max} = 480 nm transition and slight growth of the λ_{max} = 386 nm transition of **1**. Photolysis of the λ_{max} = 386 nm transition with monochromatic light (380 ± 10 nm) results in loss of the λ_{max} = 386 nm transition and a very modest growth in the λ_{max} = 480 nm transition. Reversal of the order of photolysis results in similar behavior although the effect is less pronounced. No previous attempts at photoisomerization of **1** and **2** have been reported.[2] However, Craig has reported successful photoisomerization of neat $HNNCH_3$ in a low

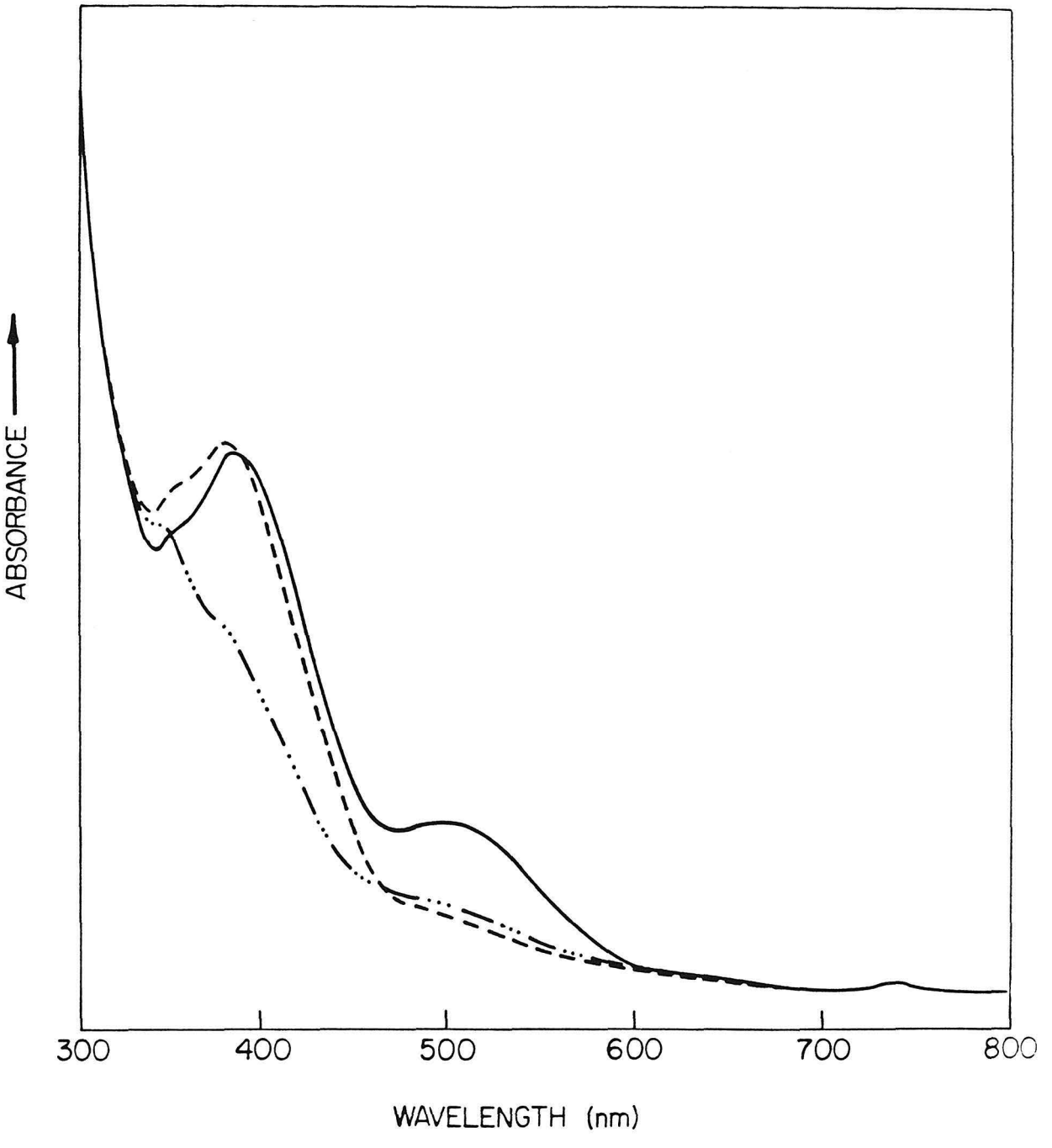

Figure 16. (a) Complete thermal decomposition of **3** at 90°K (2-MTHF) recooled to 80°K (——). (b) Photolysis (> 470 nm) 1 h, 80°K (---). (c) Photolysis (380 ± 10 nm) 2 h, 80°K (-···-).

temperature (77°K) polycrystalline matrix monitored by IR.[68] The very slight growth in the λ_{max} = 386 nm transition of **1** upon photolysis of the λ_{max} = 480 nm transition is consistent with photochemical conversion of cis **2** with a large molar extinction coefficient to trans **1** with a small molar extinction coefficient. Assuming ε for cis **2** is ten times ε trans **1**, the conversion of cis **2** to **1** is nearly quantitative. However, photolysis of the λ_{max} = 386 nm transition of **1** gives only a very slight increase in the λ_{max} = 480 nm transition amounting to only a few percent conversion of **1** to **2** with the assumed extinction coefficient ratio. Hence, these experiments must be regraded as very tentative and inconclusive. These observations may be consistent with vibrationally excited ground state cis **2** efficiently decomposing or alternatively may suggest a barrier for the excited state (S_1) collapsing to cis **2** which results in very inefficient cis production and greater decomposition yield from photolysis of **1**. Using the assumed extinction coefficient ratio, the initital ratio of **1** to **2** from thermolysis of **3** at 90°K is approximately 30:1 in favor of **1**. If this is representative of an equilibrium mixture, a free energy difference of 0.61 kcal/mol in favor of **1** is indicated. This is compared with a calculated difference of 4.7 kcal/mol in the heats of formation of **1** and **2**.[1t] All attempts to corroborate this tentative photochemical interconversion of **1** and **2** by Raman and Resonance Raman spectroscopy in a 2-MTHF glass at 77 K in the N=N double bond stretch region 1400-1700 cm^{-1} were unsuccessful. Any further attempts must overcome experimental difficulties such as efficient sample photolysis with laser excitation and excessive Rayleigh

scattering due to the sampling method. Since **1** has been characterized by Raman (ν N=N for **1** is 1529 cm^{-1}, N_2, 10°K) its assignment should be facilitated. The N=N stretch for **2** would be expected to lie at lower frequency as observed for cis and trans 1,2-dimethyl diazene.[89]

Emission Spectroscopy

For emission studies, concentrated ($\sim$0.1-0.5 M) samples of **3** were prepared by prolonged UV (VIS filtered) photolysis (14-24 h) of a 2-MTHF glass of **15** in a 5 mm OD quartz tube immersed in a liquid nitrogen cooled (77 K) Suprasil finger dewar. Irradiation of the intense blue-violet glass of **3** at its n-π^* transition (λ_{max} = 636 nm) with either monochromatic light (at various intense Hg emission lines, λ = 436, 546, 579 nm) or broad-band (λ = 480-650 nm) from a 250 watt mercury-xenon source gave no detectable emission from **3** at wavelengths 600 to 1100 nm. From the excited state studies[8g] of kinetically persistent 1,1-diazene **5** it was determined that the short lifetime (23 nanoseconds) of the n-π^* excited state S_1 was controlled by very fast internal conversion ($k_{IC} \simeq 10^8$ sec^{-1} for **5**) to ground state S_0. 1,1-Diazenes **4**[8g] and **6**[8f] were found to exhibit structureless fluorescence spectra (in contrast to a structured emission for **5**) consistent with efficient vibronic coupling in the pyramidal S_1 state for **4** and **6**. In the absence of vibrationally induced surface crossings and a low lying π,π^* triplet state, the rate of internal conversion should be determined by Franck-Condon overlap and therefore should be proportional to ΔE (state 1-state 2).[54,55] In 1,1-diazene **5** ΔE (S_1-S_0) is 50 kcal/mol and

k_{IC} is $\curvearrowright 10^8$ sec^{-1}.[8g] The quantum yield for fluorescence (ϕ_F) for **5** is 1×10^{-3}. In 1,1-diazene **6** ΔE (S_1-S_0) is 47 kcal/mol, $k_{IC} \geq 10^9$ sec^{-1} and ϕ_F is reduced to 1×10^{-4}.[8g] Energy gap considerations alone may account for the increased k_{IC} in **6**, which results in a diminished fluorescent lifetime ($\tau_F \leq 10^{-8}$ sec) and reduced ϕ_F. For comparison, in azulene ΔE (S_1-S_0) is 42 kcal/mol and k_{IC} is greater than 10^{12} sec^{-1}.[56] A rough estimate based upon energy gap considerations alone affords $k_{IC} > 10^{12}$ sec^{-1} for H_2NN **3** where ΔE (S_1-S_0) is 41.5 kcal/mol. Alternatively, the less rigid geometries of **4** and **6** may increase the contribution of vibronic coupling which could increase k_{IC}. The presence of high energy N-H stretches (2865, 2808 cm^{-1}) (see later section on infrared characterization) in **3** may result in efficient vibronic coupling and a reduced ϕ_F. Substitution of D for H in **3-d_2** could decrease vibronic coupling and slow k_{IC} resulting in an increased ϕ_F for **3-d_2** and measurable fluorescence. This effect has been demonstrated in the isoelectronic molecule formaldehyde (H_2CO).[57] In H_2CO substitution of D for H results in an increase in ϕ_F by a factor of $\curvearrowright 20$ in going from H_2CO to D_2CO. However, no emission was detected for **3-d_2** again indicative of a very low ϕ_F in **3**. Assuming $k_{IC} > 10^{12}$ sec^{-1} for **3** and $k_F \curvearrowright 10^5$ sec^{-1}, as found experimentally for 1,1- diazene **5**, affords a rough estimate of $\phi_F < 10^{-7}$ in **3**. This is consistent with no detectable emission for **3**.

Matrix Isolation Infrared Spectroscopy of H_2NN 3

For infrared studies of **3**, freshly sublimed carbomoyl azide **15** was cryo-pumped from a -20°C ice/salt bath and co-deposited with ultra high purity (UHP) argon onto a cesium iodide (CsI) inner window of the matrix isolation apparatus held at 20°K (see Experimental Section for details). The resulting argon matrix of **15** was slowly lowered to 10°K and its infrared spectrum recorded. Figure 17 shows the Fourier transform infrared (FT-IR) spectrum of **15** isolated in an argon matrix (~1:2000, Ar)[59] at 10°K. Table V lists the major FT-IR bands for **15** in Figure 17 and their assignments. Impurity peaks due to co-condensed atmospheric H_2O and CO_2 are noted. The stronger infrared bands are found to exhibit "extra" low intensity multiple bands possibly due to some site splitting, complexes with atmospheric impurities or the presence of multiple conformers. In general these "extra" bands were found to be of no consequence. Matrix ratios were adjusted to prevent the formation of hydrogen bonded "dimer" bands which are characteristically evident as lower energy multiple N-H stretch bands in the region 3400 to 3200 cm^{-1}. Achieving only two sharp N-H stretches at 3453.75 and 3572.60 cm^{-1} was indicative of a successful matrix for the desired photochemistry. Photolysis (2 h) of **15** matrix isolated in argon with UV light from two Corning CS-7-54 (UV transmitting, VIS λ = 400-680 nm cut-out) filters results in the loss of all bands due to **15** and formation of new product bands.[60] Using FT-IR subtraction programs[61] the FT-IR spectrum of **15** is subtracted from the FT-IR spectrum after UV photolysis of **15**. The resulting spectrum clearly shows the positive infrared

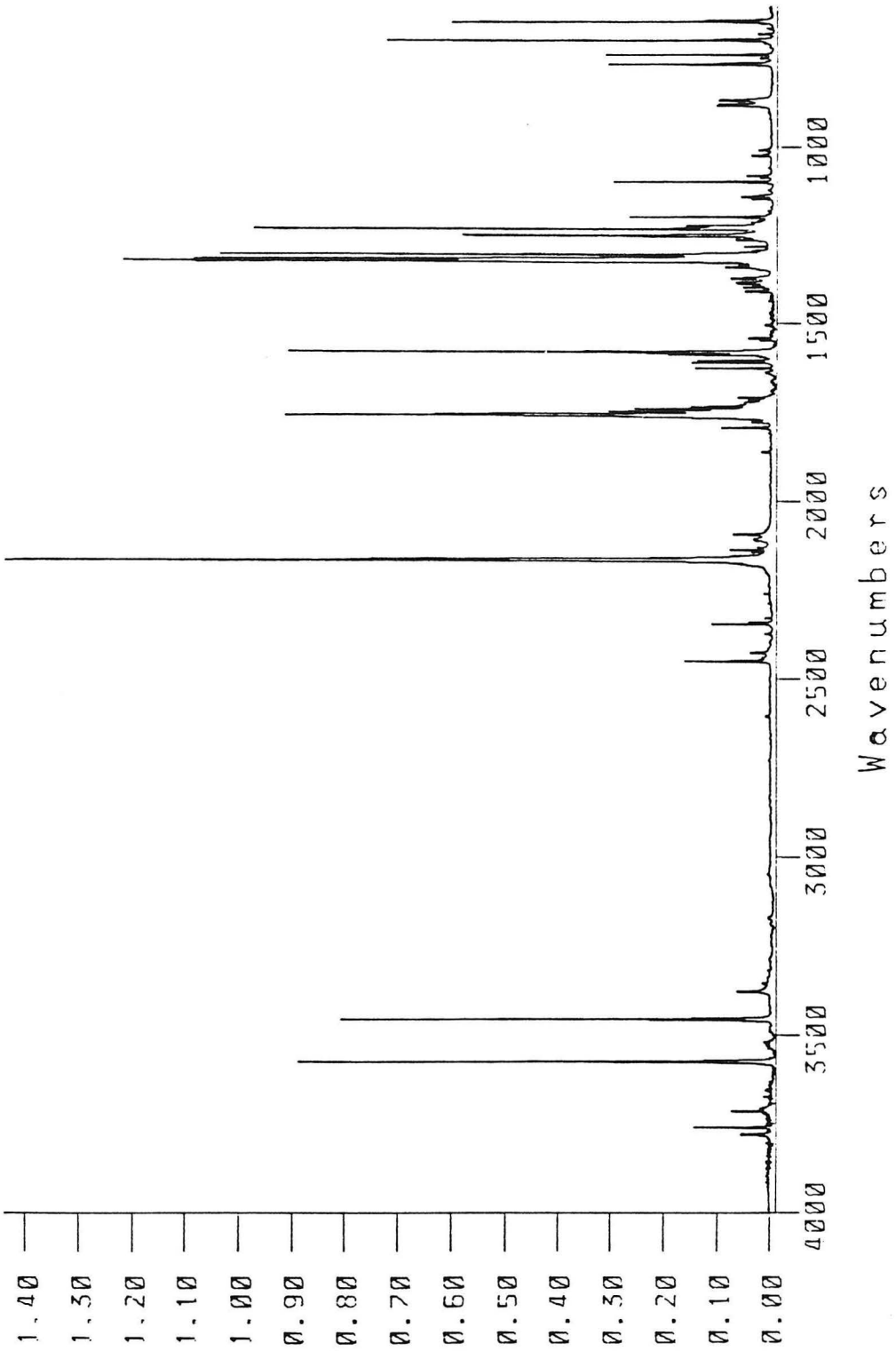

Figure 17. FT-IR spectrum of **15**, 120 mm deposition @1:2000, Ar, 10°K).

Table V. FT-IR Bands for **15** in an Argon Matrix (1:2000, 10°K) Threshold = 0.05 A.

Peak Location (cm^{-1})	Intensity (A)	Assignment
3776.05	0.05	H_2O, ν OH
3756.29	0.14	H_2O, ν OH
3711.21	0.08	H_2O, ν OH
3572.59	0.89	ν N-H
3569.70	0.12	
3453.75	0.81	ν N-H
3451.10	0.15	
3376.37	0.06	ν NH (dimer)
2448.50	0.16	overtone
2345.09	0.11	CO_2, ν CO
2339.06	0.04	CO_2, ν CO
2175.38	0.06	
2164.53	1.44	ν N_3 (asym)
2160.91	0.66	
2157.54	0.23	
2152.96	0.07	
2135.36	0.08	
2092.21	0.07	overtone
1791.84	0.09	overtone
1764.60	0.15	
1761.95	0.28	
1757.37	0.91	ν CO
1754.48	0.63	
1746.76	0.30	
1738.81	0.26	
1733.50	0.15	
1706.26	0.06	
1623.58	0.15	H_2O, δ O-H

Table V. Continued

Peak Location (cm^{-1})	Intensity (A)	Assignment
1607.91	0.15	H_2O, δ O-H
1602.36	0.14	
1586.21	0.20	
1583.80	0.10	
1578.98	0.92	δ $-NH_2$
1576.09	0.35	
1385.65	0.06	
1382.99	0.06	
1370.22	0.08	
1339.36	0.09	
1335.02	0.06	
1323.21	1.08	
1320.80	1.22	ν NCO (sym)
1315.25	1.09	
1302.96	1.04	
1250.89	0.56	
1248.24	0.58	
1243.18	0.06	
1230.88	0.97	ν N_3 (sym)
1227.26	0.15	
1221.72	0.16	
1197.13	0.26	
1098.05	0.30	ρ NH_2
881.34	0.10	ν C-N_3
878.93	0.10	
866.39	0.10	
763.94	0.31	
761.04	0.07	δ N_3
737.18	0.32	N_3
695.47	0.73	NCN
642.20	0.60	NCN

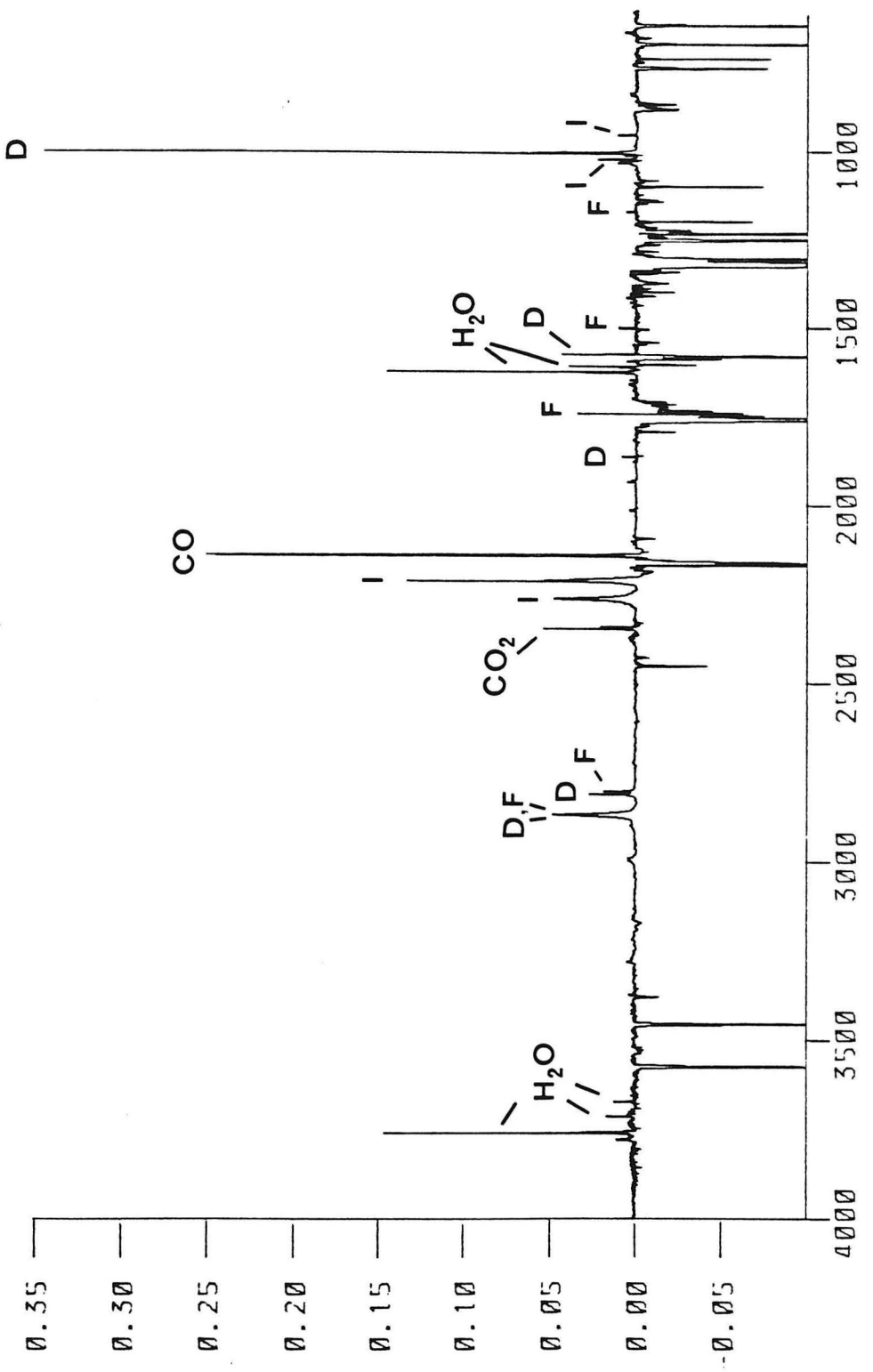

Figure 18. Difference FT-IR spectrum of products from UV (VIS filtered) photolysis (2h) of **15** (1:2000, Ar, 10°K) minus FT-IR spectrum of **15**. Subtraction factor $\alpha = 0.6$, (D) = H_2NN **3**, (F) = H_2CO, (I) = H_2N-N=C=O.

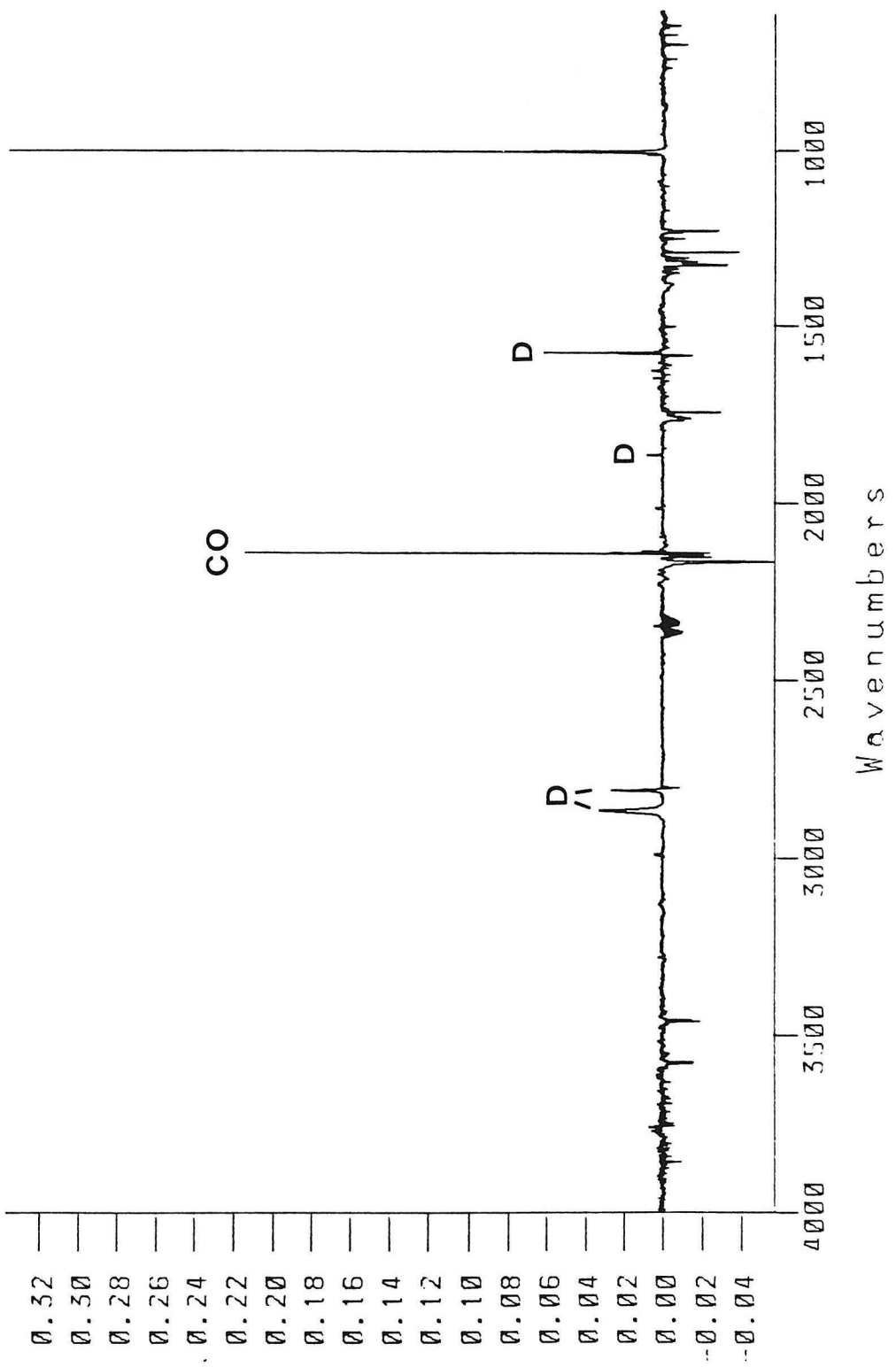

Figure 19. Difference FT-IR spectrum of H_2NN **3** (D) and CO. UV (VIS filtered) photolysis (2h) of **15** (1:2000, Ar, 10°K) minus spectrum after VIS (>500 nm) photolysis (2 h) of **3**. Subtraction factor $\alpha = 1.05$.

absorption bands due to products from photolysis of **15** together with atmospheric impurities H_2O and CO_2 (Figure 18). These bands are divided into four groups and are assigned based on their photochemical and thermal behavior together with isotopic shifts. These assignments are summarized in Table VI.

The first group of bands at 3277.53, 2989.46, 2259.03, 2212.02, 2207.68, 1021.15, 952.69, 868.08, 864.70 cm^{-1} grow in quickly with UV photolysis of **15** and decrease with prolonged UV irradiation. These are assigned to the photochemical intermediate aminoisocyanate (labeled (I) in Table VI) expected to result from the photo-Curtius rearrangement of **15**. The most intense band at 2212.02 cm^{-1} is very likely the characteristic N=C=O asymmetric stretch for aminoisocyanate.

A second group of product bands at 2865.55, 2807.20, 2140.90, 1863.20, 1574.16, and 1003.07 cm^{-1} also grow in with prolonged UV (VIS filtered) photolysis of **15** and are efficiently photolyzed away with visible irradiation at 10°K using Corning CS-1-75 and two CS-3-70 filters (> 500 nm). Recall that this filter combination resulted in decolorization of the blue-violet 2-MTHF glass of **3** and its structured n-π^* absorption curve. Subtraction of the spectrum resulting from visible light (VIS) photolysis ($\lambda > 500$ nm) from the spectrum before VIS photolysis results in positive absorption bands assigned to H_2NN **3** (labeled (D) in Table VI) (Figure 19). The bands assigned to aminoisocyanate are not affected by VIS photolysis of **3**. The band at 2140.90 is assigned to carbon monoxide (CO) resulting from photolysis of the intermediate aminoisocyanate. Curiously,

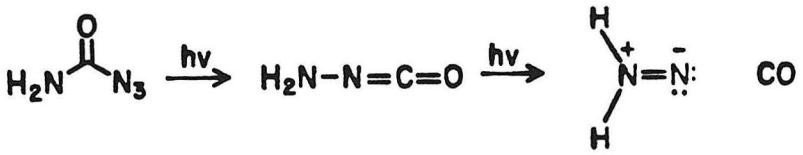

15 3

this CO band at 2140.90 cm^{-1} shows the same photochemical behavior as the group of bands assigned to H_2NN **3.** This will be addressed more fully in a later section.

Two other groups of bands resulting form UV photolysis of **15** are observed to increase with the VIS photolysis of **3.** One group of bands at 2139.94, 2137.22, and 2137.53 are also assigned to CO. The unique behavior of these CO bands suggest that they may be somehow related to the products from VIS photolysis of **3.** This will be addressed in a later section. A final set of bands at 2865.55, 2800.22, 1741.70, 1498.71, 1227.03, and 1168.45 cm^{-1} also increase in intensity with UV photolysis of **15.** Surprisingly, these bands also increase with VIS photolysis of H_2NN **3.** Based on their photochemical behavior, their isotopic shifts and spectral comparison, these bands are assigned to formaldehyde (H_2CO) (labeled (F) in Table VI) an unexpected

photolysis product. This will be addressed more fully in a later section. For comparison, literature[62] values for the infrared spectral assignment of H_2CO (1:800) in an argon matrix at 10°K are 2863, 2797, 1742, 1498, 1245, and 1168 (±1) cm^{-1}. All bands except the 1227.03 cm^{-1} (1245 cm^{-1}) band are within experimental error. This band, assigned to the δ CH_2 rocking mode of H_2CO, has been observed to shift to higher frequency in a hydrogen bonding environment. For example, forming the dimer of formaldehyde $(H_2CO)_2$ matrix isolated in argon shifts this mode from 1245 to 1251 cm^{-1}.[62b] This mode is found at 1239 cm^{-1} for H_2CO monomer in a nitrogen matrix.[62b]

Of the infrared bands assigned to **3** (Figure 19) the band at 1574.16 cm^{-1} is in the region where one would expect to find the characteristic N=N double bond stretch of H_2NN. For the kinetically persistent 1,1-diazenes **4** and **5** in CH_2Cl_2 solution, this characteristic N=N stretch is found 1595 and 1638 cm^{-1}, respectively.[8e] In order to assign these bands as the N=N double bond stretch, the terminal ^{15}N labeled 1,1-diazenes were prepared. Incorporation of the ^{15}N label results in the predicted Hooke's law shift of the $^{14}N=^{15}N$ stretch to lower energy. For kinetically persistent 1,1-diazene **4** the experimental $^{14}N=^{15}N$ double bond stretch was found at 1568 cm^{-1}.[8e] This 27 cm^{-1} shift to lower energy was identical to the Hooke's law calculated shift. In order to verify the 1574.16 cm^{-1} band observed in the FT-IR spectrum of **3** as the characteristic N=N double bond stretch for this species, a ^{15}N terminal label was desired. The Hooke's law calculated ratio ν ($^{14}N=^{14}N$)/$^{14}N=^{15}N$) is 1.0171 or a predicted shift for the $^{14}N=^{15}N$ stretch

from 1574.16 to 1547.69 cm^{-1} in **3**. Stirring carbomoyl azide **15** with an excess of (1-^{15}N) labeled sodium azide[63] in dry acetonitrile afforded **15-^{15}N**. The combination of ^{15}N NMR, high resolution mass spectroscopy and FT-IR spectroscopy demonstrates a statistical incorporation of ^{15}N into **15-^{15}N** by azide exchange in solution. Due to the symmetry of the azide anion

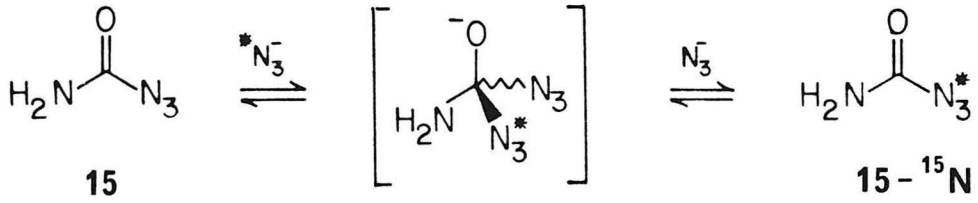

15 **15 - ^{15}N**

$$^{*}N_3^- = \left[^{15}N{=}N{=}N\right]^-$$

in solution[64] the ^{15}N label should be equally distributed between the two terminal positions of the azide moiety. Four equivalents of (1-^{15}N) sodium azide results in an approximately 80:20 mixture of **15-^{15}N:15** by mass spectroscopy. ^{15}N-NMR reveals two singlets at -140.10 and -262.32 ppm from ^{15}N-CH_3NO_2. Matrix isolation of **15-^{15}N** in argon (ca 1:2000) at 10°K (Figure 20, Table VII) reveals that the unlabeled asymmetric azide stretch at 2164.53 cm^{-1} has ^{15}N shifted multiple bands at 2159.23 cm^{-1} and 2141.15 cm^{-1} in an approximate 1:1 ratio consistent with the ^{15}N label equally distributed between the two terminal positions of the azide moiety. Photolysis of an 80:20 mixture of **15-^{15}N:15** would be expected to yield a 60:40 mixture of H_2NN **3** to $H_2N^{15}N$ **3-^{15}N** by the photo-Curtius

Table VI. Infrared Assignments for Products from Photolysis of **15** and **15-^{15}N** (~1:2000, Ar, 10°K).

120 min hν UV (VIS filtered)	120 min hν VIS (λ > 500 nm)	100 min hν VIS (λ = 360-420 nm)	Assignment
3776.05			h, νOH
3756.53			h, νOH
3710.96			h, νOH
3669.74			h, νOH
3277.53			(I), νNH
2989.46			(I), νNH
2865.55	(-)		D, νNH
2865.55	(+)	(+)	F, νC-H
2807.20	(-)		D, νNH
2800.22	(+)	(+)	F, νC-H
2345.09			CO_2, νCO
2339.06			CO_2, νCO
2259.03			I, ν^{14}N=C=O
2238.78			I*, ν^{15}N=C=O
2212.02			I, ν^{14}N=C=O (asym)
2207.68			I, ν^{14}N=C=O
2194.18			I*, ν^{15}N=C=O
	2149.82	(-)	CO/T, νCO
	2143.32	(-)	CO/T, νCO
2140.90	(-)		CO/D, νCO
2139.94	(+)	(+)	CO, νCO
2137.22			CO, νCO
2137.53	(+)	(+)	CO, νCO
1863.20	(-)		D, δN-H
1741.70	(+)	(+)	F, νC=O
1623.58			h, δO-H
1610.08			h, δO-H
1607.67			h, δO-H
1592.96			h, δO-H

Table VI. Continued.

120 min hν UV (VIS filtered)	120 min hν VIS (λ >500 nm)	100 min hν VIS (λ= 360-420 nm)	Assignment
1574.16	(-)		D, ν $^{14}N=^{14}N$
1547.64	(-)		D*, ν $^{14}N=^{15}N$
1498.71			F, δ CH_2
	1288.01	(-)	T, δ N=N-H (asym)
	1286.81	(-)	T*, δ $^{15}N=N-H$
1227.03	(+)	(+)	F, δ CH_2
	1218.83		(?)
1168.45	(+)	(+)	F, δ CH_2
1146.03			(I)
1030.32			(I)
1021.15			(I)
1003.07	(-)		D, δ $^{14}N=^{14}N-H$
1002.35	(-)		D*, δ $^{15}N=^{14}N-H$
952.69			(I)
868.08			(I)
864.70			(I)

h = H_2O
I = Aminoisocyanate ($H_2N-N=C=O$), I* = ($I-^{15}N$)
D = Diazene (H_2NN), D* = ($D-^{15}N$)
F = Formaldehyde (H_2CO)
T = Trans-1,2-diazene (HNNH), T* = ($T-^{15}N$)
CO = Carbon monoxide
(-) = Decreased
(+) = Increased
( ) = Tentative assignment

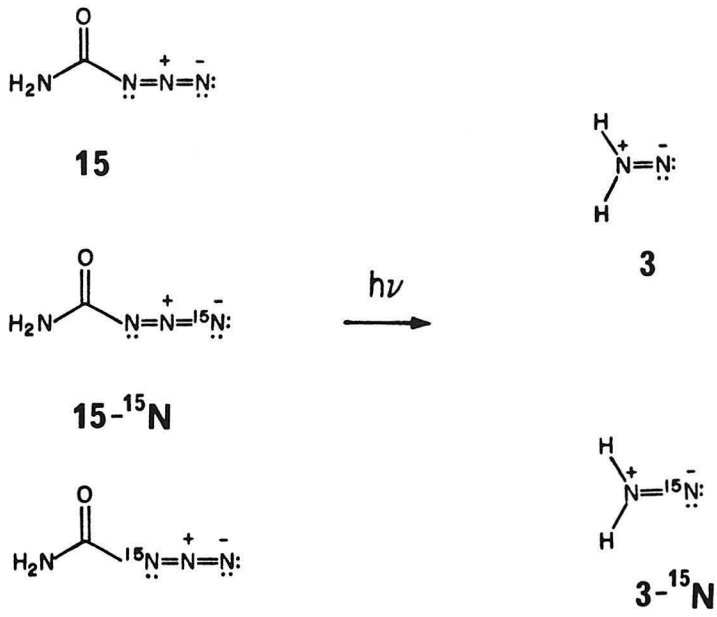

rearrangement and subsequent photolysis of the intermediate amino-isocyanate.

Photolysis of matrix isolated **15-^{15}N** (1:2000, Ar, 10°K) (Figure 20, Table VII) with two CS-7-54 filters for 2 h results in decrease in the FT-IR bands of **15-^{15}N** and formation of product bands. Figure 21 shows the product FT-IR spectrum minus the FT-IR spectrum of **15-^{15}N.** These bands are summarized in the first column of Table VI. In addition to the product bands reported from the UV photolysis of **15,** additional ^{15}N isotope shifted bands are found at 2238.78, 2194.18, 1547.64, and 1002.35 cm^{-1}. These correspond in intensity (based on ^{15}N incorporation into **15-^{15}N**) to ^{15}N shifted bands of product infrared bands at 2259.03, 2212.02, 1547.16, and 1003.07 cm^{-1}, respectively, observed from UV photolysis of **15.** The new band at 1547.64 cm^{-1} corresponds to the calculated 1547.69 cm^{-1} $\nu^{14}N=^{15}N$ stretch for **3-^{15}N** (Figure 23). Comparison with the Raman active ν $^{14}N=^{14}N$ stretch for HNNH **1** at 1529 cm^{-1} [2f] demonstrates the

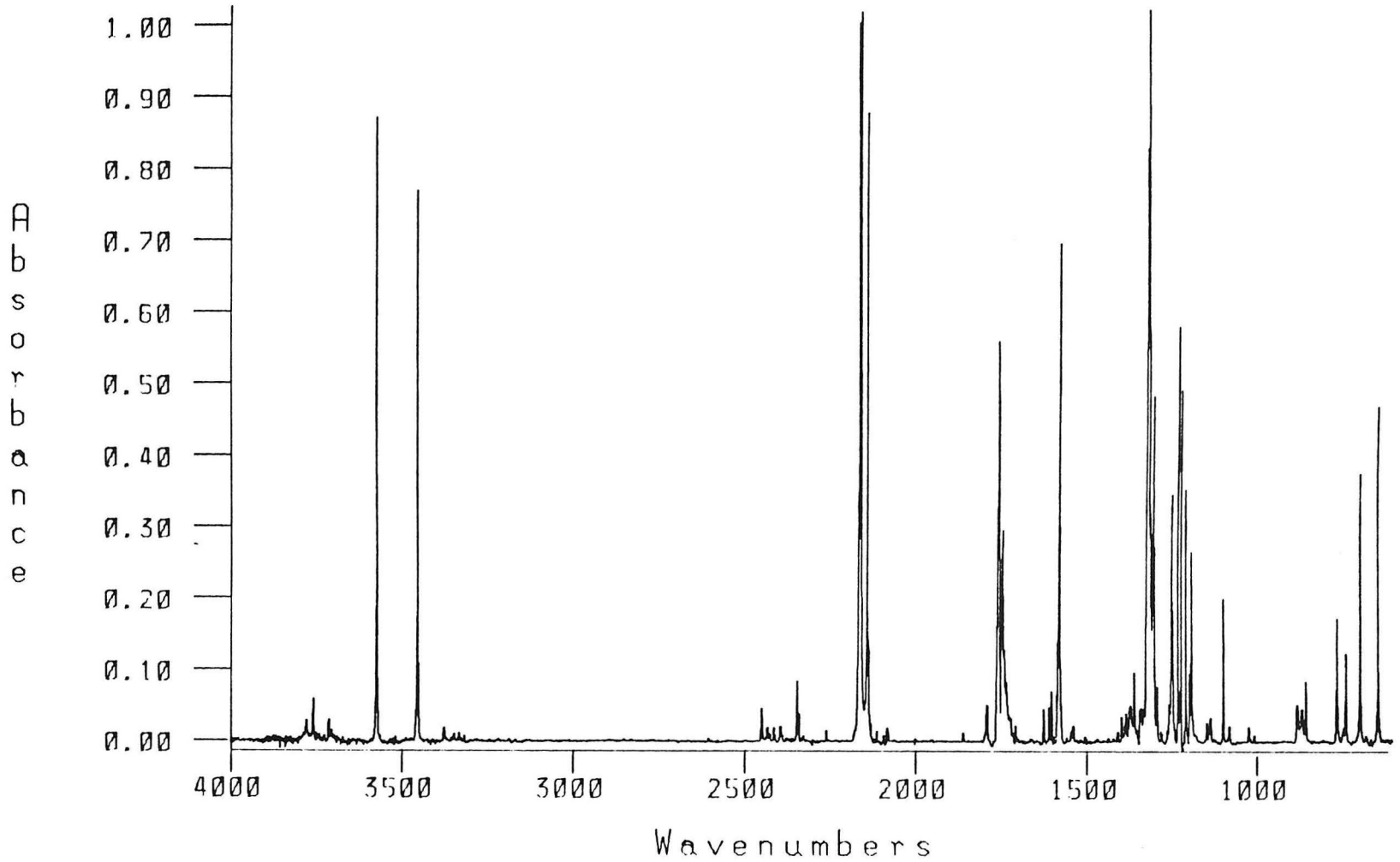

Figure 20. FT-IR spectrum of **15-^{15}N:15** (~80:20 mixture), 120 mm deposition (1:2000, Ar, 10°K).

Table VII. FT-IR Bands for **15-^{15}N** in an Argon Matrix (1:2000, 10°K) Threshold = 0.05 A.

Peak Location (cm^{-1})	Intensity (A)	Assignment
3711.21	0.02	H_2O, ν OH
3572.59	0.88	ν NH
3569.70	0.09	
3453.75	0.77	ν NH
3451.10	0.11	
2448.02	0.05	overtone
2345.09	0.09	CO_2, ν CO
2339.06	0.05	CO_2, ν CO
2164.53	1.02	ν -^{14}N=^{14}N=^{14}N (asym)
2159.22	1.04	ν -^{15}N=^{14}N=^{14}N (asym)
2155.61	0.20	
2152.96	0.09	
2151.03	0.07	
2146.93	0.06	
2141.14	1.01	ν ^{14}N=^{14}N=^{15}N (asym)
2138.01	0.14	
2136.56	0.16	
2135.36	0.14	
1761.47	0.20	
1757.70	0.61	ν C=O
1755.20	0.55	
1744.83	0.26	
1739.77	0.10	
1738.57	0.10	
1623.58	0.06	H_2O, δ OH
1607.91	0.06	H_2O, δ OH
1602.36	0.09	H_2O, δ OH
1586.21	0.08	
1583.80	0.15	
1578.98	0.71	δ NH_2
1572.95	0.06	
1359.37	0.08	

Table VII. Continued.

Peak Location (cm^{-1})	Intensity (A)	Assignment
1321.52	0.82	
1315.25	1.016	ν NCO (sym)
1311.40	0.311	
1309.50	0.289	
1302.92	0.48	
1299.83	0.27	
1248.00	0.35	
1230.88	0.60	ν N_3 (sym)
1221.96	0.60	ν $^{15}N{=}N{=}N$ (sym)
1208.22	0.40	ν $N{=}N{=}^{15}N$ (sym)
1196.89	0.10	ν $N{=}N{=}^{15}N$ (sym)
1193.03	0.11	ν $N{=}N{=}^{15}N$ (sym)
1191.35	0.28	
1098.05	0.20	ρ NH_2
881.34	0.05	ν C-N_3
878.93	0.05	
855.06	0.08	
763.96	0.18	δ N_3
736.94	0.13	δ N_3
735.97	0.13	
695.23	0.34	δ NCN
693.55	0.38	δ NCN^{15}
641.96	0.47	δ $N^{15}CN$

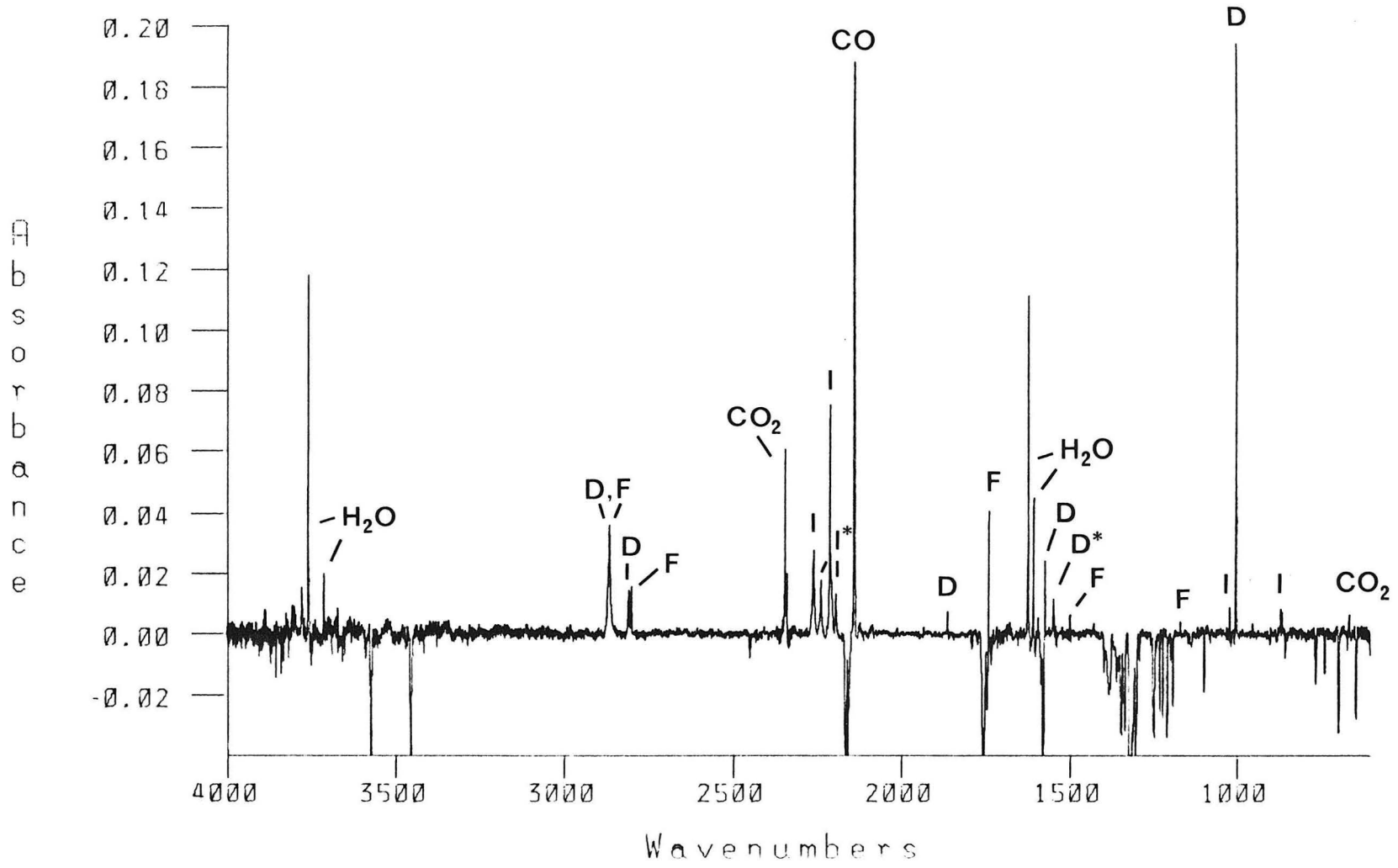

Figure 21. Difference FT-IR spectrum of products from UV (VIS filtered) photolysis (2 h) of **15-^{15}N:15** (1:2000, Ar, 10°K) minus FT-IR spectrum of **15-^{15}N:15.** Subtraction factor = 0.6, (D) = H_2NN **3**, (D*) = H_2N-^{15}N, (F) = H_2CO, (I) = H_2N-N=C=O, (I*) = H_2N-^{15}N=C=O.

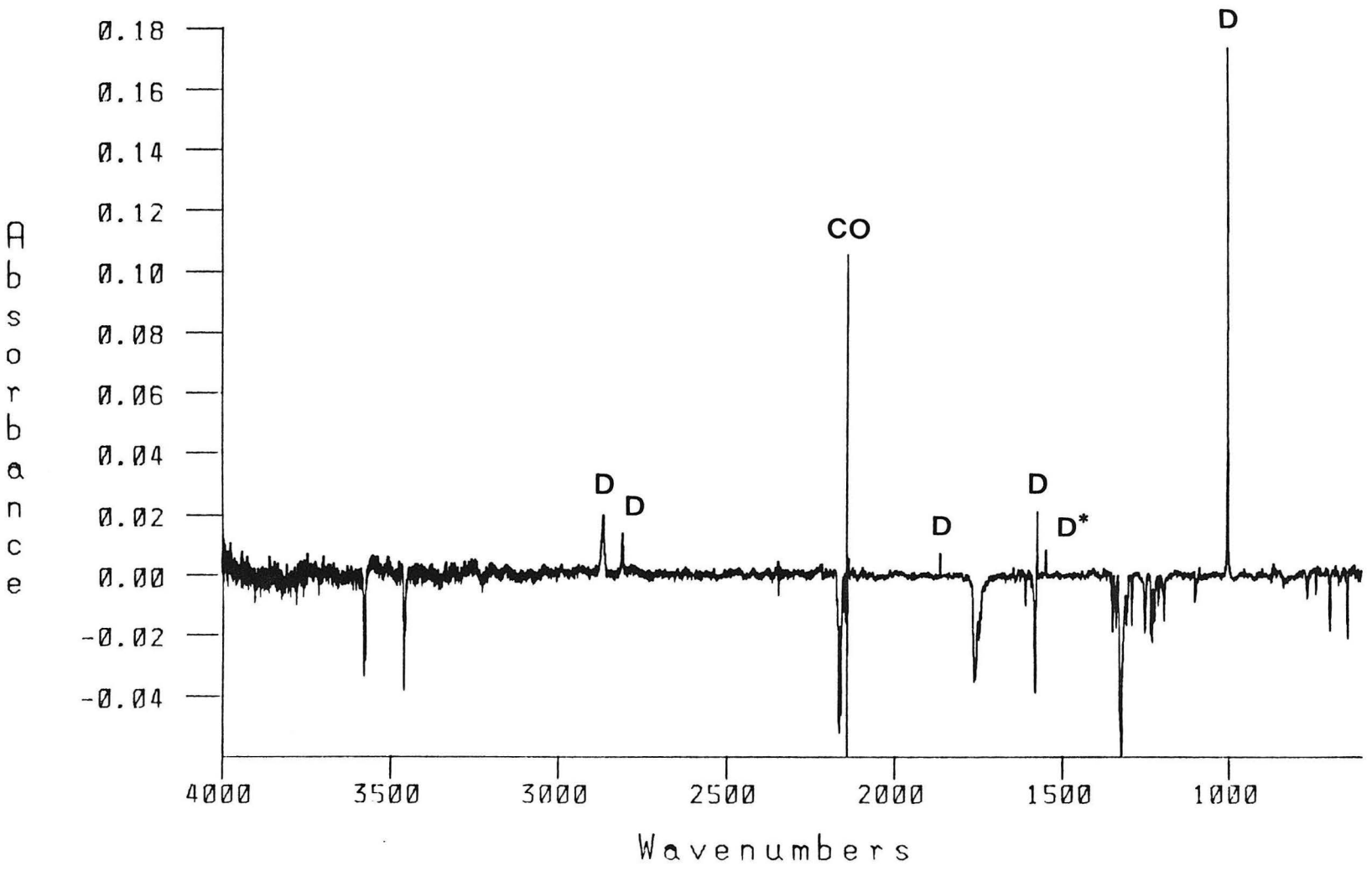

Figure 22. Difference FT-IR spectrum of H_2NN **3** (D): H_2N-^{15}N **3**-^{15}N (D*) mixture and CO. UV (VIS filtered) photolysis (2 h) of **15**-^{15}N:**15** (1:2000, Ar, 10°K) minus spectrum after VIS (>500 nm) photolysis (2 h) of **3**:**3**-^{15}N. Subtraction factor $\alpha = 1.10$.

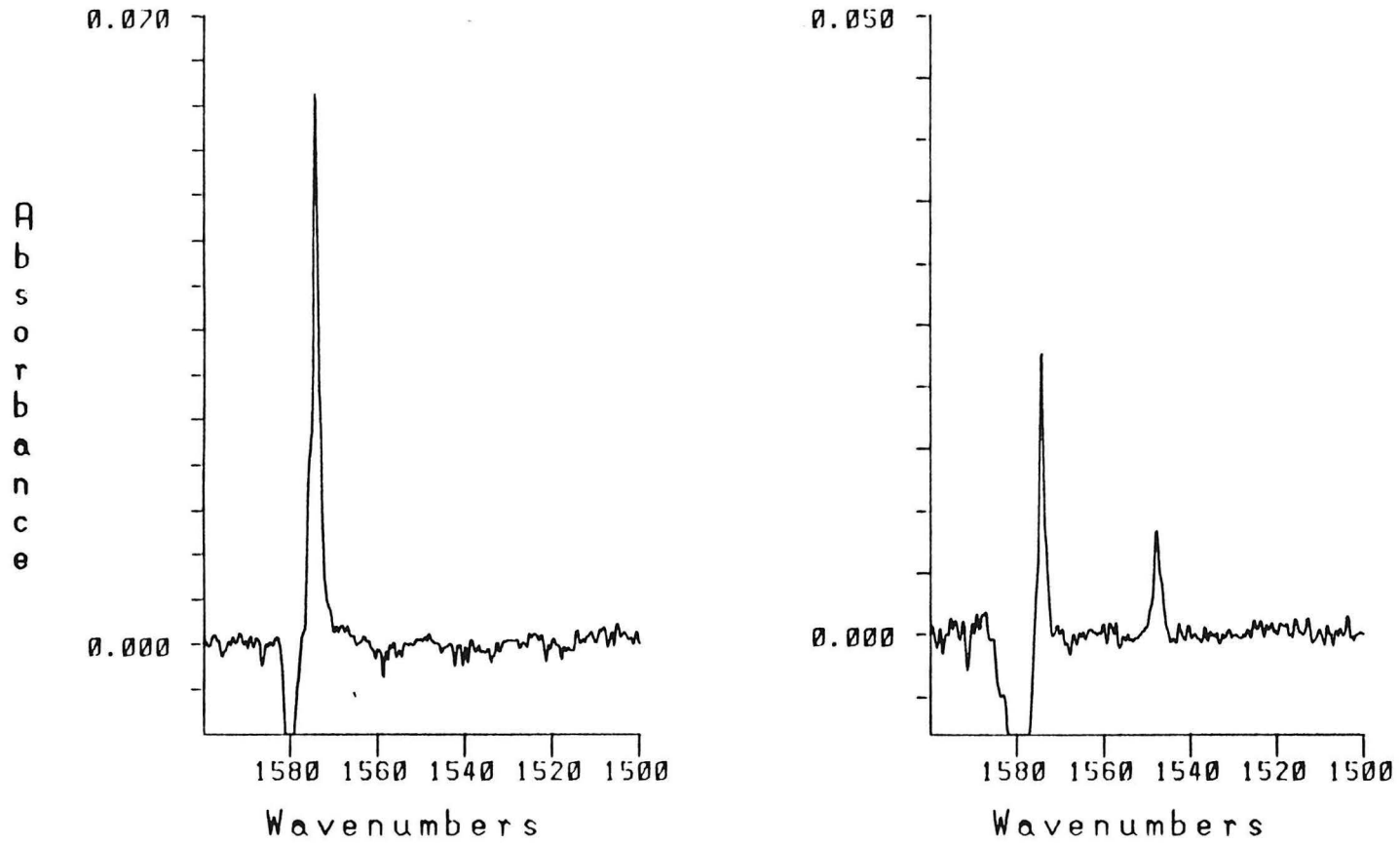

Figure 23. (a) H_2 $^{14}N=^{14}N$ stretch of **3** from Figure 19. (b) H_2 $^{14}N=^{14}N$ stretch of **3** and H_2 $^{14}N=^{15}N$ stretch of **3-^{15}N** from Figure 22.

substantial double bond character in the 1,1-diazene N=N bond in accord with the calculation of Davis and Goddard.[1n]

Photolysis of the products from UV (VIS filtered) photolysis of **15-^{15}N** with visible light (> 500 nm) results only in the loss of all bands assigned to **3-^{15}N** and **3** and the accompanying CO stretch at 2140.90. Figure 22 shows the difference FT-IR spectrum for before minus after VIS photolysis of the **3-^{15}N, 3** mixture. Table VIII summarizes the infrared bands assigned to **3** and **3-^{15}N.** The strongest FT-IR band of **3** at 1003.07 cm^{-1} is also affected by the incorporation of a ^{15}N label. This band is likely assigned to the in plane asymmetric bending mode of **3.** This band shows a small ^{15}N isotope shift of 0.72 cm^{-1} to 1002.35 cm^{-1}. For comparison, the asymmetric in plane bend is also the strongest infrared band observed for HNNH **1** at 1286 cm^{-1}.[2c] This mode also shows the small ^{15}N isotope shift expected for a bending mode from 1285.8 to 1284.3 cm^{-1} (a shift of 1.3 cm^{-1}). The infrared band at 1863.20 cm^{-1} observed for **3-^{15}N** shows no resolvable (0.25 cm^{-1} resolution) ^{15}N shift. This band is therefore likely assigned to the out of plane torsional mode for **3.** The N-H stretching modes at 2865.55 and 2807.20 cm^{-1} are also unaffected by a terminal ^{15}N label in **3-^{15}N** consistent with their assignments. Due to its C_{2V} symmetry H_2NN should exhibit six vibrational modes all of which should be both infrared and Raman active. Five of these six modes have been located in the argon matrix FT-IR spectrum described. The sixth mode is presumably obscured by other infrared bands. Conclusive assignment of the vibrational modes of **3** must await full Raman characterization and polarization studies.

Table VIII. Infrared Bands for H_2NN **3** and $H_2N^{15}N$ **3-^{15}N** (Ar, 10°K).

(cm^{-1})	Assignment
2865.55	ν N-H
2807.20	ν N-H
1863.20	δ =N-H (out of plane)
1574.16	ν $^{14}N=^{14}N$
1547.64	ν $^{14}N=^{15}N$
1003.07	δ $^{14}N=^{14}N$-H (in plane)
1002.35	δ $^{15}N=^{14}N$-H (in plane)

( ) = Tentative assignment

The remaining ^{15}N isotope shifted product bands observed from UV photolysis of **15-^{15}N** at 2238.78 and 2194.18 cm^{-1} are assigned, due to the magnitude of their shift and their relative intensities, to ν-^{15}N=C=O the ^{15}N isotope shifted isocyanate stretching modes (ν -^{14}N=C=O) of aminoisocyanate (labeled (I*) in Table VI) at 2259.03 and 2212.02 cm^{-1}. All of these bands are observed to grow in quickly with UV photolysis and decrease in intensity with prolonged UV photolysis.

Photolysis of H_2NN **3** with visible light (VIS) ($\lambda > 500$ nm) results in loss of all bands assigned to **3** and formation of new bands 2149.82, 2143.32, 1288.01, and 1218.83 cm^{-1}. In addition, VIS photolysis of **3** results in the growth of bands assigned to formaldehyde

(H_2CO) at 2865.55, 2800.22, 1741.70, 1498.71, 1227.03, and 1168.45 cm^{-1} and growth of two CO bands at 2139.94 and 2137.22 cm^{-1}. The CO bands will be discussed in a later section. Photolysis of **3**-^{15}N with visible light results in formation and growth of the same product bands observed in the photolysis of **3** together with formation of a single ^{15}N isotope shifted band at 1286.81 cm^{-1} (see second column of Table VI). VIS irradiation (> 500 nm) of **3** in a rigid 2-MTHF glass at 80°K resulted in the growth of an electronic absorption at 386 nm assigned by spectral comparison to the known electronic absorption of <u>trans</u> HNNH **1** at 386 nm. The infrared band at 1288.01 cm^{-1} and its ^{15}N shifted multiple at 1286.81 cm^{-1} (a shift of 1.20 cm^{-1}) correspond to the strongest infrared transition reported by Rosengren and Pimentel[2c] for **1** at 1285.8 ± 0.3 cm^{-1} in a nitrogen matrix. The incorporation of a single ^{15}N isotope into **1** was found by Pimentel to result in a ^{15}N shift of 1.3 cm^{-1} to 1284.5 ± 0.3 cm^{-1}. For direct comparison, **3** was matrix isolated in N_2 (1:2000, 10°K).[65] VIS photolysis (> 500 nm) results in formation of the corresponding band for **1** at

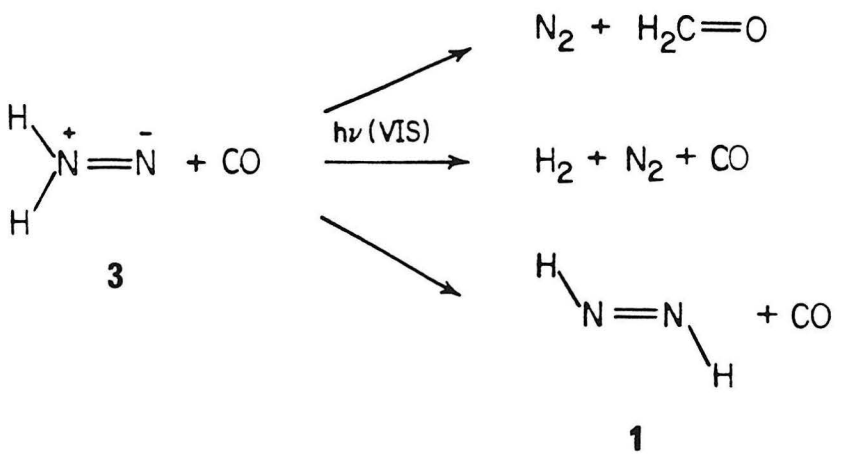

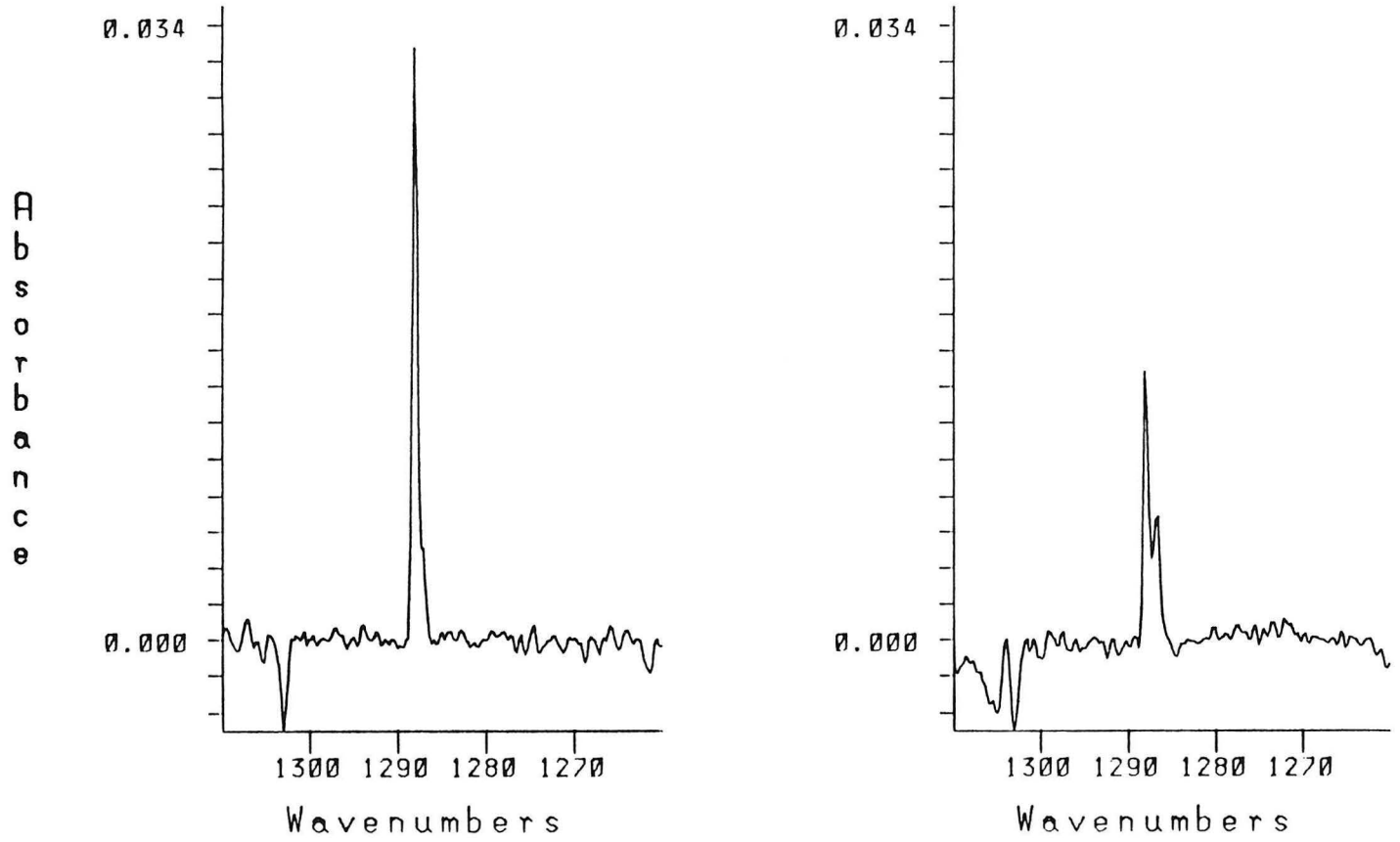

Figure 24. (a) Difference FT-IR spectrum of HNNH **1** from VIS photolysis of **3** (2 h, Ar, 10°K). Before minus after photolysis of **1** (360-420 nm), 100 min. (b) Difference FT-IR spectrum of HNNH **1** and **1**-^{15}N from VIS photolysis of **3**:**3**-^{15}N (2 h, Ar, 10°K). Before minus after photolysis of **1**; **1**-^{15}N (360-420 nm), 100 min.

1286.02 cm^{-1} in agreement with the 1285.8 ± 0.3 cm^{-1} band reported by Rosengren and Pimentel.[2c] All attempts to locate the other reported infrared band for **1** at 3131 cm^{-1} (N_2 matrix, very weak, broad, ν N-H) have been unsuccessful. This may be attributed to a low yield of **1** from VIS photolysis of **3** (estimated at ≤10%). Photolysis of trans HNNH **1** could be effected with either monochromatic light (380 ± 10 nm) or more efficiently with Corning CS-5-58 and CS-7-51 filters (λ = 360-410 nm, 2-3h) (see Figure 24). In addition to loss of the 1288.01 cm^{-1} band (Ar) (and the 1286.81 ^{15}N multiple with **1-^{15}N**) two CO stretches at 2149.82 and 2143.32 cm^{-1} are also lost with photolysis of **1**. This will be discussed in more detail in a later section. Photolysis of **1** (λ = 360-410 nm) results in growth of absorbances due to H_2CO and two CO bands at 2139.94 and 2137.53 cm^{-1}. Identical behavior was found with VIS photolysis of **3**. The third column of Table VI summarizes the effects of photolysis of **1** and **1-^{15}N**. None of the tentative cis HNNH **2** bands reported by Rosengren an Pimentel[2c] at 1279 and 3074 cm^{-1} were observed in the photolysis of **1** with either broad-band (λ = 360-410 nm) or monochromatic (λ = 380 ± 10 nm) light (Ar or N_2, 10°K). The identity of one last minor product band from photolysis of **3** and **3-^{15}N** at 1218.83 cm^{-1} remains uncertain.

In order to further support the infrared assignments for **3**, **1**, and their photochemical decomposition products, **3-d_2** and **3-d_2-^{15}N** were also prepared. Exhaustive H-D exchange of **15** and **15-^{15}N** afforded **15-d_2** and **15-d_2-^{15}N**. Photolysis of **15-d_2** (1:2000, Ar, 10°K) (Figure 25, Table IX) and **15-d_2-^{15}N** (1:2000, Ar, 10°K) (Figure 26, Table X) with UV light from two CS-7-54

filters (λ = 400-680 cut-out) results in loss of the infrared bands due to the starting carbomoyl azides and formation of product absorbances assigned to aminoisocyanate-d_2 (labeled (I) in Table XI), D_2NN (**3-d_2**), formaldehyde-d_2 (D_2CO) (labeled (F) in Table XI) and carbon monoxide (CO) listed in the first column of Table XI. Subtraction of the spectrum of the respective starting carbomoyl azide from the product mixture FT-IR spectrum (Figure 27 for **15-d_2**, Figure 28 for **15-d_2-^{15}N**) clearly reveals the product absorptions.

The first group of bands at 2259.03 and 2231.06 cm^{-1} from **15-d_2** show ^{15}N shifted multiple bands at 2237.81 and 2212.26 cm^{-1} a shift of 21.22 and 18.80 cm^{-1}, respectively. These bands are observed to grow in quickly with UV photolysis and decrease with prolonged UV irradiation. These bands are assigned to the isocyanate stretches (ν N=C=O) for aminoisocyanate-d_2 and the corresponding ^{15}N shifted modes (ν ^{15}N=C=O). No other bands for aminoisocyanate-d_2 were located suggesting that the ν N=C=O is the most intense infrared band for the aminoisocyanate as anticipated.

A second group of bands at 2140.90, 2138.73, 2109.08, 1599.23, 1571.27, 1195.69, 913.64, 899.89, and 793.83 cm^{-1} from photolysis of **15-d_2** are assigned to D_2NN **3-d_2** and CO at 2140.90 cm^{-1}. The behavior of the CO bands will be discussed in a later section. These bands all decrease with VIS irradiation ($\lambda > 500$ nm) as observed for H_2NN **3** and its accompanying identical CO band at 2140.90 cm^{-1}. The difference FT-IR spectrum resulting from the subtraction of the spectrum after VIS photolysis of **3-d_2** is shown in Figure 29. This spectrum clearly shows the absorbances assigned to **3-d_2** and CO. The bands at 1599.23 and 1571.27 cm^{-1} are in the region where the

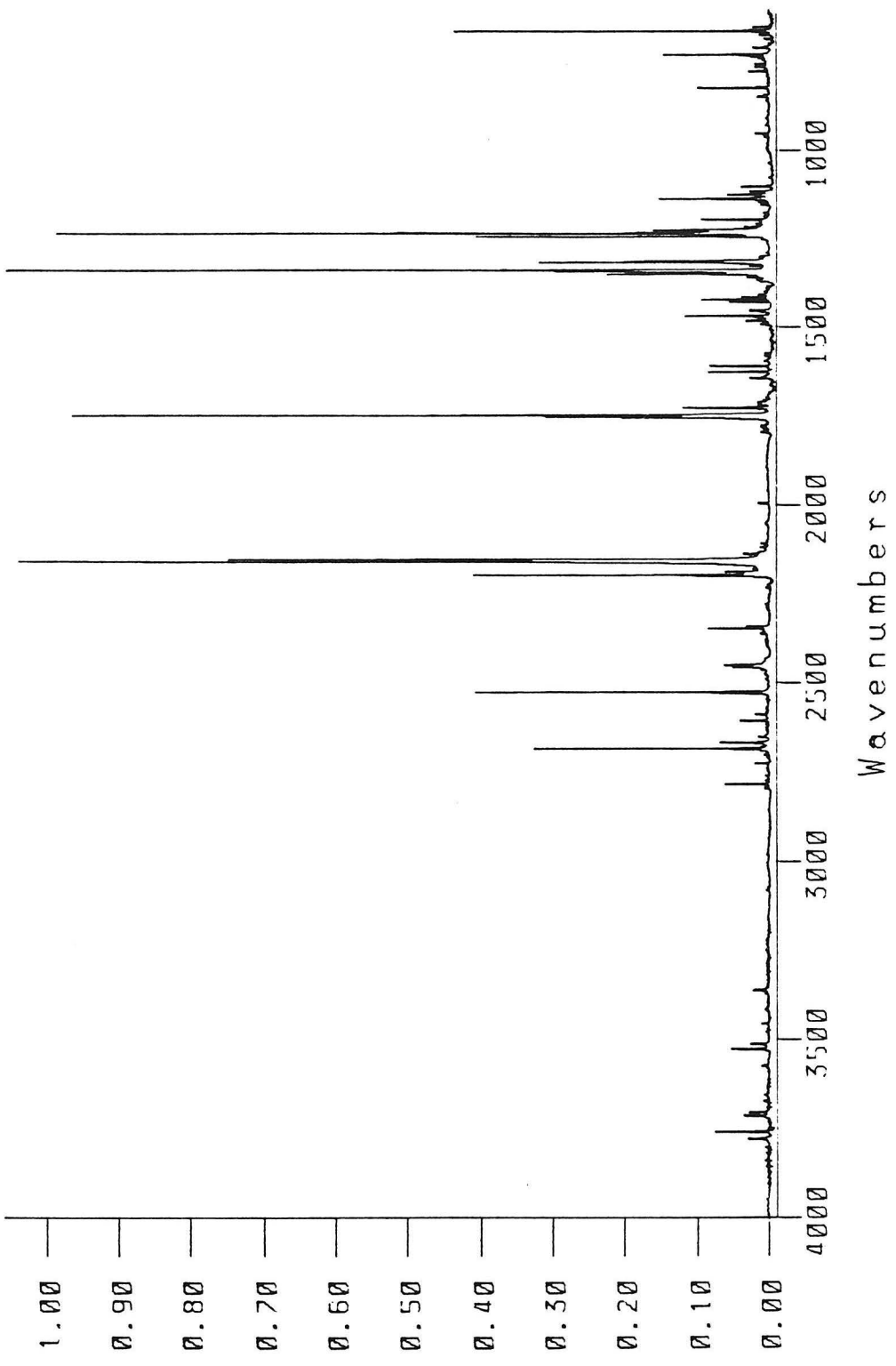

Figure 25. FT-IR spectrum of **15-d_2**, 120 mm deposition (1:2000, Ar, 10°K).

Table IX. FT-IR Bands for **15-d_2** in an Argon Matrix (1:2000, 10°K) Threshold = 0.05 A.

Peak Location (cm^{-1})	Intensity (A)	Assignment
3756.26	0.07	H_2O, ν O-H
2782.21	0.06	
2682.68	0.33	ν N-D
2664.98	0.06	
2524.18	0.40	ν N-D
2447.96	0.06	
2345.09	0.08	CO_2, ν CO
2195.69	0.41	
2185.53	0.06	
2164.54	0.07	
2157.98	1.04	ν N_3 (asym)
2154.50	0.93	
2151.57	0.75	
1753.24	0.20	
1751.45	0.31	
1747.45	0.96	ν C=O
1726.22	0.11	
1623.58	0.08	H_2O, δ O-H
1607.91	0.08	H_2O, δ O-H
1466.47	0.11	
1420.55	0.09	
1348.24	0.22	
1342.78	0.18	
1341.90	0.19	
1340.64	0.29	
1338.07	1.06	ν NCO (sym)
1315.27	0.31	
1311.80	0.19	
1243.12	0.41	
1236.49	0.12	
1234.20	0.99	ν N_3 (sym)
1224.00	0.16	

Table IX. Continued

Peak Location (cm^{-1})	Intensity (A)	Assignment
1136.35	0.15	δ ND_2
821.72	0.10	ρ N-D
727.22	0.14	δ N_3
659.23	0.44	Γ NCN

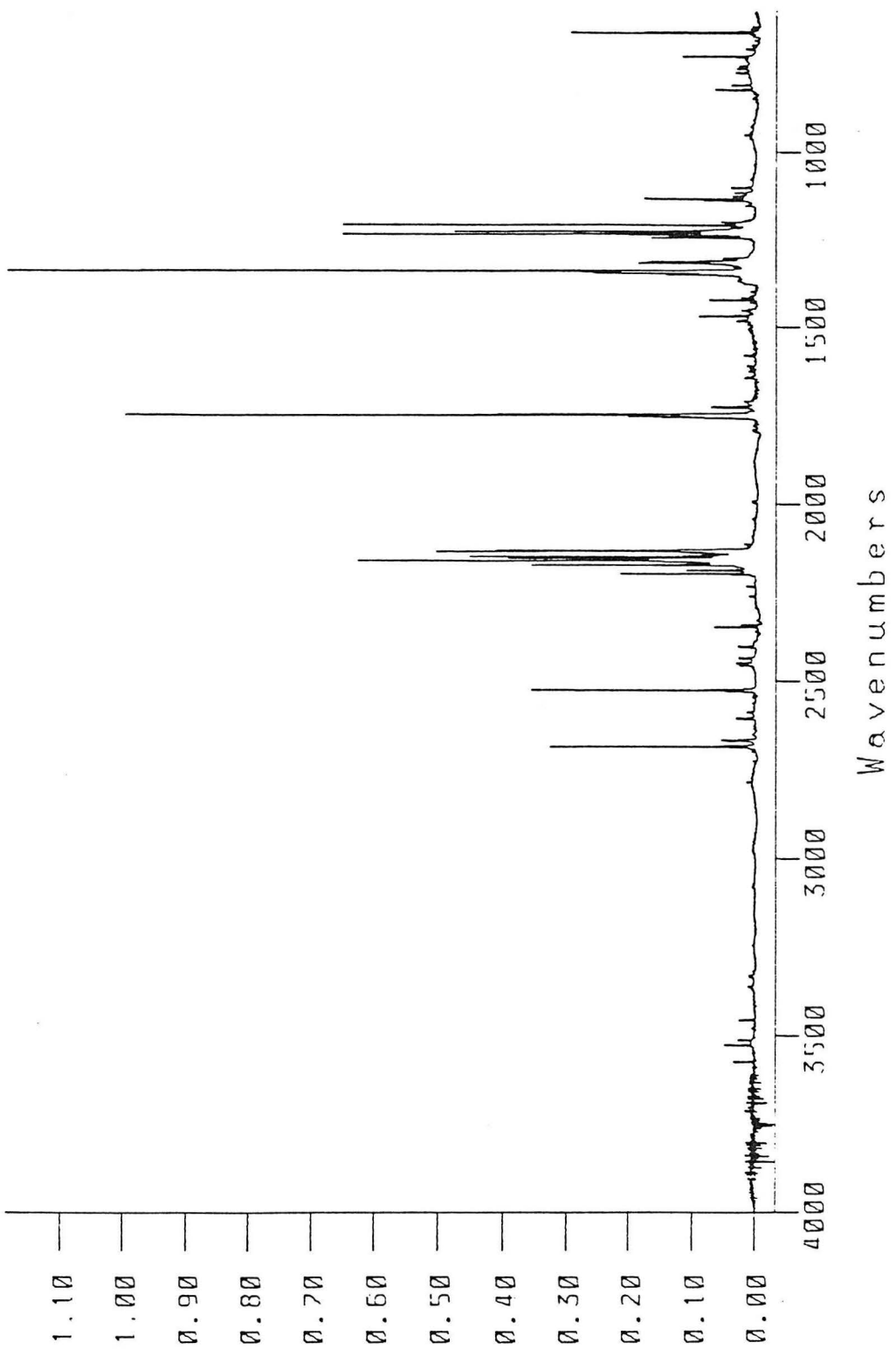

Figure 26. FT-IR spectrum of **15-d_2-^{15}N:15-d_2** (~80:20 mixture), 120 mm deposition (1:2000, Ar, 10°K).

Table X. FT-IR Bands for **15-d_2-^{15}N** in an Argon Matrix (1:2000, 10°K) Threshold 0.05 A.

Peak Location (cm^{-1})	Intensity (A)	Assignment
2782.22	0.05	
2682.69	0.32	ν N-D
2664.98	0.05	
2524.19	0.37	ν N-D
2345.09	0.06	CO_2, ν CO
2195.69	0.21	
2185.55	0.11	
2170.98	0.35	
2168.36	0.11	
2164.55	0.09	
2157.97	0.63	ν-N=N=N (asym)
2151.40	0.39	
2146.28	0.45	ν-^{15}N=N=N (asym)
2141.20	0.08	
2136.58	0.10	
2133.55	0.12	
2131.76	0.51	ν-N=N=^{15}N (asym)
2129.48	0.41	ν-N=N=^{15}N (asym)
1753.25	0.14	
1751.46	0.20	
1746.76	0.99	ν C=O
1726.23	0.06	
1466.47	0.09	
1420.55	0.07	
1348.04	0.12	
1346.41	0.14	
1343.76	0.26	
1341.10	0.23	
1337.87	1.18	ν NCO (sym)
1315.28	0.18	
1311.80	0.17	

Table X. Continued.

Peak Location (cm^{-1})	Intensity (A)	Assignment
1243.12	0.16	
1240.01	0.13	
1234.24	0.65	ν N=N=N (sym)
1231.59	0.23	
1225.55	0.47	ν ^{15}N=N=N (sym)
1220.44	0.10	
1207.22	0.65	ν N=N=^{15}N (sym)
1136.35	0.18	δ ND_2
821.73	0.06	ρ N-D
727.23	0.11	δ N_3
659.00	0.29	Γ NCN
656.75	0.18	Γ NC^{15}N

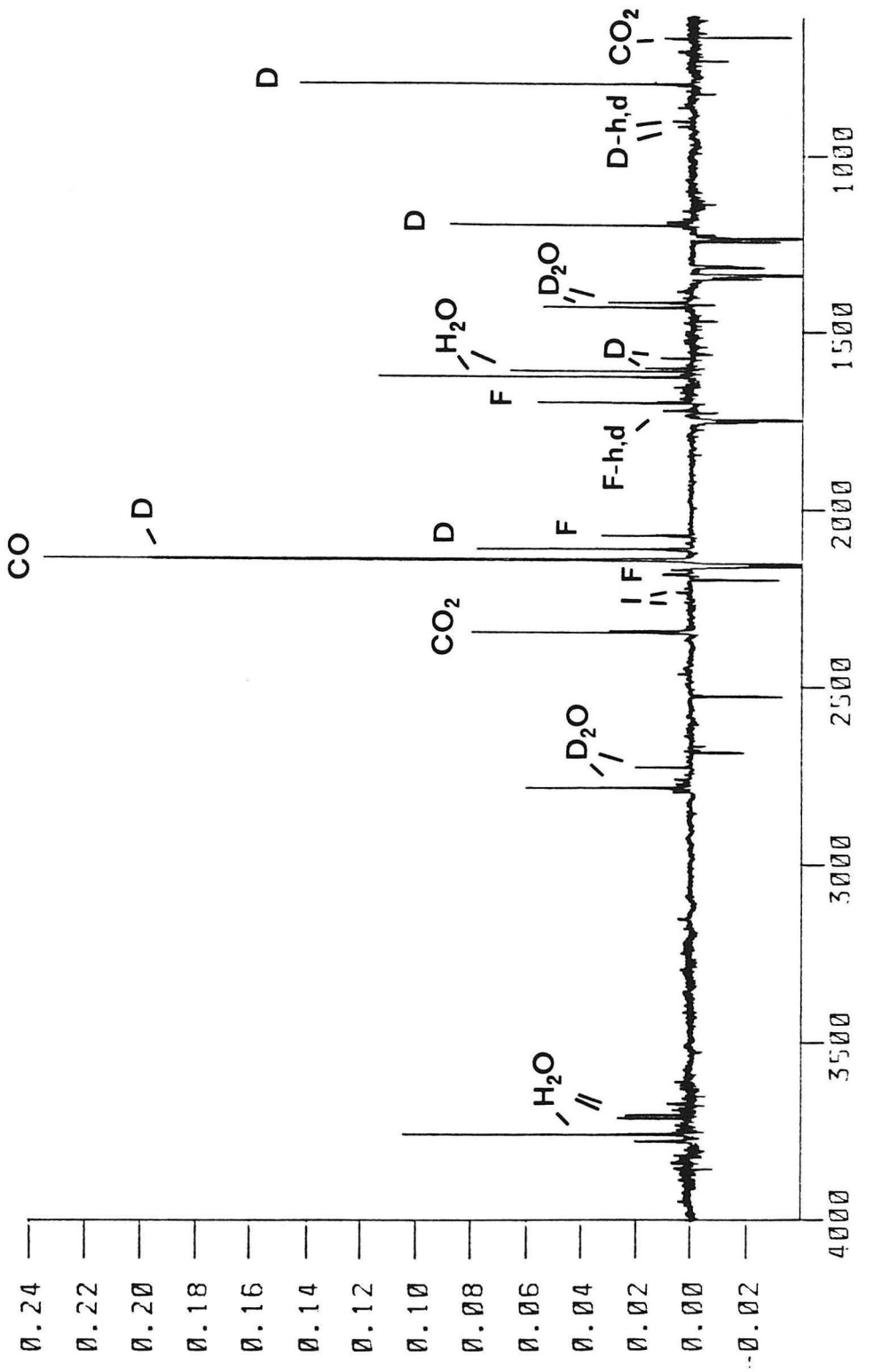

Figure 27. Difference FT-IR spectrum of products from UV (VIS filtered) photolysis (90 min) of **15-d2** (1:2000, Ar, 10°K) minus spectrum of **15-d2**. Subtraction factor $\alpha = 0.10$. (D) = D_2NN **3-d2**, (F) = D_2CO, (I) = D_2N-N=C=O.

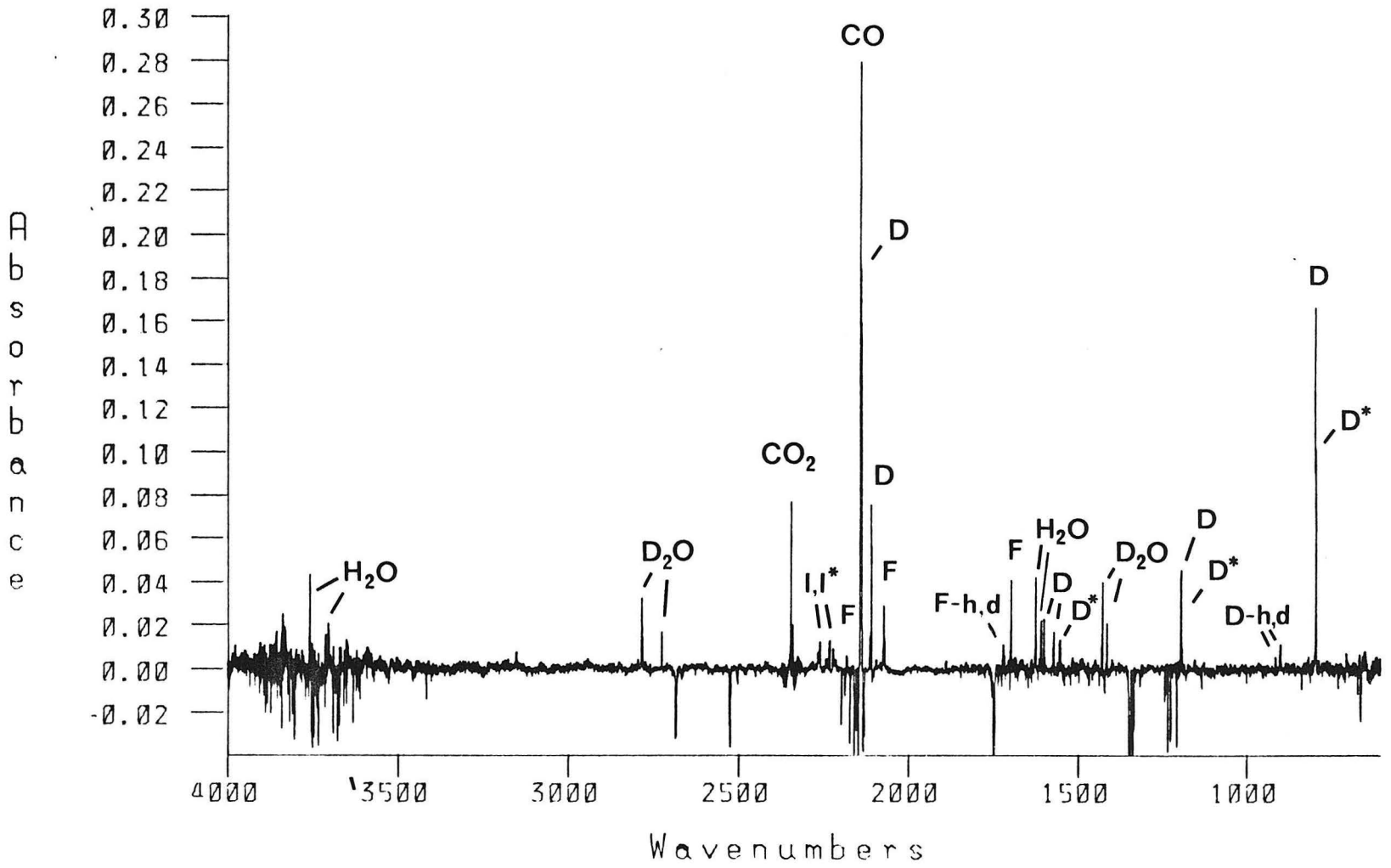

Figure 28. Difference FT-IR spectrum of products from UV (VIS filtered) photolysis (90 min) of $15\text{-}d_2\text{-}^{15}N{:}15\text{-}d_2$ mixture (1:2000, Ar, 10°K) minus spectrum of $15\text{-}d_2\text{-}^{15}N{:}15\text{-}d_2$ mixture. Subtraction factor $\alpha = 0.30$. (D) = D_2NN $3\text{-}d_2$, (D*) = $D_2N\text{-}^{15}N$ $3\text{-}d_2\text{-}^{15}N$, (D) = D_2CO, (I) = $D_2N\text{-}N{=}C{=}O$, (I*) = $D_2N\text{-}^{15}N{=}C{=}O$.

Table XI. Infrared Assignments for Products from Photolysis of **15-d_2** and **15-d_2-^{15}N** (~1:2000, Ar, 10°K).

90 min hν UV (VIS filtered)	240 min hν VIS (λ >500 nm)	150 min hν (λ = 360-420 nm)	Assignment
3776.05			h, ν OH
3756.53			h, ν OH
3710.96			h, ν OH
3701.81			h, ν OH
2782.14			d, ν O-D
2723.80			d, ν O-D
2345.09			CO_2, ν CO
2339.06			CO_2, ν CO
2259.03			I, ν -^{14}N=C=O
2237.81			I*, ν -^{15}N=C=O
2231.06			I, ν -^{14}N=C=O
2212.26			I*, ν -^{15}N=C=O
2179.96	(+)	(+)	F, ν C-D
	2149.82	(-)	CO/T, ν CO
	2143.32	(-)	CO/T, ν CO
2140.90	(-)		CO, ν CO
2139.94	(+)	(+)	CO, ν CO
2138.73	(-)		D, ν N-D
2137.53	(+)	(+)	CO, ν CO
2109.08	(-)		D, ν N-D
2071.48	(+)	(+)	F, ν C-D
1720.00	(+)	(+)	F (H,D), ν C=O
1697.58	(+)	(+)	F, ν C=O
1623.58			h, δ OH
1607.67			h, δ OH

Table XI. Continued

90 min hν UV (VIS filtered)	240 min hν VIS (λ > 500 nm)	150 min hν (λ = 360-420 nm)	Assignment
1599.23	(-)		D, δ N-D
1572.95			h, δ OH
1571.27	(-)		D, ν $N^{14}=^{14}N$
1552.22	(-)		D, ν $N^{14}=^{15}N$
1427.35			d, δ O-D
1413.61			d, δ O-D
1195.69	(-)		D, δ N=N-D
1194.72	(-)		D*, δ ^{15}N=N-D
984.99	(+)	(+)	F, δ C-D
	965.95	(-)	(?)
	964.50	(-)	(?*)
	947.39	(-)	T, δ N=N-D (asym)
	945.46	(-)	T*, δ ^{15}N=N-D
913.64	(-)		D (H,D), δ N=N-D,H
912.92	(-)		D* (H,D), δ ^{15}N=N-D,H
899.89	(-)		D (H,D), δ N=N-D,H
899.18	(-)		D* (H,D), δ ^{15}N=N-D,H
793.83	(-)		D, δ N=N-D
793.11	(-)		D*, δ ^{15}N=N-D

h = H_2O
I = Aminoisocyanate-d_2 (D_2N-N=C=O), I* = (I-^{15}N)
D = Diazene (D_2NN), D* = (D-^{15}N)
F = Formaldehyde-d_2 (D_2C=O)
T = Trans-1,2-diazene-d_2 (DNND), T* = (T-^{15}N)
CO = Carbon monoxide
d = D_2O
(-) = Decreased
(+) = Increased
( ) = Tentative assignment

characteristic N=N stretch for **3** is found. Photolysis of **15-d_2-^{15}N** yields **3-d_2-^{15}N**. Subtraction of spectrum after VIS photolysis of **3-d_2-^{15}N** results in the difference FT-IR spectrum clearly showing the absorbances due to **3-d_2-^{15}N** and CO (Figure 30). The resulting spectrum reveals ^{15}N shifted bands for **3-d_2-^{15}N** at 1552.22, 1194.72, 912.92, 899.18, and 793.11 cm^{-1}. The 1552.22 cm^{-1} corresponds to the Hooke's law ^{15}N shifted $\nu D_2{}^{14}N{=}^{15}N$ stretch of the characteristic $\nu D_2{}^{14}N{=}^{14}N$ stretch at 1571.27 cm^{-1}. The remainder of the ^{15}N shifted bands of **3-d_2-^{15}N** are assigned to ^{15}N shifts of the N=N-D bending modes of **3-d_2** by analogy to **3**. The bands at 913.64 and 899.89 cm^{-1} and their ^{15}N multiples are assigned to the H,D counterparts of the strongest bands observed for **3** at 1003.07 cm^{-1} and **3-d_2** at 793.83 cm^{-1} due to some **15-h,d** (and **15-h,d-^{15}N**) impurity in **15-d_2** (and **15-d_2-^{15}N**). The infrared transitions for **3-d_2** and **3-d_2-^{15}N** are summarized and assigned in Table XII. All six infrared modes of D_2NN **3-d_2** have been located. Failure to observe a ^{15}N multiple band (0.25 cm^{-1} resolution) for the absorption for **3-d_2** at 1599.23 cm^{-1} is consistent with its assignment as the out of plane torsion mode.

A third group of bands from UV photolysis of **15-d_2** and **15-d_2-^{15}N** at 2139.94 and 2137.53 are identical to the CO stretches observed in the UV photolysis of **15** and **15-^{15}N**. These CO stretches are observed to increase with photolysis of **3-d_2** and **3-d_2-^{15}N** with visible light consistent with their assignment as CO's somehow associated with the photochemical decomposition products of **3**, **3-^{15}N**, **3-d_2**, and **3-d_2-^{15}N**.

The final group of product bands from photolysis of **15-d_2** and **15-d_2-**

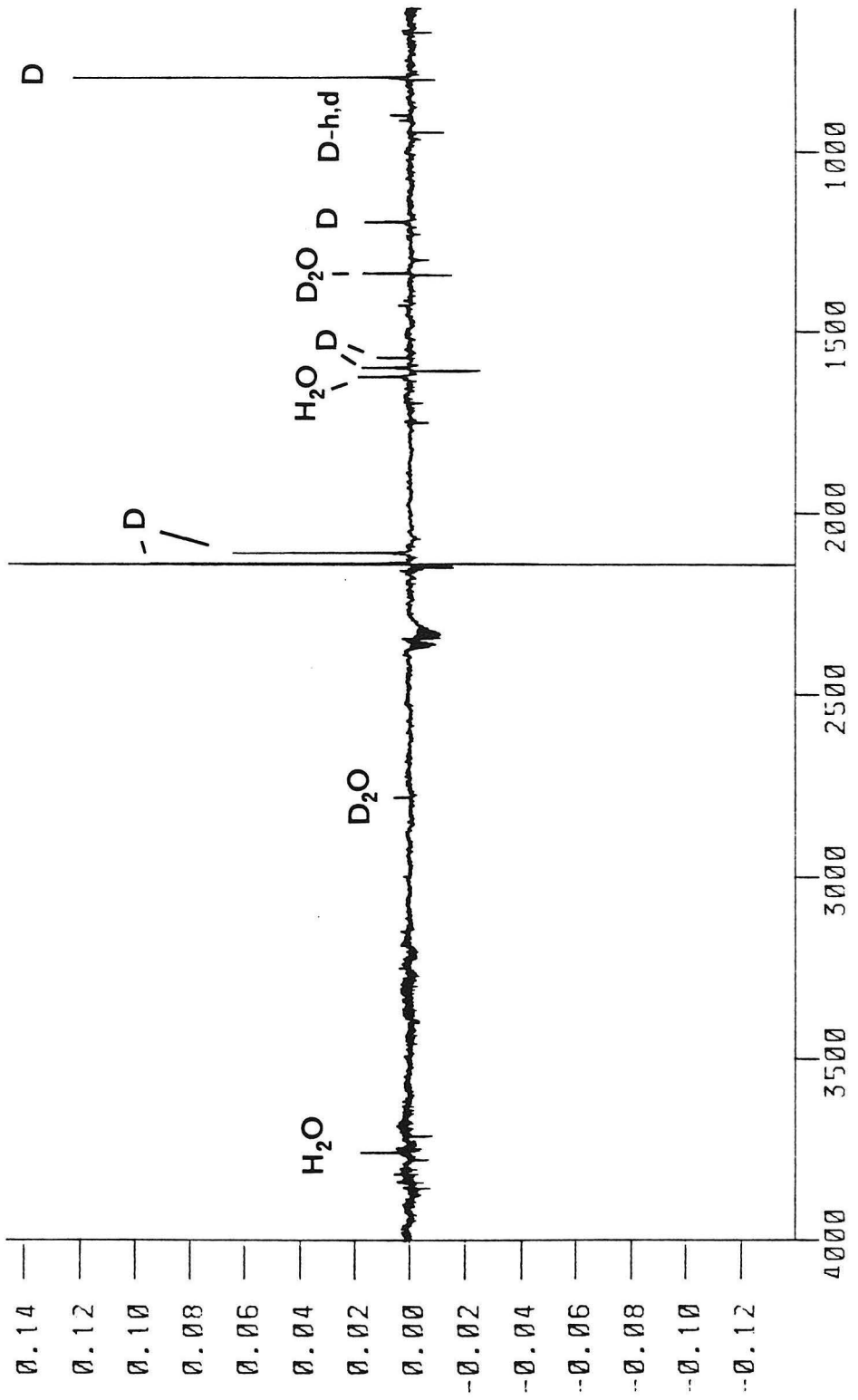

Figure 29. Difference FT-IR spectrum of D_2NN **3-d2** (n) and CO. UV (VIS filtered) photolysis (90 min) of **15-d2** (1:2000, Ar, 10°K) minus spectrum after VIS (>500 nm) photolysis (4 h) of **3-d2**. Subtraction factor $\alpha = 1.0$.

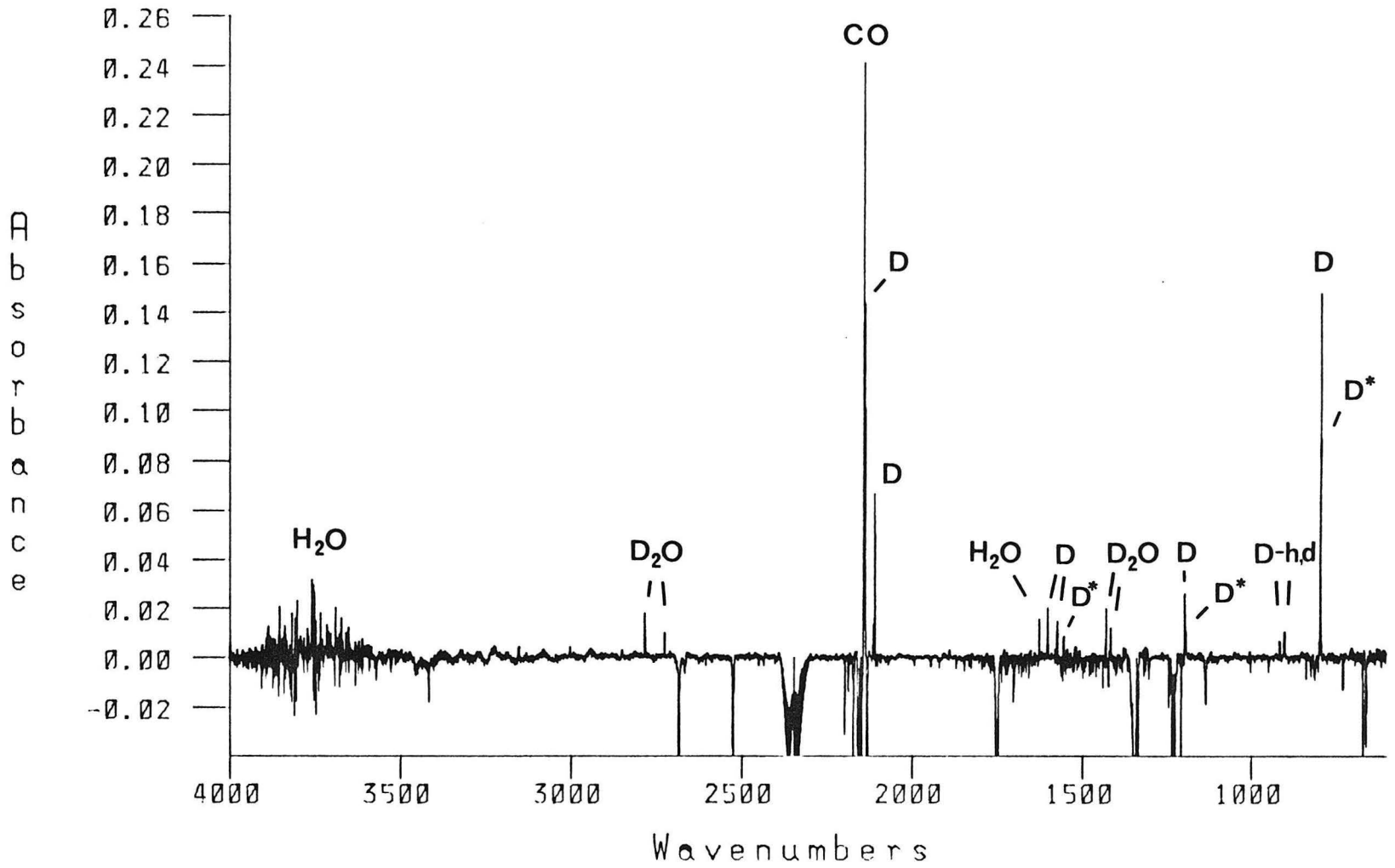

Figure 30. Difference FT-IR spectrum of D_2NN 3-d_2 (D): D_2N-^{15}N 3-d_2-^{15}N (D*) mixture and CO. UV (VIS filtered) photolysis (90 min) of 15-d_2-^{15}N:15-d_2 mixture (1:2000, Ar, 10°K) minus spectrum after VIS (>500 nm) photolysis (4 h) of 3-d_2:3-d_2-^{15}N. Subtraction factor $\alpha = 1.10$.

Table XII. Infrared Transitions of D_2NN **3-d_2** and D_2N-^{15}N **3-d_2-^{15}N** (Ar, 10°K).

(cm^{-1})	Assignment
2138.73	ν N-D
2109.08	ν N-D
1599.23	δ N=N-D (out of plane)
1571.27	ν $^{14}N=^{14}N$
1552.22	ν $^{14}N=^{15}N$
1195.69	δ $^{14}N=N-D$
1194.72	δ $^{15}N=N-D$
(913.64)	δ N=N-H (H,D)
(912.92)	δ $^{15}N=N-H$ (H,D)
(899.89)	δ N=N-D (H,D)
(899.18)	δ $^{15}N=N-D$ (H,D)
793.83	δ N=N-D
793.11	δ $^{15}N=N-D$

( ) = Tentative assignment

^{15}N show no ^{15}N multiples. These bands are assigned by spectral comparison to formaldehyde-d_2 (D_2CO) and formaldehyde-h,d (H,DCO). These bands are listed in the first column of Table XI (F-d_2, F-hd). These bands are observed to increase with VIS photolysis of **3-d_2** and **3-d_2-^{15}N** (see second column Table XI) demonstrating, as found for **3**, that formaldehyde is a photochemical decomposition product of **3** in the presence of CO. This will be discussed

fully in a later section. The observed infrared bands for isotopically labeled formaldehydes are compared with their literature[62,66] values in Table XIII.

Table XIII. Formaldehyde Infrared Bands from Photolysis of **3** and **3-d_2(h,d)** in the Presence of CO (Ar, 10°K)[a] (cm^{-1}). Literature Comparison.

H_2CO	(lit.)[b]	D_2CO	(lit.)[b]	H,DCO	(lit.)[c]	Assignment
2865.55	2863.0	2179.96	2176.8	--	2873.8	ν C-H
2800.22	2797.1	2071.48	2069.1	--	2764.3	ν C-H
1741.70	1742.0	1697.58	1697.8	1720.00	1723.2	ν C=O
1498.71	1498.8	--	1099.1	--	1399.1	δ CH_2 (scissor)
1227.03	1244.8	984.99	987.1	--	1028.0	δ CH_2 (rock)
1168.45	1168.0	--	938.3	--	1074.0	δ CH_2 (out of plane)

[a]This work ±0.05 cm^{-1}. [b]Ref. 62 (Ar, 10°K). [c]Ref. 66 (Ar, 10°K).

Photolysis of matrix isolated **3-d_2** with visible light (>500 nm) also results in formation of new infrared bands at 2149.82, 2143.32, 965.95, and 947.39 cm^{-1}. The bands at 2149.82 and 2143.32 cm^{-1} are identical to two of the new bands observed in VIS photolysis of **3** and **3-^{15}N.** These bands are assigned to CO's and will be fully discussed in a later section. The bands at 965.95 and 947.39 show ^{15}N shifted multiples with VIS photolysis of **3-d_2-^{15}N** at 964.50 (a ^{15}N shift of 1.45 cm^{-1}) and 945.46 (a

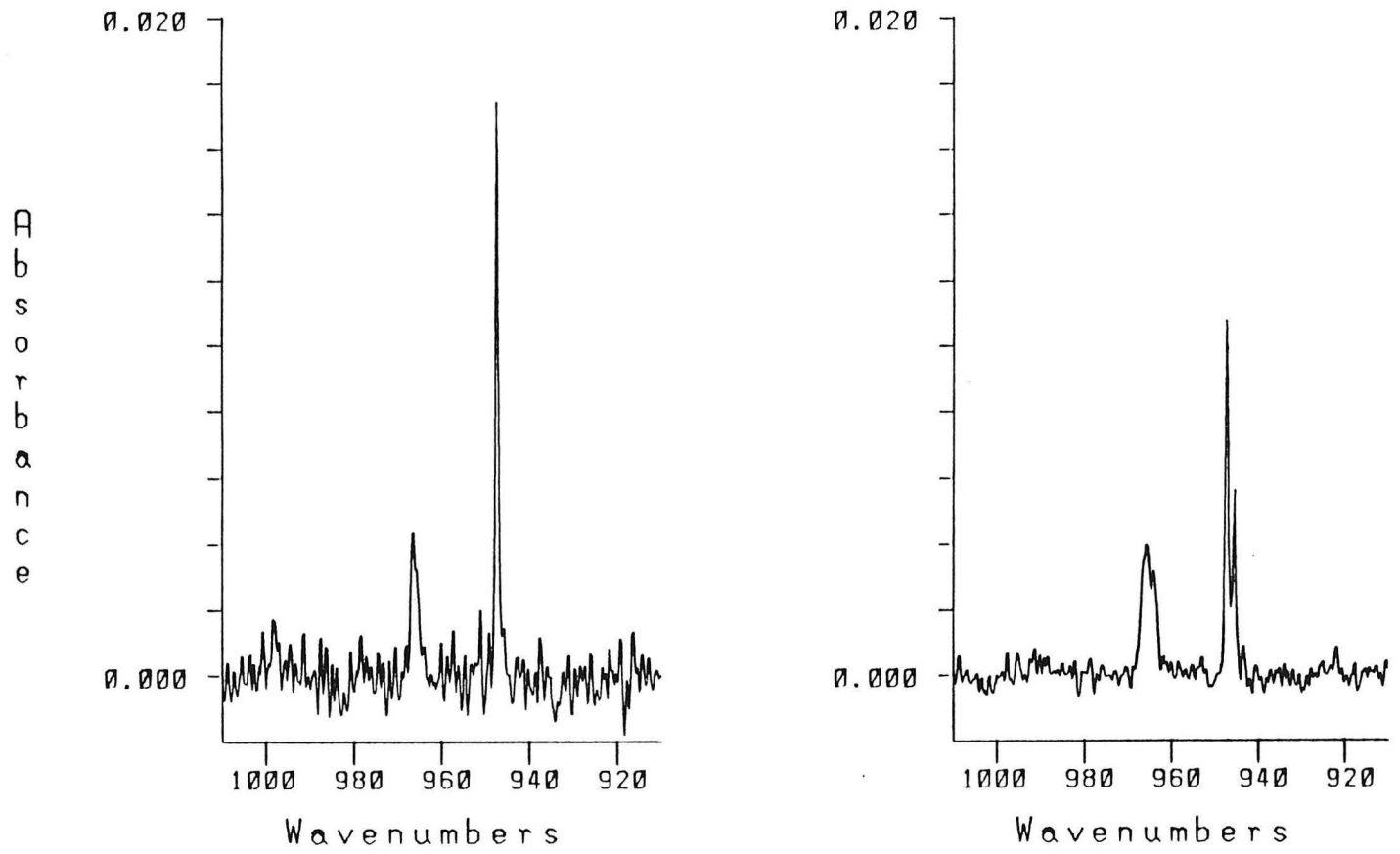

Figure 31. (a) Difference FT-IR spectrum of DNND **1-d_2** from VIS photolysis (4 h) of **3-d_2** (Ar, 10°K). Before minus after photolysis of **1-d_2** (360-420 nm), 150 min. (b) Difference FT-IR spectrum of DNND **1-d_2** and **1-d_2-^{15}N** from VIS photolysis (4 h) of **3-d_2:3-d_2-^{15}N** mixture (Ar, 10°K). Before minus after photolysis **1-d_2:1-d_2-^{15}N** (360-420 nm), 150 min.

shift of 1.93 cm^{-1}), respectively. The band at 947.39 cm^{-1} corresponds to the known strong infrared band for trans DNND **1-d_2** found by Rosengren and Pimentel[2c] at 946.2 ± 0.3 cm^{-1} in a nitrogen matrix. The reported ^{15}N isotope shift for this band is 2.0 cm^{-1} to 944.2 cm^{-1}. This is very close to the observed 1.93 cm^{-1} ^{15}N shift to 945.46 cm^{-1} in an argon matrix. These bands are efficiently photolyzed away with either monochromatic light (λ = 380 ± 10 nm) or broad band irradiation (λ = 360-410 nm) (see third column Table XI) consistent with the assignment to trans DNND **1-d_2** and **1-d_2-^{15}N** (Figure 31). Table XIV summarizes the observed FT-IR assignments for HNNH **1**, DNND **1-d_2** and their literature assignments.[2c] The band at 965.95 and its ^{15}N multiple at 964.50 cm^{-1} are also photolyzed away with **1-**

Table XIV. Infrared Bands for HNNH **1** and DNND **1-d_2**. Literature Comparison.[2c]

1,2-Diazene	Observed[a] (cm^{-1})	Literature[b] (cm^{-1})	Difference (Obs.-Lit.) (cm^{-1})
1	1288.01 (1286.02)[c]	1285.8	+2.2 (+0.2)[c]
1-^{15}N	1286.81	1284.5	+2.3
^{15}N shift	1.20	1.3	-0.1
1-d_2	947.39	946.2	+1.2
1-d_2-^{15}N	945.46	944.2	+1.3
^{15}N shift	1.93	2.0	-0.07

[a]This work (Ar, 10°K). [b]Ref. 2c (N_2, 10°K). [c]This work (N_2, 10°K).

d_2. The assignment of these bands remains uncertain. Attempts to selectively photolyze or interconvert these bands with the bands due to **1-d_2** (as a possible assignment to **2-d_2**) have been unsuccessful. Photolysis of **1-d_2** as for **1** results in the increase of the bands due to formaldehyde (D_2CO) and two CO bands at 2139.94 and 2137.53 cm^{-1}. Two CO bands at 2149.82 and 2143.32 are lost concomitant with the bands due to **1-d_2**. Identical behavior was observed in the CO stretch region with **1**. This will be discussed in a later section. The third column of Table XI summarizes the photochemical behavior of **1-d_2**.

H_2NN Product Analysis

For product analysis, samples of **3** were prepared by photo-Curtius rearrangement/photodecarbonylation of carbomoyl azide **15** isolated in a rigid 2-MTHF glass contained in a 5 mm O.D. quartz tube immersed in a liquid nitrogen filled finger dewar at 77°K. Gaseous products H_2, N_2, and CO were identified by VPC coinjection and mass spectral analysis and quantitated by Toepler pump analysis. Ammonia (NH_3), hydrazine (N_2H_4), ammonium azide ($\overset{+}{N}H_4\overset{-}{N}_3$), and formaldehyde ($H_2CO$) were quantitated by standard colorimetric analysis. Product ammonium azide was compared with independently synthesized $\overset{+}{N}H_4\overset{-}{N}_3$ by FT-IR.

Warming a blue-violet 2-MTHF glass of **3** from 80°K to 90°K results in the loss of **3** and formation of HNNH **1** (yellow, λ_{max} = 386 nm), 2-tetrazene (H_4N_4) **25** (λ_{max} = 260 nm) and an orange species λ_{max} = 480 nm (see Figure 14). Warming further results in loss of the

yellow-orange color together with vigorous gas evolution and formation of an insoluble precipitate of ammonium azide. Analysis of the products for thermal decomposition of **3** reveals the formation of NH_3, N_2H_4, $\overset{+}{N}H_4\overset{-}{N}_3$ together with H_2, N_2, and CO. Carbon monoxide (CO) and N_2 are the expected side products for photo-Curtius rearrangement of **15** to aminoisocyanate and N_2 followed by photo-decarbonylation to form **3** and CO. These products are summarized in Table XV. Ammonia, hydrazine, ammonium

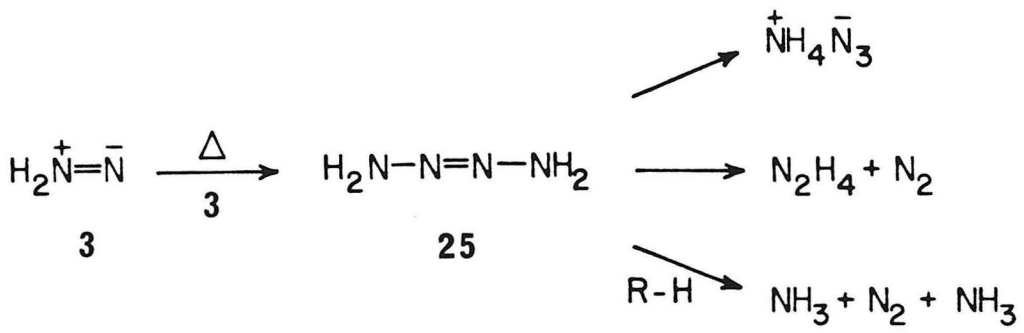

azide, and N_2 are known thermal decomposition products of 2-tetrazene **25**. Observation of these products together with a thermally labile intermediate λ_{max} = 260 nm (large extinction-coefficient) suggests that **3** dimerizes to form the expected 2-tetrazene **25** (λ_{max} = 260 nm) which subsequently thermally decomposes to NH_3, N_2H_4, and N_2 and tautomerizes to $\overset{+}{N}H_4\overset{-}{N}_3$. The mechanism for the thermal decomposition of tetrazene **25** is unknown. Attempts to directly monitor its disappearance by electronic spectroscopy are severely impeded due to simultaneous formation of $\overset{+}{N}H_4\overset{-}{N}_3$ precipitate

Table XV. Products from UV Photolysis of **15** Followed by Thermolysis of **3**.[a]

Product	Ratio[b]	% Yield[c]	Ratio[d]	% Yield[e]
CO	1	29.0	--	--
N_2	1.65	50.0	21.7	49.3
H_2	0.40	12.0	13.3	30.2
NH_3	0.12	4.0	4.0	9.1
N_2H_4	0.03	0.90	1	2.3
$\overset{+}{N}H_4\overset{-}{N}_3$	0.12	4.0	4.0	9.1
H_2CO[f]	--	--	--	--

[a]Typically 1.50 mg **15** in 300 μL 2-MTHF, [**15**] = 58 mM; $h\nu$ 2-CS-7-54 filters, 5 h, 77°K; warmed to R.T. [b]Molar ratio, normalized. Average of three determinations. Individual yields ±10% of each. Total mass 97 ± 10% typically. [c]Normalized from ratio in b. [d](c) Corrected for CO and 1 equivalent of N_2 as side products of photo-Curtius/decarbonylation of **15** → **3** + N_2 + CO. [e]Normalized from ratio in d. [f]Formaldehyde not detected.

together with vigorous gas evolution. Hence, kinetic studies were not attempted. The rapid and spontaneous nature of the thermal decomposition of **25** may support a radical chain decomposition mechanism (together with rapid self-heating) or the presence of a catalyzed pathway (e.g., trace acid). Correcting the yields of products from thermal decomposition of **3** for the formation of CO and one equivalent of N_2 as side products of the photo-Curtius rearrangement/decarbonylation route to **3** reveals an added component of H_2 and N_2 as products (see Table XV). The ratios of H_2, N_2, and CO products from thermal and photochemical decomposition of **3** in 2-MTHF

are summarized in Table XVI.

Visible light (>340 nm) photolysis of a blue-violet glass of **3** results in decolorization and formation of H_2, N_2, and CO in a 0.98:1.95:1.0 ratio. The nearly quantitative yield of gaseous products is consistent with a sequence consisting of UV photo-Curtius/decarbonylation of **15** to **3** + N_2 + CO followed by direct photolysis of **3** in the visible to produce H_2 + N_2 in an

Table XVI. Thermal and Photochemical Decomposition of H_2NN **3**. H_2, N_2, and CO Ratios.[a]

Conditions	N_2/CO	H_2/CO
hν,[b] Δ[c]	1.65	0.40
hν,[b] hν (λ >500 nm)[d,e]	1.88	0.82
hν,[b] hν (λ >340 nm)[e,f]	1.95	0.98
hν,[b] hν (λ >500 nm),[d] hν (λ >340 nm)[e,f]	1.94	0.96
hν (UV + VIS)[e,g]	1.96	1.04

[a]Molar ratios from Toepler pump analysis. CO yield 95 ± 10% from warmed (R.T.) reaction mixture. [b] hν (2-CS-7-54 filters, 5 h, 77°K). [c]Warmed to R.T. Other products summarized in Table XV. [d]hν (CS-1-75, 2-CS-3-70 filters, 5 h, 77°K). Remaining products summarized in Table XVII. [e]H_2CO not detected, see Experimental. [f]hν (CS-1-75 filter, 5 h, 77°K). [g]hν (no filters, 5 h, 77°K).

overall expected ratio for H_2:N_2:CO of 1.0:2.0:1.0. UV photolysis of **15** with no visible absorbing filters results in no blue-violet color due to **3** and a nearly quantitative yield of H_2, N_2, and CO in a ratio of 1.04:1.96:1.0.

The added component of H_2 and N_2 in the photochemical generation followed by thermolysis of **3** may represent actual thermal decomposition products from **3**. Alternatively H_2 and N_2 may be the result of secondary photolysis (S_1 or T_1) during photochemical generation of **3**. Competing relaxation/decomposition pathways from photoexcited aminoisocyanate to excited **3** (S_1, T_1) and CO followed by decomposition of excited **3** to H_2 and N_2 products represents a reasonable alternative source of H_2 and N_2. Additionally, excited **3** may isomerize to **1** which would be efficiently decomposed at the wavelengths used to generate **3** from **15**.

Irradiation of **3** with visible light ($\lambda > 500$ nm) affords yellow **1** (λ_{max} = 386 nm). Subsequent warming to room temperature results in loss of **1** and formation of $\overset{+}{N}H_4\overset{-}{N}_3$, N_2H_4, NH_3 in addition to H_2, N_2, and CO in a 0.82:1.88:1.0 ratio. These products are summarized in Table XVII. Photolysis of **3** appears to afford **1** in approximately 10 to 15% yield based on the reduced yield of H_2 when compared to that obtained upon photolysis (>340 nm) of **3**. Thermolysis of **1** appears to result in formation of NH_3, N_2H_4, and $\overset{+}{N}H_4\overset{-}{N}_3$ as observed from thermolysis of **3**, which to some extent also yields **1**. Wiberg found[2g] N_2H_4, NH_3, $\overset{+}{N}H_4\overset{-}{N}_3$, N_2 and H_2 as thermal products from decomposition of neat **1** near 77°K. Willis found[37] only N_2H_4, H_2, and N_2 as thermal products for gas phase decomposition of **1** (100°C). Willis proposed that hydrazine results from isomerization of <u>trans</u> **1** to <u>cis</u> **2** followed by disproportionation. The mechanism for NH_3, N_2H_4, and $\overset{+}{N}H_4\overset{-}{N}_3$ formation from **1** is less obvious. Dimerization of **1** to form tetrazene **25** has been reported.[35] Subsequent thermolysis of **25** would explain the

observed products. The greater proportion of N_2H_4 obtained from thermolysis of **1** produced from VIS photolysis of **3** compared with that obtained from thermolysis of **3** could result from competing isomerization to **2** followed by disproportionation. The orange λ_{max} = 480 nm species from thermolysis of **3** (tentatively identified as cis **2**) is also seen transiently in thermolysis of **1** produced from photolysis of **3** [VIS Photolysis (>500 nm) of concentrated samples (0.5 M) of **3** and **3-d$_2$** occasionally resulted in formation of the orange λ_{max} = 480 nm species.[69]] Attempts to trap H_2N_2

Table XVII. Decomposition Products from Photoisomerization of **3** to **1** Followed by Thermal Decomposition.

Product	Ratio[a]	% Yield[b]	Ratio[c]	% Yield[d]
CO	1	26	--	--
N_2	1.88	50	44.0	49
H_2	0.82	22	41.0	46
NH_3	0.02	0.5	1	1.1
N_2H_4	0.05	1.3	2.5	2.8
$NH_4^+N_3^-$	0.3	0.8	1.5	1.7

[a]Molar ratios see experimental. Typically 1.50 mg **15** in 300 μL 2-MTHF, hν 2-CS-7-54 filters, 5 h, 77 K; hν CS-1-75, 2-CS-3-70 filters, 5 h, 77 K; warmed to R.T. [b]Total mass yield 90 ± 10% typically. Normalized from ratio in a. Average of two determinations each. Formaldehyde not detected. Individual yields ±10% of each. [c]Corrected for CO and 1 equivalent of N_2 as side products of photo-Curtius/decarbonylation of **15** → **3** + N_2 + CO. [d]Normalized from ratio in c.

with a large excess of reactive olefin (which could result in reduction if cis **2** is present) are summarized in Table XVIII. Norbornene has been shown to be among the most reactive olefins toward diimide reduction[70] (presumably cis HNNH **2**). Thermolysis of **3** produced from VIS filtered photolysis of **15**, in a 2-MTHF glass containing a 50 to 100 molar excess of norbornene does result in a low but measurable yield of norbornane. VIS photolysis of **3** (>500 nm or >340 nm) in the presence of the same excess of norbornene followed by thermolysis results in approximately the same degree of reduction (approximately 7% of 1 equivalent of **15**). However, UV photolysis

Table XVIII. Reduction of Norbornene.

Conditions[a,b]	**15**		% Yield[c] 
hν,[d] Δ[e]	1	50	7.1 ± 0.3
hν,[d,f] Δ	1	100	6.8 ± 0.3
hν,[d] hν (>340 nm),[g] Δ	1	50	6.6 ± 0.3
hν,[d] hν (>500 nm),[h] Δ	1	50	6.7 ± 0.3
hν (full lamp),[i] Δ	1	50	7.2 ± 0.3

[a]Photolysis in 5 mm quartz sample tube, Suprasil finger dewar, 77 K. [b]Molar ratio **15**:norbornene (**15**) = 4.5×10^{-2} M, in 2-MTHF, 300 μL sample. [c]% Yield based on (**15**), n-octane as internal standard, 15 m SE-54 capillary, R.T. [d]hν, 2-CS-7-54 filters, H_2O filter, quartz optics, 4 h. [e]Warmed to R.T. [f]Forms opaque, fractured glass. [g]hν, CS-1-75 filter, 4 h. [h]hν, CS-1-75, 2-CS-3-70 filters, 4 h. [i]hν, quartz optics, H_2O filter, 4 h.

of **15** with no visible filters (which gives no blue-violet color of **3**) results in the same degree of reduction within experimental error. These studies implicate a mechanism other than direct H_2N_2 reduction of norbornene. Direct H abstraction by an excited state of norbornene[72] and/or H· addition (produced from photolysis of **3**) are possible alternative reduction mechanisms. This was not explored in greater detail.

Matrix FT-IR Studies of Carbon Monoxide

Several groups of bands showing no isotope shifts in the photo-Curtius rearrangement/photodecarbonylation of **15**, **15**-^{15}N, **15**-d_2, and **15**-d_2-^{15}N have been assigned to CO, a co-product in the photochemical generation of isotopically labeled **3**. The appearance of several groups of CO bands each mirroring the behavior of the photogenerated diazenes **3** and **1** and their photochemical decomposition products (H_2, N_2) suggests an intimate association or matrix site arrangement of these products with a contiguous CO molecule in an argon matrix.[91] UV (VIS filtered) photolysis of **15** affords CO, N_2,and **3** in addition to formaldehyde and aminoisocyanate FT-IR bands (see Figure 18). Figure 32b shows the CO stretch region of the infrared spectrum obtained from UV (VIS filtered) photolysis of **15**. Four CO bands at 2140.90, 2139.94, 2137.22, and 2137.53 cm^{-1} are observed. Photolysis of **3** with visible light (λ >500 nm) results in loss of the CO band at 2140.90 cm^{-1} with loss of the bands due to **3** (Figure 32c), growth of two CO bands at 2139.94 and 2137.53 cm^{-1} together with formation of two new CO bands of equivalent intensity at 2149.82 and 2143.32 cm^{-1}. As described earlier, VIS photolysis

of **3** affords mainly H_2 and N_2 (2-MTHF, 77°K), trans HNNH **1** (2-MTHF, 77°K or Ar, 10°K), and formaldehyde H_2CO (Ar, 10°K). Formaldehyde very likely results from successive hydrogen radical reduction of CO[62a] contiguous to **3** and will be discussed in a later section. Photolysis of **1** (Ar, 10°K) results in loss of its infrared bands, loss of the two CO bands at 2145.82 and 2143.32 cm^{-1} together with growth of the two CO bands at 2139.94 and 2137.53 (Figure 32d). The photolysis products of **1** are mainly H_2 and N_2 (2-MTHF, 77 K) (Table XVI).

Matrix isolated complexes of CO with various small molecules has been demonstrated to result in shifts of the CO infrared stretch due to hydrogen bonding (e.g., H_2O, NH_3), dipole-dipole (e.g., CO dimers) and electrostatic (e.g., N_2) interactions.[71] Some of these effects together with the observed and assigned CO bands from matrix studies of isotopically labeled **3**, **1**, and their photodecomposition products are listed in Table XIX.

Matrix isolation of CO (1:2000, Ar, 10°K) affords a single infrared band at 2138.25 cm^{-1} in argon (Figure 33a). In a nitrogen matrix (1:2000, N_2, 10°K) the CO stretch is observed at 2139.69 cm^{-1} (Figure 33b). Matrix isolation of CO in a mixture of nitrogen and argon, $CO/N_2/Ar$ (1:20:1000, 10°K) shifts the CO stretch to 2136.32 cm^{-1}. The two CO bands which are observed to grow in with photolysis of **3** and **1** is an argon matrix at 2139.94 and 2137.53 cm^{-1} are likely assigned to "complexes" or sites of CO contiguous to N_2 (possibly two N_2's) and H_2 (photolysis products of **3** and **1**). The nearly one-to-one ratio of intensities of these bands suggests two equally formed $N_2 + H_2/CO$ sites in an argon matrix from photolysis of **15**, **3**, and **1**.

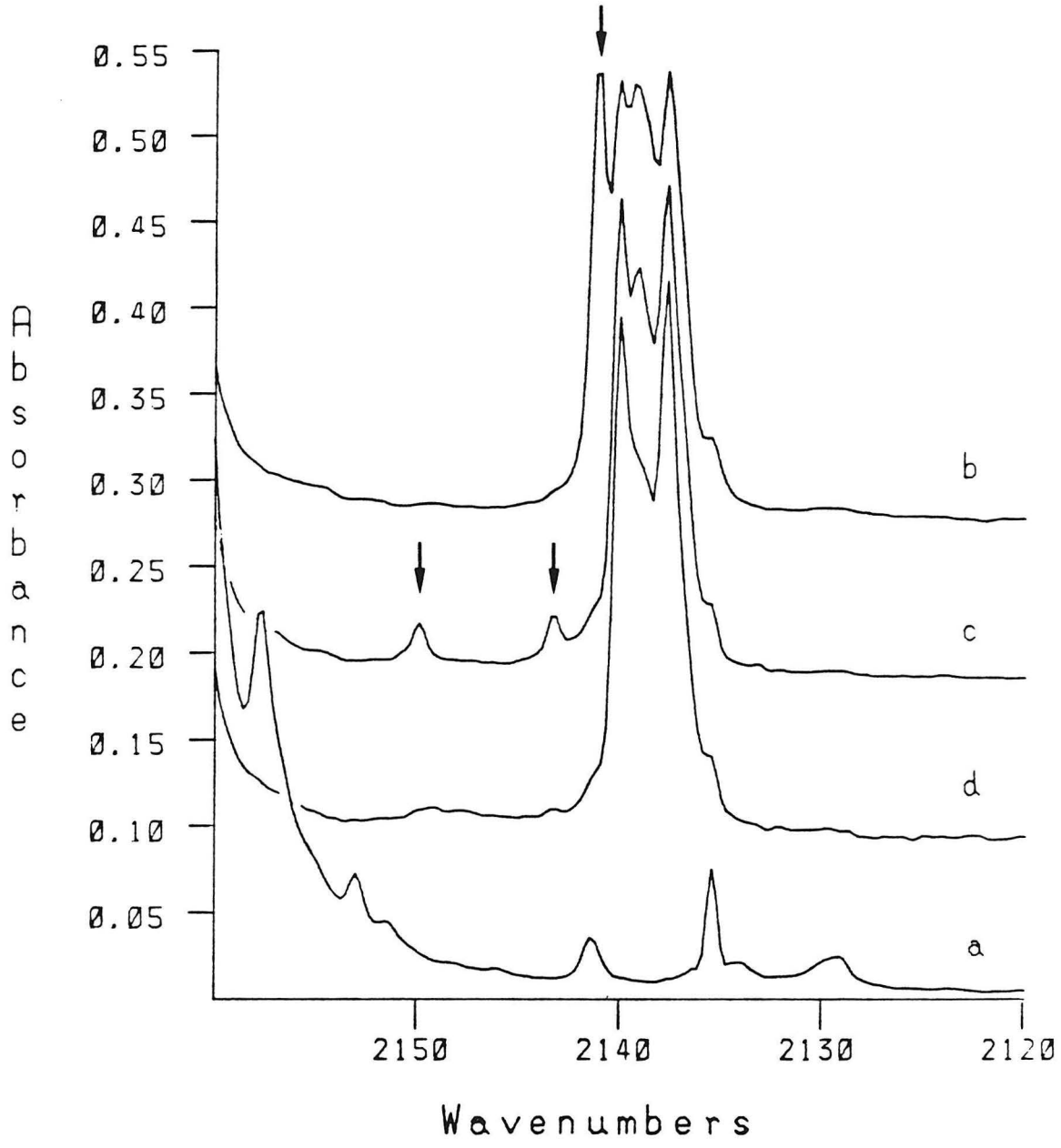

Figure 32. Successive FT-IR spectra of CO region (Ar, 10°K). (a) Before photolysis of **15** (1:2000, Ar, 10°K). (b) After UV (VIS filtered) photolysis of **15** (2 h) to form H_2NN **3** and CO. (c) After VIS (>500 nm) photolysis of **3** (2 h) to form HNNH **1**. (d) After photolysis of **1** (360-420 nm) 100 min.

Table XIX. Matrix Isolated Carbon Monoxide (CO) Infrared Stretch Frequencies.

CO/Matrix	(Ratio)	Obs.[a] ν CO (cm^{-1})	Lit.[b] ν CO (cm^{-1})	(Ratio)
CO/Ar	(1:2000)	2138.25	2138.40	(1:1000)
CO/N_2	(1:2000)	2139.69	2139.69	(1:1000)
$CO/N_2/Ar$	(1:9:1800)	2136.32	2136.60	(1:20:2000)
$CO/H_2O/Ar$	(1:2:2000)	2148.60	2148.8	(2:5:1000)
$CO/NH_3/Ar$			2143.3	(1:1:1000)
CO "dimers"/Ar	[c]	2139.40	2139.9	[c]
$CO/H_2NN/Ar$	[d]	2140.90		
$CO/D_2NN/Ar$	[d]	2140.90		
$CO/H_2NN/N_2$	[d]	2135.84		
CO/t-HNNH/Ar	[d]	2149.82 2143.32		
CO/t-DNND/Ar	[d]	2149.82 2143.32		
$CO/t\text{-}HNNH/N_2$	[d]	2143.80 2135.84		
$CO/H_2/N_2/N_2/Ar$	[d]	2139.94 2138.97 2137.53		
$CO/D_2/N_2/N_2/Ar$	[d]	2139.94 2137.53		
$CO/H_2/N_2/N_2/N_2$	[d]	2139.69		

[a]This work (10°K). [b]Ref. 71 (10°K). [c]CO/Ar warmed to 30°K and back to 10°K. [d]Matrix ratio unknown estimated at (1:1:>2000) from photolysis of **15** (~1:2000, 10°K).

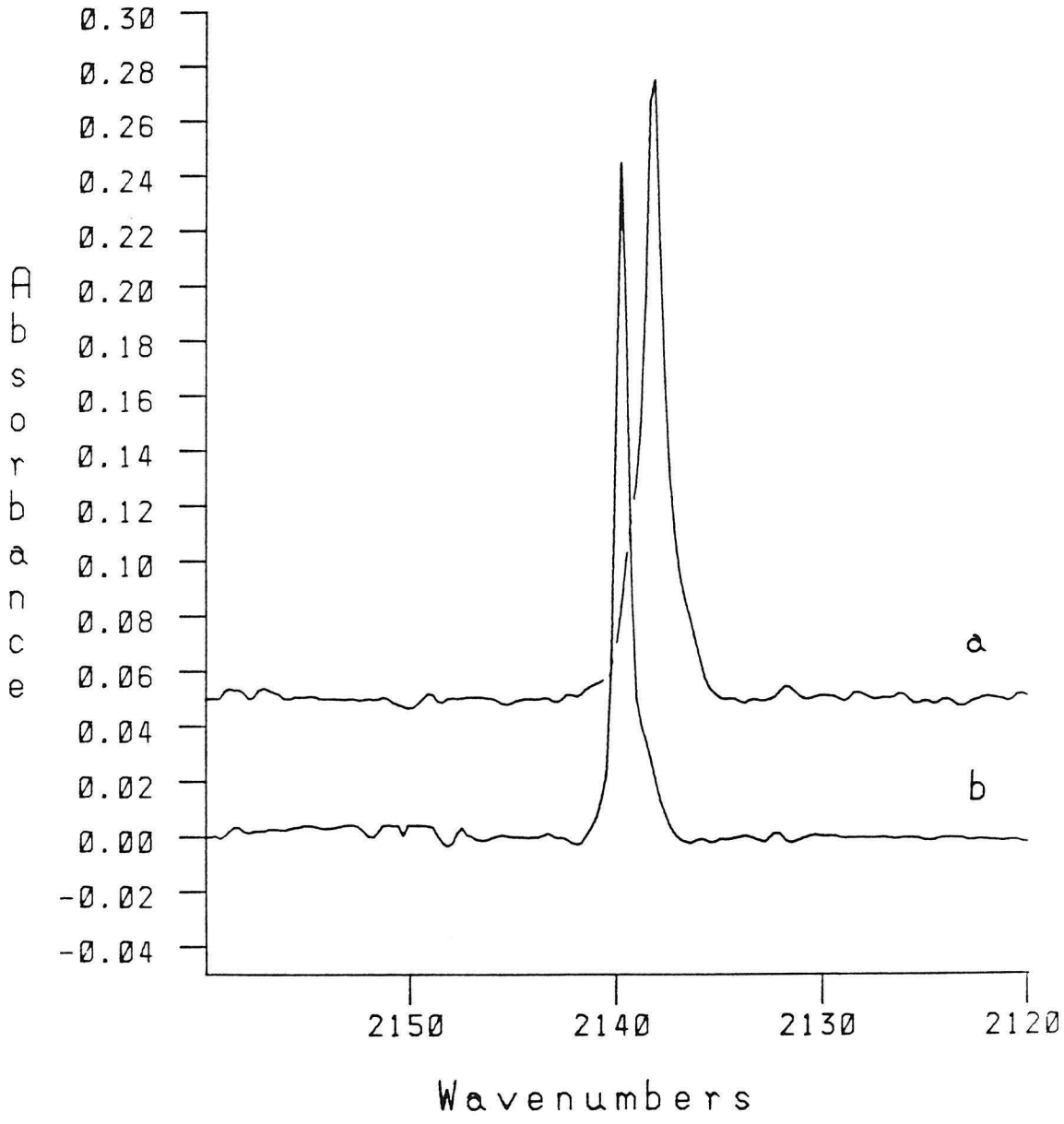

Figure 33. (a) FT-IR spectrum of CO (1:2000, Ar, 10°K). (b) FT-IR spectrum of CO (1:2000, N_2, 10°K).

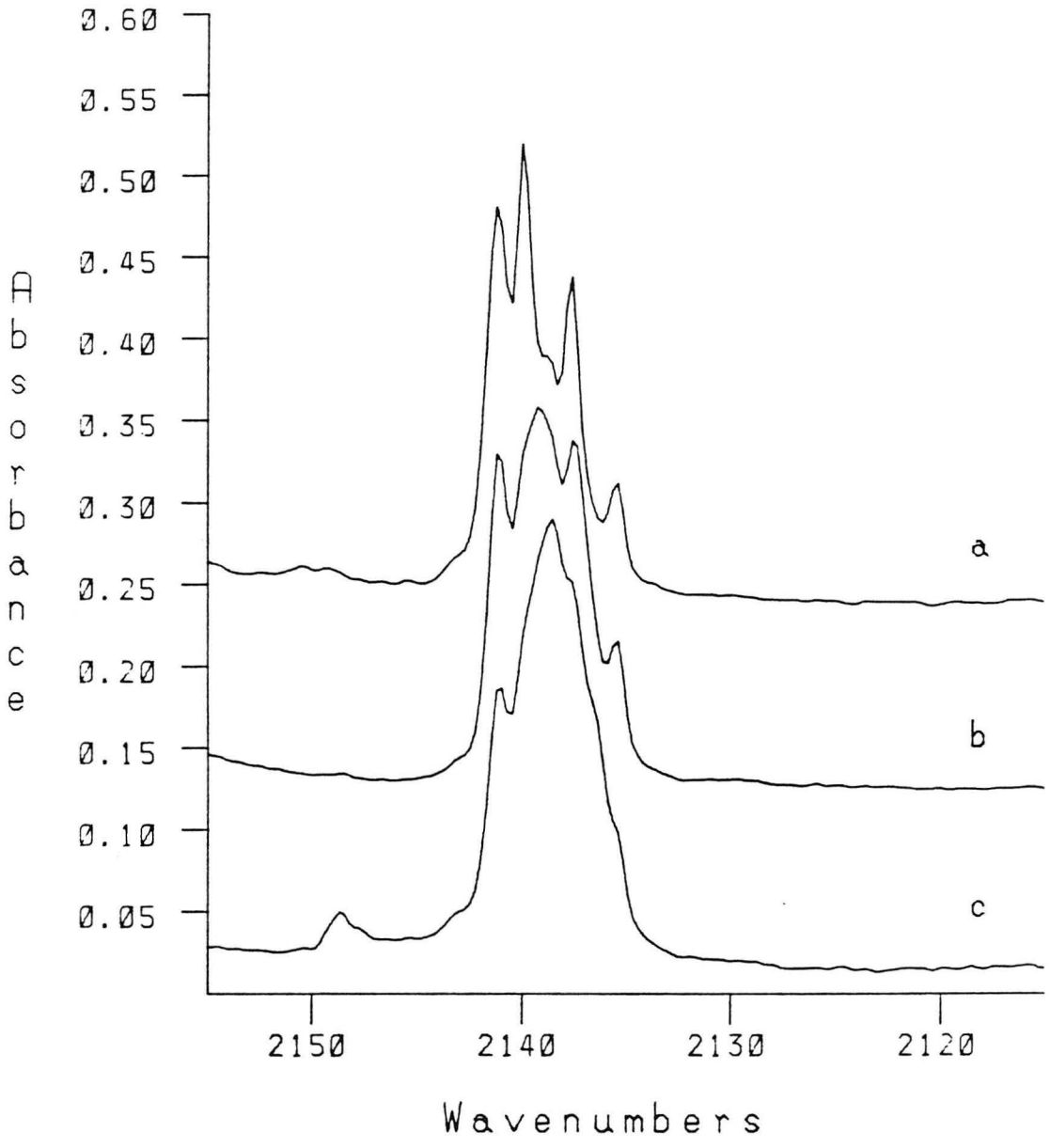

Figure 34. (a) FT-IR spectrum of CO region after UV (VIS filtered) photolysis (2 h) of **15** (1:2000, Ar, 10°K) to form **3** and CO. (b) After warming (a) to 35°K 3 min back to 10°K. (c) After warming (b) to 35°K 10 min back to 10°K.

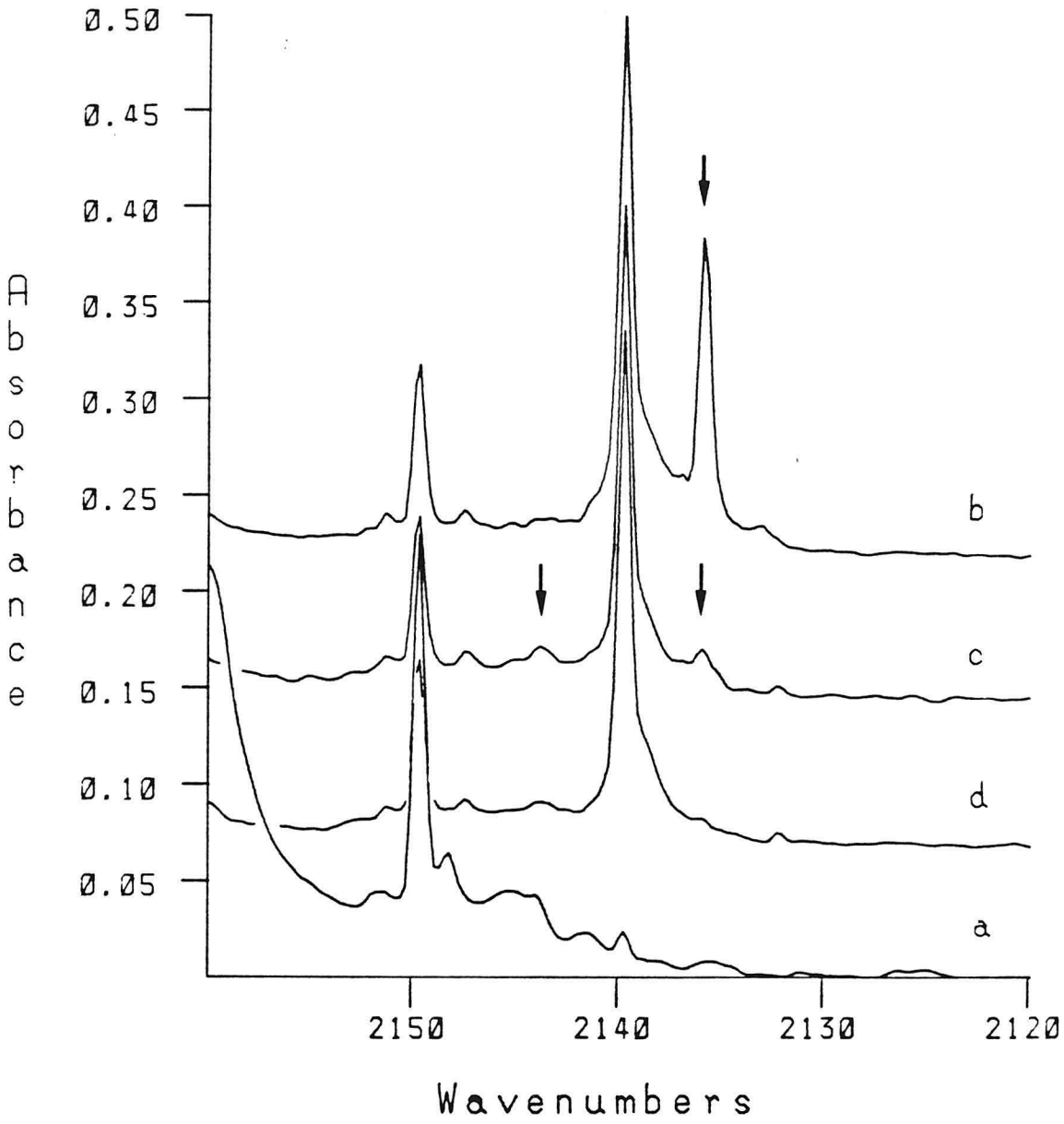

Figure 35. Successive FT-IR spectra of CO region (N_2, 10°K). (a) Before photolysis of **15** (1:2000, N_2, 10°K). (b) After UV (VIS filtered) photolysis of **15** (2 h) to form **3** and CO. (c) After VIS (> 500 nm) photolysis (2 h) of **3** to form **1**. (d) After photolysis of **1** (360-420 nm), 2 h.

The growth of these CO bands with sequential photolysis of **15** to **3** to **1** and **1** to products (H_2, N_2, H_2CO) supports the assignment of these CO bands at 2139.94 and 2137.53 cm^{-1} to two CO/N_2 sites. Warming an argon matrix of **3** to 35°K allows diffusion of small molecules (e.g., CO, N_2) and results in broadening and "merging" of the CO stretches (Figure 34). As an added test for these unique N_2/CO site assignments, UV (VIS filtered) photolysis of **15** in a nitrogen matrix (~1:2000, N_2, 10°K) affords only two CO bands at 2139.69 and 2135.84 cm^{-1} (Figure 35b) together with bands due to **3**.[65] VIS photolysis of **3** results in a diminished band at 2135.84 cm^{-1} (Figure 35c) together with loss of the infrared bands of **3** and growth of the CO band at 2139.69 cm^{-1}. This is consistent with loss of the unique N_2/CO sites found in an argon matrix due to replacement of Ar with N_2 molecules (degeneracy). VIS photolysis of **3** in a nitrogen matrix also results in formation of two CO bands at 2135.84 and 2143.80 cm^{-1} (Figure 35c) (analogous to the 2149.82 and 2143.32 cm^{-1} bands in Ar, 10°K) together with an infrared band of **1**. Photolysis of **1** results in loss of these bands (Figure 35d).

Hydrogen bonding to CO (e.g., H_2O, NH_3) shifts the CO stretching frequency to higher energy (Table XIX). The shift is H-bond donor dependent (e.g., pKa).[73] The stabilization results from H-bonding to the 5σ lone pair of CO at carbon which reduces antibonding character in the CO bond (higher energy stretch).[73,74] Dipole-dipole stabilization of CO also results in a higher energy CO stretch. The small dipole moment of CO (μ= 0.12 D) is oriented toward carbon.[75] Matrix isolated CO dimers (head-to-tail) show a higher energy infrared stretch than free CO (Table XIX). The

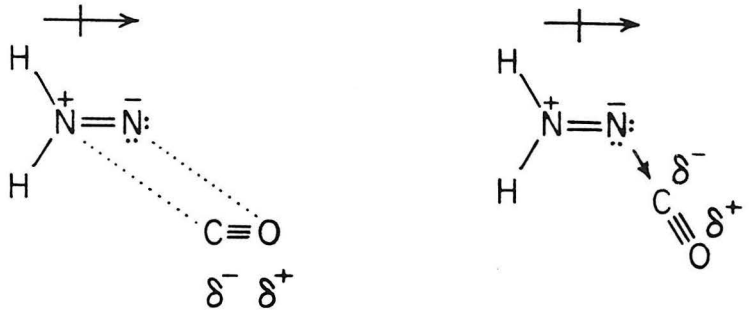

Ar Matrix N_2 Matrix

CO band at 2140.90 cm^{-1} (Ar, 10°K) which is lost with VIS photolysis of **3** is consistent with CO stabilized by dipole-dipole interaction and/or hydrogen bonding to **3**. The large calculated dipole moment for **3** (4.036 D)[1n] should lead to favorable dipole-dipole stabilization of CO in the proper orientation. The corresponding CO band in a nitrogen matrix is found at 2135.84 cm^{-1} which is destabilized (lower energy stretch) compared to CO in N_2 (2139.69 cm^{-1}). The destabilization may be due to the inability for CO to rotate to a favorable dipole-dipole or hydrogen bond stabilized orientation to **3** in N_2 at 10°K. The two equivalent intensity CO bands at 2149.82 and 2143.32 cm^{-1} formed from VIS photolysis of **3** (Ar, 10°K), which are lost with subsequent photolysis of **1** suggests their assignment to two types of stabilized CO/**1** complexes. The magnitude of the higher energy shifts correlates well with the hydrogen bond stabilization of CO encountered with H_2O or NH_3 in an

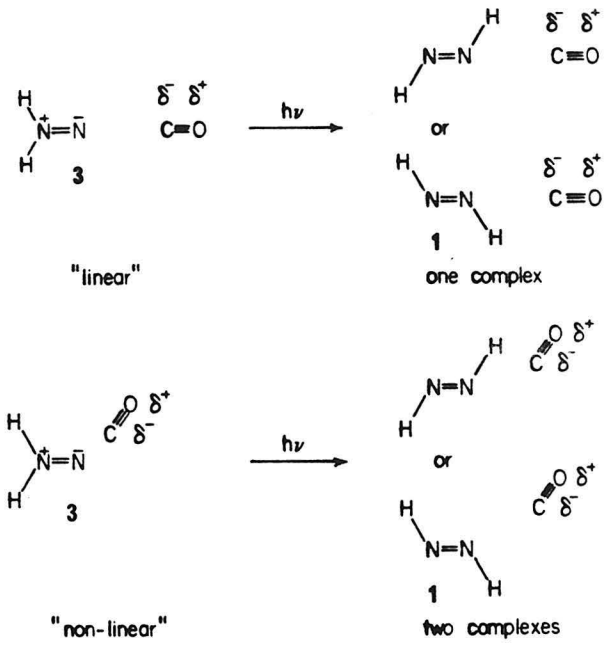

argon matrix (Table XIX). Photoisomerization of **3** to **1** could occur as a simple 1,2 H shift[94] in electronically excited **3** (S_1, T_1) or alternatively, through bond cleavage to diazenyl radical (HNN·) and H· followed by recombination.[95] If in the CO/**3** complex CO and the N=N double bond of **3** lie coaxial (C_{2v} symmetry) then the complex of CO and **1** resulting from 1,2 H shift of excited **3** should result in a <u>single</u> complex of CO and **1** by symmetry (assuming no rotational diffusion). However, if the CO axis is non-linear relative to the C_2 axis of **3**, the photoisomerization of **3** to **1** should

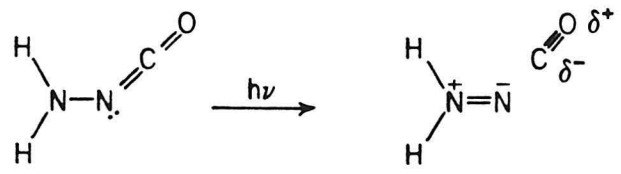

3

result in <u>two</u> CO/**1** complexes due to symmetry. Photolysis of aminoisocyanate to H_2NN **3** plus CO would be expected to yield a non-linear arrangement of CO and **3** due to the anticipated bent geometry of aminoisocyanate.[44] Observation of two CO stretches assigned to two complexes of 1 and CO formed with equal probability (1:1 intensities) at 2149.82 and 2143.32 cm^{-1} is consistent with a photochemical 1,2 H shift of **3** to **1** in a non-linear

Scheme III

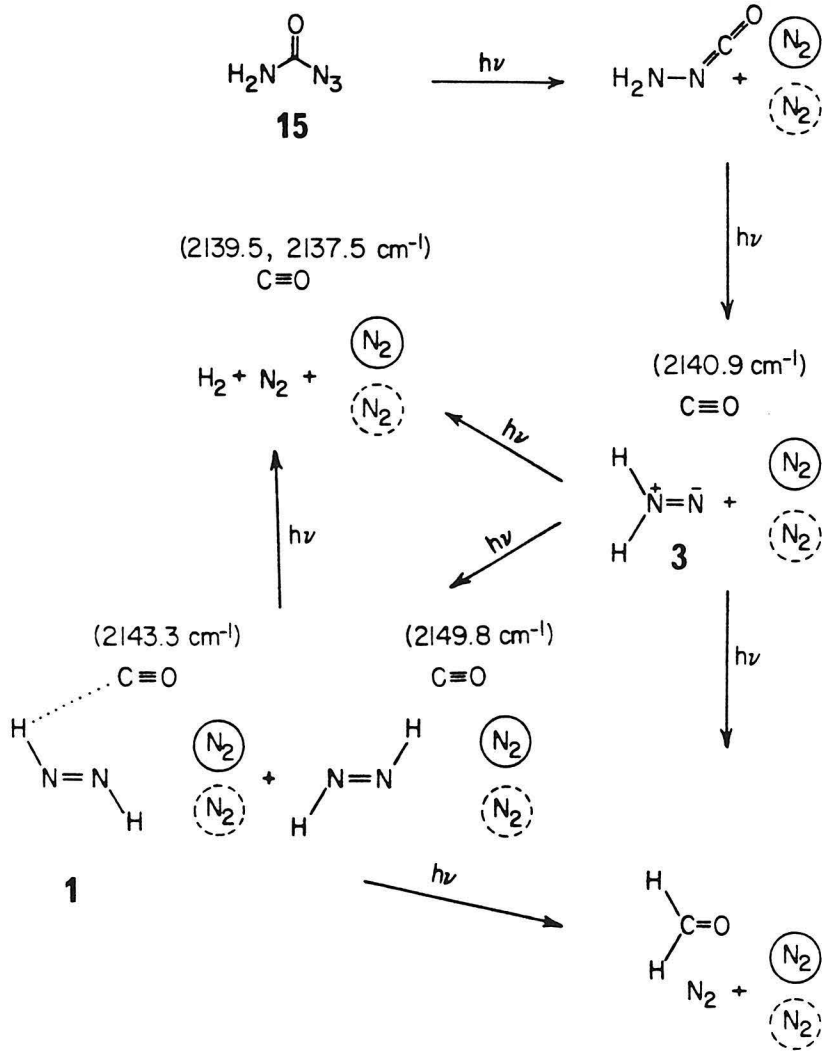

complex with CO. The lower energy CO stretches observed in a nitrogen matrix 2135.84 and 2143.80 cm^{-1} suggest a less stabilizing orientation of **1** and CO in N_2 produced from photolysis of a destabilized **3**/CO complex. Scheme III summarizes the CO matrix behavior.

ESR Studies

The derivative electron spin resonance (ESR) spectrum of a 2-MTHF glass of **3** (10°K) reveals a structural signal in the g = 2 region, an apparent superposition of two signals (Figure 36a). The anisotropic nature of the glass precludes a precise determination of the ~20 gauss hyperfine splittings. The ESR spectrum of a 2-MTHF glass of **3-d_2** reveals an identical signal. VIS irradiation of **3** or **3-d_2** with ($\lambda > 500$ nm, ~10°K) results in growth of the structural portion of the signal with the center doublet portion unchanged. The structured portion of the signal corresponds to 2-MTHF radical(s) independently produced from photolysis of trans-1,2-dimethyldiazene **8t** or di-tert-butyl peroxide in a 2-MTHF glass (77°K) (Figure 36b). The identity of the center doublet portion of the spectrum is unknown.[76] A similar spectrum to Figure 36a has been obtained from γ-irradiation of a 2-MTHF glass.[77] Prolonged UV (VIS filtered) photolysis of a 2-MTHF glass alone (77°K) under conditions used to generate **3** does not yield the spectrum of Figure 36a. The formation of 2-MTHF radical(s) in photolysis of **15** or **3** is consistent with the generation of H· from **3** followed by abstraction from the matrix. VIS photolysis of **3-d_2** prepared form **15-d_2** (>97% d_2) results in a mixture of D_2:HD:H_2 in a ratio of 75:23:2 by mass spectroscopy. This is consistent with

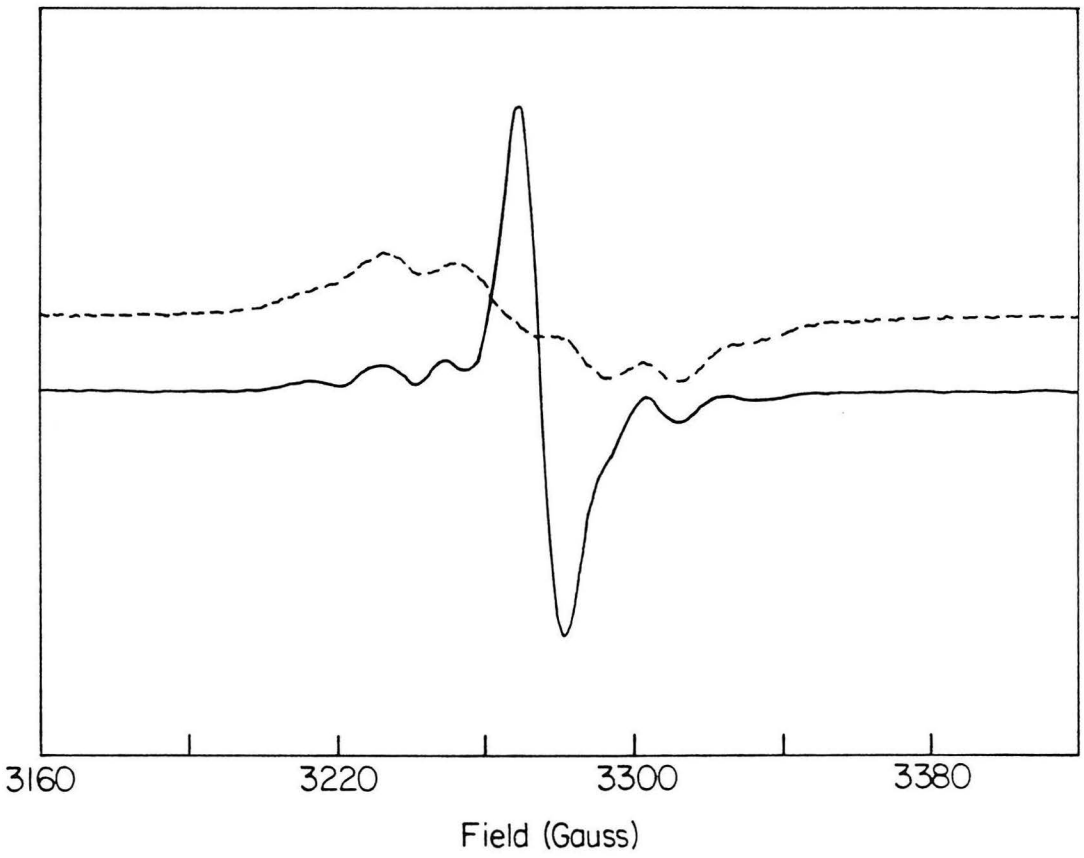

Figure 36. (a) ESR spectrum of blue-violet glass of H_2NN **3** (2-MTHF, 10°K). (b) ESR spectrum (10°K) of 2-MTHF radical(s) produced from photolysis of either trans-1,2-dimethyldiazene **8t** or di-tert-butyl peroxide in 2-MTHF glass, 77°K.

H abstraction from 2-MTHF solvent by D•. Failure to observe formaldehyde as a product from **3** in 2-MTHF may reflect a preference for H abstraction from solvent to H• addition to CO. However, in the absence of an abstraction pathway (Ar, 10°K) photolysis of **3** and **1** in the presence of CO then affords formaldehyde. No signal attributable to diazenyl radical (HNN•) was observed from VIS photolysis of **3** in 2-MTHF (10°K)[78] or in an argon matrix 10°K.[79] A concerted photochemical reduction of CO by **3** or **1** cannot be ruled out.

Thermal Decomposition Kinetics

The difficulties and perils associated with kinetic studies in rigid and softened organic glasses have been noted by others.[81] Frequently, very rapid non-exponential decays are noted in the decomposition of reactive intermediates in these media. A rigorous interpretation of this behavior is lacking, but may be ascribed to matrix site effects or contributions of quantum mechanical tunnelling. The rapid thermal decomposition of H_2NN **3** in a softened 2-MTHF glass at 90 ± 1°K was monitored spectroscopically at 636 nm. Early kinetic points prior to temperature equilibration (~30 min) were discarded. A linear least squares analysis reveals an apparent bimolecular decomposition pathway for **3** from the "best fit" 1/absorbance versus time plot (Figure 37). Assuming a molar extinction coefficient (ε) of 20 M^{-1} cm^{-1} (for kinetically persistent 1,1-diazenes $\varepsilon = 20 \pm 3\ M^{-1}\ cm^{-1}$) yields a corrected bimolecular rate constant of 7.2×10^{-4} M^{-1} sec^{-1} (r^2 = 0.991) at 90 ± 1°K. The estimated diffusional rate constant for 2-MTHF at

$90 \pm 1^{o}K$ is 4×10^{-6} 10^{2} M^{-1} sec^{-1}.[82] Hence, the observed bimolecular decay of **3** (k_2) is apparently greater than or equal to the estimated diffusional rate constant. Due to the extreme variation of solvent viscosity with temperature[82] the rate of decay of **3** was not determined as a function of temperature.

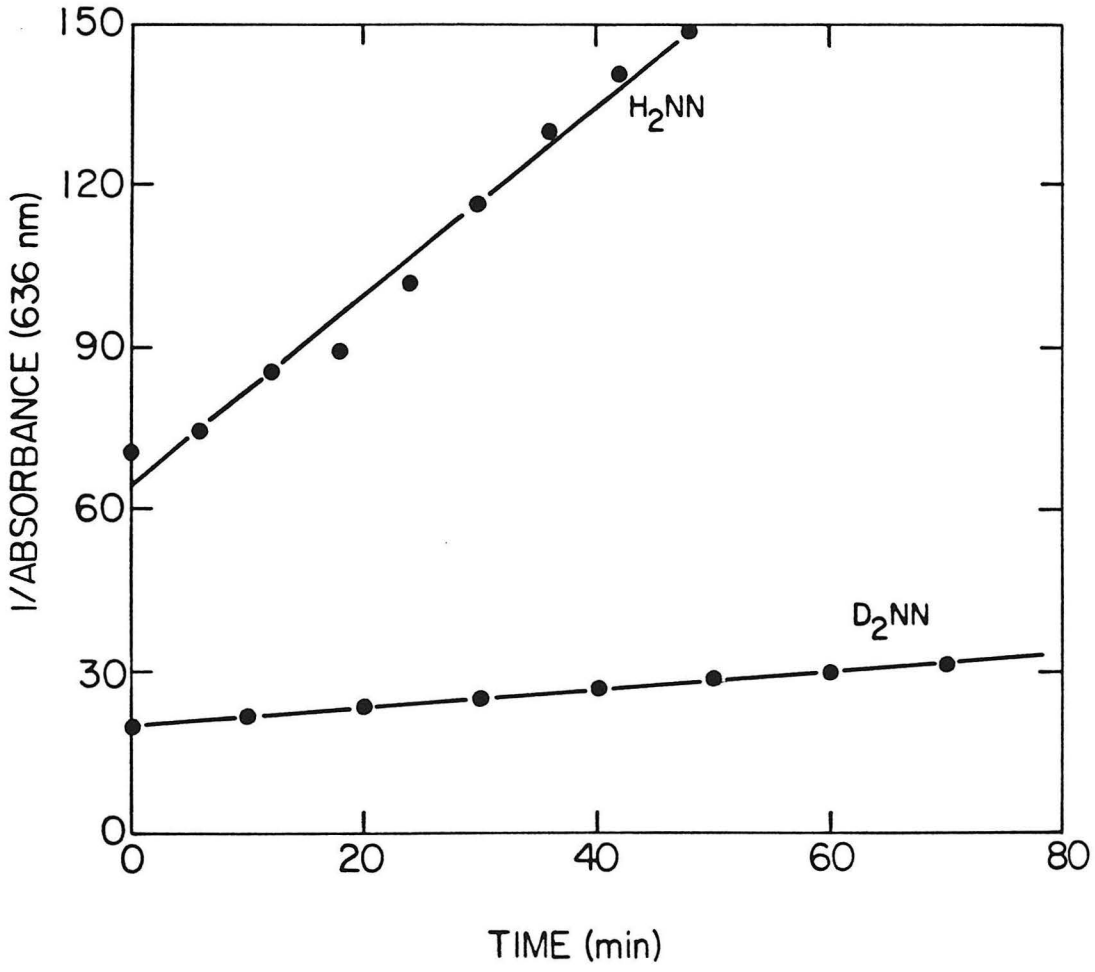

Figure 37. Bimolecular kinetic plots for decomposition of **3** and **3-d_2** at $90 \pm 1^{o}K$ in 2-MTHF from same initial concentration at $80^{o}K$.

Thermal decomposition of D_2NN **3-d$_2$**, prepared indentically to H_2NN **3**, in softened 2-MTHF at 90 ± 1°K affords the "best fit" kinetic plot shown in Figure 37. The corrected bimolecular rate constant of 6.8×10^{-5} M^{-1} sec^{-1} ($r^2 = 0.998$) is indicative of a substantial deuterium kinetic isotope effect $k_H/k_D \simeq 10.6 + 3$ at 90 ± 1°K. Simple head to head dimerization of **3** to afford 2-tetrazene **25** (as is observed for kinetically persistent 1,1-diazenes in solution)[8g] would be expected to show only a small inverse secondary isotope effect.

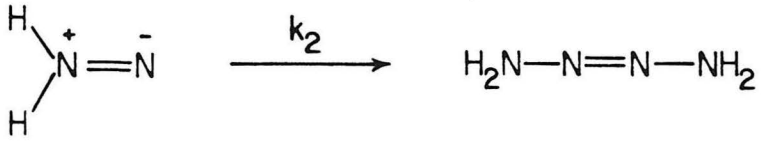

3 **25**

For a hybridization change from sp^3 to sp^2, a normal secondary isotope effect is typically $k_H/k_D \simeq 1.1$ to 1.4 per deuterium at 298°K. This would correspond to $k_H/k_D = 1.4$ to 3.1 per deuterium at 90°K. For comparison, a normal primary isotope effect $k_H/k_D \simeq 5$ at 298°K corresponds to a $k_H/k_D \simeq 200$ at 90°K. Clearly a simple head-to-head dimerization of **3** to **25** at 90°K (sp^2 to sp^3, $k_H/k_D \simeq 0.71$ to 0.32 per deuterium) would not account for the observed isotope effct for bimolecular decomposition of **3**.

The observed kinetic isotope effect may be consistent with the mechanism proposed in Scheme IV.

Scheme IV

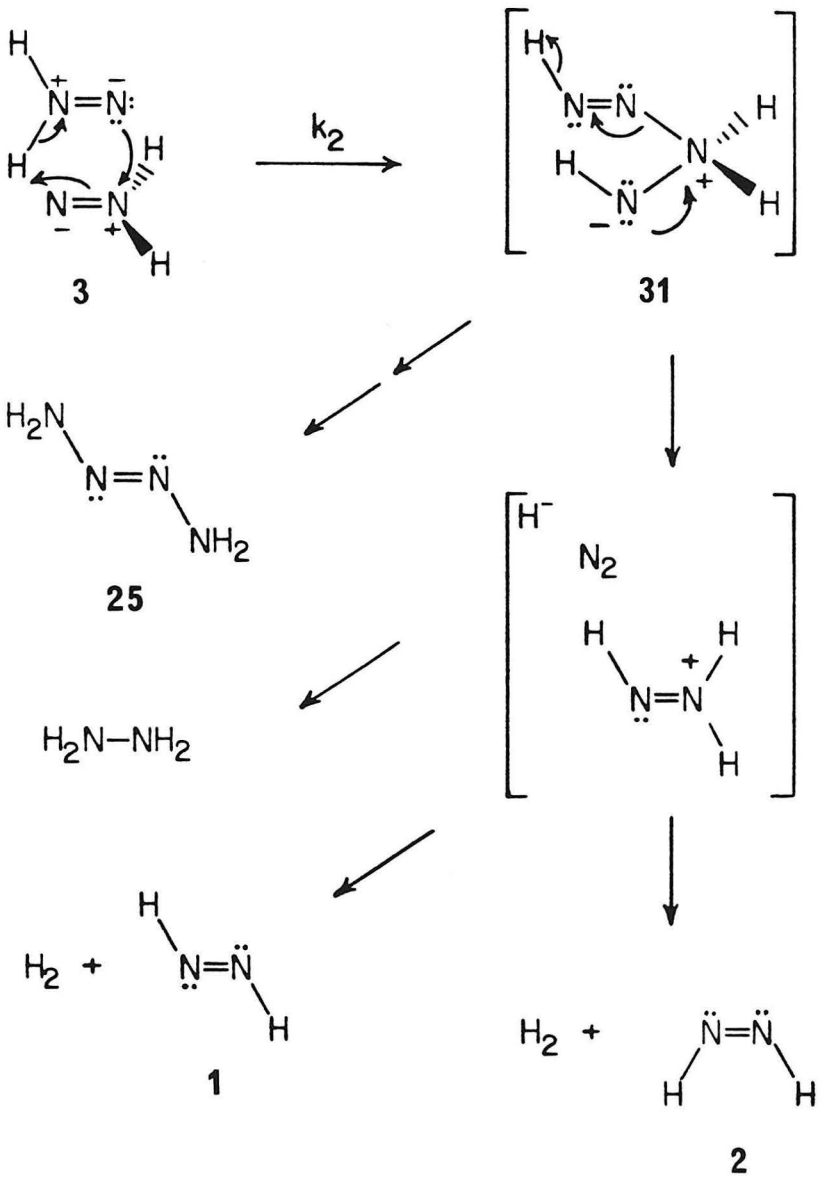

An initial concerted $w2s + \pi 2s + \sigma 2s$ head-to-tail dimerization of **3** to afford intermediate **31** as the rate determining step would be expected to show the observed bimolecular decomposition kinetics and a deuterium isotope effect of approximately $k_H/k_D \simeq 200/(3.2)^2 \simeq 20$. This value is comparable to the observed value $k_H/k_D = 10.6 \pm 3$ at 90 ± 1^oK. Tautomerization of **31** to afford 2-tetrazene **25** competitive with hydride elimination and subsequent disproportionation to afford trans HNNH **1**, cis HNNH **2**, H_2 and N_2 or addition to afford hydrazine would account for the products observed from thermal decomposition of **3**. Unfortunately, kinetics for formation of **1** ($\lambda_{max} = 386$ nm), **2** ($\lambda_{max} = 480$ nm) (tentative identification) and tetrazene **25** gave inconsistent results. Subsequent thermal decomposition of **1** and the $\lambda_{max} = 480$ nm species at 90 to 100^oK were also inconsistent and do not support a clear interpretation.

The mechanism of Scheme IV may be consistent with the low activation energy ($E_a \leq 5$ kcal/mol) necessary for the facile thermal decompositions observed at these low temperatures (assuming $\log A \leq 5$). However, any mechanistic considerations derived from the limited kinetic data presented must be tempered with the consideration of alternative mechanisms. Due to the presence of radicals (e.g., •MTHF) in samples of **3** prior to thermolysis (see previous section) a facile radical chain decomposition of **3**, **1**, **2**, and **25** cannot be excluded. This alternative mechanism could provide the necessary rapid, low E_a pathway for the observed decompositions.

Unsuccessful attempts were made to prepare **3** isolated in a "rigid" high temperature matrix (e.g., adamantane, polymethylmethacrylate,

polyethylene) in order to investigate the "non-diffusive" unimolecular thermochemistry of **3**. It was hoped that activation parameters could be derived for comparison with theoretical calculations for the N-H bond strength of **3** and the H_2N_2 energy surface. However, in all cases the blue-violet color of **3** was lost well below 200°K, resulting in formation of the yellow color of trans **1**. It is unknown whether this isomerization of **3** to **1** is the result of diffusion of **3** in these "rigid" matrices, well below their softening points or whether a low activation energy pathway for unimolecular decomposition of **3** (e.g., tunnelling) exists. The yellow color of **1** persists for several days at 298°K in a polymethylmethacrylate matrix. This is suggestive of slow diffusion in this matrix. In contrast, the blue-violet color of **3** in this matrix is gone in less than 20 seconds upon warming from 77°K to 120°K.

Summary

The low temperature matrix isolation and direct spectroscopic characterization of the parent 1,1-diazene H_2NN **3** has been described. The UV (VIS filtered) photolysis of carbamoyl azide **15** in a rigid medium (2-MTHF glass, 80°K or Ar matrix, 10°K) provides a new method for the generation of reactive 1,1-diazenes. This photochemical rearrangement is considered to proceed by the photo-Curtius rearrangement of **15** to aminoisocyanate followed by photodecarbonylation of the aminoisocyanate to afford H_2NN **3** and carbon monoxide. H_2NN is a blue-violet species λ_{max} = 636 nm displaying the now characteristic structured absorption curve

of a 1,1-diazene. The characteristic N=N double bond stretch for **3** is located at 1574.16 cm^{-1}. This is consistent with the theoretical (GVB-CI) prediction for H_2NN. Isotopic labeling (D, ^{15}N) has provided identification of the infrared active modes for **3**, **3-^{15}N**, **3-d_2**, **and 3-d_2-^{15}N**. No emission was detected from irradiation of **3** at its n-π^* transition consistent with very rapid internal conversion ($k_{IC} \sim 10^{12}$ sec^{-1}) controlling the lifetime of the excited state (S_1). This in turn is consistent with the relatively small S_0-S_1 gap of 41.5 kcal/mol in **3**. The products of thermal and photochemical decomposition of **3** were determined. Thermolysis of **3** (2-MTHF, 90°K) affords tetrazene **25** (λ_{max} = 260 nm) at a nearly diffusion controlled rate as expected. Additionally, thermolysis of **3** affords yellow <u>trans</u> HNNH **1** (λ_{max} = 386 nm) and another species λ_{max} = 480 nm tentatively identified as <u>cis</u> HNNH **2**. The mechanism for formation of these unexpected products is unknown but suggests that **3** is indeed a higher energy species than **1** and **2**. Photolysis of **3** (2-MTHF, 80°K and Ar, 10°K) affords some <u>trans</u> HNNH **1** together with H_2 and N_2. Photolysis of **3** in the presence of CO (Ar, 10°K) also affords formaldehyde (H_2CO). The photochemical isomerization of **3** to **1** can be compared to the proposed isoelectronic photochemical isomerization of H_2CO to hydroxycarbene which has been invoked to explain the much disputed formaldehyde photochemistry.[66,94] Attempts to detect diazenyl radical (HNN·) in the photodecomposition of **3** by ESR and matrix FT-IR were unsuccessful. Attempts at photochemical isomerization of <u>trans</u> **1** to <u>cis</u> **2** were inconclusive. The observation of several FT-IR stretching frequencies for CO mirroring the photochemical behavior of diazenes **3**

and **1** and their photodecomposition products in solid matrices (Ar, N_2, 10°K) suggests an intimate association of these diazenes and the CO side product in a rigid low temperature matrix.

RESULTS AND DISCUSSION

CHAPTER 2

1,1-Diazenes With α-Hydrogens. Matrix Isolation and Characterization of 1,1-Dimethyldiazene and 1,1-Diisopropyldiazene

Synthesis of Carbamoyl Azides

Reaction of the requisite dialkyl amine with phosgene at low temperatures affords dialkyl carbamoyl chlorides **21**[47] and **22**.[83] Carbamoyl azides **13** and **17** are easily prepared by the reaction of sodium azide with the corresponding carbamoyl chloride in dry acetonitrile.[47] Preparative VPC affords analytically pure carbamoyl azides **13** and **17**.

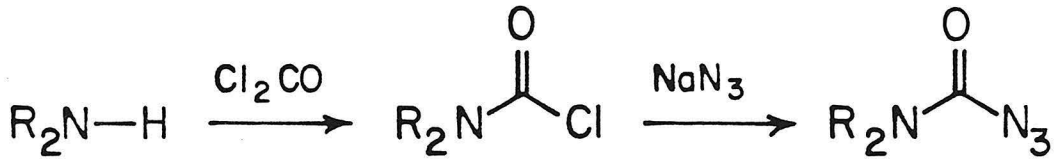

$R = CH_3$	**21**	**13**
$R = (CH_3)_2CH$	**22**	**17**

Electronic Absorption Spectra of 1,1-Diazenes 7 and 18

For electronic absorption spectroscopy of 1,1-diazenes **7** and **18**, a dilute ($\sim 5 \times 10^{-3}$ M)[102] solution of the freshly purified carbamoyl azide in dry, degassed 2-methyltetrahydrofuran (2-MTHF) was loaded into a 1.0 cm path length low temperature spectroscopic cell[50] attached to the low temperature matrix isolation apparatus. The solution was loaded under a positive pressure of argon through Teflon tubing with syringe suction. Cooling the solution to 80°K results in the formation of a rigid optically transparent glass.

Irradiation of carbamoyl azide **13** in a 2-MTHF glass at 80°K with ultraviolet (UV) light from a 1000 watt xenon lamp[51] through two Corning CS-7-54 (UV transmitting, visible (VIS) λ 400-680 nm cut-out) filters results in loss of the UV absorption of the carbamoyl azide and formation of a red-orange glass. Electronic absorption spectroscopy of this red-orange glass reveals a structured absorption curve λ_{max} = 556 nm (51.5 kcal/mol) and $\lambda_{0,0}$ = 653 nm (43.9 kcal/mol)[52a] assigned to 1,1-dimethyldiazene **7** together with a structureless absorption due to another species λ_{max} = 464 nm (Figure 38). Similarly, irradiation of carbamoyl azide **17** in a dilute glass (~ 5 x 10^{-3} M, 2-MTHF, 80°K)[102] affords a purple glass. Electronic absorption spectroscopy reveals a structured absorption curve λ_{max} = 504 nm (52.7 kcal/mol) and $\lambda_{0,0}$ = 620 nm (46.2 kcal/mol)[52a] of 1,1-diisopropyldiazene **18** (Figure 39). These structured absorptions are close to

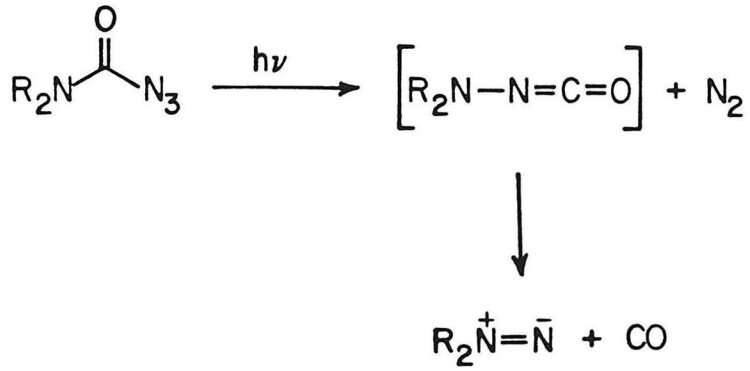

R = CH_3	**13**	**7**
R = $(CH_3)_2CH$	**17**	**18**

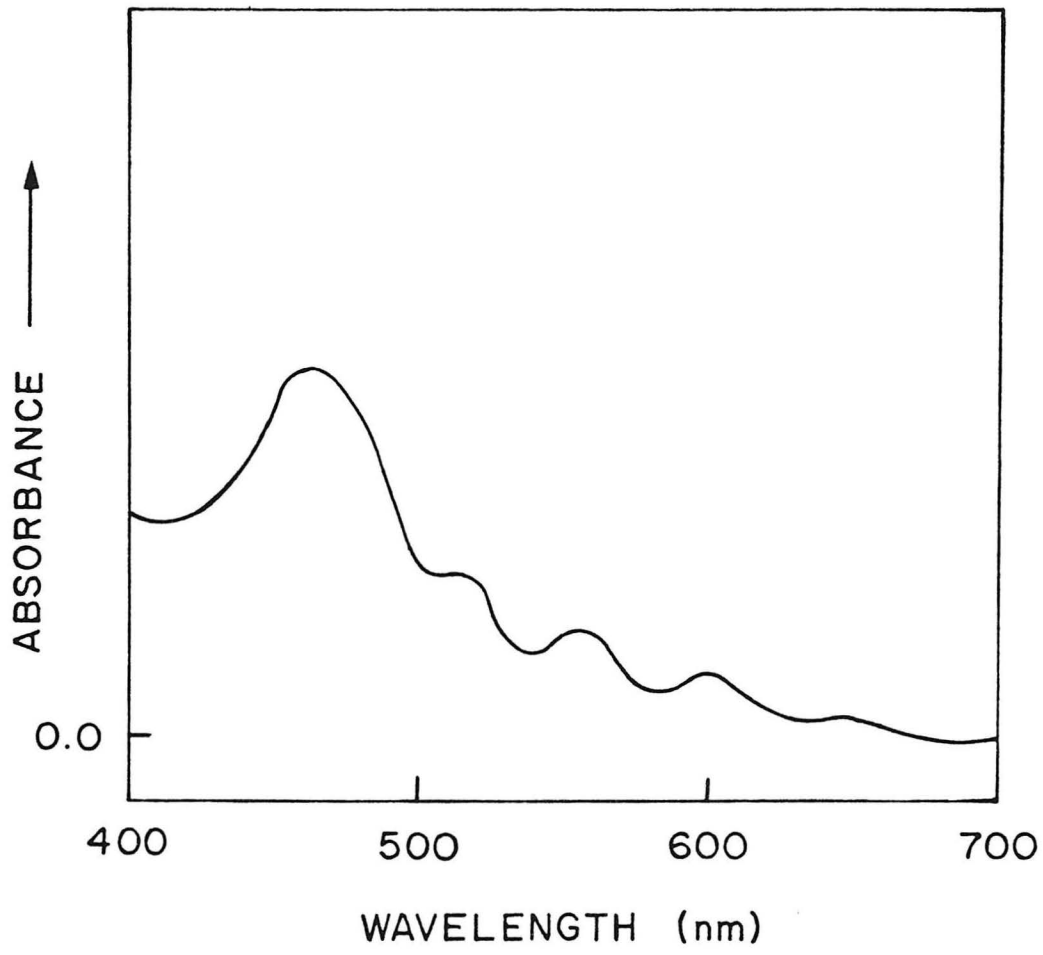

Figure 38. Electronic absorption spectrum of 1,1-dimethyldiazene **7** and λ_{max} = 464 nm co-product (2-MTHF glass, 80°K).

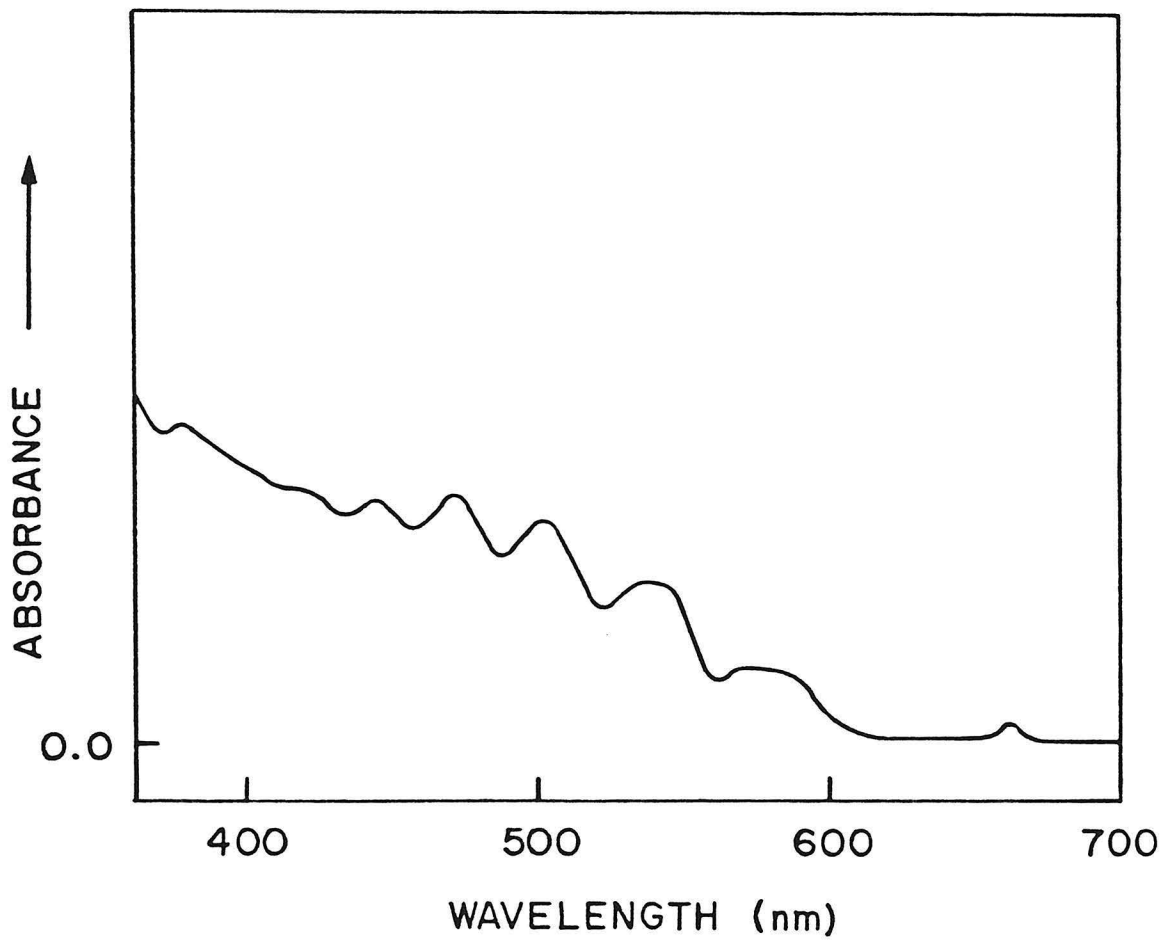

Figure 39. Electronic absorption spectrum of 1,1-diisopropyldiazene **18** (2-MTHF glass, 80°K)

Table XX. 1,1-Diazene Electronic Transitions.

1,1-Diazene		λ_{max} (nm)	$\lambda_{0,0}$ (nm)	$\bar{\nu}$ cm^{-1}	$E(S_0\text{-}S_1)$ (max) (kcal)
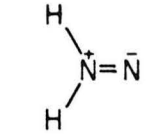	**a**	636	695	1315	45.1
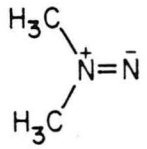	**a**	556	653	1315	51.5
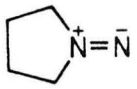	**c**	528	614	1340	54.6
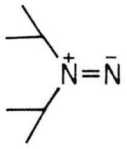	**a**	504	580	1306	56.8
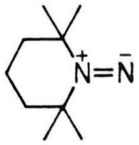	**b**	543	610	1040	52.7
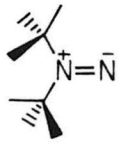	**b**	506	620	1200	56.6
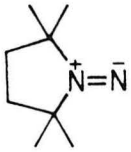	**b**	497	572	1238	57.6

[a]This work. 2-MTHF glass, 80°K. [b]Me_2O solution. Ref. 8e,f. [c]Ref. 84. 2-MTHF glass, 80°K.

the n-π* transition calculated by Davis and Goddard[1n] for H_2NN **3** near 560 nm. The kinetically persistent 1,1-dialkyl diazenes **4**, **5**, and **6** prepared earlier in the Dervan group were found to have similar structured absorptions (λ_{max} = 497 to 543 nm) due to this n-π* transition in the visible.[8e,f] The parent 1,1-diazene **3** has also been shown to be a blue-violet species with a structured absorption λ_{max} = 636 nm in a 2-MTHF glass at 80°K.[4] The characteristic n-π* transitions for 1,1-diazenes are summarized in Table XX.

The structure in the absorption spectrum of 1,1-diazenes is assigned to the vibrational spacing of the excited state (S_1). The prominence of this N-N stretching mode is indicative of a substantial change in Re(NN) on excitation from ground state (S_0) to S_1. The calculations of Davis and Goddard[1n] indicate an optimal pyramidal geometry for S_1 of **3**. The experimental average vibrational spacing for **3** is 1315 cm^{-1}. Comparison with the calculated N-N stretch for S_1 of **3** (1357 cm^{-1})[52b] may indicate a preference for pyramidalization over two center three electron bonding in S_1 of **3**. The average vibrational spacing in S_1 of 1,1-dimethyldiazene **7** is 1315 cm^{-1} comparable to that of **3**. By comparison, the average spacing in S_1 of 1,1-diisopropyldiazene is 1306 cm^{-1}. The smaller vibrational spacings observed for the kinetically persistent 1,1-diazenes with tertiary alkyl substituents in solution (1040 to 1238 cm^{-1}) may be reflective of the poorer resolution of their vibrational structure. In general, pyramidalization should stabilize 1,1-diazene S_1 states by relieving nitrogen lone pair-alkyl group repulsions. These interactions are certainly more severe in tertiary substituted 1,1-diazenes. The observed lower S_1 N-N vibrational frequencies in the

Table XXI. Comparison of 1,1-Diazene and Corresponding Carbonyl Electronic Transitions.

1,1-Diazene	λ_{max} (nm)	$E(S_0-S_1)$ (kcal)	$E(S_0-S_1)$ (kcal)	λ_{max} (nm)	Carbonyl[c]
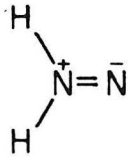 [a]	636	45.1	92.4	310	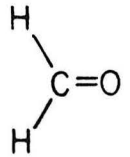
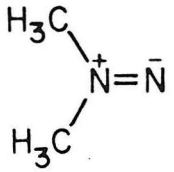 [a]	556	51.5	102.6	279	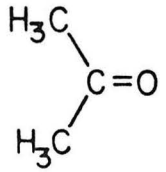
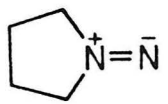 [d]	528	54.6	95.5	300	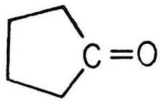
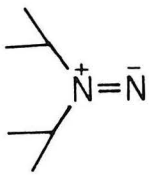 [a]	504	56.8	99.4	288	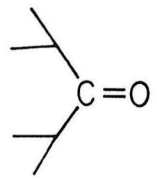

Table XXI. Continued.

1,1-Diazene	λ_{max} (nm)	$E(S_0-S_1)$ (kcal)	$E(S_0-S_1)$ (kcal)	λ_{max} (nm)	Carbonyl [c]
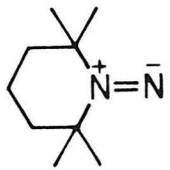 [b]	543	52.7	93.9	305	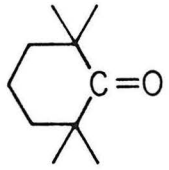
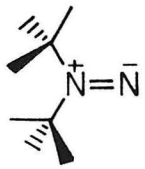 [b]	506	56.6	96.4	297	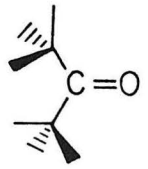
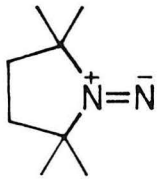 [b]	497	57.6	96.7	296	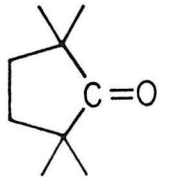

[a]This work. 2-MTHF glass, 80°K. [b]Me_2O solution. Ref. 8e,f. [c]n-Alkane solution. Ref. 85. [d]Ref. 84. 2-MTHF glass, 80°K.

kinetically persistent 1,1-diazenes would be consistent with this explanation. However, in the absence of tertiary alkyl-lone pair repulsive interactions the average vibrational frequency in S_1 should follow a trend indicative of the necessity to relieve alkyl-lone pair repulsions. Small groups (e.g., H, Me) should require less pyramidalization. Larger groups (e.g., i-Pr) should require more pyramidalization resulting in a lower S_1 vibrational frequency (as is observed). In the unsubstituted five-membered ring 1,1-diazene pyramidalization is restricted resulting in more two center three electron bonding and higher N-N vibrational frequency in S_1. The electronic n-π^* transitions of 1,1-diazenes show a trend similar to that observed in the isoelectronic carbonyl compounds (Table XXI).

1,1-Dimethyldiazene **7** was also prepared by UV (VIS filtered) photolysis of (Z)-3,3-dimethyl-1-phenyltriazene-1-oxide[40] **16** in a rigid 2-MTHF glass (80°K) affording the structured absorption curve of **7** (purple, λ_{max} = 556 nm) together with the structured absorption of nitrosobenzene (blue, λ_{max} 780 nm, ε = 45) (Figure 40). Comparison of these absorbances

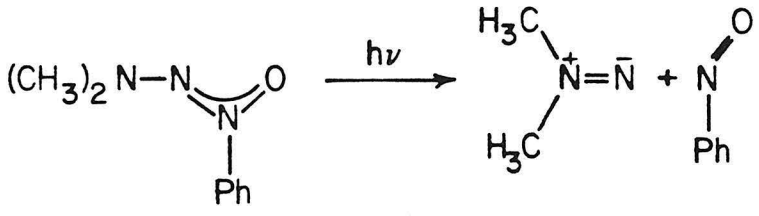

16 **7**

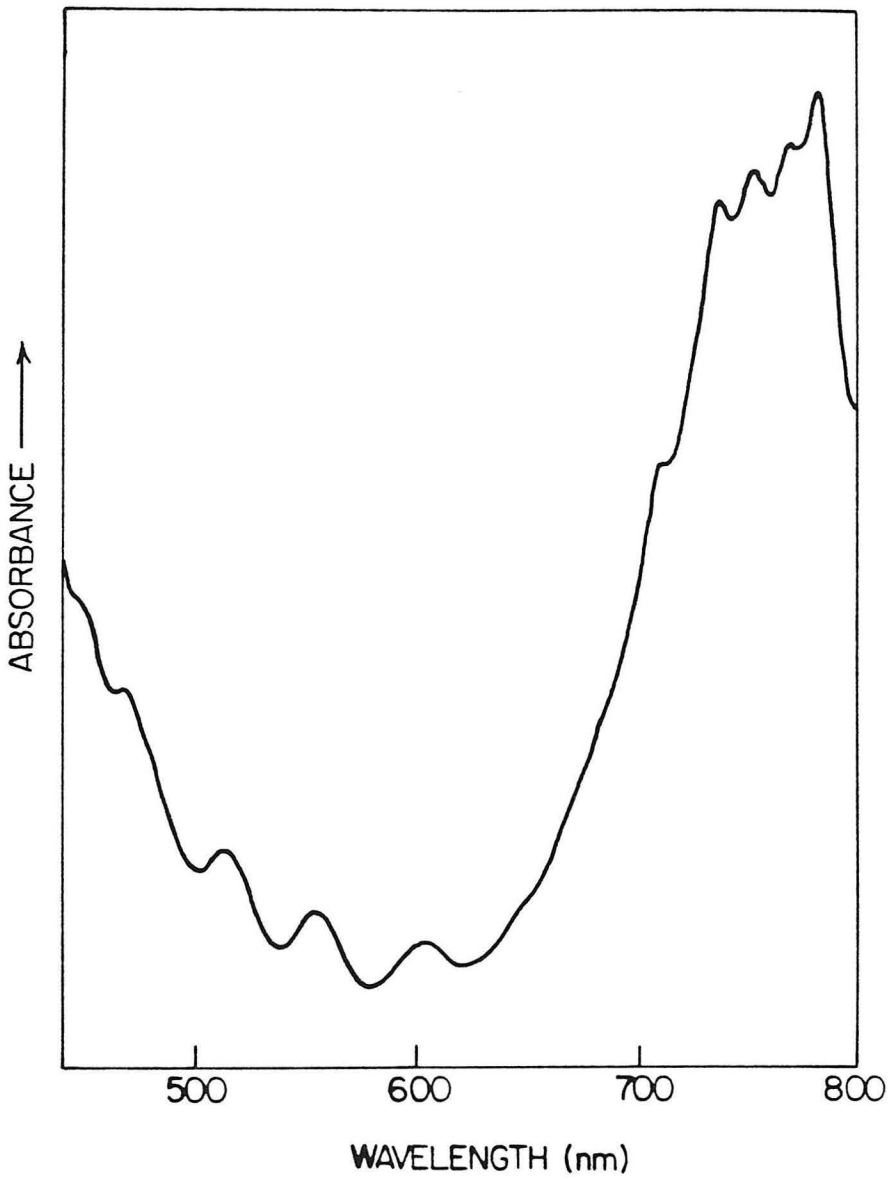

Figure 40. Electronic absorption spectrum of 1,1-dimethyldiazene **7** (λ_{max} = 556 nm) and co-product nitrosobenzene (λ_{max} = 780 nm) from UV (VIS filtered) photolysis of **16** (2-MTHF, 80°K).

provides an estimate for the molar extinction coefficient for **7** of $\varepsilon = 6$ (M^{-1} cm^{-1}). Warming the glass gives a nearly quantitative (>90%) yield of tetramethyl-2-tetrazene **19** and nitrosobenzene.

Thermal Decomposition of 1,1-Diazenes 7 and 18

Warming a 2-MTHF glass of **7** to softening at 90°K results in loss of the structured absorption curve due to **7** (Figure 38) and formation of a red-orange species (λ_{max} = 464 nm) (Figure 41) together with growth of the UV absorption due to tetramethyl-2-tetrazene **19** (λ_{max} = 280 nm). Warming this softened glass to greater than 180°K results in loss of the λ_{max} = 464 nm absorption and growth of the UV absorption due to tetrazene **19**. Tetrazene **19** is obtained in nearly quantitative yield from **13** overall.

Similarly, warming a 2-MTHF glass of 1,1-diisopropyldiazene **18** to 90°K results in loss of the structured absorption curve due to **18** (Figure 39) and formation of a red-orange species (λ_{max} = 474 nm) (Figure 42) together with growth of the UV absorption due to tetraisopropyl-2-tetrazene **20** (λ_{max} = 290 nm). Warming this softened glass to greater than 200°K results in loss of the red-orange species (λ_{max} = 474 nm) and formation of products expected from thermal decomposition of **18**. Attempts to detect the 1,1-diazenes **7** and **18** in these warmed red-orange solutions in possible equilibrium with the λ_{max} = 464 or λ_{max} = 474 nm species, respectively, by electronic spectroscopy were unsuccessful.

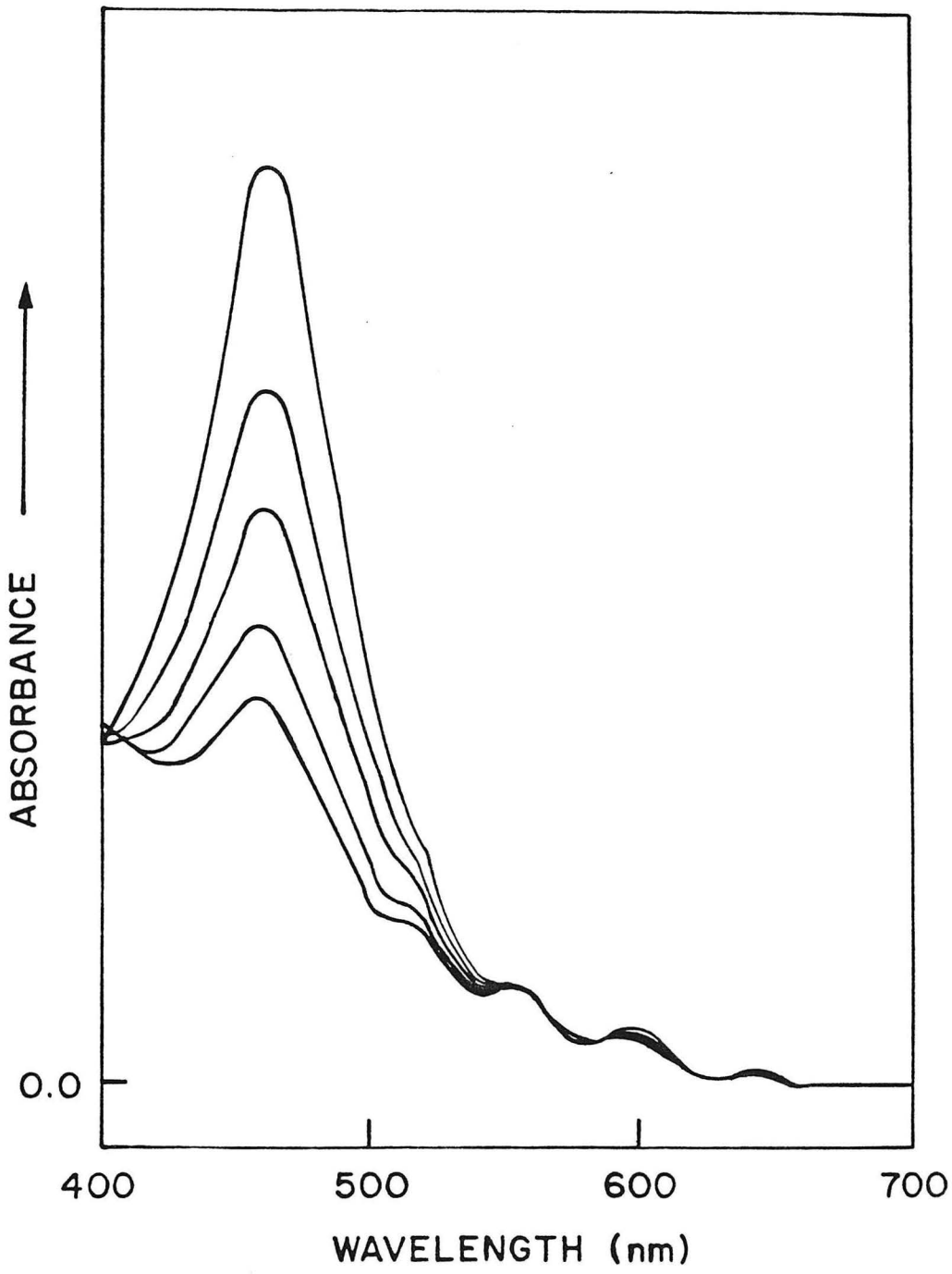

Figure 41. Thermolysis of 1,1-diazene **7** (2-MTHF, 90°K), 10 min intervals.

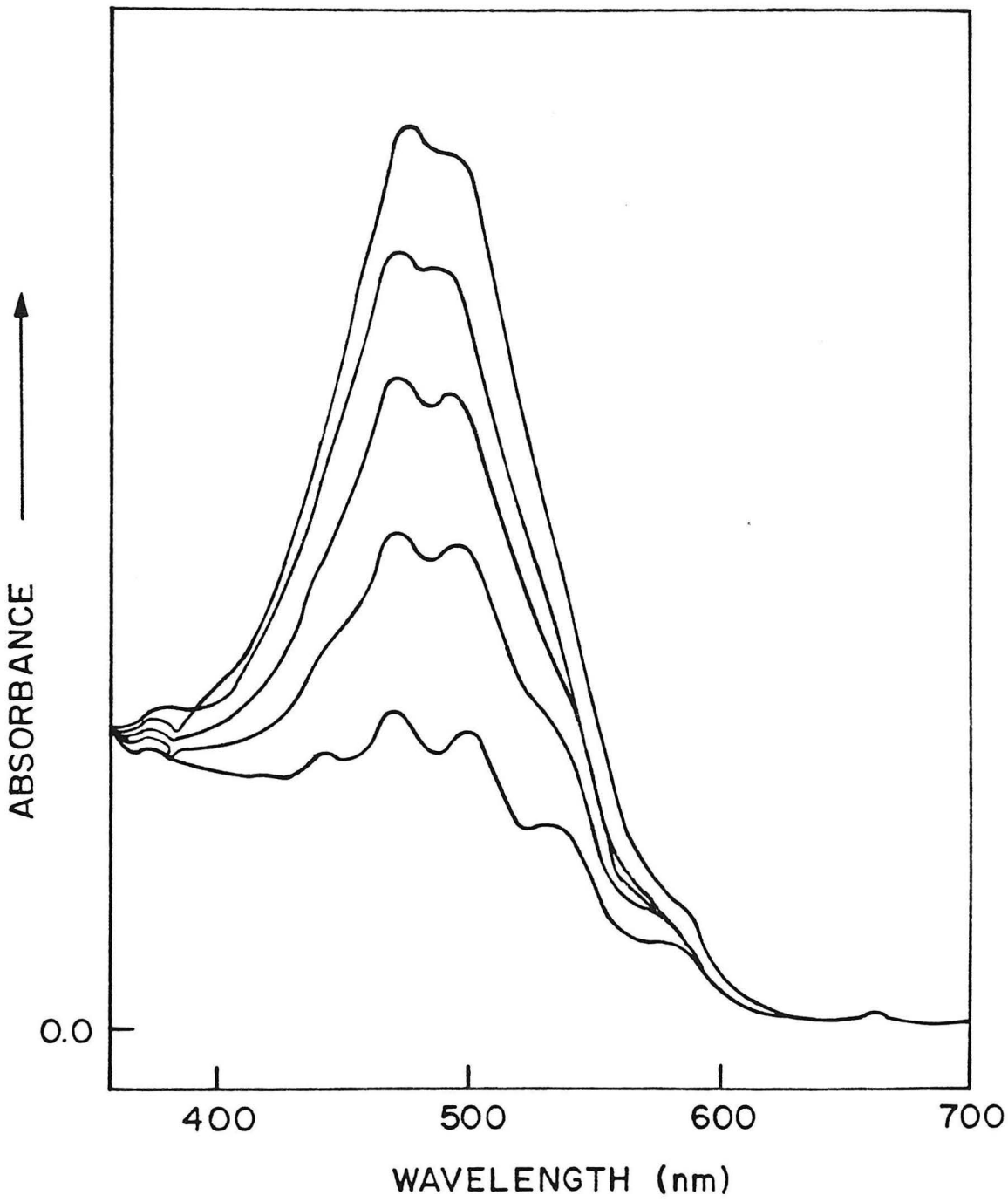

Figure 42. Thermolysis of 1,1-diazene **18** (2-MTHF, 90-^{o}K), 10 min intervals.

Photochemical Decomposition of 1,1-Diazenes 7 and 18

1,1-Diazenes have been shown to decompose when irradiated at their n-π^* transitions in the visible. Irradiation of a 2-MTHF glass of **7** with visible light (VIS, 2 h) from Corning filters CS-1-75, CS-3-70, and CS-4-96 (λ 470-610 nm) results in loss of the structured absorption of **7** and growth of the absorption λ_{max} = 464 nm due to the red-orange species. Extended VIS photolysis results in no detectable decrease in the 464 nm absorption. A mixture of ethane and tetrazene **19** are obtained upon warming the glass to room temperature. Ethane is the expected photochemical decomposition product of **7**. Similarly, VIS photolysis of a 2-MTHF glass of **18** with Corning filters CS-1-75 and CS-3-70 (>470 nm) results in loss of the structured absorption of **18** and formation of the red-orange species λ_{max} 474 nm. Extended VIS irradiation (10 h) results in no detectable loss of the λ_{max} = 474 nm transition. A mixture of hydrocarbon products expected from thermal and photochemical decomposition of **18** together with tetrazene **20** are obtained upon warming the red-orange glass. Full product analysis for thermal and photochemical decomposition of **7**, **18** and kinetics for thermal decomposition are reported in a later section. Similar behavior was obtained in several other glass forming solvents including 3-methyl pentane, triacetin and methylmethacrylate. One possible explanation for the red-orange species obtained from 1,1-diazenes **7** and **18** might be the cis-2-tetrazene isomers of the corresponding trans-2-tetrazene products ultimately observed. However, UV (VIS filtered) irradiation of trans-2-tetrazenes **19** and **20** in a rigid 2-MTHF glass (80°K) gave no red-orange coloration and no detectable visible

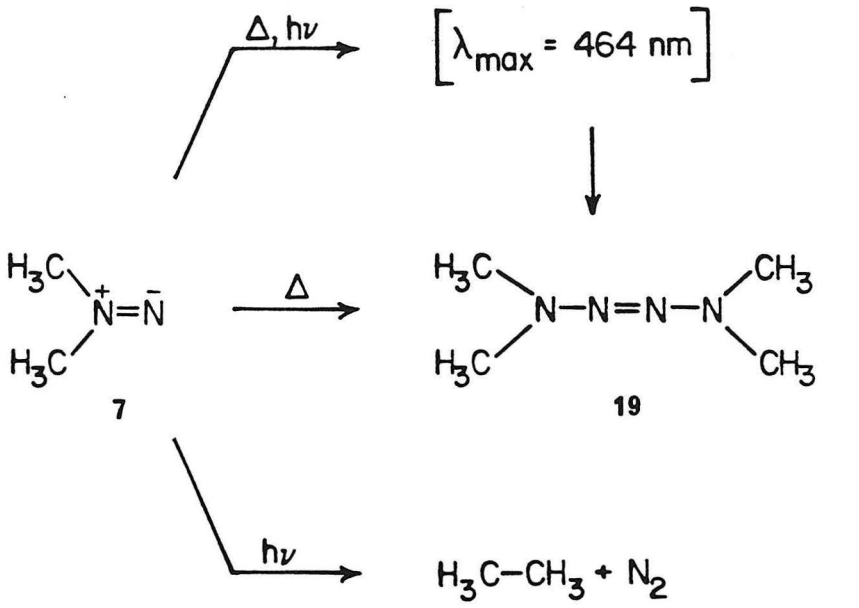
Δ, hν
[λmax = 464 nm]
H3C
N=N
H3C
Δ
H3C
N–N=N–N
H3C
CH3
CH3
7
19
hν
H3C–CH3 + N2

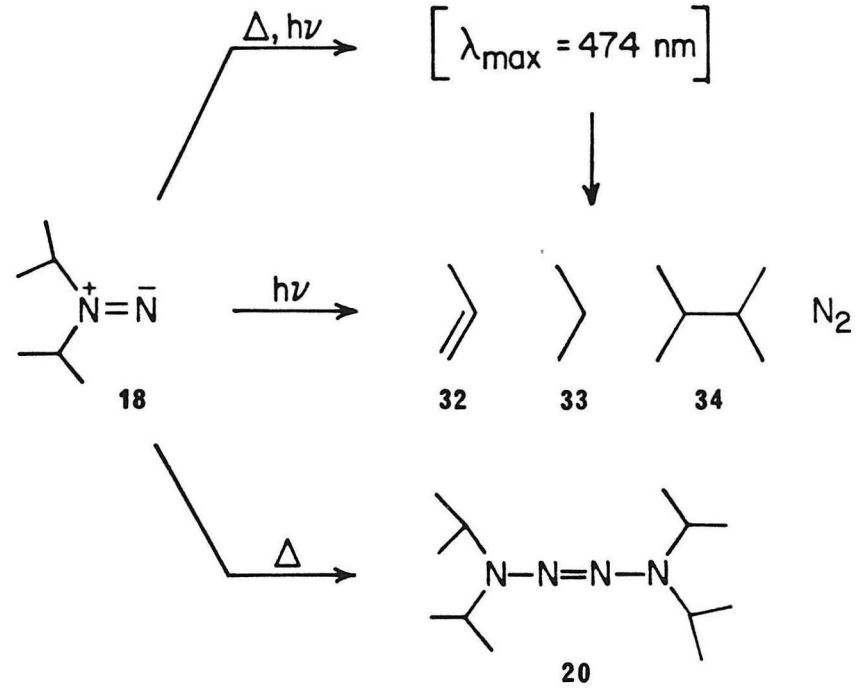
Δ, hν
[λmax = 474 nm]
N=N
hν
N2
18
32
33
34
Δ
N–N=N–N
20

transitions between 350 and 750 nm. This is consistent with exclusion of the corresponding cis-2-tetrazenes as the species responsible for the λ_{max} 464 and 474 nm transitions from 1,1-diazenes **7** and **18**, respectively. In addition, warming a rigid glass of **7** or **18** in triacetin to 150°K (still rigid), results in loss of **7** and **18** and formation of the λ_{max} = 464 and λ_{max} = 474 nm species respectively. Hence, diffusion of the 1,1-diazenes is apparently unnecessary for the observed thermal decomposition.

Matrix Isolation Infrared Spectroscopy of 1,1-Dimethyldiazene 7

For infrared studies a gas mixture of freshly purified dimethyl carbamoyl azide **13** in ultra high purity argon (1:1400, Ar) was deposited onto a cesium iodide (CsI) inner window of the matrix isolation apparatus at 20°K. The resulting argon matrix of **13** was slowly lowered to 10°K. Figure 43 shows the FT-IR spectrum of **13**. Table XXII summarizes the assignments for the infrared bands of **13** and co-condensed atmospheric impurities (H_2O, CO_2). Irradiation (1 h) of matrix isolated **13** with UV (VIS filtered) light from two Corning CS-7-54 filters results in loss of the infrared bands of **13** and formation of product bands. Subtraction of the FT-IR spectrum of **13** from the FT-IR spectrum resulting from UV photolysis of **13** clearly shows these product bands (Figure 44). These bands are divided into five groups. Assignments are based on thermal and photochemical behavior and comparison to authentic argon matrix infrared spectra. The first column of Table XXIII lists the products from UV photolysis of **13** and their assignments.

The first group of bands labeled (I) are assigned to dimethylaminoiso-

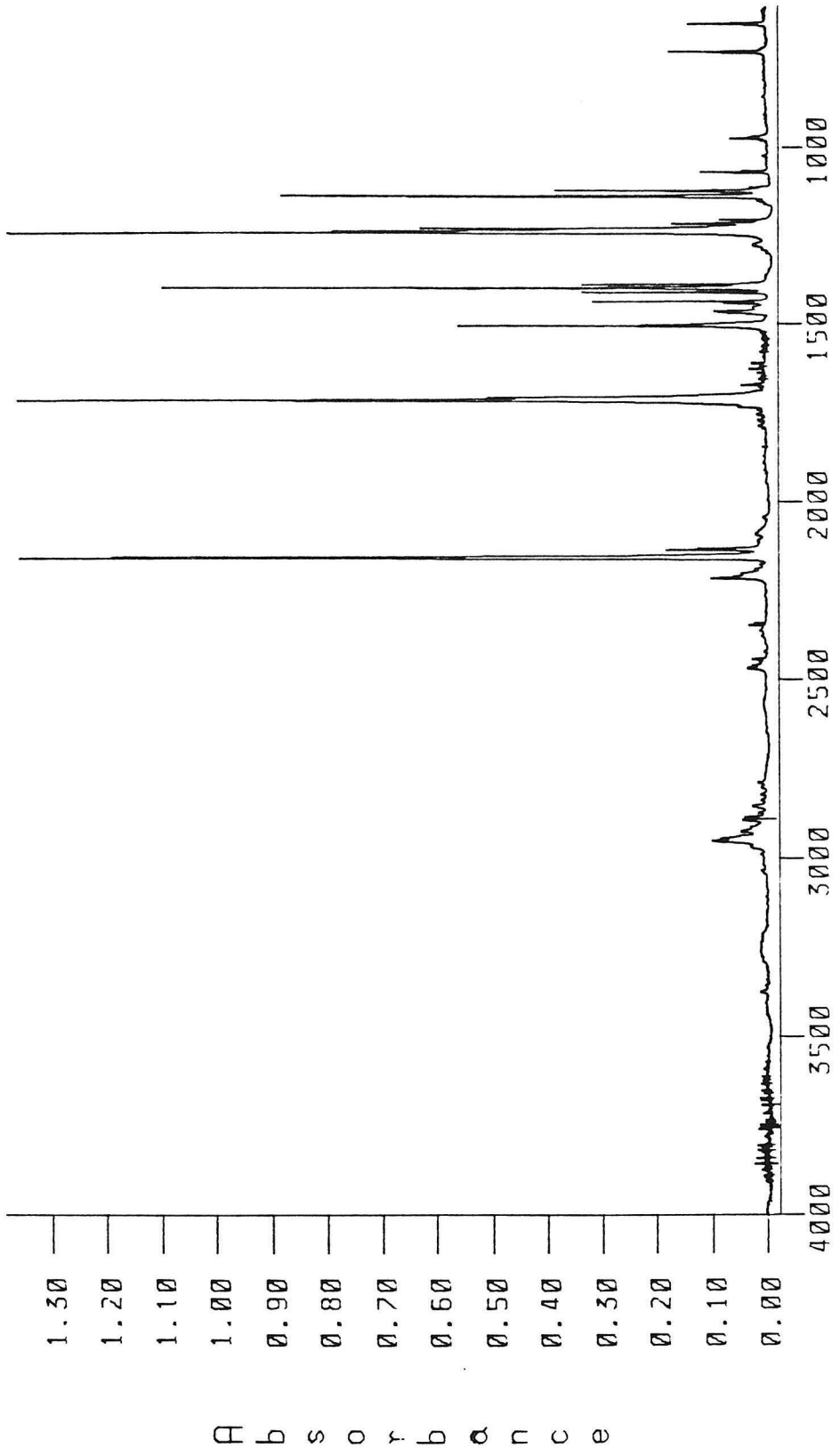

Figure 43. FT-IR spectrum of **13**, 120 mm deposition (1:1400, Ar, 10°K).

Table XXII. FT-IR Bands for **13** in Argon Matrix (120 mm) (1:1400, 10°K) Threshold 0.05 A.

Peak Location (cm^{-1})	Intensity (A)	Assignment
2949.45	0.10	ν C-H
2943.25	0.09	
2936.07	0.05	
2923.22	0.05	
2345.03	0.08	CO_2, ν CO
2339.00	0.05	CO_2, ν CO
2213.05	0.06	
2208.53	0.06	
2156.75	1.36	ν N_3 (asym)
2152.91	1.20	ν N_3
(2146.12)	0.14	
(2133.80)	0.18	
(2128.99)	0.12	
1713.47	1.36	ν NCO (asym)
1705.59	0.51	
1502.88	0.56	
1466.83	0.07	
1461.09	0.09	
1439.14	0.08	
1434.59	0.32	δ CH_3
1432.92	0.15	
1410.45	0.11	
1408.85	0.34	δ CH_3
1407.49	0.22	
1398.37	0.64	
1396.22	1.10	ν NCO (sym)
1386.22	0.34	

Table XXII. Continued.

Peak Location (cm^{-1})	Intensity (A)	Assignment
1240.60	1.39	ν N_3 (sym)
1236.59	0.79	
(1232.42)	0.56	
1228.31	0.63	
(1221.28)	0.10	
(1215.58)	0.17	
(1212.51)	0.09	
(1203.72)	0.09	
1138.53	0.83	ρ CH_3
1136.89	0.89	
1124.99	0.14	
1121.41	0.39	
1071.63	0.06	
1069.83	0.12	γ CH_3
1066.23	0.05	
973.81	0.07	ν C-N (asym)
729.76	0.08	
726.51	0.18	δ N_3
648.12	0.14	ν N-C (sym)
644.85	0.06	

( ) = ^{15}N labeled (13-^{15}N) as impurity

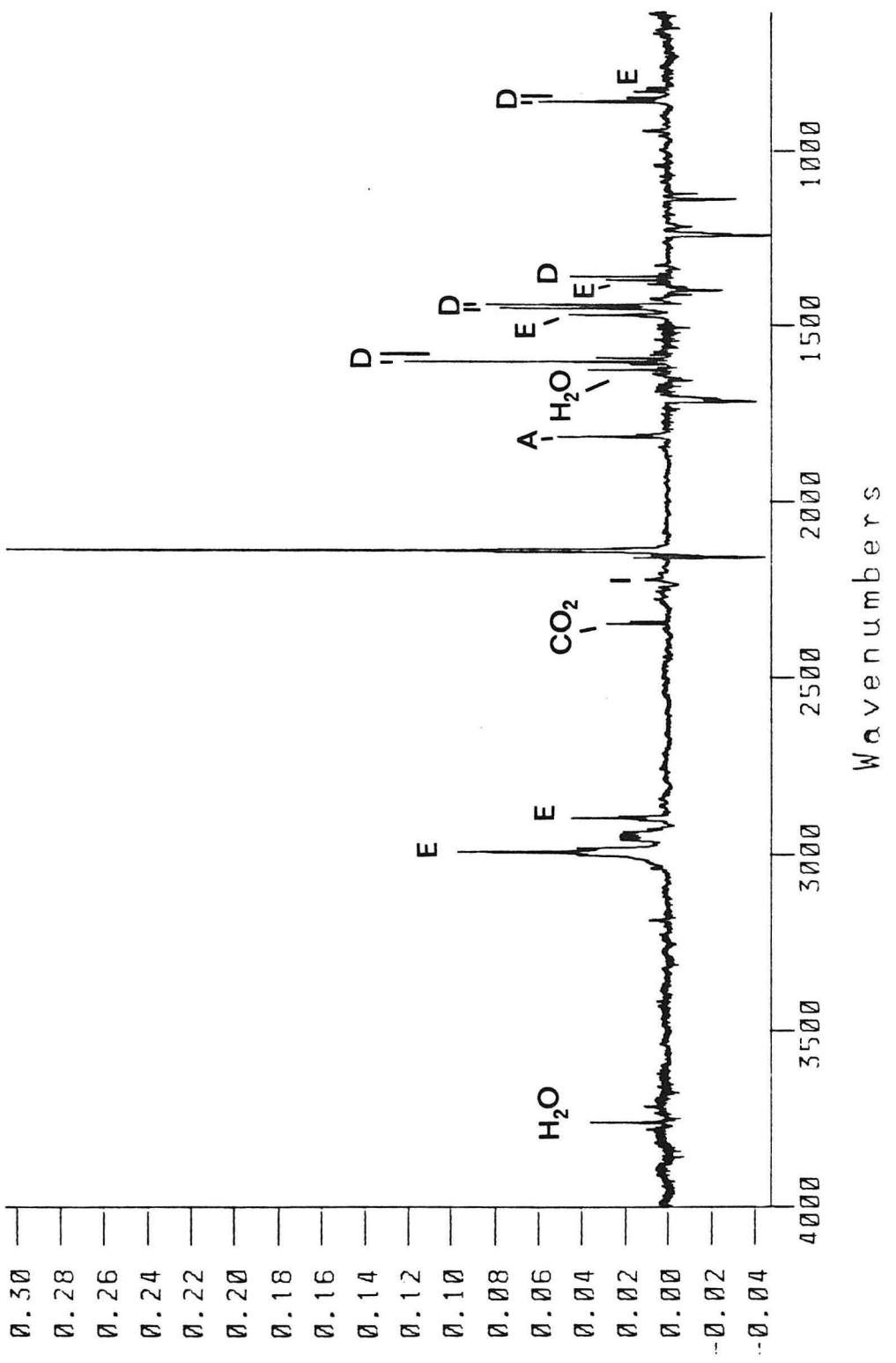

Figure 44. Difference FT-IR spectrum of products from UV (VIS filtered) photolysis (1 h) of **13** (1:1400, Ar, 10°K) minus spectrum of **13**. Subtraction factor α = 0.10.

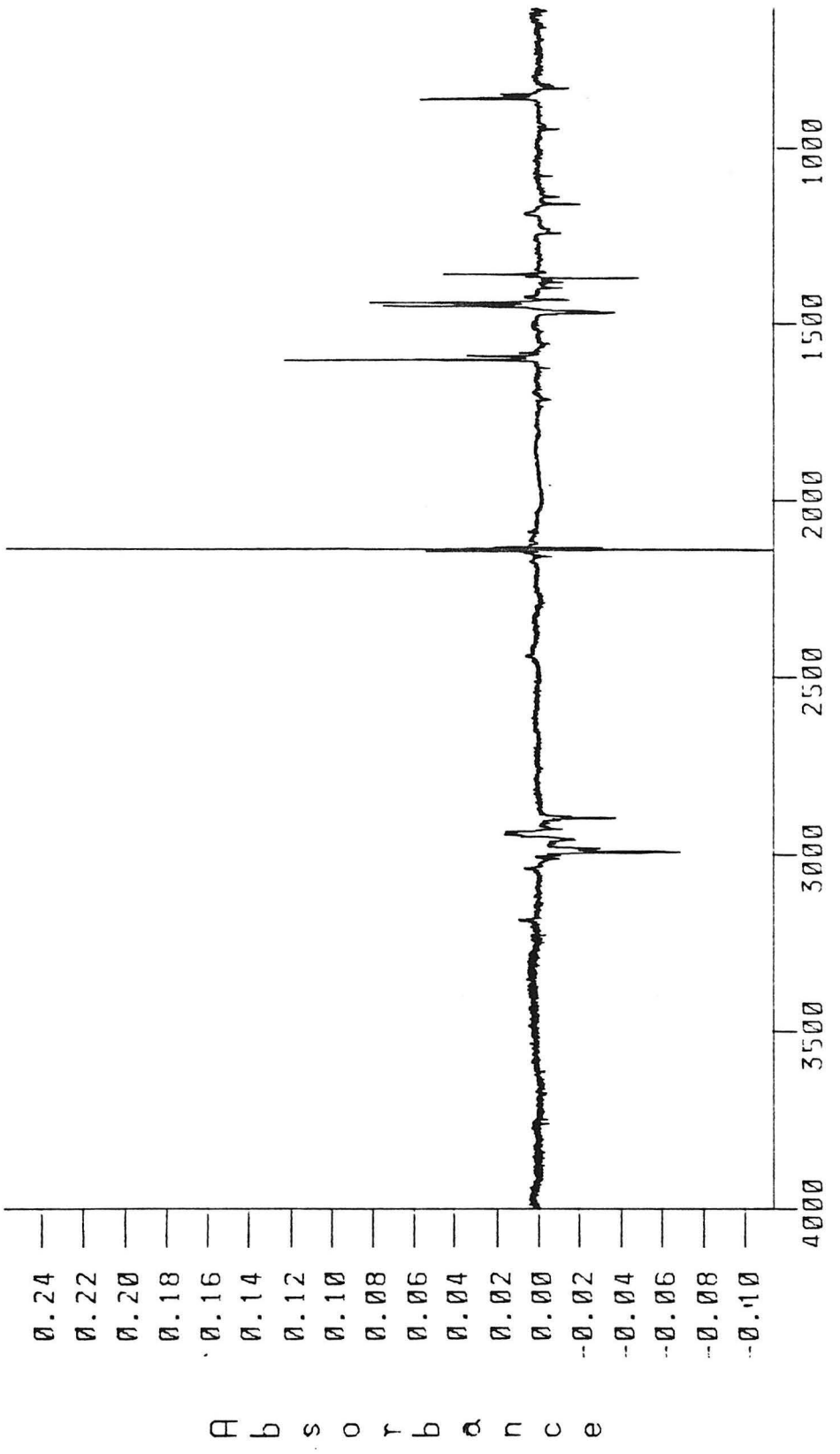

Figure 45. Difference FT-IR spectrum of 1,1-dimethyldiazene **7** and CO. UV (VIS filtered) photolysis (1 h) of **13** (1:1400, Ar, 10°K) minus spectrum after VIS (470-610 nm) photolysis (1 h) of **7**. Subtraction factor $\alpha = 1.0$.

cyanate, the expected product from the photo-Curtius rearrangement of **13**. These bands grow in quickly with UV photolysis of **13** and decrease with extended UV photolysis. Photolysis with wavelengths 340-410 nm also results in decrease in their intensity (see third column of Table XXIII). These bands are unaffected by warming the matrix to 30-35°K. The most intense band of (I) at 2219 cm^{-1} is likely assigned to the isocyanate stretching frequency. For comparison, Lwowski[47] reported this stretch at 2230 ± 2 cm^{-1} in a neon matrix at 6°K.

A second group of bands are observed to grow in with UV (VIS filtered) irradiation of **13**. These bands assigned to 1,1-dimethyldiazene **7** are labeled (D) in Table XXIII. Recall that VIS irradiation of **7** in a rigid 2-MTHF glass (80°K) resulted in loss of **7**. The infrared bands assigned to **7** are all efficiently photolyzed away with VIS irradiation at 10°K using Corning filters CS-1-75, CS-3-70, and CS-4-96 (λ 470-610 nm). Subtraction of the FT-IR spectrum after VIS photolysis from the spectrum before VIS photolysis results in positive absorption bands assigned to **7** (D) (Figure 45) together with a third group of bands at 2142.02 and 2134.75 cm^{-1} assigned to carbon monoxide (CO). All of the bands assigned to **7** are unaffected by warming the matrix to 30-35°K.

The third group of bands, assigned to CO, show the same behavior as the bands assigned to **7** (D). This type of CO behavior was demonstrated in the infrared studies of isotopically labeled H_2NN **3** (see Chapter 1). The formation of two distinct CO bands mirroring the behavior of 1,1-diazene **7** will be discussed in a later section.

A fourth group of product bands from UV photolysis of **13** also increase in intensity with VIS photolysis of **7** in argon at 10°K. These bands labeled (E) in Table XXIII, are assigned to ethane. Ethane is a product of VIS photolysis of **7** in a 2-MTHF glass (80°K).

A fifth group of product bands from UV photolysis of **13** remain unaffected by VIS photolysis of **7**. Irradiation with wavelengths 340-410 nm

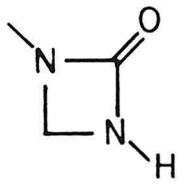

26

also has no effect. These bands are tentatively assigned to the unknown N-methyl-diazetedinone **26**, labeled (A) in Table XXIII. The strongest band observed for **26** (Figure 44) at 1815.06 cm^{-1} is consistent with the stretching frequency of a carbonyl in a four-membered ring. For comparison, dimethyl-

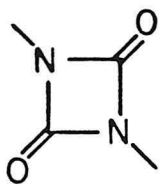

27

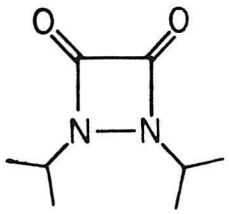

28

diazetedinedione **27** has a carbonyl stretch at 1780 cm^{-1} in $CHCl_3$ solution.[86a] N,N'-diisopropyl-1,2-diazetedinedione **28** has a C=O stretch at 1815 cm^{-1},[86b] whereas β-lactams have a stretch near 1800 cm^{-1}.[87] Diazetedinone **26** would result from intramolecular insertion of dimethyl carbamoyl nitrene into a methyl C-H bond. This intramolecular insertion is precedented for diethyl carbamoyl carbene yielding the corresponding four- and five-membered ring compounds.[88] No previous evidence for intermolecular or intramolecular dialkyl carbamoyl nitrene insertion chemistry has been noted.[45b,6] Attempts to isolate and fully characterize **26** have not been successful to date.

Of the infrared bands assigned to 1,1-dimethyl diazene **7** the major band at 1600.96 cm^{-1} and a minor band at 1590.83 cm^{-1} with a shoulder at 1591.53 cm^{-1} are all in the region where one would expect to find the characteristic N=N double bond stretch of the 1,1-diazene. This N=N stretch has been shown in the kinetically persistent 1,1-dialkyldiazenes in solution and in the parent 1,1-diazene H_2NN in an argon matrix to be Hooke's law shifted to lower energy with the incorporation of a terminal ^{15}N label at the nitrene nitrogen. In order to verify the assignment of the characteristic N=N double bond stretch for **7** a ^{15}N terminal label was desired. Reaction of dimethyl carbamoyl chloride **21** with (1-^{15}N) labeled sodium azide[63] in dry acetonitrile afforded **13-^{15}N.** The combination of ^{15}N NMR, high resolution mass spectroscopy and FT-IR spectroscopy demonstrates an equal distribution of the ^{15}N label between the two terminal positions of the azide moiety. ^{15}N NMR reveals two singlets at -141.40 and -266.02 ppm from ^{15}N-CH_3NO_2.

Table XXIII. Infrared Bands for Products from Photolysis of **13** and **13-^{15}N** (1:1400, Ar, 10°K) (cm^{-1}).

60 min hν UV (VIS Filtered)	60 min hν VIS (λ 470-610 nm)	60 min hν (λ 340-410 nm)	Assignment
3776.01			H_2O, ν O-H
3756.53			H_2O, ν O-H
3711.10			H_2O, ν O-H
3184.24	(-)		D (overtone)
3037.18	(-)		D (?)
	3009.44	(-)	(U)
3004.64	(-)		D_M, ν C-H
3000.50	(+)	(+)	E, ν C-H
2991.15	(+)	(+)	E, ν C-H
2982.65	(+)	(+)	E, ν C-H
2980.53	(+)	(+)	E, ν C-H
	2967.28	(-)	(U)
2958.15	(+)	(+)	E, ν C-H
2955.91	(+)	(+)	E, ν C-H
2942.97	(-)		D, ν C-H
2941.17	(-)		D, ν C-H
2938.23	(-)		D, ν C-H
2933.79	(-)		D, ν C-H
2926.06	(+)	(+)	E, ν C-H
	2909.42	(-)	(U)
2900.38	(+)	(+)	E, ν C-H
2895.21	(+)	(+)	E, ν C-H
2890.90	(+)	(+)	E, ν C-H
2345.00			CO_2, ν CO
2339.01			CO_2, ν CO

Table XXIII. Continued.

60 min hν UV (VIS Filtered)	60 min hν VIS (λ 470-610 nm)	60 min hν (λ 340-410 nm)	Assignment
2219.49		(-)	I, ν-N^{14}=C=O
2207.00		(-)	I*, ν-N^{15}=C=O
2142.02	(-)		CO, ν CO
2137.80	(+)		CO, ν CO
2135.93			CO, ν CO
2134.75	(-)		CO, ν CO
2132.95	(+)	(-)	CO, ν CO
1815.06			(A, ν ^{14}NCO)
1811.97			(A*, ν ^{15}NCO)
1623.60			H_2O, δOH
1607.73			H_2O, δ OH
1600.96	(-)		D_M, ν ^{14}N=^{14}N
1591.53	(-)		D_m, ν ^{14}N=^{14}N
1590.83	(-)		D_m, ν ^{14}N=^{14}N
1581.83	(-)		D_M*, ν ^{14}N=^{15}N
1572.26	(-)		D_m*, ν ^{14}N=^{15}N
1473.12		(-)	I, δ CH_3
1471.62		(-)	I, δ CH_3
1467.84	(+)	(+)	E, δCH_3
1464.97	(+)	(+)	E, δ CH_3
	1463.03	(-)	(U)
1448.50	(-)		D_M, δ CH_3
1438.16	(-)		D_M, δ CH_3
	1430.01	(-)	(U)
1423.25	(-)		D (?)
1380.12	(+)	(+)	E, ω CH_3
1375.12	(+)	(+)	E, ω CH_3
	1369.10	(-)	(U), ω CH_3

Table XXIII. Continued.

60 min hν UV (VIS Filtered)	60 min hν VIS (λ 470-610 nm)	60 min hν (λ 340-410 nm)	Assignment
1358.17	(-)		D_M, $^{\omega}$ CH_3
1184.35	(-)		D_M, $^{\rho}$ CH_3
	1158.79	(-)	(U), $^{\delta}$ $CN^{14}N$
	1154.24 *	(-)	(U*), $^{\delta}$ $CN^{15}N$
	1078.77	(-)	(U)
	1077.80 *	(-)	(U*)
	946.18	(-)	(U)
	937.02	(-)	(U)
859.37	(-)		D_M, $^{\nu}$ C-N
857.56	(-)		D_M, $^{\nu}$ C-N
856.49	(-)		D (?)
849.74	(-)		D_m, $^{\nu}$ C-N
845.90	(-)		D_m
829.20	(+)	(+)	E
825.85	(+)	(+)	E, $^{\nu}$ C-C
822.27	(+)	(+)	E
818.16		(-)	I
606.67	(+)	(+)	(E)
605.56	(+)	(+)	(E)

D_M = 1,1-Dimethyldiazene **7**, D_M* = **7**-^{15}N
D_m = Minor species (**7**), D_m* = D_m-^{15}N
E = Ethane
I = Dimethylaminoisocyanate, I* = I-^{15}N
A = N-Methyldiazetedinone (**26**), A* = A-^{15}N
( ) = Tentative assignment
(+) = Increased with photolysis
(-) = Decreased with photolysis
(U) = Unidentified. (U*) = (U-^{15}N).

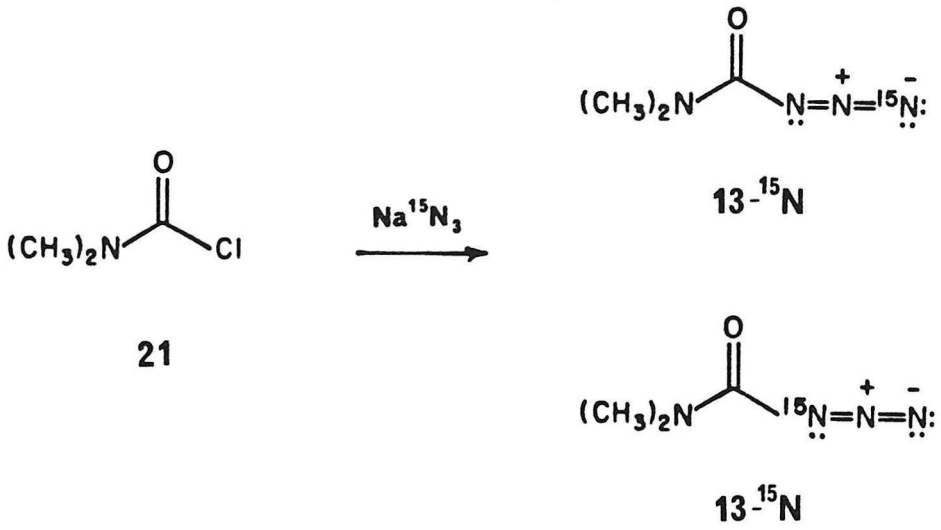

21

Matrix isolation of 13-^{15}N in argon (1:1400, Ar, 10°K) (Figure 46, Table XXIV) reveals the two ^{15}N labeled asymmetric azide stretches at 2151.04 and 2133.74 cm^{-1} in an approximate 1:1 ratio. Photolysis of a 13-^{15}N would be expected to yield a 1:1 mixture of unlabeled 1,1-diazene 7 and terminally labeled 7-^{15}N by the photo-Curtius rearrangement and subsequent photodecarbonylation of the intermediate dimethylaminoisocyanate.

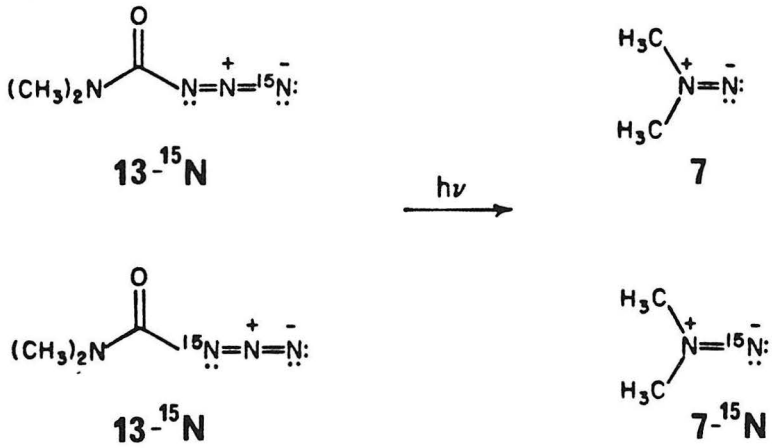

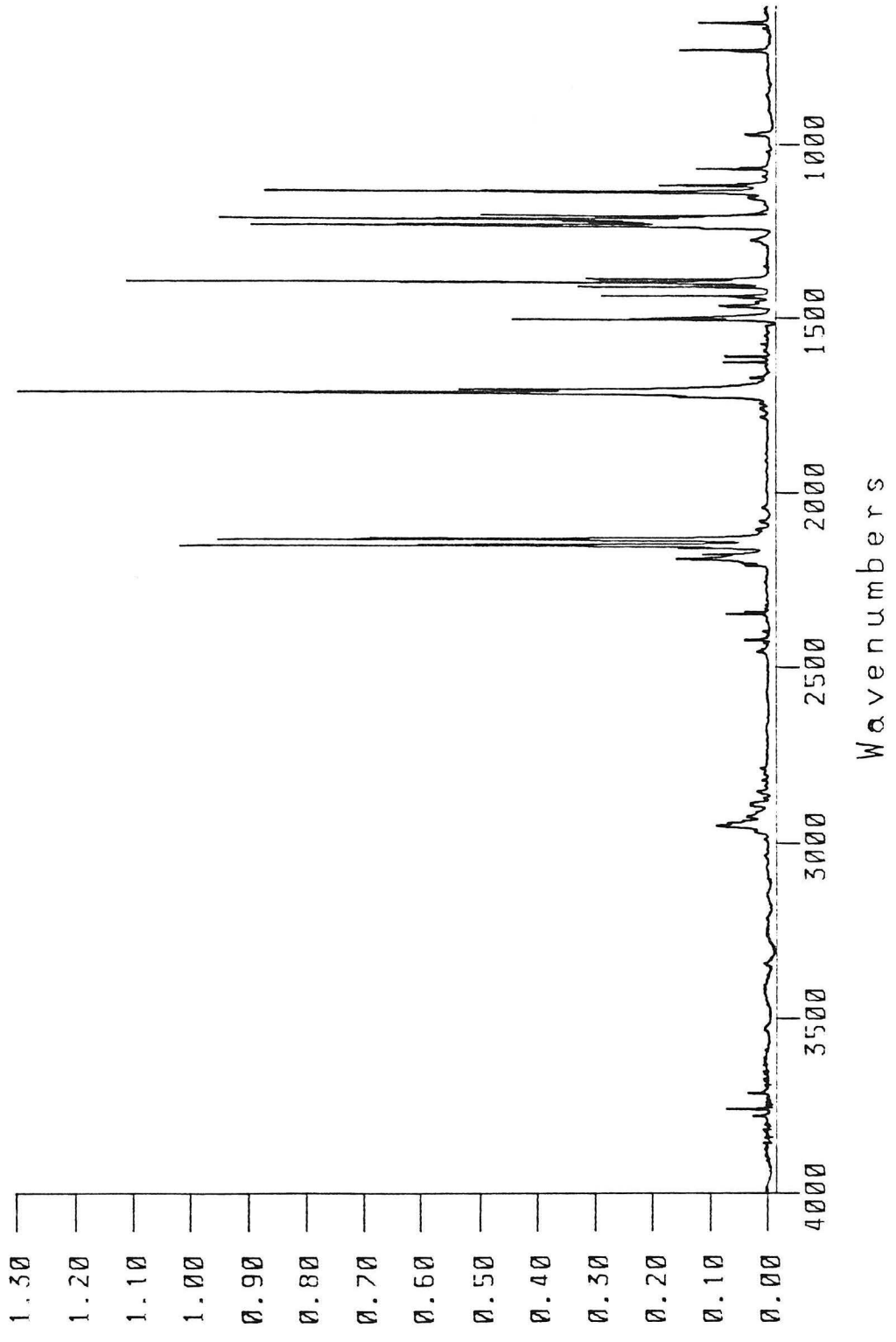

Figure 46. FT-IR spectrum of **13-^{15}N**, 120 mm deposition (1:1400, Ar, 10°K).

Table XXIV. FT-IR Bands for **13-^{15}N** in Argon Matrix (120 mm) (1:1400, 10°K) Threshold 0.05 A.

Peak Location (cm^{-1})	Intensity (A)	Assignment
3756.37	0.07	H_2O, ν OH
3711.02	0.05	H_2O, ν OH
2949.45	0.09	ν C-H
2942.84	0.06	
2935.50	0.05	
2923.22	0.05	
2345.03	0.08	CO_2, ν CO
2339.00	0.06	CO_2, ν CO
2187.43	0.14	
2183.24	0.09	
2174.27	0.10	
(2157.48)	0.15	
2151.04	1.02	ν-N^{15}=N=N (asym)
2148.07	0.60	
2146.00	0.51	
2133.74	0.96	ν-N=N=^{15}N (asym)
2129.05	0.70	
1724.13	0.16	
1721.45	0.17	
1712.93	1.31	ν NCO (asym)
1704.02	0.54	
1692.51	0.07	
1623.65	0.08	H_2O, δ OH
1607.77	0.08	H_2O, δ OH
1502.78	0.53	
1466.42	0.07	
1462.11	0.09	
1439.04	0.06	
1434.45	0.30	δ CH_3
1432.76	0.14	
1410.45	0.11	
1408.83	0.34	δ CH_3
1407.49	0.22	

Table XXIV. Continued.

Peak Location (cm^{-1})	Intensity (A)	Assignment
1398.13	0.64	
1395.99	1.12	ν NCO (sym)
1385.92	0.32	
(1240.39)	0.13	
1233.60	0.92	ν-N^{15}=N=N (sym)
1229.73	0.67	
1225.75	0.34	
1220.94	0.38	
1215.53	0.98	ν-N=N=^{15}N (sym)
1212.52	0.60	
1207.82	0.33	
1203.75	0.54	
1136.03	0.88	ρ CH_3
1134.78	0.89	
1117.10	0.19	
1112.15	0.05	
1071.62	0.06	
1069.83	0.13	γ CH_3
1066.23	0.05	
973.41	0.07	ν C-N (asym)
970.53	0.05	ν C-^{15}N (asym)
729.69	0.05	
726.82	0.15	δ N_3
648.12	0.12	ν N-C (sym)
644.85	0.10	

( ) = Unlabeled (13) as impurity

UV (VIS filtered) photolysis **13-^{15}N** (1 h) (1:1400, Ar, 10°K) results in loss of the infrared bands of **13-^{15}N** and formation of product bands. Figure 47 shows the product FT-IR spectrum minus the FT-IR spectrum of **13-^{15}N.** These product bands are summarized in the first column of Table XXIII. In addition to the product bands from photolysis of **13,** additional ^{15}N shifted bands are found at 2207.00, 1811.97, 1581.83, and 1572.26 cm^{-1}. These bands correspond in intensity to ^{15}N shifted multiples of unlabeled product bands at 2219.49, 1815.06, 1600.96, and 1590.83 cm^{-1}, respectively. The major band at 1581.83 cm^{-1} and a minor band at 1572.26 cm^{-1} are lost with VIS irradiation together with the bands of unlabeled **7** and are assigned to **7-^{15}N.** Subtraction of the FT-IR spectrum after VIS photolysis from the FT-IR spectrum before VIS photolysis results in the spectrum of **7, 7-^{15}N,** and bands due to carbon monoxide (CO) (Figure 48). The more intense bands at 1600.96 and 1581.83 cm^{-1} are assigned to the characteristic ν ^{14}N=^{14}N and ν ^{14}N=^{15}N stretches of **7** and **7-^{15}N,** respectively. Figure 49 shows the N=N stretch region. The observation of a minor band at 1590.83 cm^{-1} which shows the same behavior as bands due to **7** and also shows a large ^{15}N shift to 1572.26 cm^{-1} is surprising. One possible explaination for this would be matrix site splitting of the bands of **7** yielding small multiple bands of **7** due to different sites. The minor band at 1590.83 cm^{-1} would correspond to the 1600.96 cm^{-1} ν ^{14}N=^{14}N stretch in a different site environment. However, attempts to remove this possible site splitting by warming the matrix to 30-35°K were unsuccessful. This observation is consistent with assigning the 1590.83 cm^{-1} band to another species with a N=N stretch which is also efficiently photolyzed with VIS irradiation

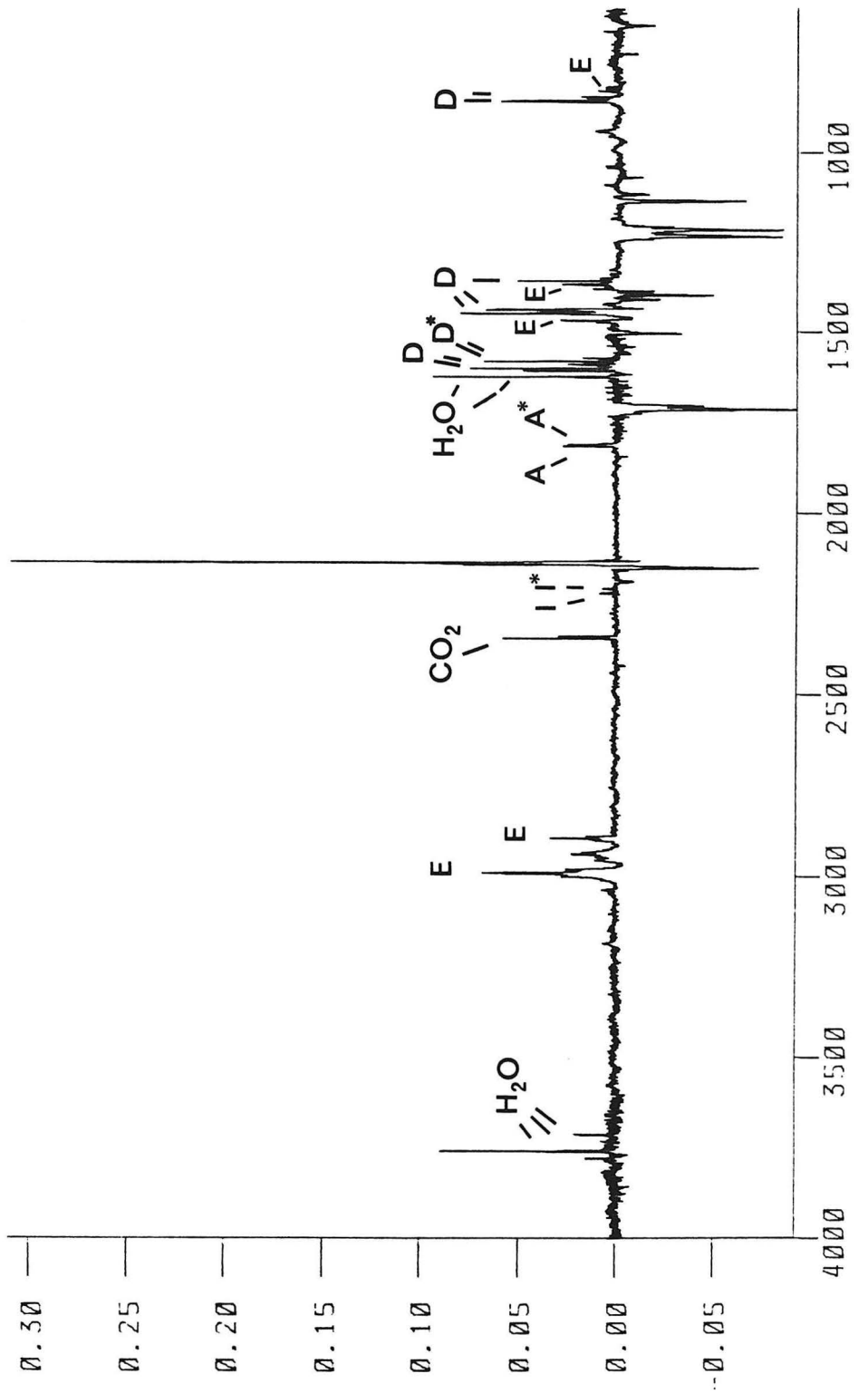

Figure 47. Difference FT-IR spectrum of products from UV (VIS filtered) photolysis (1 h) of **13-^{15}N** (1:1400, Ar, 10°K) minus spectrum of **13-^{15}N**. Subtraction factor $\alpha = 0.16$.

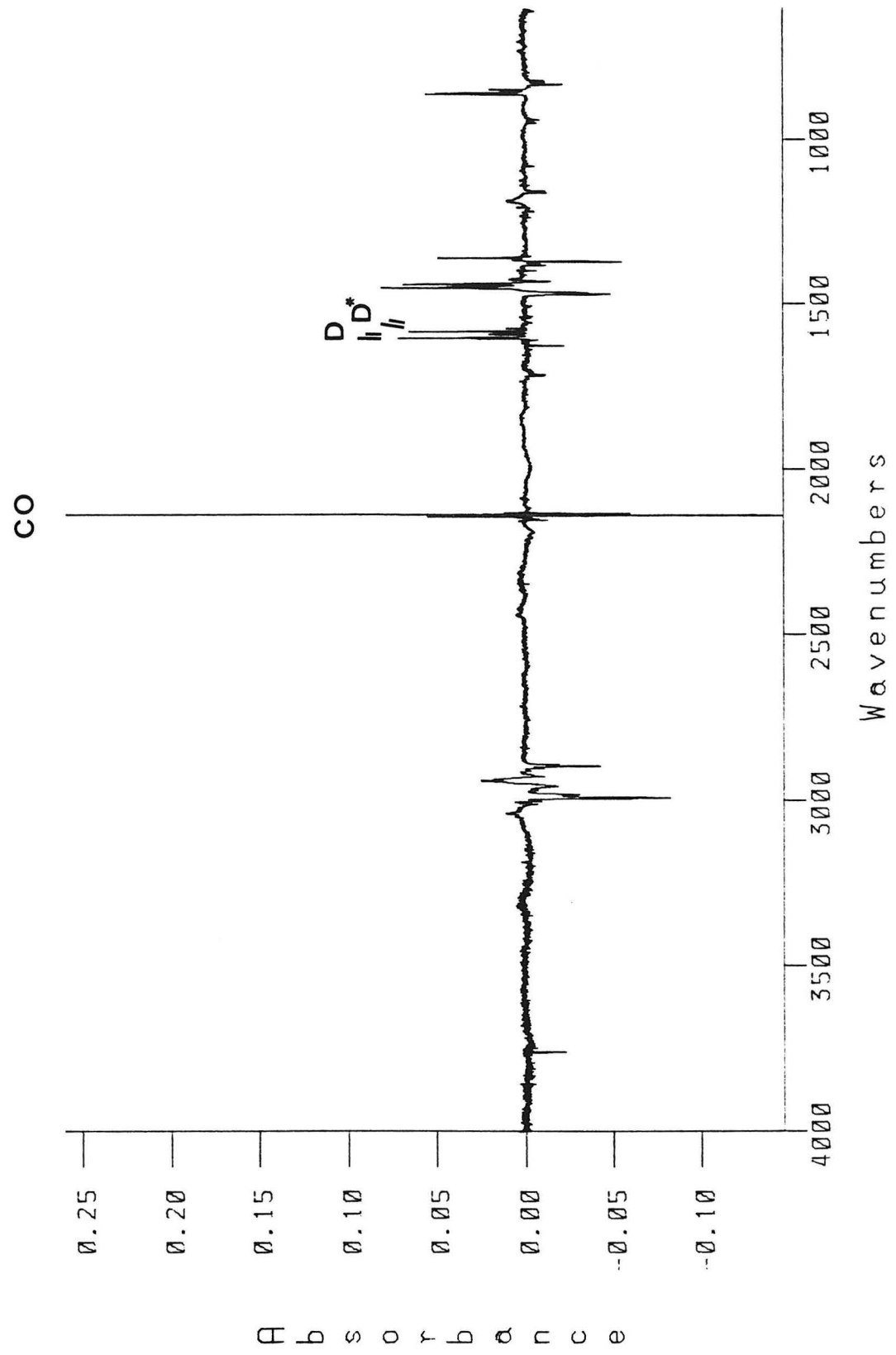

Figure 48. Difference FT-IR spectrum of **7, 7-^{15}N** and CO. UV (VIS filtered) photolysis (1 h) of **13-^{15}N** (1:1400, Ar, 10°K) minus spectrum after VIS (470-610 nm) photolysis (1 h) of **7:7-^{15}N** mixture. Subtraction factor $\alpha = 1.0$.

Table XXV. Infrared Bands for 1,1-Dimethyldiazene **7** and **7-^{15}N** (Ar, 10°K).

Peak Location (cm^{-1})	Assignment
3184.24	(overtone)
3037.13	(?)
3004.64	M, ν C-H
2942.97 2941.17 2939.27 2938.23 2933.79	M, ν C-H
1600.96	M, ν $^{14}N=^{14}N$
1591.53	m, ν $^{14}N=^{14}N$
1590.39	m, ν $^{14}N=^{14}N$
1581.83	M, ν $^{14}N=^{15}N$
1572.26	m, ν $^{14}N=^{15}N$
1448.50	M, δ CH_3
1438.46	M, δ CH_3
1423.25	(?)
1358.17	M, ω CH_3
1184.35	M, ρ CH_3
859.37	M, ν C-N
857.56	M, ν C-N
856.49	(?)
849.74	m, ν C-N
845.90	m, ν C-N

M = Major species (**7**, **7-^{15}N**). m = Minor species. (?) = Uncertain. ( ) = Tentative assignment.

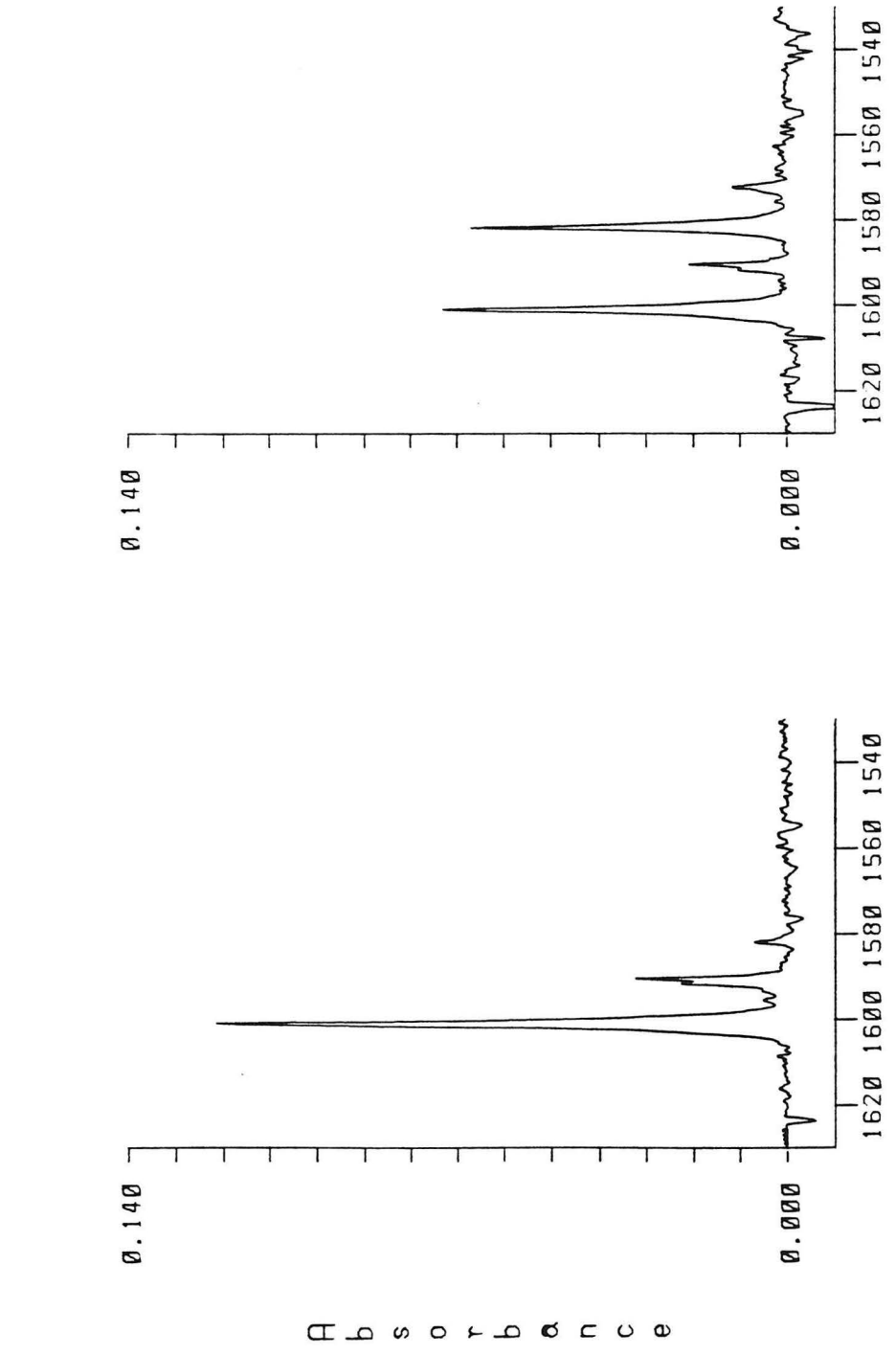

Figure 49. (a) R_2 $^{14}N=^{14}N$ stretch of **7** (ν_M) and minor component (ν_m) from Figure 45. (b) R_2 $^{14}N=^{14}N$ stretch of **7** and R_2 $^{14}N=^{15}N$ stretch of **7-15N** and minor component stretches from Figure 48.

(λ 470-610 nm) or its assignment to **7** in a different matrix site which is not altered by warming to 30-35°K. The band at 1590.83 cm^{-1} and other additional "minor" bands which show matrix behavior similar to **7** and **7-^{15}N** are labeled (D_m) in Table XXIII. The major bands (greater intensity) assigned to **7** and **7-^{15}N** are labeled (D_M). Table XXV summarizes the infrared bands of **7** and **7-^{15}N** and their tentative assignments. Only the N=N double bond stretch mode shows a ^{15}N shift. This is consistent with the assignment of these bands to 1,1-dimethyldiazene **7** and **7-^{15}N** with ^{15}N incorporation only into the terminal "nitrene" nitrogen.

Two other product bands from UV photolysis of **13-^{15}N** also show a ^{15}N shift to lower energy. The asymmetric isocyanate stretch ν ^{14}N=C=O of dimethylaminoisocyanate (labeled (I) in Table XXIII) at 2219.49 cm^{-1} shows a ^{15}N shift to 2207.00 cm^{-1}. For comparison, the isocyanate stretch for the parent aminoisocyanate (H_2N-N=C=O) was found to ^{15}N shift from 2212.02 cm^{-1} to 2194.18 cm^{-1} in an argon matrix at 10°K (see Chapter 1). In addition, the band at 1815.06 cm^{-1} shows a small ^{15}N shift to 1811.97. This band is tentatively assigned to the asymmetric NCO stretch of N-methyl diazetedinone **26** (labeled (A) in Table XXIII).

Photolysis of **7** with visible light (VIS) (λ 470-610 nm) results in loss of all infrared bands of **7** and formation of new bands assigned to ethane (labeled (E) in Table XXIII) together with a CO band at 2137.80 cm^{-1}. Ethane and nitrogen are the expected photolysis products of 1,1-diazene **7**. Ethane is a product of photolysis of **7** in a 2-MTHF glass (80°K). A

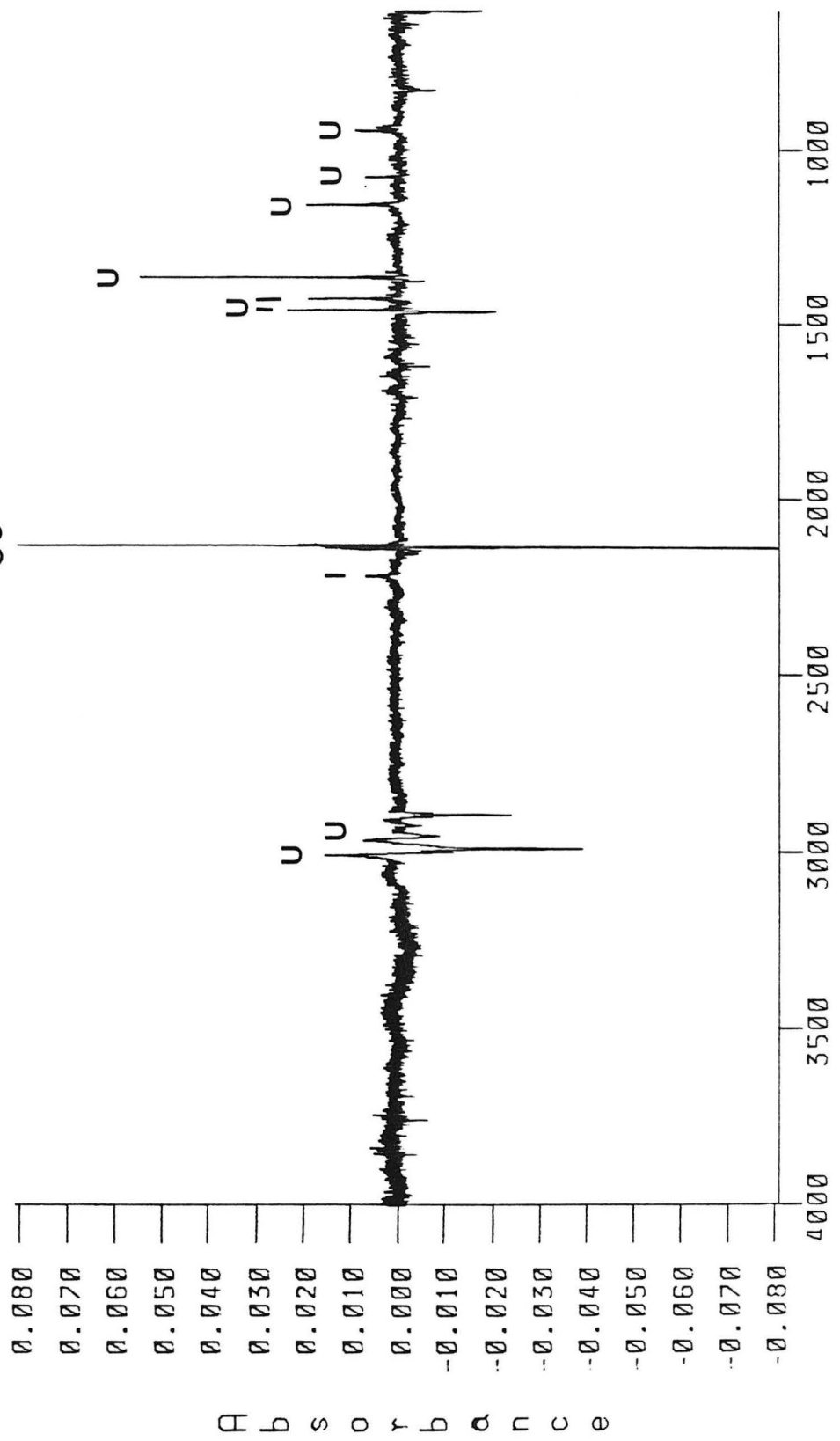

Figure 50. Difference FT-IR spectrum of (U) resulting from VIS (470-610 nm) photolysis (1 h) of **7**. Spectrum resulting from VIS photolysis of **7** minus spectrum after photolysis (1 h) of (U) (340-410 nm). Subtraction factor $\alpha = 1.0$.

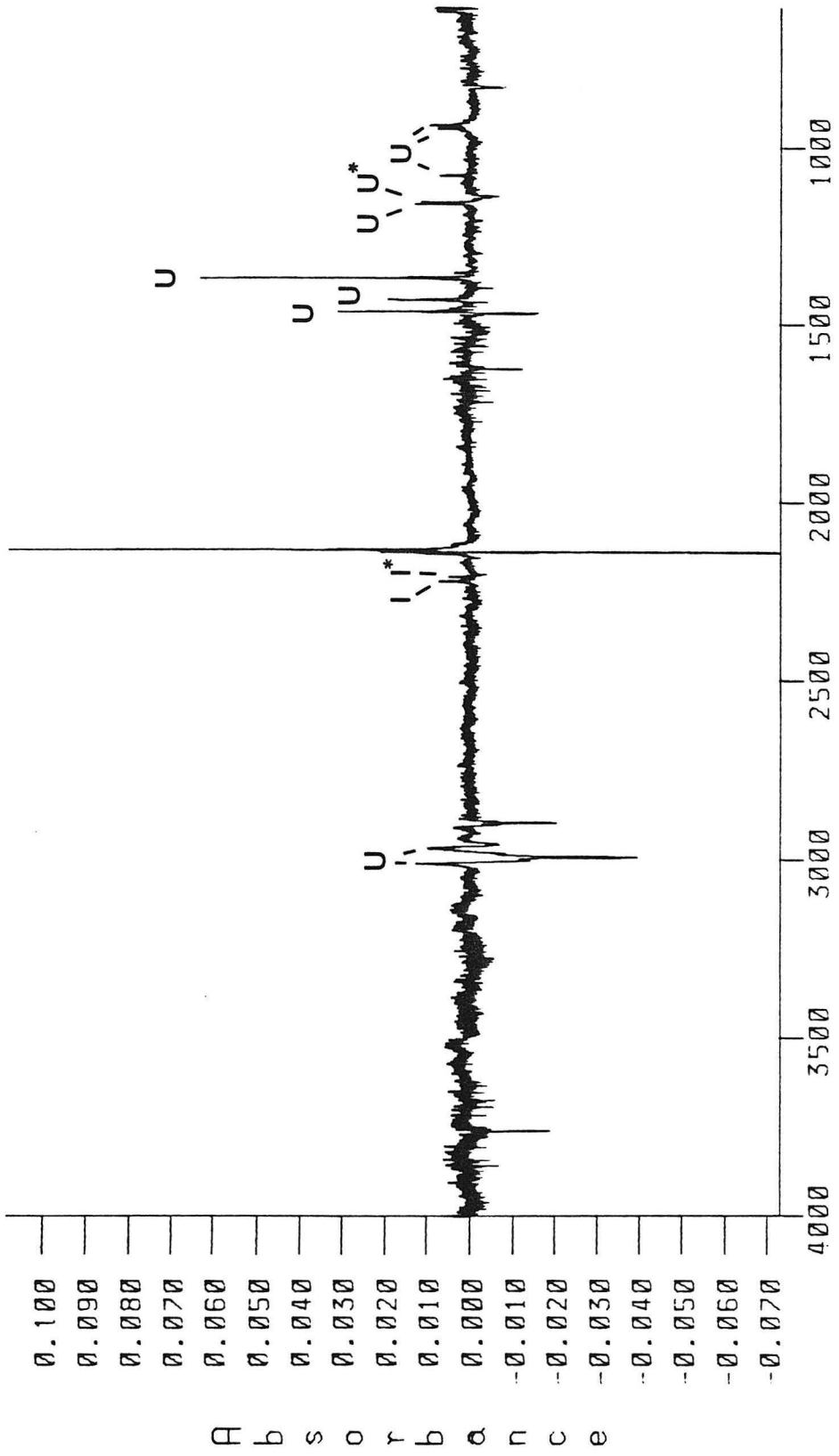

Figure 51. Difference FT-IR spectrum of (IJ) and (IJ-^{15}N) resulting from VIS (470-610 nm) photolysis (1 h) of **7:7-^{15}N** mixture. Spectrum resulting from VIS photolysis (1 h) of **7:7-^{15}N** minus spectrum after photolysis (1 h) of (IJ):(IJ-^{15}N) mixture (340-410 nm) subtraction factor $\alpha = 1.0$.

Table XXVI. Comparison Ethane Infrared Bands (Ar, 10°K) (cm^{-1}).[a]

hν VIS 1,1-Diazene **7**	hν UV t-1,2-Diazene **8t**	Ethane/Ar	Assignment
3000.50	3001.15	3000.50	
2991.15	2991.82	2991.97	
		2986.74	ν C-H
2982.65	2982.05	2984.16	
2980.53	2979.50	2979.84	
2958.15	2960.81		
2955.91	2956.23		
2952.91	2952.64	2951.26	
2926.00	2926.06	2920.83	
2900.38	2901.74		
2895.21	2895.57		
2893.02		2893.75	
2890.90	2891.17	2891.52	
1467.84	1468.00	1467.40	δ CH_3
1464.97		1464.21	
1380.12	1379.80		
1375.12	1378.17	1374.50	ω CH_3
832.16			
829.20	829.64	822.26	
825.85	828.30	820.34	
822.27	826.13	818.09	
(606.67)	(610.03)		
(605.56)	(608.28)		

[a] ~1:1400, Ar, 10°K. ( ) Tentative assignment. Close to strongest observed bands for methyl radical (CH_3·) at 602-620 cm^{-1} (Ar, 10°K). Ref. 90.

comparison of the infrared spectrum of matrix isolation ethane (1:1400, Ar, 10°K) with that produced from **7** is made in Table XXVI. Some additional unidentified minor product bands (labeled (U) in the second column of Table XXIII) are also obtained from VIS photolysis of **7**. VIS photolysis of **7**-^{15}N produces the same set of product bands together with ^{15}N shifted multiple bands at 1154.24 and 1077.80 cm^{-1}. The 4.55 cm^{-1} ^{15}N shift of the band at 1158.79 cm^{-1} to 1154.24 cm^{-1} suggests its assignment to a bending mode involving a ^{15}N labeled nitrogen. The same is true for the band at 1078 .77 cm^{-1}, which shows a 0.97 cm^{-1} ^{15}N shift to 1077.80 cm^{-1}. Photolysis of (U) with wavelengths 340 to 410 nm results in loss of these unidentified product bands and growth of bands due to ethane. Subtraction of the FT-IR spectrum after 340-410 nm photolysis from the FT-IR spectrum of (U) before photolysis results in the difference spectrum of Figure 50. Positive absorbance bands of (U) and a CO band at 2132.95 cm^{-1} are clearly displayed. Additionally, bands due to dimethylaminoisocyanate are also apparently photolyzed with light 340 to 410 nm. The negative absorbances correspond to ethane and a CO band at 2137.80 cm^{-1}. The behavior of CO bands will be discussed in a later section. Similarly, Figure 51 shows the differenced spectrum resulting from 340-410 nm photolysis of ^{15}N-labeled (U). The observation of ethane as a product from photolysis of (U) between 340 and 410 nm suggests the 1,2-dimethyldiazene isomers **8** as possible candidates for (U). The argon matrix infrared spectrum of trans-1,2-dimethyldiazene **8t** (1:1400, Ar, 10°K) (Figure 52, Table XXVII) easily rules out **8t** as the species responsible for the bands labeled (U). Photolysis of matrix isolated **8t** (λ 340-410 nm) results in loss

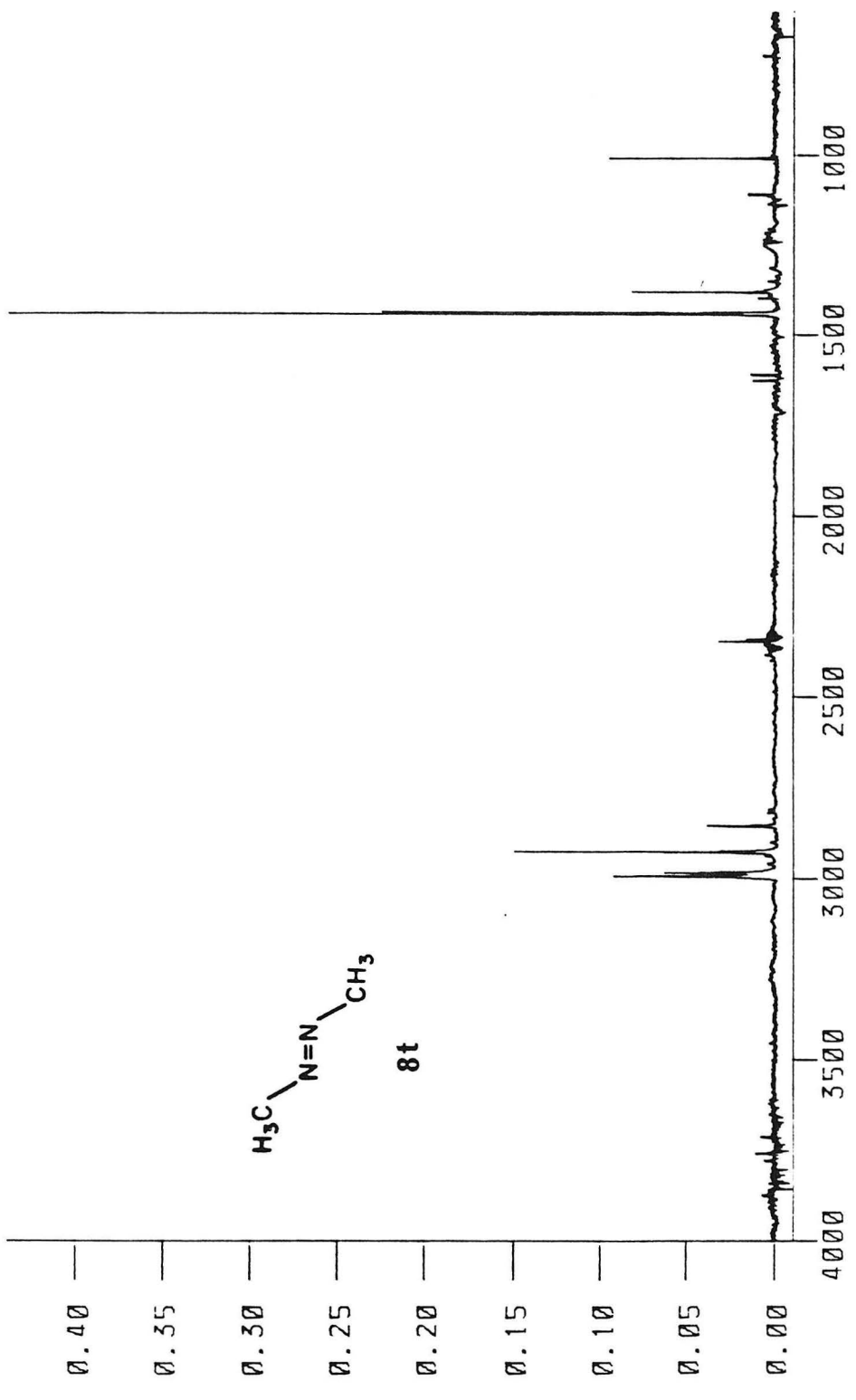

Figure 52. FT-IR spectrum of trans-1,2-dimethyldiazene **8t** (1:1400, Ar, 10°K).

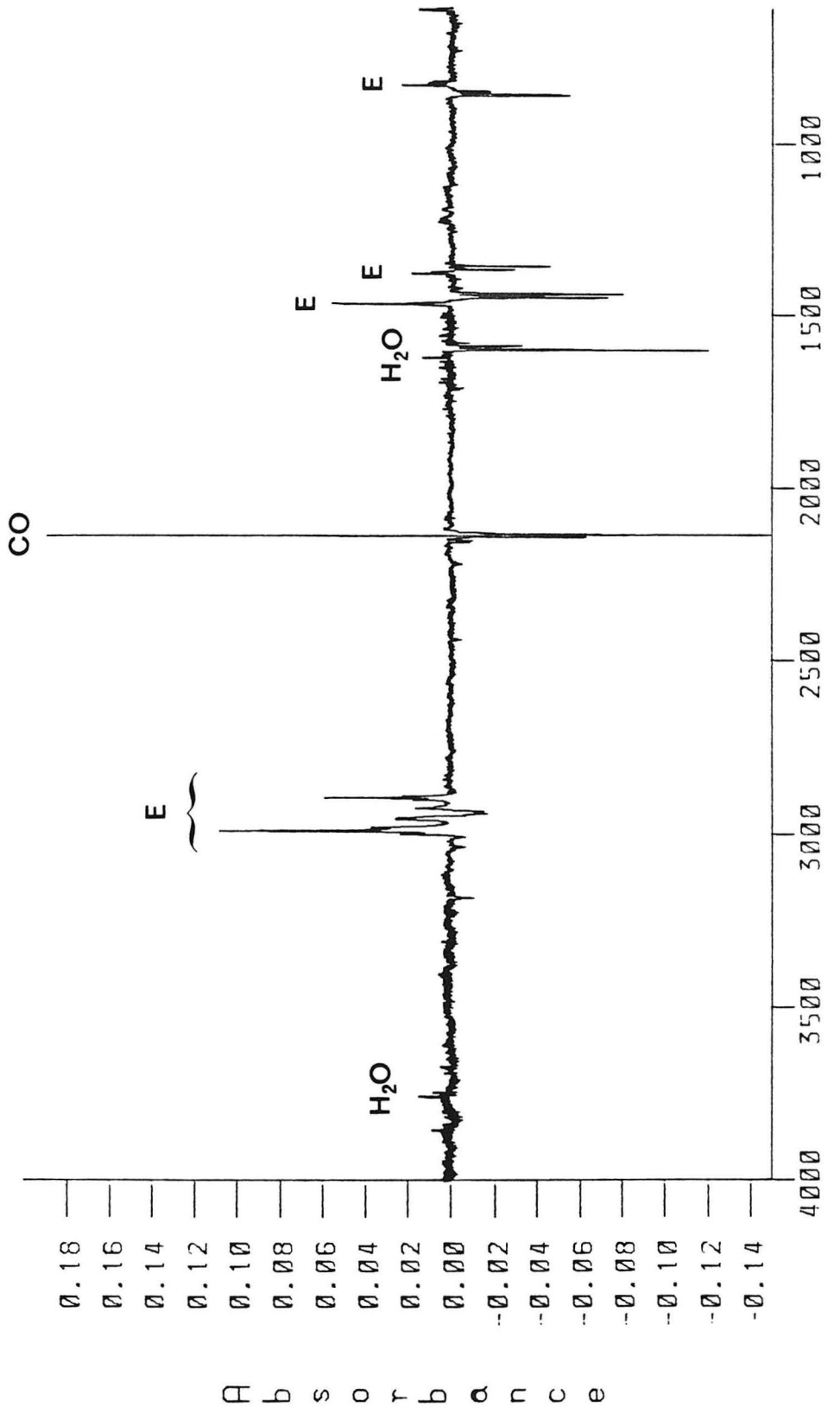

Figure 53. Difference FT-IR spectrum of ethane/CO from VIS photolysis of 1,1-diazene **7**/CO. Spectrum after VIS photolysis of **7** and subsequent photolysis of (1) minus spectrum before VIS photolysis of **7**. Subtraction factor $\alpha = 1.0$.

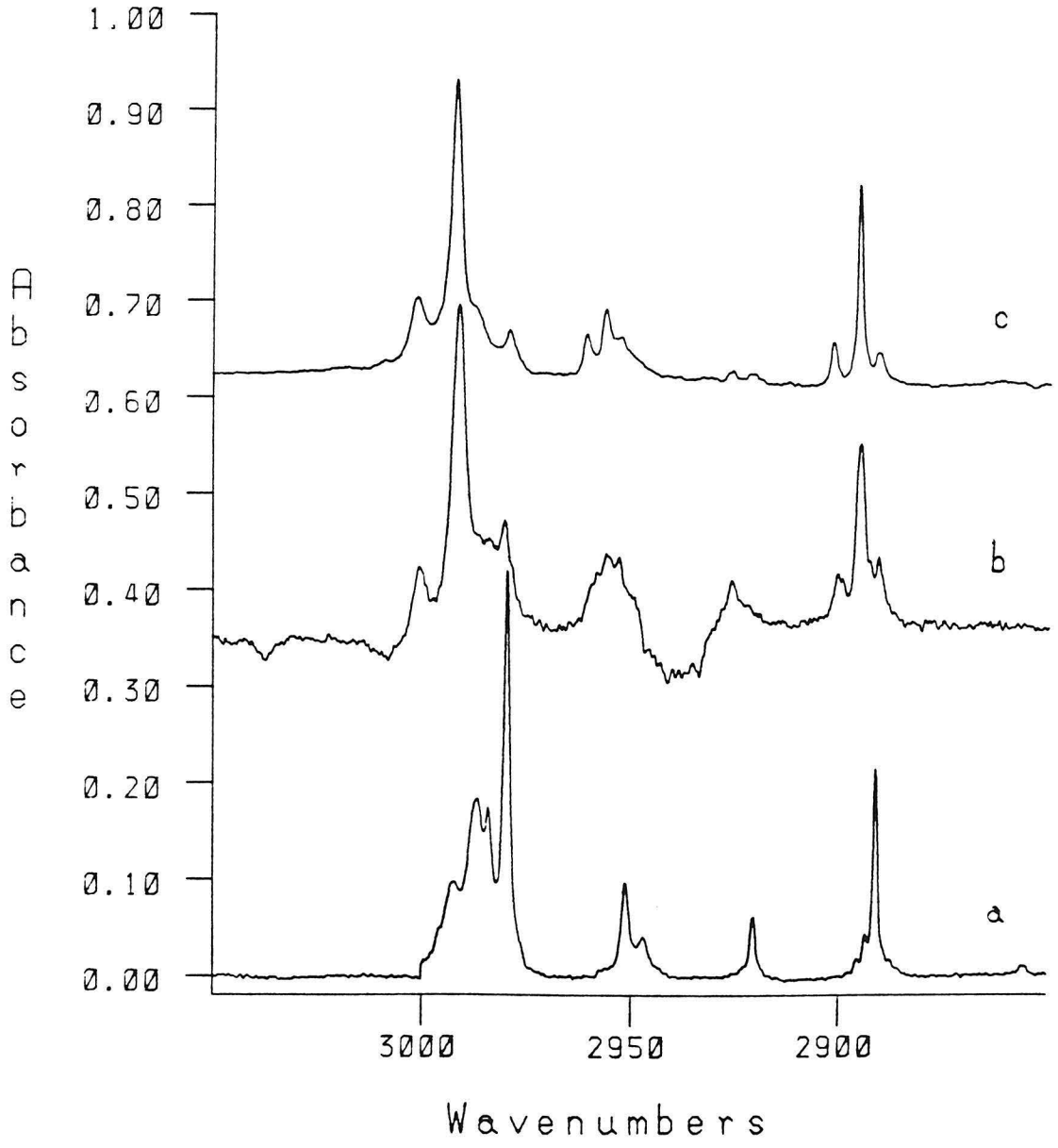

Figure 54. Comparison ethane FT-IR spectra of the C-H stretch region. (a) Ethane (1:1400, Ar, 10°K). (b) Ethane from VIS photolysis of 1,1-diazene **7** (Figure 53). (c) Ethane from photolysis (340-410 nm) of trans-1,2-diazene **8t** (1:1400, Ar, 10°K) 1 h.

Table XXVII. Infrared Bands for 1,2-Diethyldiazenes **8t** and **8c** (cm^{-1}).

Trans-1,2-Diazene **8t**[a]	Cis-1,2-Diazene **8c**[b]
2992.91 (m)	3018 (m)
2983.65 (m)	2960 (s)
2981.46 (w)	2910 (m)
2926.12 (s)	1561 (w)
2923.26 (w)	1477 (m)
2854.03 (w)	1460 (s)
1441.52 (s)	1430 (m)
1436.76 (s)	
1379.46 (m)	1370 (s)
1377.72 (w)	1159 (s)
1108.72 (w)	1110 (m)
1008.26 (m)	935 (m)

[a]This work (1:1400, Ar, 10°K). [b]Ref. 89 (gas). w = weak, m = medium, s = strong.

of the bands of **8t** and formation of bands due to ethane. Subtraction of the FT-IR spectrum after photolysis from the FT-IR spectrum before photolysis of **8t** clearly displays the infrared spectrum of ethane produced from photolysis of **8t** (Figure 53, Table XXVI). No bands of (U) were obtained from photolysis of **8t**. No infrared bands attributable to cis-1,2-dimethyl diazene **8c** were observed to grow in the photolysis of trans-1,2-diazene **8t**. Table

XXVI shows a comparison of the ethane infrared bands produced from photolysis of 1,1-diazene **7**, 1,2-diazene **8t**, and argon matrix isolated ethane (1:1400, Ar, 10°K). Close inspection of the C-H stretch region (Figure 54) reveals that infrared spectrum of matrix isolated ethane is noticeably different from that of ethane produced photochemically from either **7** or **8t** which give nearly identical ethane product spectra. The single nitrogen molecule produced together with ethane from photolysis of **7** and **8t** apparently perturbs the matrix site around ethane in solid argon. Although **8t** can be ruled out as a possible assignment for (U), the cis-1,2-diazene isomer **8c** remains a possible choice. Table XXVII shows a comparison of the infrared band for cis and trans 1,2-diazenes **8t** and **8c**. The bands for **8c** correlate fairly well with those for (U) in Table XXIII.

Another possible candidate for (U) would be H, ethyl-1,2-diazene[103] (λ_{max} = 367 nm) which would also yield ethane as a photodecomposition product. However, no infrared band attributable to an N-H stretch is observed for (U) in the region 2800-3400 cm^{-1}. Additionally, comparison with the literature matrix infrared spectra for cis- and trans-H, methyl-1,2-diazene do not support H, ethyl-1,2-diazene as a candidate for (U).[33]

Tetramethyl-2-tetrazene **19** was also ruled out as a possible candidate for (U) by comparison with its argon matrix infrared spectrum (see Experimental). UV (VIS filtered) photolysis of **19** (1:700, Ar, 10°K) results in formation of products from disproportionation/recombination of two dimethylamino radicals.[93] The disproportionation products N-methyl-methylenimine (ν $-N=CH_2$ 1663 cm^{-1}) and dimethylamine (ν NH = 3340

cm^{-1}) are also easily ruled out as candidates for (U).

Matrix Isolation Infrared Spectroscopy of 1,1-Diisopropyldiazene 18

UV (VIS filtered) photolysis of matrix isolated diisopropyl carbamoyl azide **17** and ^{15}N labeled **17-^{15}N** yielded infrared product bands for comparison with those obtained from photolysis of **13** and **13-^{15}N**. A band assigned to ν-^{14}N=C=O, the characteristic isocyanate stretch of diisopropylaminoisocyanate, was found at 2241.91 cm^{-1}. Photolysis of **17-^{15}N** resulted in a ^{15}N shift to 2231.55 cm^{-1} for the ^{15}N labeled isocyanate stretch ν-^{15}N=C=O (Figure 55). UV photolysis of **17** also yields a minor product infrared band at 1815.95 cm^{-1} and a major product band at 1795.94 cm^{-1}. These bands are tentatively assigned to the carbonyl stretches of **29** and **30**. The four and five-membered ring compounds would result from intramolecular C-H insertion of the diisopropyl carbamoyl nitrene into a methine or methyl C-H bond, respectively. Photolysis of **17-^{15}N** results in a ^{15}N shift of the

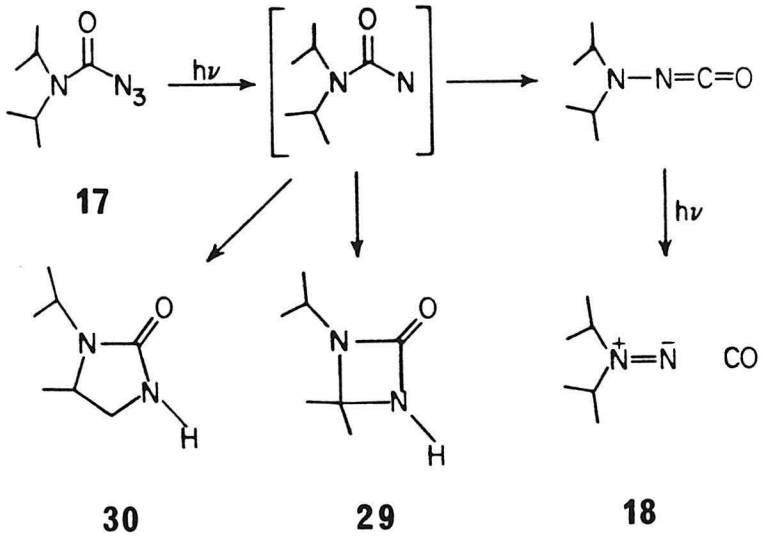

17 **30** **29** **18**

minor band at 1815.95 cm^{-1} to 1810.45 cm^{-1} in support of this assignment. The corresponding four-membered diazetedinone **26** obtained from photolysis of **13** showed a ^{15}N shift from 1815.06 to 1811.97 cm^{-1} (Figure 56).

The characteristic N=N double bond stretch for 1,1-diisopropyldiazene **18** is found at 1600.92 cm^{-1}. Photolysis of **17-^{15}N** results in a Hooke's law shift to 1579.46 cm^{-1} (Figure 57). The characteristic 1,1-diazene N=N double bond stretch frequencies are summarized in Table XXVIII. A comparison of the 1,1-diazene N=N double bond stretch frequencies with the isoelectronic carbonyl stretch frequencies is made in Table XXIX. The N=N stretch frequencies for 1,1-diazenes parallel the trend in the isoelectronic carbonyl compounds. One effect in this trend is indicative of increasing p-orbital character in the N-C bonds with decreasing CNC bond angle. This results in increased s-orbital character of the NN bond and higher energy N=N stretch frequency. Superimposed on this effect is an apparent inductive/ hyperconjugative stabilization of the positive charge on the amino nitrogen of the 1,1-diazene. Greater electronic donation (alkyl <u>vs.</u> H) results in a stronger $\overset{+}{N}{=}\overset{-}{N}$ double bond and a higher energy N=N stretch frequency. The opposite electronic effect is realized in the isoelectronic carbonyl compounds

1,1-Dimethyldiazene 7 Product Analysis

For product analysis, samples of **7** were prepared by UV (VIS filtered) photolysis of **13** in a rigid 2-MTHF glass contained in either a 5 mm O.D. quartz tube immersed in a liquid nitrogen filled finger dewar or contained in

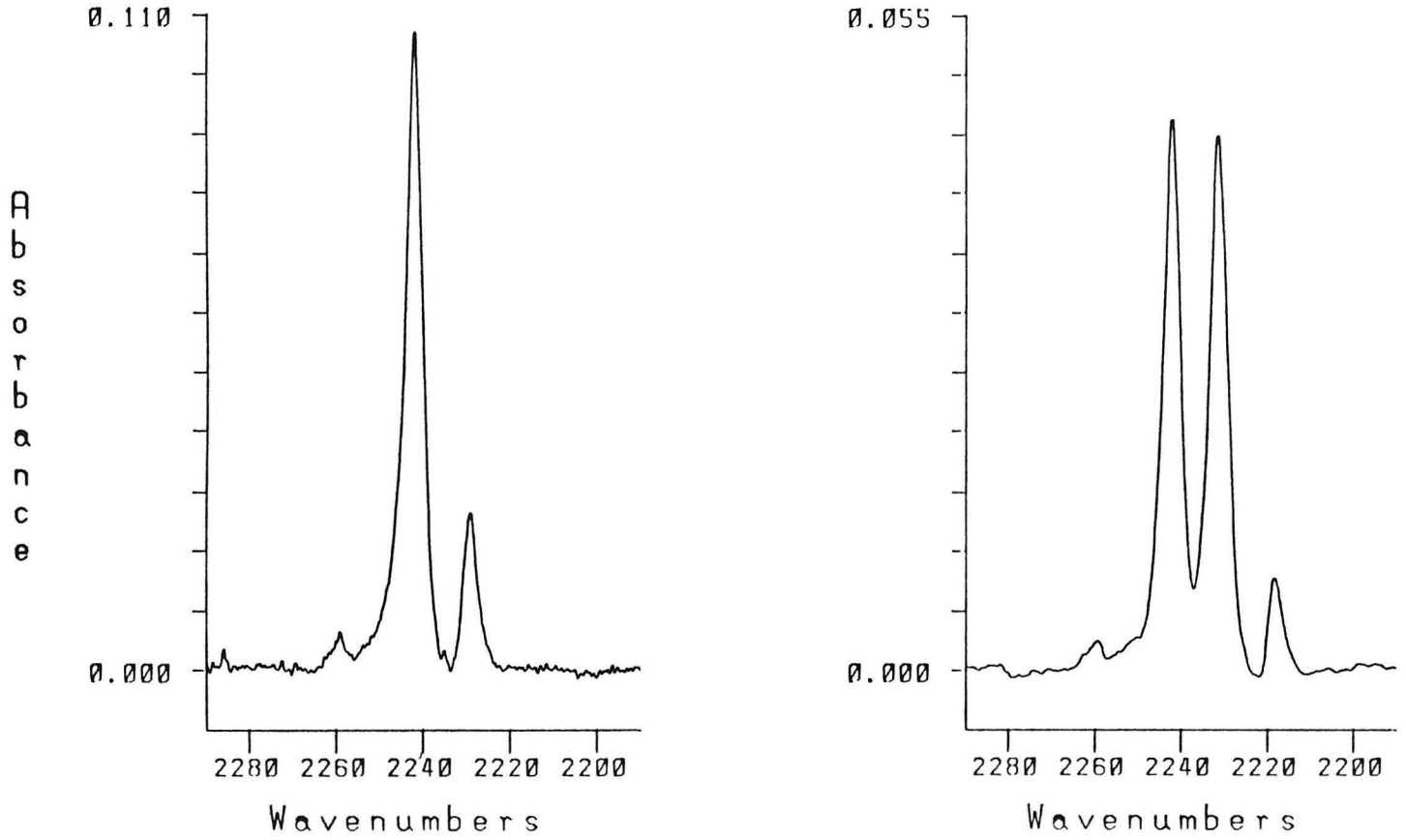

Figure 55. FT-IR spectra of diisopropylaminoisocyanate. (a) $-^{14}N=C=O$ stretch from UV (VIS filtered) photolysis of **17**. (b) $-^{14}N=C=O$ and $-^{15}N=C=O$ stretches from UV (VIS filtered) photolysis of **17**-^{15}N.

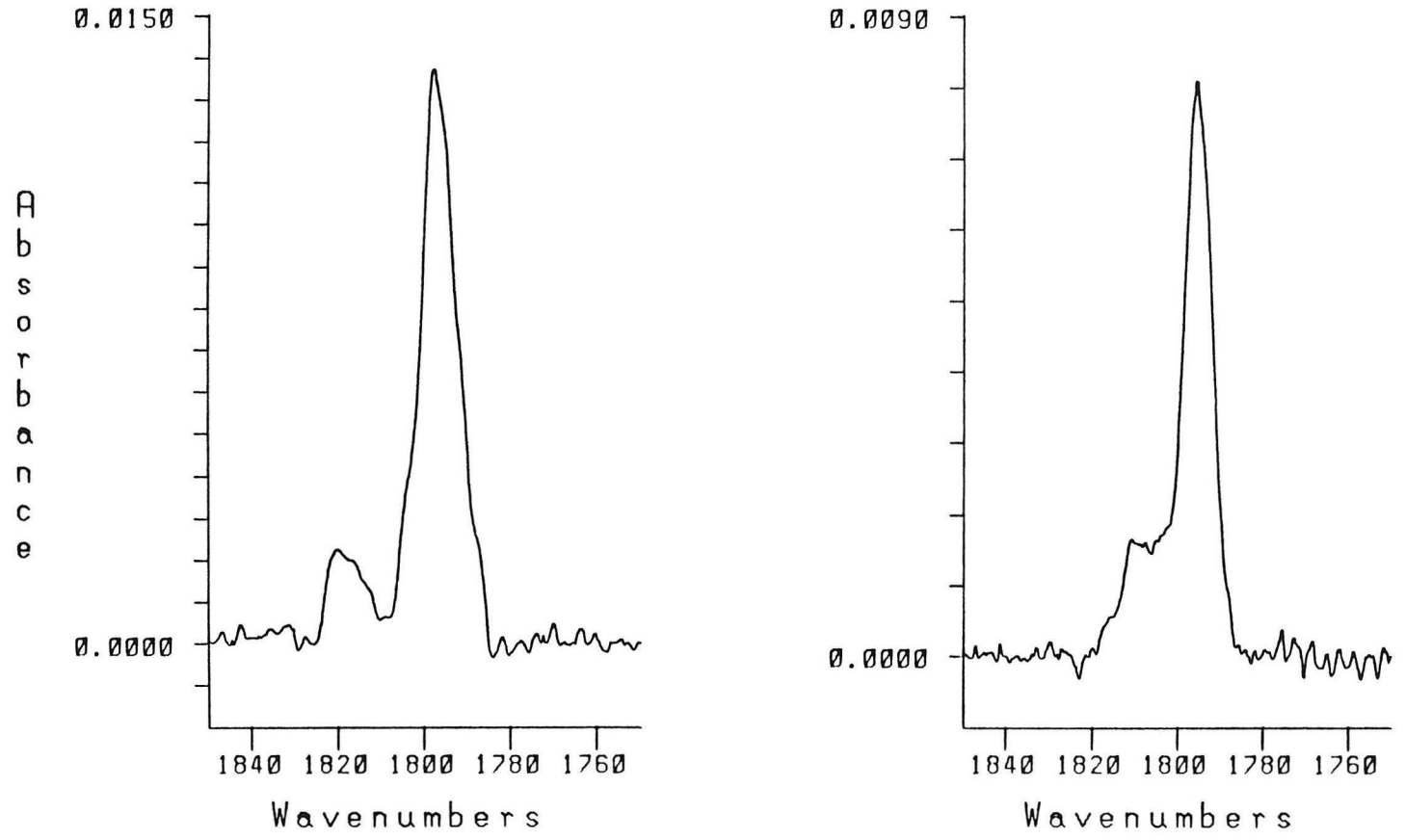

Figure 56. FT-IR spectra of carbonyl stretches for **29** and **30**. (a) From UV (VIS filtered) photolysis of **17**. (b) From UV (VIS filtered) photolysis of **17**-^{15}N.

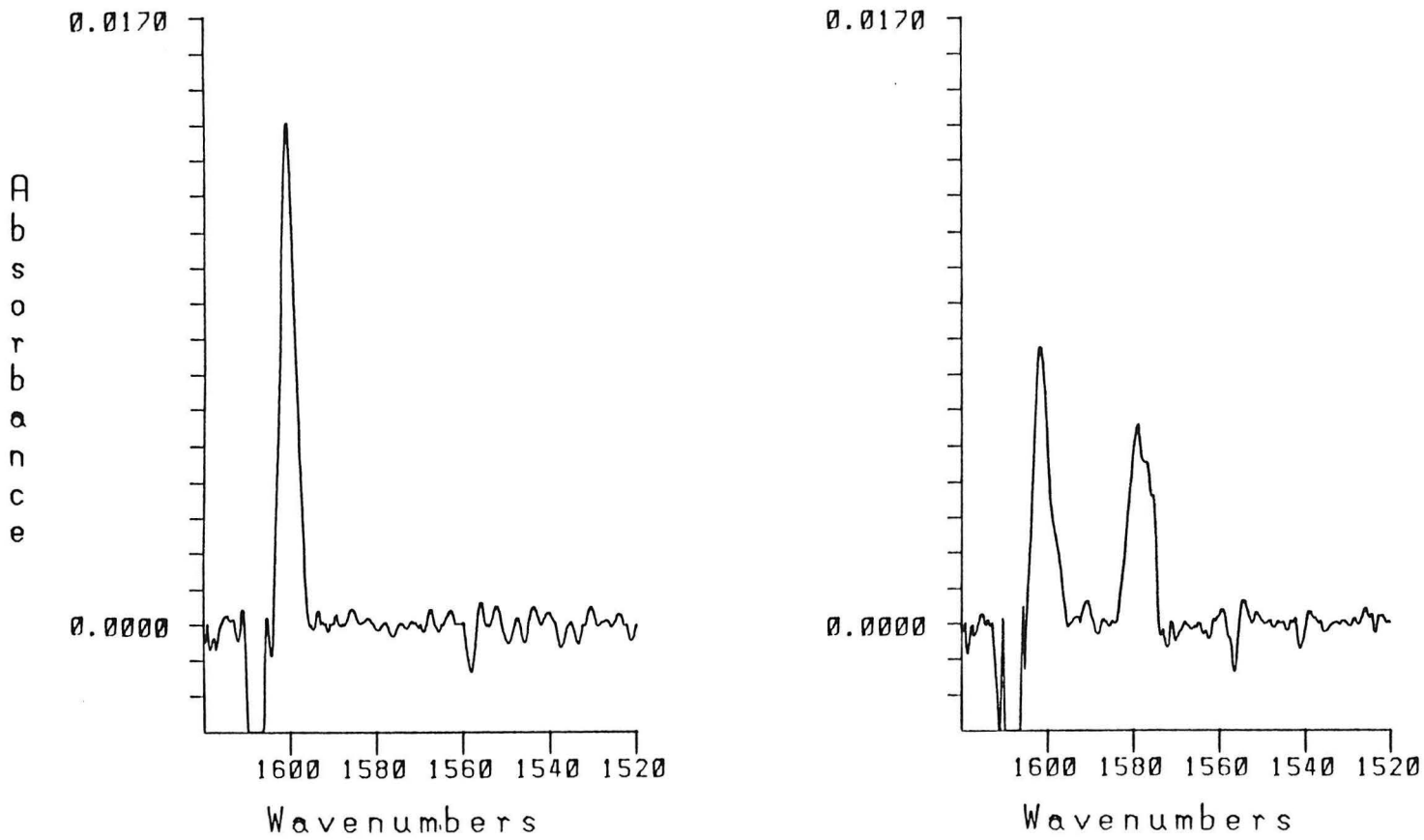

Figure 57. (a) R_2 $^{14}N=^{14}N$ stretch of **18** from UV (VIS filtered) photolysis of **17**. (b) R_2 $^{14}N=^{14}N$ and R_2 $^{14}N=^{15}N$ stretches of **18** and **18-^{15}N** from UV (VIS filtered) photolysis of **17-^{15}N**.

Table XXVIII. 1,1-Diazene Infrared Transitions.

1,1-Diazene		$^{14}N=^{14}N$	$^{14}N=^{15}N$	$^{14}N=^{15}N$ (calc.)[c]
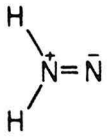	a	1574	1548	1548
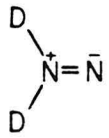	a	1571	1552	1545
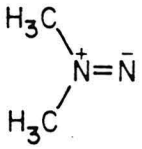	a	1601	1582	1574
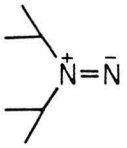	a	1601	1579	1574
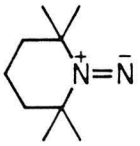	b	1595	1568	1568
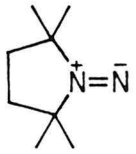	b	1638	1612	1610

[a]This work. Ar/100K. [b]Ref. 8e,f. CH_2Cl_2/-78°C. [c]Hooke's law calculated.

Table XXIX. Comparison of 1,1-Diazene and Isoelectronic Carbonyl Infrared Transitions.

1,1-Diazene	N=N	C=O	Carbonyl
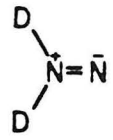	1571[a]	1698[d]	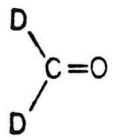
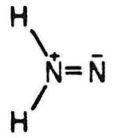	1574[a]	1742[d]	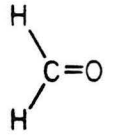
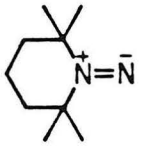	1595[b]	1690[c]	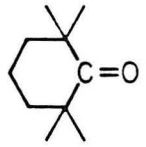
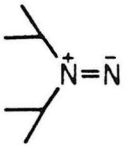	1601[a]	1713[c]	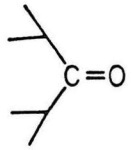
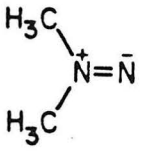	1601[a]	1719[c]	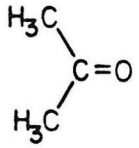
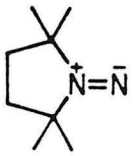	1638[b]	1725[c]	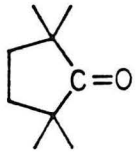

[a]This work. Ar/10°K. [b]CH_2Cl_2/-78°C. Ref. 8e,f. [c]CCl_4/R.T. [d]Ar/10°K.

the low temperature UV/VIS spectroscopy cell at 80°K.

Warming a 2-MTHF glass of **7** results in loss of **7** and growth of transition due to tetramethyl-2-tetrazene **19** and a red-orange species λ_{max} = 464 nm. Warming to greater than 170°K results in decolorization. Product analysis by analytical vapor phase chromatography (VPC) reveals tetramethyl tetrazene **19** as the major product together with ethane, N_2 and CO. Photochemical decomposition of **7** with visible light (VIS) (470-610 nm) (2-MTHF, 80°K) also results in loss of **7** and formation of the red-orange species λ_{max} = 464 nm. The λ_{max} = 464 species appears unaffected by futher visible photolysis (>340 nm). Warming to decolorization and VPC analysis reveals a greater yield of ethane than obtained from thermolysis of **7**

Table XXX. 1,1-Dimethyldiazene **7** Decomposition Products.[a]

Conc. **13** (M)	Conditions	C_2H_6	**19**
1×10^{-1}	Thermal[b,c]	1	9.7
1×10^{-1}	hν(VIS)[b,d]	1	6.1
5×10^{-3}	Thermal[e,f]	1	9.3
5×10^{-3}	hν(VIS)[e,g]	1	6.0

[a]Molar VPC ratios, n-Octane internal standard. [b]Quartz finger dewar, 77 K, hν UV (2-CS-7-54 filters), 3 h, 0.1 M, **13** 2-MTHF. [c]hν UV, warmed to R.T., 95% conversion, 95% product yield. [d]hν UV, hν (VIS) (CS-1-75, CS-3-70, CS-4-96 filters), 3 h, warmed, 92% conversion, 96% product yield. [e]UV/VIS spectroscopic cell, 82 K, hν UV (2-CS-7-54 filters),3 h, 5×10^{-3} M, **13** 2-MTHF. [f]hν UV, warmed, 92% conversion, 94% product yield. [g] hν UV, hν (VIS), 3 h, warmed, 90% conversion, 92% product yield.

together with tetrazene **19** as the major product. The product ratios for thermal and photochemical decomposition of **7** are listed in Table XXX.

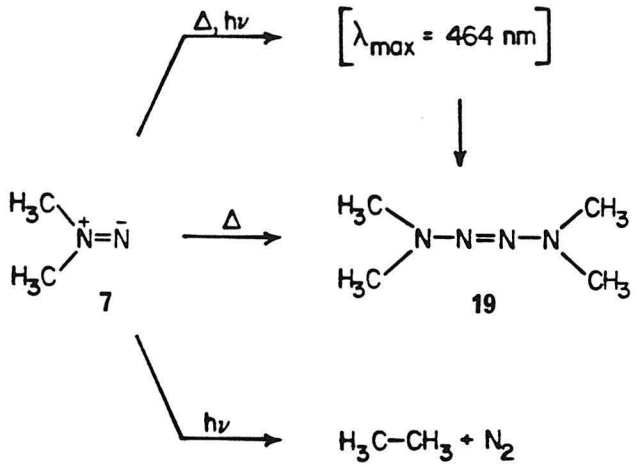

Tetrazene **19** was synthesized independently by oxidation of 1,1-dimethyldiazene. Tetrazene **19** isolated from decomposition of **7** by preparative VPC was compared spectroscopically (^{1}H NMR, UV, IR) and by analytical VPC coinjection. Methane, 1,2-dimethyldiazene **8** and formaldehyde dimethyl hydrazone **10** were not detected by ^{1}H NMR or analytical VPC (SE-54 capillary) from decomposition of **7** in 2-MTHF. Ethane was the major photochemical decomposition product of **7** in an argon matrix at 10°K. It can be inferred that the red-orange λ_{max} = 464 nm species which reuslts from thermal and photochemical decompositions of **7** in 2-MTHF ultimately yields tetrazene **19**.

The activation energy for nitrogen extrusion from **7** is estimated to be 23-26 kcal/mol. Hence, thermal decomposition of **7** to afford ethane and N_2 is unlikely at the low temperatures where the structured absorption of **7** is lost (<100°K). The ethane detected in the products from UV photolysis of **13**

to produce **7** followed by thermal decomposition of **7** very likely results, at least in part, from competitive decomposition/relaxation of excited **7** produced photochemically.

1,1-Diisopropyldiazene 18 Product Analysis

Warming a 2-MTHF glass of **18** results in loss of **18** and formation of a red-orange species λ_{max} = 474 nm. Warming to greater than 180°K results in decolorization. Product analysis by capillary VPC reveals tetrazene **20** and hydrocarbon products **32, 33,** and **34.**

Photochemical decomposition of **18** with visible light (VIS) (>470 nm) also results in loss of **18** and formation of the red-orange species λ_{max} = 474 nm. The products for thermal and photochemical decompositions of **18** are summarized in Table XXXI.

Tetrazene **20** is the expected dimerization product of 1,1-diazene **18.** Hydrocarbons **32, 33,** and **34** are the expected products of thermal and photochemical decomposition of **18** to two isopropyl radicals and N_2. It is unlikely that 1,1-diazene **18** extrudes N_2 at the low temperatures (<100°K) where the structured absorption curve of **18** is lost and the red-

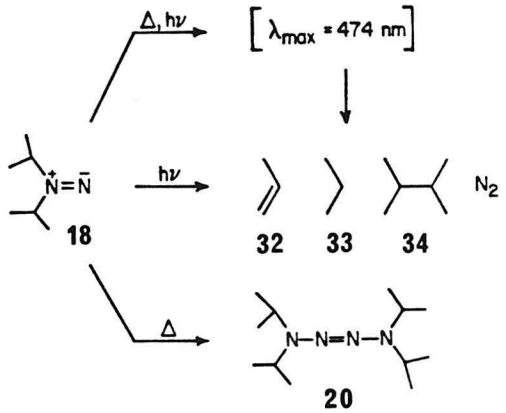

orange λ_{max} = 474 nm species grows in. Thus, it could be inferred that the λ_{max} = 474 nm species which subsequently decomposes (>200°K) ultimately yields the observed hydrocarbon products **32**, **33**, and **34** (at least in part). Higher initial concentrations of **18** afford a greater ratio of tetrazene **20** to hydrocarbons from both thermal and photochemical decomposition of **18**. For comparison, 1,1-di-tert-butyldiazene **6**, showed only unimolecular thermal decomposition to hydrocarbons **35**, **36**, and **37** at -78°C. Direct dimerization of **6** to tetra-tert-butyltetrazene was not

6 **35** **36** **37**

observed.[8f] The ratio of disproportionation products **32** and **33** to recombination product **34** from thermal decompositoin of 1,1-diazene **18** is comparable to that obtained from 1,1-di-tert-butyldiazene **6**. Comparison with the thermal and photochemical decomposition of 1,2-diisopropyl diazene is made in Table XXXII. The greater ratio of disproportionation to recombination products from **18** (or the red-orange λ_{max} = 474 species) may favor a competitive thermal decomposition of **18** via a β-hydrogen elimination. Subsequent radical chain decomposition of the H,

Table XXXI. 1,1-Diisopropyldiazene Decomposition Products.[a]

Conditions	32	33	34	20
Thermal[b,c]	15	13	1.0	4.8
hν(VIS)[b,d]	11	12	3.8	1.0
hν(VIS)[e]	2.8	3.3	1.0	1.0
Thermal[e,g]	16	15	1.0	160

[a]Molar VPC ratios n-dodecane and n-pentane internal standards. [b]UV/VIS spectroscopic cell, 3×10^{-3} M, **17** 2-MTHF, 82 K, hν UV (2-CS-7-54 filters), 3 h. [c]hν UV, warmed, 95% conversion, 94% product yield. [d]hν UV, hν (VIS) (CS-1-75, CS-3-70), 10 h, warmed, 95% conversion, 93% product yield. [e]Quartz finger dewar, 77 K, 0.1 M **17** 2-MTHF, hν UV (2-CS-7-54 filters), 3 h. [f]hν (VIS) (CS-1-75, CS-3-70 filters), 10 h, warmed, 99% conversion, 94% product yield. [g]hν UV, warmed, 96% conversion, 92% product yield.

Table XXXII. Molar Product Ratios for Some Related Decompositions.

Compound	Conditions	32	33	34
1,2-Diisopropyldiazene[a]	hν, R.T., octane	1.0	1.2	1.6
1,2-Diisopropyldiazene[a]	hν, R.T., gas	1.0	1.0	1.6
Diisopropyl ketone[b]	hν, 100°C, gas	1.0	1.0	3.5

[a]*Cis* or *trans*, Ref. 104. [b]Ref. 105.

isopropyl-1,2-diazene would give the observed disproportionation products **32** and **33.** Although a concerted β-elimination pathway cannot be ruled out, the formation of 2,3-dimethylbutane appears to indicate a nitrogen extrusion pathway for **18.**

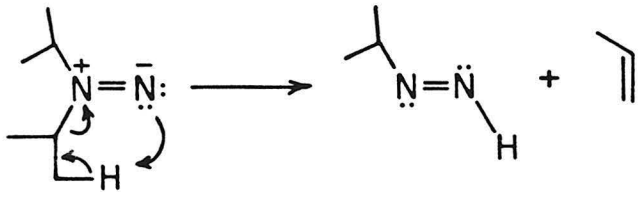

18 **32**

1,1-Diazene Tautomerization

The identity of red-orange species λ_{max} = 464 nm and λ_{max} = 474 nm produced thermally or photochemically from **7** and **18,** respectively, which apparently yields tetrazene and hydrocarbon products (the expected thermolysis products from **7**) of the 1,1-diazenes, is intriguing. The tautomer of a 1,1-diazene **7** (analogous to the enol form of a ketone) is azomethinimine **9.** Stabilized azomethinimines with N-aryl substituents

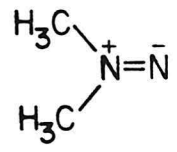

7

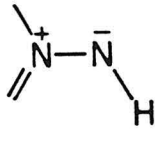

9

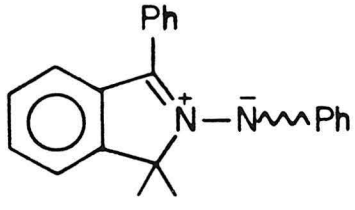

38

such as **38** have been prepared.[96,97] These species are known to be deeply colored (red-orange, λ_{max} = 460 nm, $\varepsilon \simeq$ 10,600). Azomethinimines have also been postulated as intermediates in a number of chemical reactions. The reaction of alkyl and aryl lithium reagents with N-nitrosamines affords transient deeply colored species which can be trapped to give products consistent with the intermediacy of an azomethinimine.[98] Neutralization

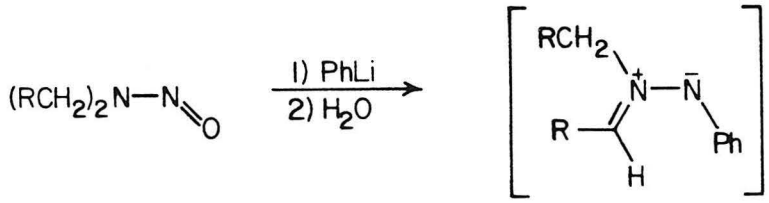

of dimethyldiazenium salts with base in aqueous solution affords a transitory red species.[99] Tetramethyl tetrazene **19** is the major product. This transient red color has been interpreted as evidence for 1,1-diazene **7**. However, competitive deprotonation of dialkyl diazenium salts is also likely to occur at the α C-H resulting in formation of the tautomer of the 1,1-diazene, an azomethinimine.[100]

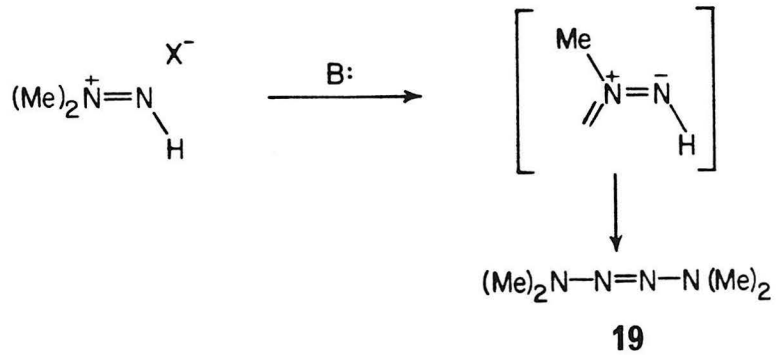

19

Theoretical treatments for azomethinimines tend to indicate a singlet biradical ground state analogous to that found for the isoelectronic ozone.[97] The relative heats of formation of a 1,1-diazene and its azomethinimine tautomer have not been calculated.

The electronic transitions for the deep red-orange species obtained from the corresponding 1,1-dialkyldiazenes with α-hydrogens are compared in Table XXXIII. These transitions follow the trend expected for substituent

Table XXXIII. Electronic Transitions for Proposed 1,1-Diazene Tautomers.

Tautomer	λ_{max} (nm)[a]
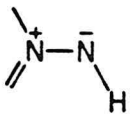	464[b]
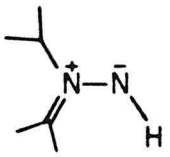	474[b]
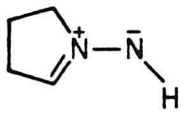	491[c]
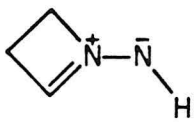	496[c],[d]

[a] 2-MTHF solution. [b] This work. [c] Ref. 84. [d] Shows reversible thermochromism (λ_{max} = 466 at 90°K, λ_{max} = 496 at 200°K).

effects on a π-π^* transition ($\sim$5 nm red shift per alkyl substituent) as predicted by Woodwards rules for alkenes.[87] The observation of these deeply colored species ($\varepsilon \simeq 3000\ M^{-1}\ cm^{-1}$) in a number of solvents, the substituent effects on the electronic transitions, the observed thermal chemistry, and a comparison with the spectroscopic properties of stabilized azomethinimines suggests their tentative assignments as the tautomers of 1,1-dialkyl diazenes (azomethinimines). The apparent facile thermal rearrangement of **7** to **9** and

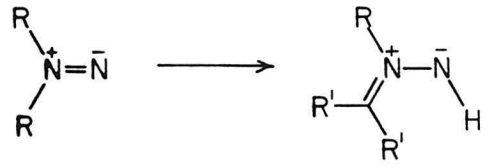

R = Me **7** R' = H **9**

R = i-Pr **18** R' = Me **30**

18 to **30** at 90°K suggests a very small barrier for this transformation. Observation of this transformation in a triacetin glass well below the softening temperature may be indicative of a unimolecular pathway. Failure to detect 1,1-diazenes **7** and **18** in equilibrium with **9** and **30** by electronic spectroscopy suggests that **9** and **30** are indeed lower in energy than the corresponding 1,1-diazenes. For comparison, a free energy difference $\Delta G = 1$ kcal/mol at 90°K corresponds to an equilibrium constant K = 268.

Thermal Decomposition Kinetics

The kinetics for thermal decomposition of 1,1-diazenes **7** and **18** in a

softened 2-MTHF glass (see Figures 41 and 42) do not bear interpretation due to the limited data attainable and baseline effects due to overlap of the very strong transitions attributable to **9** and **30**. In addition, the kinetics for growth of the λ_{max} = 464 nm and λ_{max} = 474 nm transitions of **9** and **30** at 90°K in a softened 2-MTHF glass are non-exponential and fit no simple kinetic treatment. The non-exponentiality may be attributable to the non-fluid nature of the softened glass (viscosity or site effects).[81,82] Kinetic treatments for presumed site effects on unimolecular decompositions in rigid media (e.g., ln A vs. $t^{1/2}$, $t^{1/3}$, etc.) did not yield interpretable data.[101]

Although kinetic treatments at 90°K proved inconclusive, thermal decomposition of **9** and **30** at warmer temperatures in 2-MTHF solution gave excellent kinetics. Thermal decomposition of **9** monitored at 464 nm gave bimolecular decomposition kinetics over a range of initial absorbances (Figure 58, Table XXXIV). Attempts to measure kinetics for formation of tetramethyl-2-tetrazene **19** ($\lambda_{max} \simeq 280$ nm) which grows in with decay of **9** were unsuccessful presumably due to an overlapping UV absorption due to **9**.

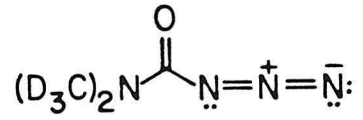

13-d_6

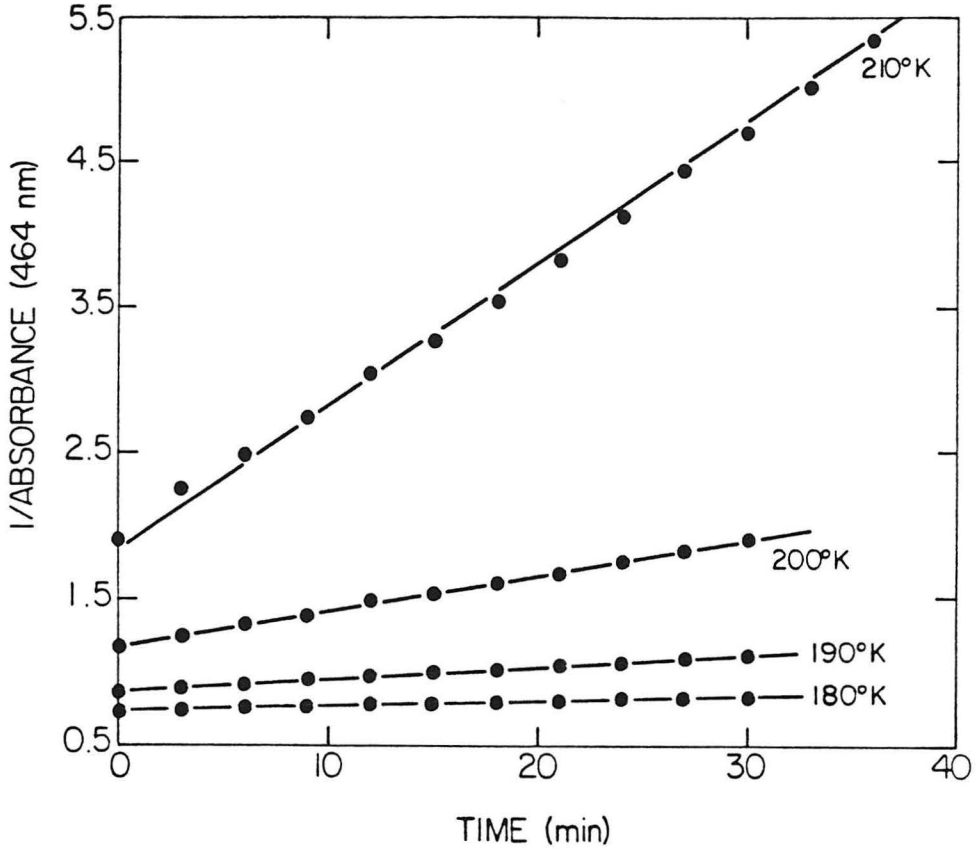

Figure 58. Bimolecular decay kinetics for λ_{max} = 464 nm species (**9-h$_6$**) from thermolysis of **7** (2-MTHF).

Table XXXIV. Second Order Rate Constants for Decomposition of **9-h$_6$**.[a]

Temperature (°K)	k_2 (A^{-1} sec^{-1})	r^2
180	5.45×10^{-5}	0.999
190	1.40×10^{-4}	0.999
200	4.02×10^{-4}	0.999
210	1.49×10^{-3}	0.999

[a]2-MTHF.

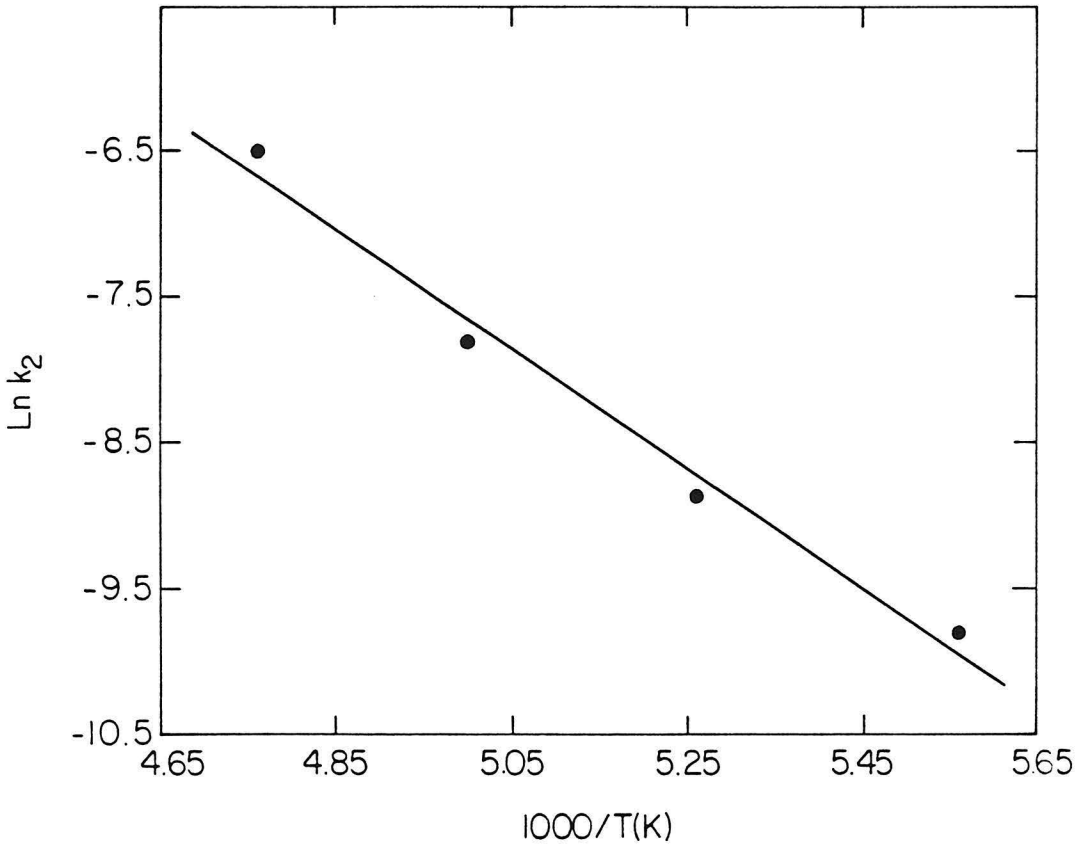

Figure 59. Arrhenius plot for bimolecular decomposition kinetics of λ_{max} = 464 nm species (**9-h$_6$**) from **7** in 2-MTHF.

For comparison, fully deuterated (>99% d_6) **13-d$_6$** was prepared. UV (VIS filtered) photolysis of **13-d$_6$** in a 2-MTHF glass at 80°K afforded a structured absorption curve of **7-d$_6$** (λ_{max} = 556 nm) identical to that obtained for **7**. Warming the glass to 90°K afforded **9-d$_6$** λ_{max} = 464 nm. From the same initial absorbance the rate of formation of **9-h$_6$** ($\Delta A/\Delta t$) is only a factor of $\sim$3 times the rate of formation of **9-d$_6$**. This surprising result

would be consistent with the lack of a primary deuterium kinetic isotope effect for tautomerization of **7** to **9** and the presence of only secondary isotope effects. For a change in hybridization from sp^3 to sp^2, a normal secondary deuterium isotope effect ranges from k_H/k_D = 1.4 to 3.1 per deuterium at 90°K.

The thermal decomposition of **9-d_6** shows a strong deuterium isotope effect (Figure 60, Table XXXV). At 190°K k_H/k_D = 6.7 for bimolecular decomposition of **9**. The magnitude of the deuterium isotope effect is consistent with a combination of primary and secondary isotope effects. A normal primary isotope effect of k_H/k_D = 5 at 298°K would correspond to k_H/k_D = 12.5 at 190°K. For a change in hybridization from sp^2 to sp^3 a normal secondary isotope ranges from k_H/k_D = 0.59 to 0.83 per deuterium at 190°K. A combination of two secondary isotope effects and a primary isotope effect would be expected to range from k_H/k_D = 4.3 to 8.6. The observed k_H/k_D = 6.7 at 190°K is well within this range.

Assuming an extinction coefficient of $\varepsilon \simeq 3000\ M^{-1}\ cm^{-1}$ for **9** allows calculation of Arrhenius activation parameters for bimolecular decomposition of **9**. For **9-h_6** $E_a = 8.2 \pm 0.5$ kcal/mol and $\log_{10} A = 1.8 \pm 0.6$ ($\Delta H^{\ddagger}$ = 7.8 kcal/mol, $\Delta S^{\ddagger}$ = -51.3 e.u.). For **9-d_6** $E_a = 8.6 \pm 0.5$ kcal/mol and $\log_{10} A = 1.4 \pm 0.6$. The apparent low A factors are consistent with severe stereochemical constraints on the transition state. For comparison, direct dimerization of kinetically persistent diazene **4** $E_a = 6.4 \pm 0.9$ kcal/mol and $\log_{10} A = 3.8 \pm 0.7$.

Mechanistically, the presence of a deuterium isotope effect for

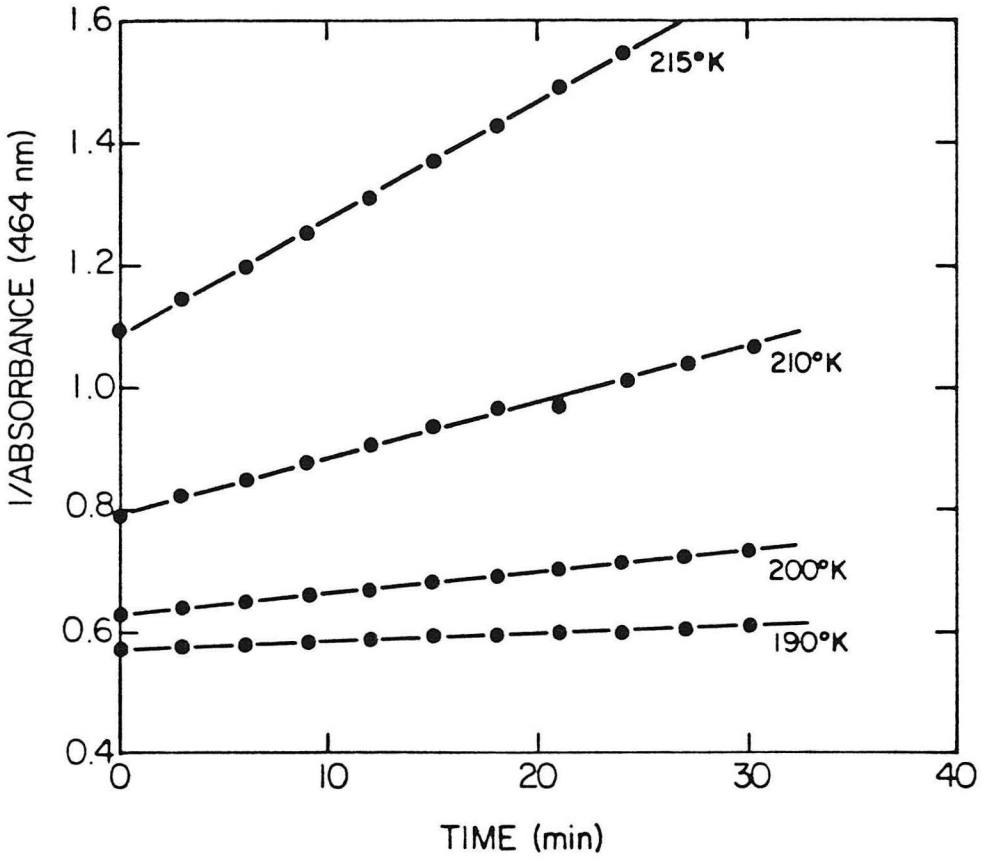

Figure 60. Bimolecular decay kinetics for λ_{max} = 464 nm species (**9-d_6**) from thermolysis of **7-d_6** (2-MTHF).

Table XXXV. Second Order Rate Constants for Decomposition of **9-d_6**.[a]

Temperature (°K)	k_2 (A^{-1} sec^{-1})	r^2
190	2.10×10^{-5}	0.997
200	5.83×10^{-5}	0.999
210	1.52×10^{-4}	0.995
215	3.20×10^{-4}	0.999

[a] 2-MTHF.

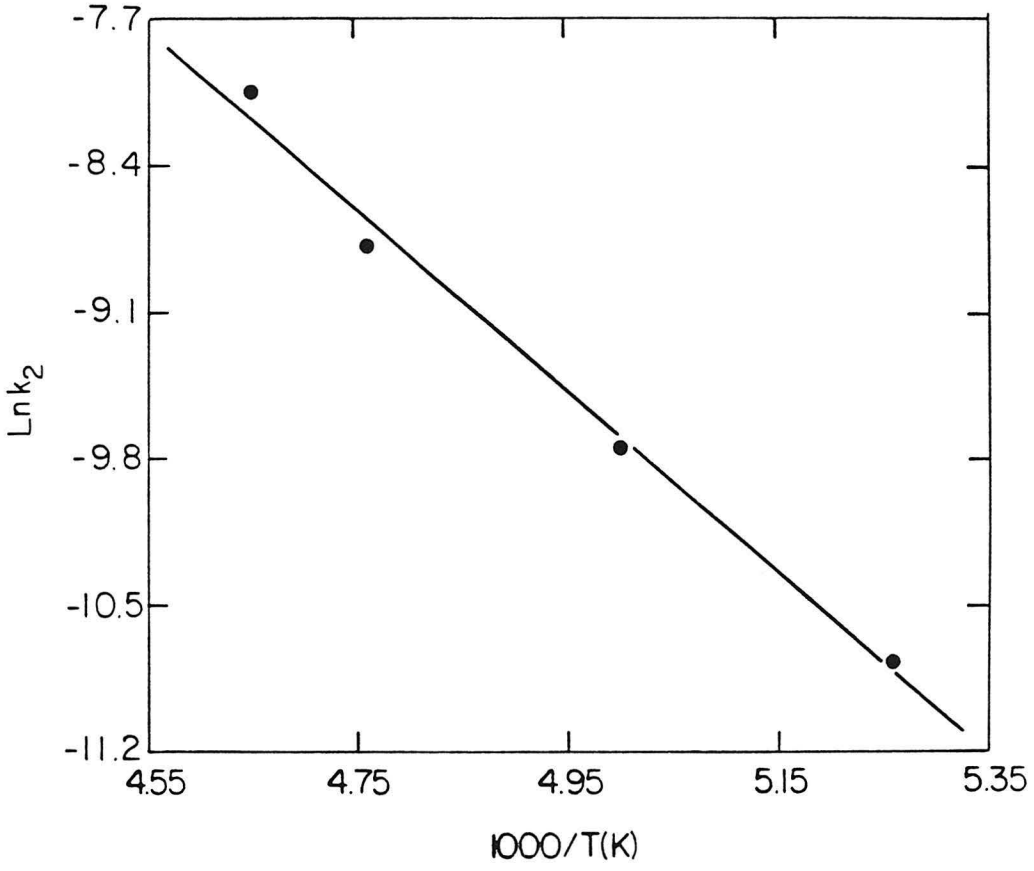

Figure 61. Arrhenius plot for bimolecular decomposition kinetics of λ_{max} = 464 nm species (**9-d_6**) from **7-d_6** in 2-MTHF.

bimolecular loss of **9** may be consistent with a mechanism involving an equilibrium of **9** and 1,1-diazene **7** followed by dimerization of **7** with **7** (unlikely, no isotope effect expected) or dimerization of **7** with **9** to form tetrazene **19** (Scheme V). A mechanism involving rate determining tautomerization of **9** to **7** followed by dimerization of two **7**'s should show unimolecular decay of **9** (see Appendix Mechanism A). A rapid equilibration of **9** to **7**, with equilibrium favoring **9**, followed by rate determining dimerization of **9** and **7** to form tetrazene **19** should show the observed bimolecular kinetics

Scheme V

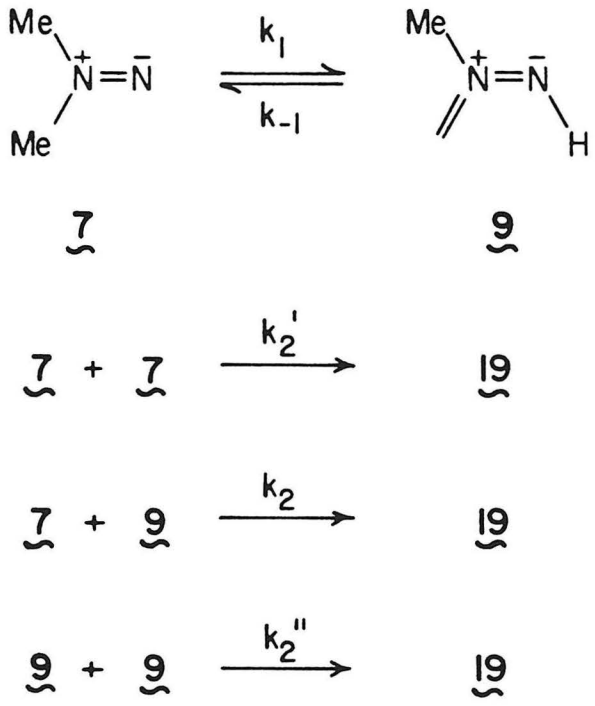

(see Appendix Mechanism B) if $k_1 >> k_2(\mathbf{9})$, and a deuterium isotope effect as observed.

$$\frac{-d(\mathbf{9})}{dt} = k_{-1}(\mathbf{9}) \left(\frac{2\ k_2(\mathbf{9})}{k_1 + k_2(\mathbf{9})} \right)$$

$$= 2 \left(\frac{k_{-1}}{k_1} \right) k_2(\mathbf{9})^2$$

Dimerization of **9** with **7** may be similar to the known facile acid catalyzed dimerization of 1,1-diazenes (diazenium ion plus 1,1-diazene followed by deprotonation). One resonance form of **9** is similar to a 1,1-diazenium ion with an anionic substituent **9a.**

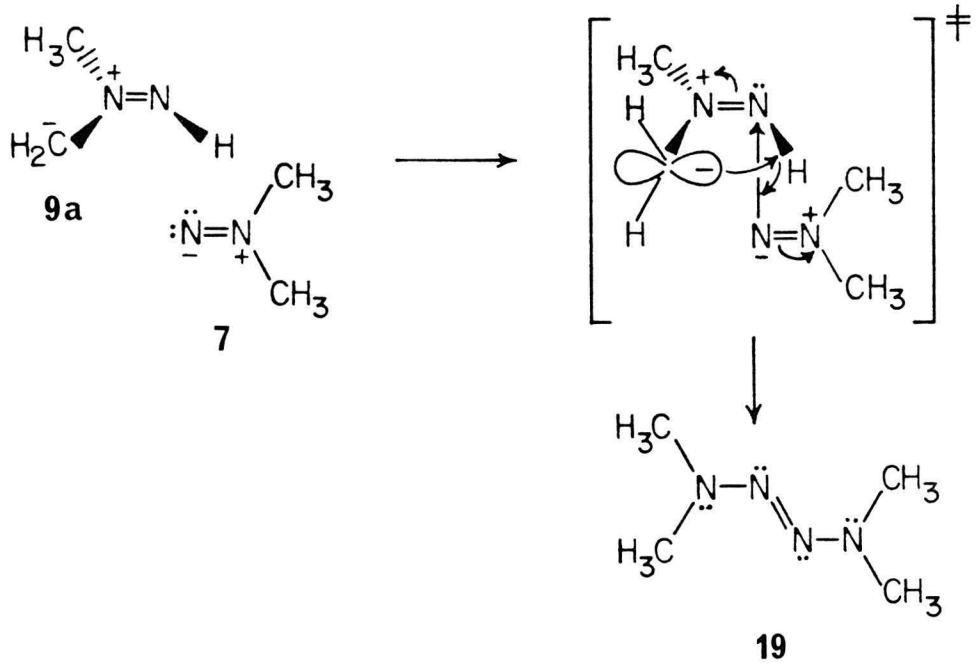

9a **7** **19**

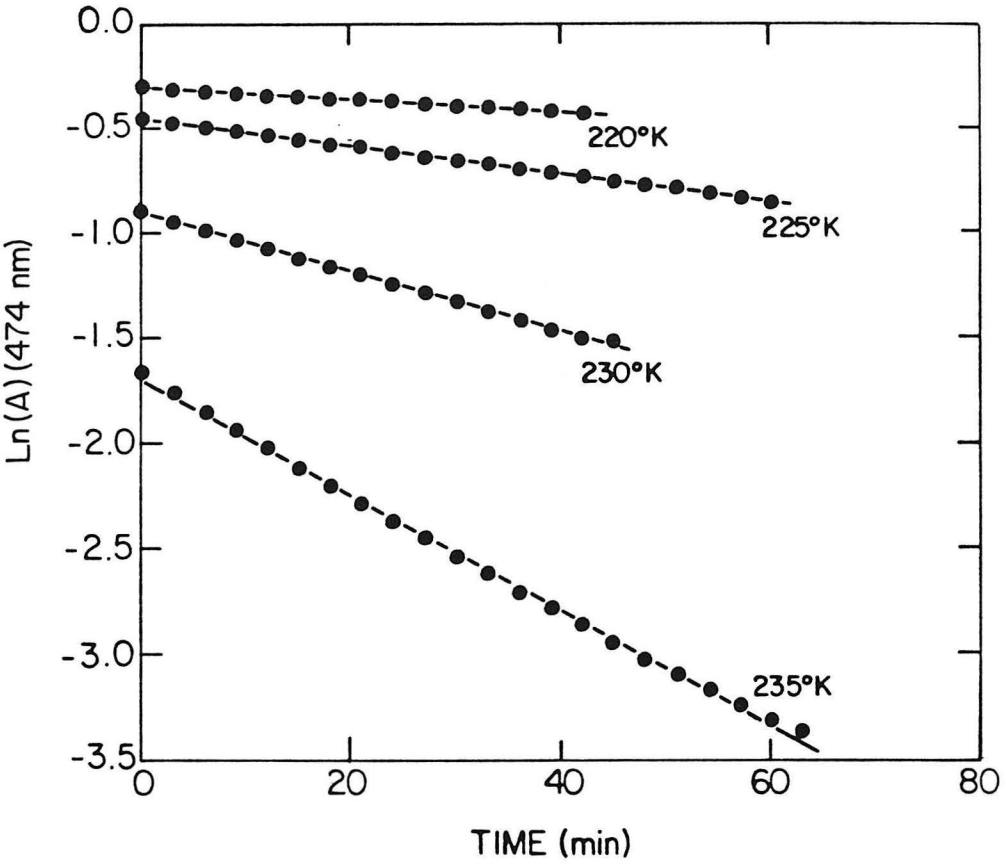

Figure 62. Unimolecular decay kinetics for decomposition kinetics of λ_{max} = 474 nm species (**30**) from thermolysis of **18** (2-MTHF).

Table XXXVI. First Order Rate Constants for Decomposition of **30**.[a]

Temperature (°K)	k_1 (A^{-1} sec^{-1})	r^2
220	4.68×10^{-5}	0.999
225	1.09×10^{-4}	0.999
230	2.35×10^{-4}	0.998
235	4.53×10^{-4}	0.999

[a]2-MTHF.

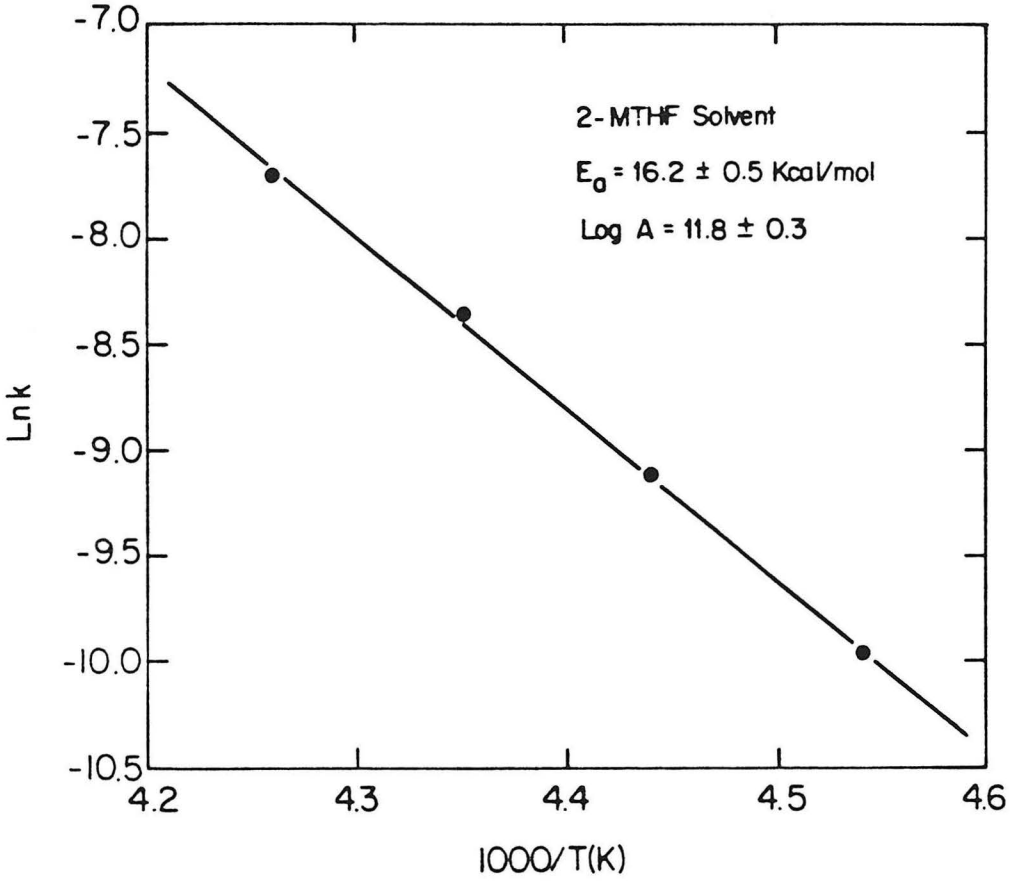

Figure 63. Arrhenius plot of unimolecular decomposition of λ_{max} = 474 species (**30**) from **18** in 2-MTHF .

Scheme VI

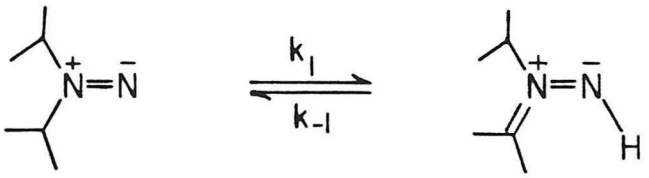

18 30

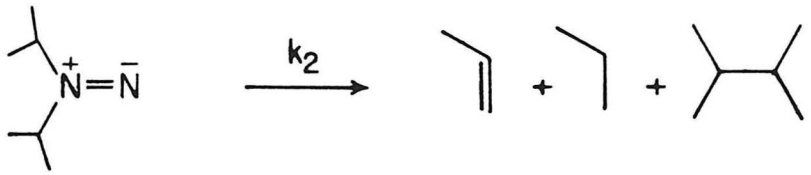

18 32 33 34

$$\frac{-d(30)}{dt} = k_{-1}(30) - k_1(18)$$

$$= \frac{k_{-1}k_2}{k_1 + k_2}(30)$$

if $k_1 >> k_2$

$$= \left(\frac{k_{-1}}{k_1}\right) k_2(30)$$

Table XXXVII. Relative Rates and $\Delta G^{\ddagger}$'s for 1,1-Diazene Decompositions at -94°C (179°K).

1,1-Diazene	$\Delta G^{\ddagger}$	k rel
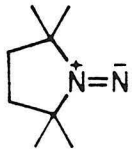	19.4[a]	4×10^{-9}
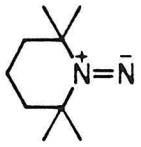	19.1[a]	1×10^{-8}
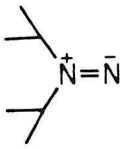	16.8[b]	6×10^{-6}
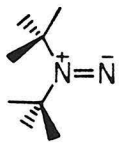	12.5[c]	1

[a]Ref. 8g (Et_2O). [b]This work, intermediacy of **18** assumed, $k = k_2/K$ see text (2-MTHF). [c]Ref. 8f (Me_2O).

The thermal decomposition of 1,1-diisopropyl diazene and formation of red-orange **30** λ_{max} = 474 nm at 90°K did not give interpretable kinetics as previously discussed for 1,1-diazene **7**. The decay of **30** monitored at 474 nm gave unimolecular decomposition kinetics (Figure 62, Table XXXVI). The UV absorption of tetraisopropyl-?-tetrazene **20** does not grow in with thermal decomposition of **30**. The major products from thermolysis of 1,1-diazene **18** are hydrocarbons **32**, **33**, and **34**. This is consistent with a mechanism involving rapid equilibrium of 1,1-diazene **18** and tautomer **30** followed by rate determining thermal decomposition of **18** to afford hydrocarbon products expected from decomposition of **18** (Scheme VI) (see Appendix Mechanism C).

The Arrhenius activation parameters for unimolecular decomposition of **30** E_a = 16.8 ± 0.5 kcal/mol and $\log_{10}$ A = 11.8 ± 0.3 ($\Delta H^{\ddagger}$ = 15.8 kcal/mol, $\Delta S^{\ddagger}$ = -5.7 e.u.) are consistent with the activation parameters expected for nitrogen extrusion from 1,1-diisopropyldiazene **18**. For comparison the activation parameters for cyclic kinetically persistent 1,1-diazene **5** are E_a = 19.1 ± 0.4 kcal/mol, $\log_{10}$ A = 12.1 ± 0.3 in THF solution while the activation parameters for 1,1-di-tert-butyldiazene **6** are $E_a \simeq 13$ kcal/mol for an assumed $\log_{10}$ A = 13. The activation free energies for 1,1-diazenes are compared in Table XXXVII.

Matrix FT-IR Studies of Carbon Monoxide

A group of infrared bands assigned to CO show photochemical behavior which mirrors the behavior of 1,1-dimethyldiazene **7** and its photochemical decomposition products. Similar behavior was observed for CO bands

associated with H_2NN **3** and its products (see Chapter 1).

UV (VIS filtered) photolysis of **13** (1:1400, Ar, 10°K) (Figure 64a) yields CO bands at 2142.02, 2137.80, 2135.93, 2134.75, and 2132.95 cm^{-1} (Figure 64b) in addition to FT-IR bands of 1,1-diazene **7**, dimethylaminoisocyanate and ethane (see Figure 44). Photolysis of **7** with visible light results in loss of two of the CO bands at 2142.02 (minor) and 2134.75 (major) and growth of two CO bands at 2137.80 and 2132.95 cm^{-1} (Figure 64c). One CO band at 2135.93 cm^{-1} remains apparently unchanged as a shoulder on the 2137.80 cm^{-1} band. Coincident with this transformation in the CO stretch region, infrared bands due to 1,1-diazene **7** (a major set of bands (D_M) and a minor set (D_m)) are lost while infared bands due to ethane and an unknown species (U) grow in. Further photolysis (λ 340-410 nm) results in loss of FT-IR bands of (U) and growth of ethane bands. Coincident with this transformation, the CO band at 2132.95 cm^{-1} is lost while the CO band at 2137.80 cm^{-1} grows in (Figure 64d).

Shifts of the CO stretch frequency due to hydrogen bonding (e.g., H_2O, NH_3), dipole-dipole and electrostatic interactions[71] (e.g., N_2) allows the qualitative assessment of the matrix environment of a CO-molecule complex (see Chapter 1) (Table XXXVIII).

The CO bands at 2142.03 (minor) and 2134.75 cm^{-1} (major) correspond in intensity ratio and photochemical behavior to two sets of bands assigned to 1,1-diazene **7** (D_M, D_m). The shift of the minor CO band at 2142.03 cm^{-1} (CO/D_m) to higher energy relative to CO in an argon matrix (2138.25 cm^{-1}) or CO in a nitrogen matrix (2139.69 cm^{-1}) suggests a hydrogen bonding or

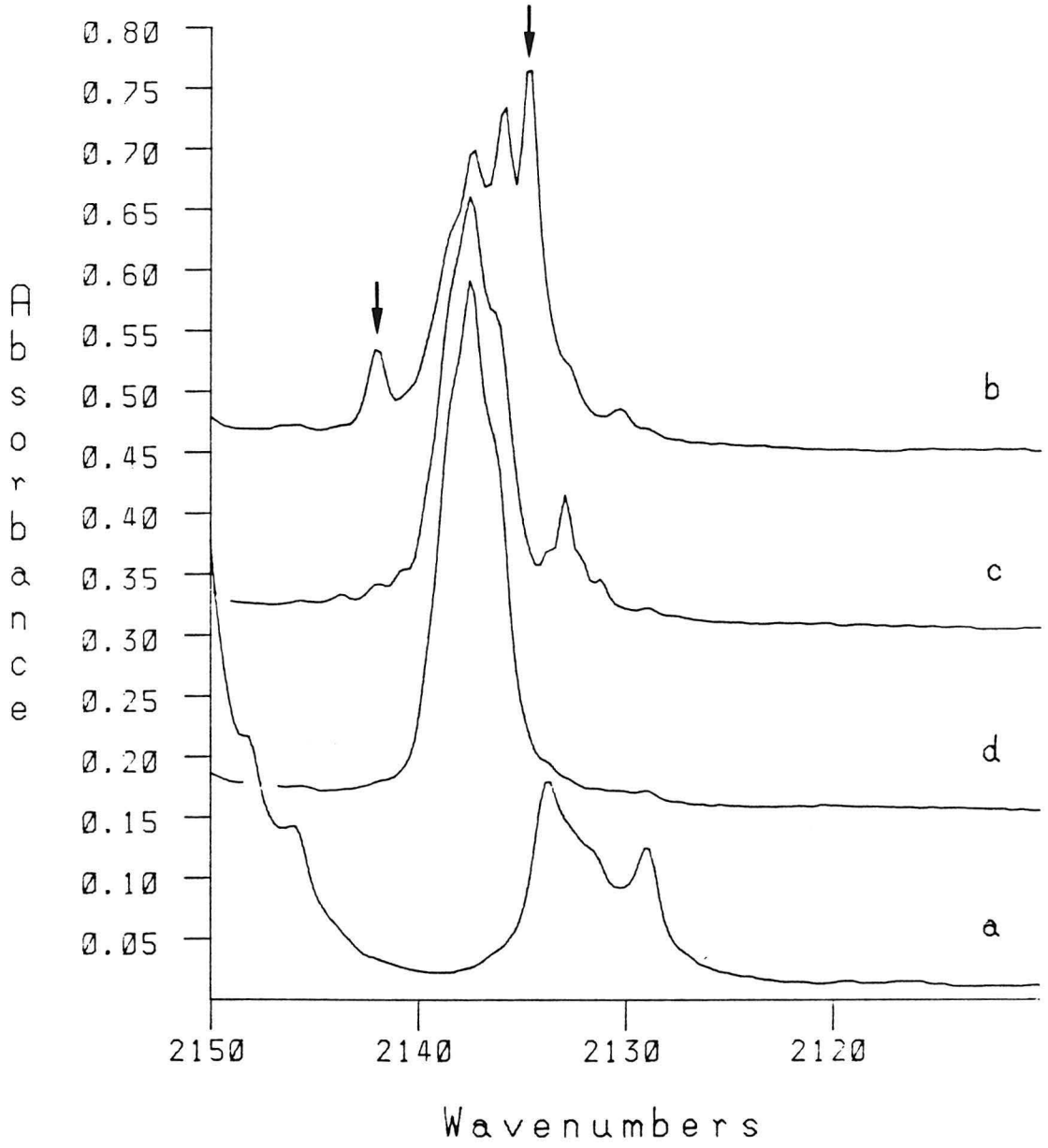

Figure 64. Successive FT-IR spectra of the CO stretch region (Ar, 10°K). (a) Before photolysis of **13** (1:1400, Ar, 10°K). (b) After UV (VIS filtered) photolysis of **13** (1 h) to form **7** and CO. (c) After VIS (470-610 nm) photolysis (1 h) of **7** to form ethane and (U). (d) After photolysis of (U) 340-410 nm) (1 h) to form ethane.

Table XXXVIII. Matrix Isolation Carbon Monoxide (CO) Infrared Stretch Frequencies.

CO/Matrix	(Ratio)	Obs.[a] ν CO (cm^{-1})	Lit.[b] ν CO (cm^{-1})	(Ratio)
CO/Ar	(1:2000)	2138.25	2138.40	(1:1000)
CO/N_2	(1:2000)	2139.69	2139.69	(1:1000)
$CO/H_2O/Ar$	(1:2:2000)	2148.60	2148.8	(2:5:1000)
$CO/NH_3/Ar$			2143.3	(1:1:1000)
$CO/H_2NN/Ar$	[c]	2140.90		
$CO/H_2/N_2/N_2/Ar$	[c]	2139.94 2138.97 2137.53		
$CO/(CH_3)_2NN(D_M)/Ar$	[d]	2134.75		
$CO/(CH_3)_2NN(D_m)/Ar$	[d]	2142.02		
$CO/C_2H_6/N_2/N_2/Ar$	[d]	2137.80 2135.93		
CO/(U)/Ar	[d]	2132.95		

[a]This work (10°K). [b]Ref. 71 (10°K). [c]Matrix ratio approximately (1:1:2000, Ar). [d]Matrix ratio approximately (1:1:1400, Ar).

dipole-dipole stabilizing interaction (higher energy stretch) for this CO. The lower energy stretch (relative to free matrix) for the major CO stretch at 2134.75 cm^{-1} (CO/D_M) suggests a destabilizing dipole-dipole or electrostatic interaction for this CO. The orientation of CO relative to 1,1-diazene **7** could give rise to either a dipole-dipole stabilized (CO, D_m) or destabilized (CO/D_M) CO environment. A steric interaction with the methyl groups of **7**

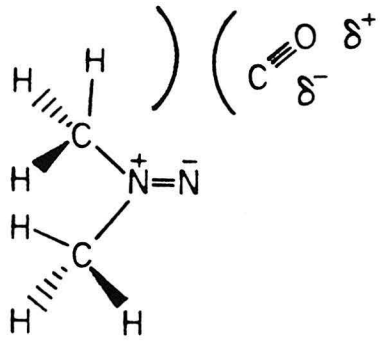

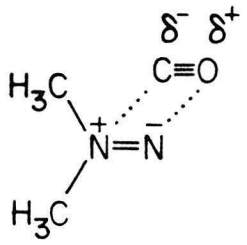

may be sufficient to prevent a stabilizing interaction with CO.

Two CO bands at 2137.80 and 2135.93 cm^{-1} mirror the behavior of bands due to ethane which grow in with photolysis of **7** and (U). The lower energy stretch frequencies of these CO's (relative to free matrix CO) suggest an intimate association of CO with ethane and N_2 (possibly two N_2's) in a matrix site. For comparison, the stretching frequency for CO in a rigid 3-methyl pentane matrix is 2132 cm^{-1}.

In addition to ethane, VIS photolysis of **7** affords infrared bands of a minor unidentified species (U). A low frequency CO stretch at 2132.95 cm^{-1} grows in with (U) and is subsequently lost with photolysis of (U) (λ 340-410 nm). The low frequency of the CO band at 2132.95 suggests a destabilizing dipole-dipole or electrostatic interaction of CO with (U). A destabilizing dipole-dipole interaction of CO with the lone pairs of <u>cis</u> 1,2-dimethyldiazene **8c** would be consistent with the observed CO stretch frequency. Interestingly, the FT-IR bands of (U) correlate well with those of **8c**.

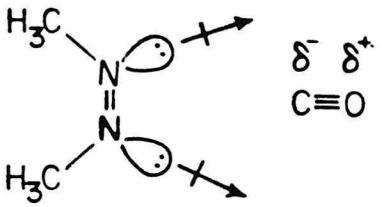

Summary

The low temperature matrix isolation and direct spectroscopic characterization of 1,1-dimethyldiazene **7** and 1,1-diisopropyldiazene **18** have been described. The UV (VIS filtered) photolysis of carbamoyl azides **13** and **17** in a rigid medium (organic glass, 80°K or Ar matrix, 10°K) provides a new general method for the photochemical generation of reactive 1,1-dialkyldiazenes. This photochemical route is considered to proceed by the photo-Curtius rearrangement of a carbamoyl azide to an aminoisocyanate followed by photodecarbonylation of the aminoisocyanate to a 1,1-diazene and CO. The 1,1-diazenes are purple showing structured absorption curves in the visible λ_{max} = 556 nm for **7** and λ_{max} = 504 nm for **18**. 1,1-Diazene **7** was independently generated by photolysis of (Z)-3,3-dimethyl-1-phenyltriazene-1-oxide **16** (2-MTHF, 80°K) to form **7** and nitrosobenzene. Comparison of the absorptions permits estimation of the extinction for **7** of 6 (M^{-1} cm^{-1}). The characteristic N=N double bond stretches of the 1,1-diazenes are located at

1600.96 cm^{-1} for **7** and 1600.92 for **18**. The spectroscopic characterization of matrix isolated 1,1-dialkyldiazenes is consistent with the theoretical (GVB-CI) prediction for H_2NN **3** and the experimental characterization of **3** and kinetically persistent 1,1-diazenes **4**, **5**, and **6**.

Thermolysis of **7** and **18** yields deeply colored species **9** (λ_{max} = 464 nm) and **30** (λ_{max} = 474 nm), respectively. These species are tentatively identified as the azomethinimine tautomers of the 1,1-diazenes with α-hydrogens. Photolysis of 1,1-diazenes **7** and **18** at their n-π* transitions in the visible also results in formation of **9** and **30** (organic glasses, 80°K). The products of subsequent thermolysis of **9** and **30** are the 2-tetrazene and hydrocarbon products expected from the respective 1,1-diazenes.

The kinetics for thermal decomposition of **9** and **30** are consistent with an equilibrium with the corresponding 1,1-diazenes **7** and **18** followed by bimolecular dimerization of **7** to 2-tetrazene **19** and unimolecular nitrogen extrusion for **18**. Photochemical decomposition of **7** (Ar, 10°K) yields infrared bands of ethane and an unidentified species (U) which is subsequently photolyzed to ethane. The observation of several FT-IR stretches for CO which mirror the photochemical behavior of 1,1-diazene **7** and its photodecomposition products in an argon matrix (Ar, 10°K) suggests an intimate association of CO with these products in a rigid environment.

EXPERIMENTAL SECTION

Melting points were determined using a Thomas-Hoover melting point apparatus and are uncorrected. Infrared spectra were recorded on either a Perkin-Elmer 257 or a Shimadzu IR-435 spectrophotometer. Fourier transform infrared spectra (FT-IR) were recorded on a Mattson Instruments Sirius 100 FT-IR equipped with Starlab minicomputer data station and high resolution graphics terminals under a positive nitrogen purge at 0.25 cm^{-1} using HgCdTe (MCT) detector cooled to 77°K unless otherwise noted. Proton NMR spectra were obtained on either a Varian Associates EM-390, Jeol FX-90O or Varian Associates XL-200 spectrometer. Chemical shifts are reported as parts per million (ppm) downfield from tetramethylsilane (TMS) in δ units and coupling constants are in Hertz (Hz). NMR data are reported in this order: chemical shift; multiplicity, s = singlet, d = doublet, t = triplet, m = multiplet; number of protons; coupling constants. Nitrogen (^{15}N) NMR spectra were obtained on either a Jeol FX-90O or Brucker WM-500 spectrometer. Chemical shifts are reported in parts per million (ppm) from ^{15}N nitromethane with a negative value indicating an upfield position. Deuterium (^{2}H) NMR spectra were recorded on a Jeol GX-400 spectrometer. Chemical shifts are reported in ppm from TMS. Electronic spectra were obtained using a Varian associates 219 spectrophotometer. Electronic spin resonance (ESR) spectra were recorded using a Varian Associates E-line spectrometer equipped with an Air Products and Chemicals Helitran LTD-3-110 liquid helium transfer apparatus. Emission spectroscopy was performed with assistance of members of Professor H. B. Gray's group at Caltech using

a noncommercial spectrophotometer with a 250-watt xenon source and Hamamatsu R-406 and R-955 photomultiplier tubes. Raman spectroscopy was performed with assistance of members of Professor S. I. Chan's research group at Caltech using a Spex Industries model 14018 double monochromator equipped with 2400 line/mm holographic gratings and a Hamamatsu R-955 photomultiplier tube. Spectral slit widths were 3 cm^{-1}. A Spectra-Physics model 170 argon iron laser was used directly or in conjunction with a Spectra-Physics 375 dye laser. Samples were prepared in 5 mm O.D. quartz tubes immersed in a liquid N_2 filled quartz finger dewar. Light scattered at 90° relative to the incident beam was collected. A Spex Industries SC-32 SCAMP controller/data processor was used for data manipulation.

For analytical vapor phase chromatography (VPC), a Hewlett-Packard 5700A gas chromatograph equipped with a Hewlett-Packard 18704A inlet splitter and flame ionization detector was used. Hydrogen was employed as the carrier and nitrogen was used as the makeup gas. Packed column analytical VPC was done using a Hewlett-Packard 5720A gas chromatograph equipped with a flame ionization detector and nitrogen carrier gas. This instrument was used with 1/8 in. steel columns. All quantitative VPC was accomplished with a Hewlett-Packard 3390A electronic integrator. VPC response factors for aliphatic hydrocarbons were assumed to be 1.00 relative to n-alkanes. Quantitative analysis of other products were corrected for detector response. For preparative VPC, a Varian 920 instrument equipped with a thermal conductivity detector and helium carrier gas was used. This instrument was used with 0.25 in. or 0.375 in. aluminum packed columns and

Table XXXIX. VPC Columns

Disignation	Description
Carbowax 20M	10 ft. x 3/8 in. aluminum; 25% Carbowax 20M on 60/80 Chrom W-AW-DMCS
DMS	20 ft. x 1/8 in. aluminum; 25% 2,4-dimethyl-sulfolane on 80/100 Chrom P-NAW
Pennwalt	6 ft. x 1/4 in. glass; 28% Pennwalt 223 80/100 Chrom R
SE-30	40 meter x 0.2 mm ID fused silica capillary
SE-54	15 meter x 0.32 mm ID fused silica SE-54 capillary
Sieve 5 A	3 ft. x 1/8 in. 60/80 sieve 5 A

adapted for use with 1/8 in. packed columns. VPC columns are listed in Table XXXIX. Identities of products were established by coinjection techniques with authentic samples from preparative VPC and spectroscopic characterization. Isotope compositions were determined from combination of mass spectroscopy and FT-IR. Gas pressures were measured from known volumes with an MKS type 221 capacitance manometer. Mass spectra (MS) were recorded on a DuPont 24-492B Mass Spectrometer. Combustion analyses were performed at the Caltech Microanalytical Laboratory.

All reactions were run under a positive pressure of argon. Linde UHP argon and UHP nitrogen were used as received. Ethane (Matheson) was passed through a -78°C trap prior to use. CO (Matheson) was used as received. Methyltetrahydrofuran (2-MTHF) was distilled from calcium

hydride then distilled from sodium/benzophenone ketyl using excess sodium prior to use. Toluene, pentane and acetonitrile (CH_3CN) were dried over type 4 A molecular sieves. Diisopropyl amine was distilled from barium oxide. Dimethyl carbamoyl chloride (Aldrich) was used as received. Sodium-1-^{15}N azide (Prochem 97 atom %) was used as received. Butyronitrile ($nPrCN$) was distilled from P_2O_5. Dimethylamine d_6-hydrochloride (KOR Isotopes, 99+% d_6)[110] was used as received. 3-Methylpentane was distilled from calcium hydride. Triacetin was dried over type 4 A molecular sieves. Para-dimethylamino benzaldehyde was treated with activated charcoal and recrystallized from ethanol. Norbornene was purified by distillation from sodium. Acetyl acetone was purified by preparative VPC (Carbowax 20M).

Low Temperature Matrix Isolation Apparatus. The low temperature apparatus is of conventional design[9] constructed on a mobile cart employing an Air Products Displex CSW-202 DMX-1E closed cycle helium refrigeration unit with rotating optical shroud.[116] The expander module is mounted on a rack and pinion gear assembly for horizontal positioning suspended from a threaded crank lift for precise vertical positioning of the optical portion of the rotating shroud. High vacuum ($< 10^{-7}$ mbar) was achieved with an Edwards Mk.2 Diffstack[119] and measured with an Edwards Penning 8 gauge mounted on a 3" copper manifold equipped with Veeco[123] brass bellows type high vacuum valves. Temperature control was maintained with an Air Products Displex-E heater/controller unit with an iron-doped gold/chromel thermocouple (2-300°K ± 0.1 K). Calibration was checked against LHe (4.2°K) and LN_2 (77.5°K) by immersion. The thermocouple tip is embedded in

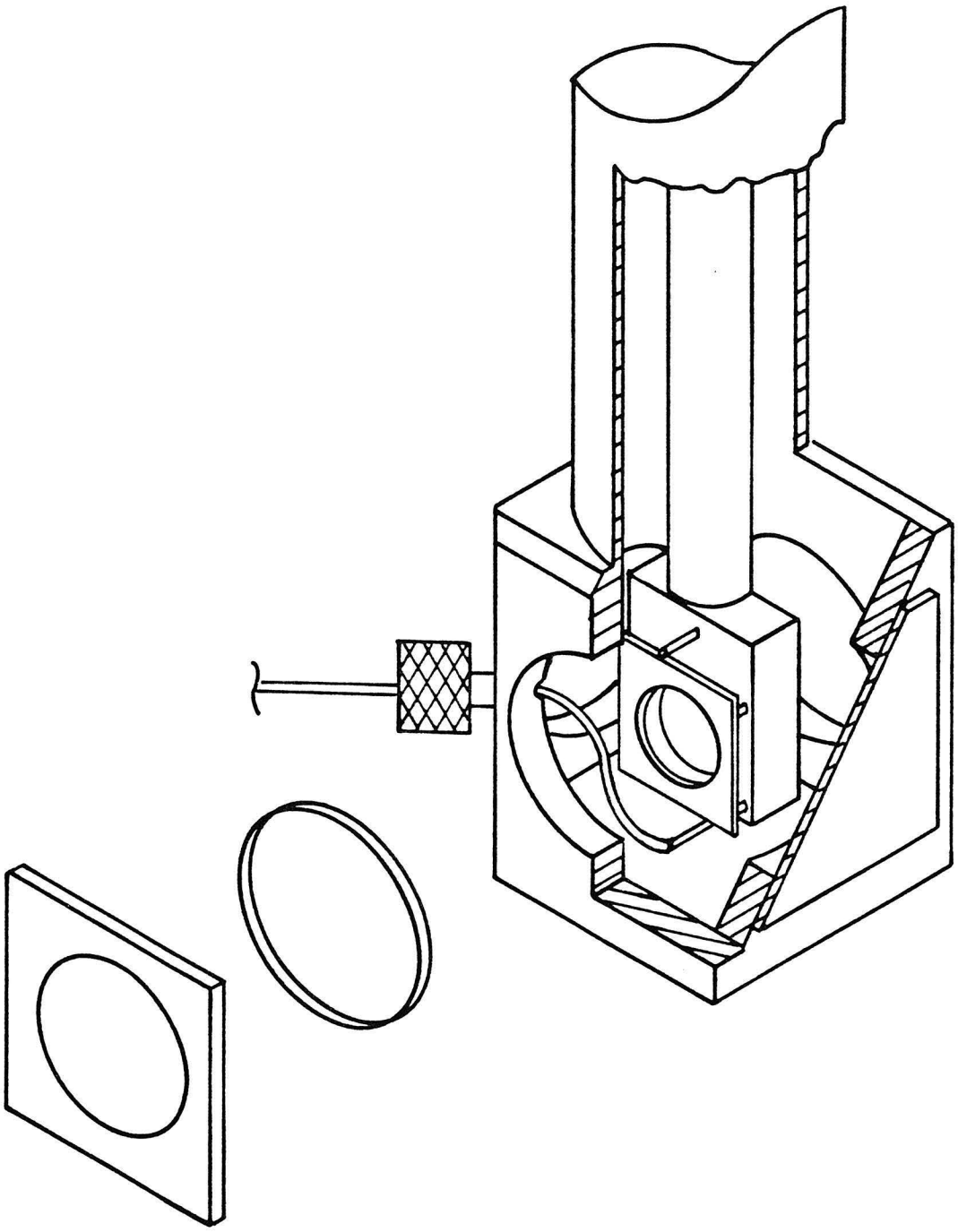

Figure 65. Low temperature spectroscopic cell[50] for electronic (UV-VIS) spectroscopy and rotatable shroud.

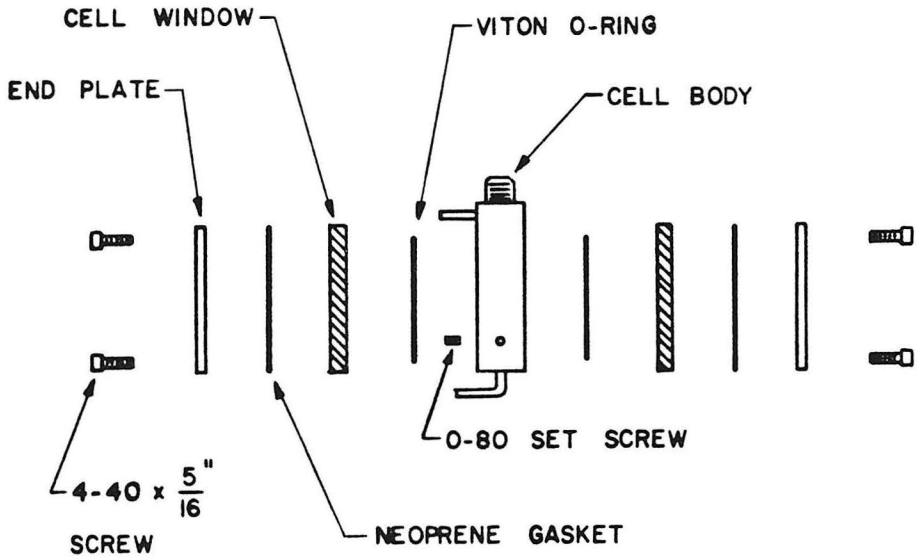

Figure 66. Low temperature UV-VIS spectroscopic cell components.[50]

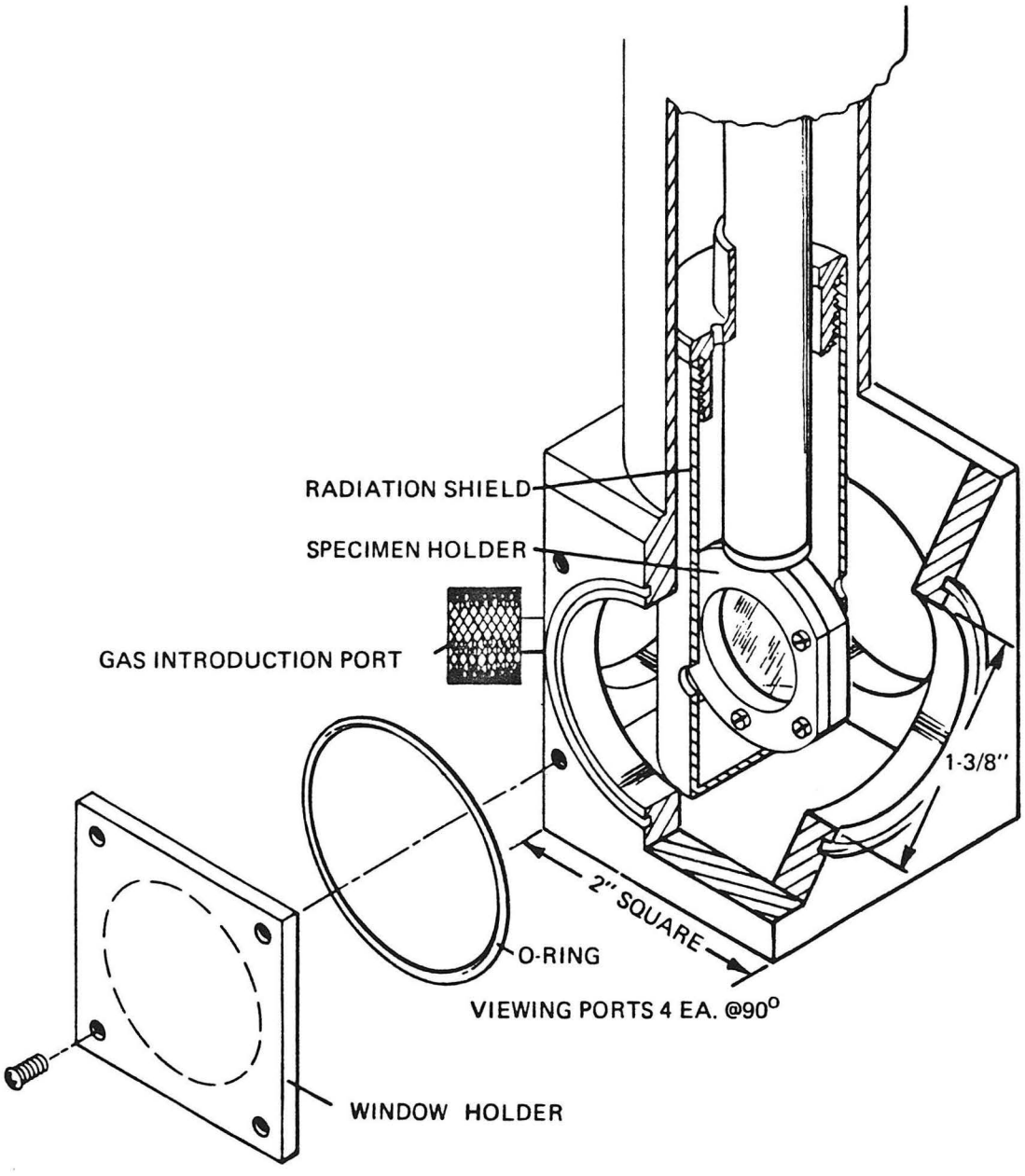

Figure 67. Rotatable spectroscopic shroud for matrix studies.

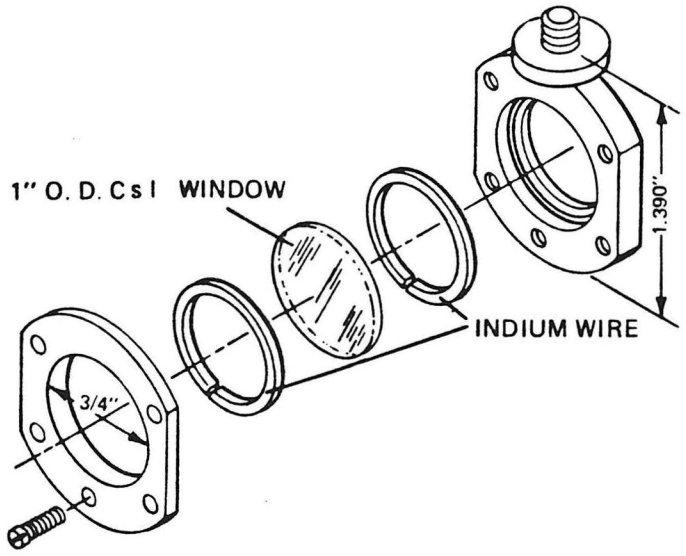

Figure 68. Inner window (e.g., CsI for matrix FT-IR) mounting assembly.

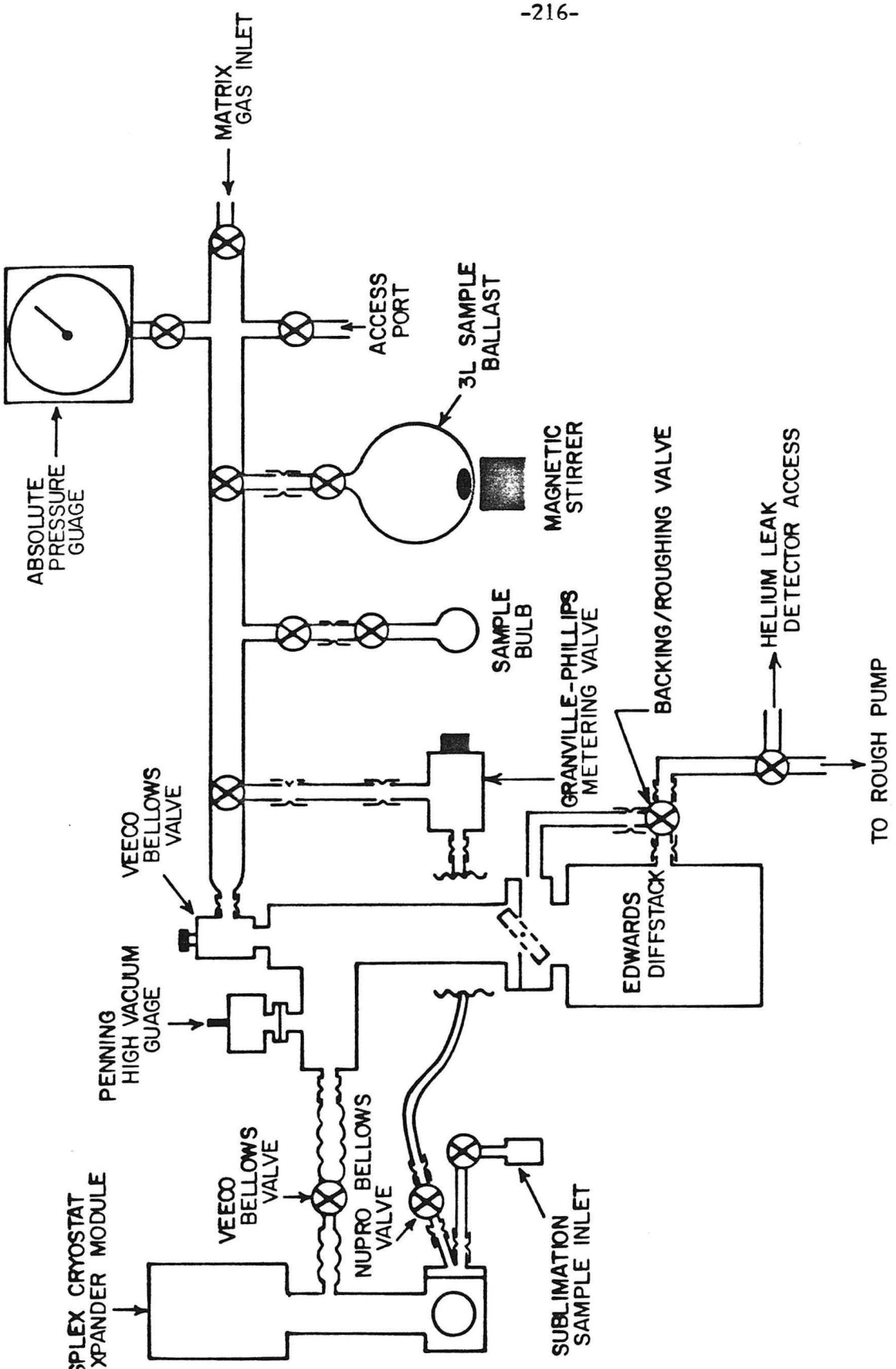

Figure 69. Schematic of low temperature matrix isolation apparatus vacuum system and gas handling manifold (not to scale).

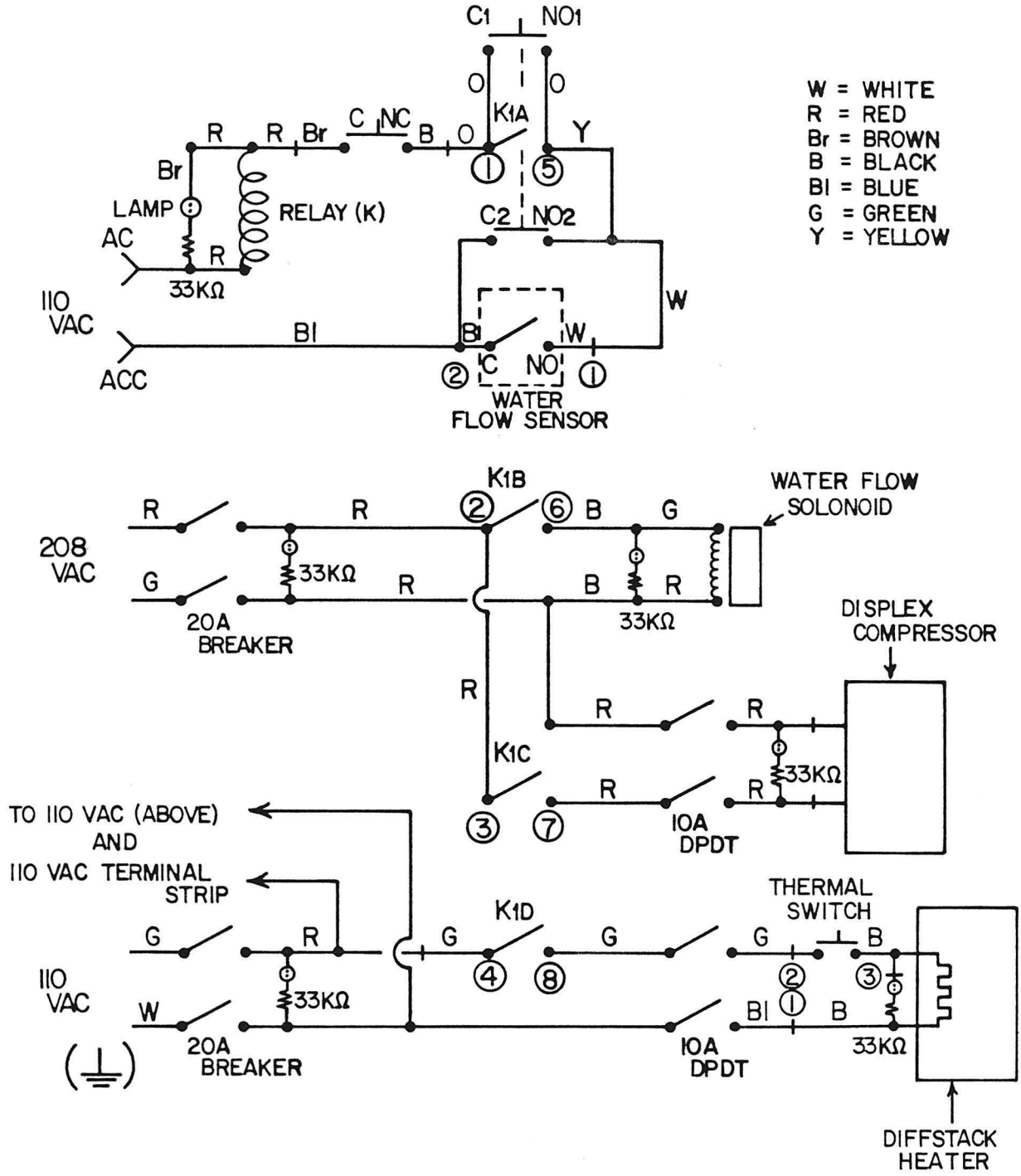

Figure 70. Schematic of cryostat/diffstack cooling water protection circuitry.

the cold tip of the expander module just above the window mount. Matrix gas mixtures were prepared using standard manometric techniques in a glass vacuum manifold equipped with high vacuum greaseless joints (Witeg) and double O-ring Teflon stopcocks (Ace Glass).[126] Manifold pressures were measured with a Pennwalt Model 1500 absolute pressure gauge (0-800 torr).[121] Matrix gas and gas mixture deposition rates were controlled with a Granville-Phillips variable leak valve.[122] Matrix gas was admitted through a Nupro[125] brass bellows type high vacuum valve. Sublimation deposition and cryopump deposition samples were co-deposited with matrix gas from a 1/4 in. I.D. pyrex sublimation tube connected with a Cajon Ultra-Torr fitting from a low temperature bath. For IR spectroscopy an inner CsI window and KBr outer windows (International Crystal Labs) were used. Photolysis was carried out through an outer Suprasil I (Amersil) window through the back of the inner CsI window with defocused light from a 1000 watt ozone free xenon source (Oriel).[120] The copper vacuum manifold, flex hoses, mobile cart, expander module positioning crank, and rack and pinion assemblies were constructed in the Caltech mechanical shops. The glass vacuum manifold was constructed in the Caltech glass shops.

Carbamoyl Azide (15).[49] To a solution of 33.5 g (0.3 mol) semicarbazide hydrochloride in 150 mL distilled water cooled in an ice bath was added dropwise with stirring a solution of 22.8 g (0.33 mol) sodium nitrite in 50 mL distilled water. After the addition was complete, three drops concentrated sulfuric acid was added and the stirring was continued for 10 min. in the ice bath. The solution was saturated with ammonium sulfate and extracted with

ether (4 x 50 mL). The ether was removed under reduced pressure and the resulting solid was recrystallized from hot ether affording 16.4 g (63%) **15** as large prisms; mp. 98°C (lit. 97°C).[49] This recrystallized material was freshly sublimed to a 0°C cold finger (bath temp. 30-70°C, 1.0 mm Hg) prior to use. NMR ($CDCl_3$) δ 5.24 (bs); UV (MeOH) λ_{max} = 214 nm (log ε = 3.3), λ = 266 nm (log ε = 2); IR (CH_3CN) 3450, 3350, 2155, 1724, 1600, 1322, 1225, 1115, 864, 699, 564, 510, 455 cm^{-1}; MS m/e 86.0533 (M^+).

Carbamoyl Azide ^{15}N (15-^{15}N). A solution of 100 mg (1.2 mmol) carbamoyl azide (**15**) in 5.0 mL dry acetonitrile was stirred with an excess (typically 4 equiv) 320 mg (4.8 mmol) 1-^{15}N-sodium azide for 48 to 60 h at room temperature in the dark. The mixture was filtered and the solvent removed in vacuo. The remaining solid was purified by sublimation to a 0°C cold finger (1.0 mm Hg) affording 70-75 mg (75%) **15-^{15}N** approximately 80% ^{15}N labeled, 20% unlabeled. ^{15}N NMR (CH_2Cl_2) δ -140.08 (s), -266.31 (s) (from $CH_3{}^{15}NO_2$); IR (CH_3CN) 3450, 3350, 2155, 2145, 2125, 1724, 1600, 1322, 1225, 1218, 1200, 1115, 860, 695, 560, 510, 450 cm^{-1}; MS m/e = 87.0503 (M^+), m/e = 87/86 = 46/12.

Carbamoyl Azide-d_2 (15-d_2). Carbamoyl azide (500 mg, 5.8 mmol) was stirred with 400 equiv (2.3 mol) 42 mL D_2O (99.8% D) for 48 h in the dark at room temperature. The excess D_2O was removed in vacuo and the product purified by sublimation under reduced pressure to a 0°C cold finger (bath temp. 30-70°C, 1.0 mm Hg), affording 390 mg (76%) **15-d_2** as a colorless solid. IR (CH_3CN) 3360, 2670, 2590, 2480, 2425, 2200, 2170, 1720, 1340, 1320, 1245, 1218, 1200, 1192, 820, 735, 695, 658 cm^{-1}; MS m/e = 88.0656

(M^+), m/e = 88/87/86 = 22/2/1.

Carbamoyl Azide-d_2 ^{15}N (15-d_2-^{15}N). The procedure for carbamoyl azide-d_2 (15-d_2) was followed with 50 mg (0.58 mmol) carbamoyl azide (15-d_2) was followed with 50 mg (0.58 mmol) carbamoyl azide ^{15}N (15-^{15}N) affording 30 mg (59%) as a colorless solid. ^{15}N NMR (D_2O) δ -140.10 (s), -262.32 (s); IR (CH_3CN) 3360, 2670, 2590, 2480, 2425, 2170, 2145, 2125, 1720, 1340, 1320, 1245, 1218, 1200, 1192, 820, 735, 695, 658 cm^{-1}; MS m/e = 89.0627 (M^+), m/e = 89/88/87 = 23/5/1.

Ammonium Azide.[128] To a paste of 6.5 g (0.1 mol) sodium azide in 6.5 mL distilled water was added 40 mL benzene. The slurry was cooled to -5°C in an ice-salt bath. To this was added dropwise with stirring 2.7 mL (0.05 mol) concentrated sulfuric acid. Once the addition was complete, the benzene layer was decanted, dried briefly over anhydrous sodium sulfate and added to 40 mL anhydrous ether at -5°C. Dry ammonia gas was bubbled through this solution at -5°C yielding an insoluble precipitate. The product was filtered, washed with anhydrous ether and dried in a desicator yielding 4.5 g (75%), 133°C sublimes (lit. 133° sublimes).[128] IR (KBr) 3110, 2020, 1620, 1500, 646, 640 cm^{-1}.

Dimethyl Carbamoyl Azide (13).[47] To 14.0 g (0.22 mol) sodium azide in 25 mL dry acetonitrile was added with stirring under argon 10 mL (0.11 mol) dimethyl carbamoyl chloride (21) in 10 mL dry acetonitrile at room temperature in the dark. The mixture was stirred for 24 h or until complete as determined by IR (CH_3CN) (ν_{CO}, 1740 cm^{-1} of the carbamoyl chloride replaced by ν_{CO}, 1685 cm^{-1} of carbamoyl azide) or VPC (15 m SE-54 60°C).

The mixture was filtered and the acetonitrile removed in vacuo. The resulting clear oil was distilled under reduced pressure yielding 11.7 g (92%) (**13**) as a colorless oil; bp 53-55°C (5 nm Hg). Preparative VPC (Carbowax 20M, 180°C, 180°C injector) afforded analytically pure **13**. NMR ($CDCl_3$, 22°C) δ 2.97 (s, 3H), 2.92 (s, 3H); IR (CCl_4) 2930, 2445, 2167, 2145, 1697, 1485, 1438, 1409, 1390, 1270, 1230, 1135, 1119, 1060, 963, 725, 647 cm^{-1}; UV (MeOH) λ_{max} = 228 nm (log ϵ = 3.7), λ = 250 nm (log ϵ = 2.7); MS m/e = 114.05466 (M^+) (theor. 114.05415).

Dimethyl Carbamoyl Azide ^{15}N (13-^{15}N). To 0.25 g (3.8 mmol) 1-^{15}N-sodium azide in 2 mL dry acetonitrile under argon was added 0.40 g (3.72 mmol) dimethyl carbamoyl chloride (**21**) via syringe. The mixture was stirred in the dark for 24 h at room temperature. The mixture was filtered and the acetonitrile removed under reduced pressure affording 0.41 g (97%) **13-^{15}N** as a colorless oil. Preparative VPC (Carbowax 20M, 180°C, 180°C injector) afforded analytically pure **13-^{15}N.** NMR ($CDCl_3$, 22°C) δ 2.97 (s, 3H), 2.92 (s, 3H); ^{15}N NMR (CH_2Cl_2 vs $CH_3{}^{15}NO_2$) δ -141.40 (s), -266.02 (s); IR (CCl_4) 2930, 2395, 2162, 2135, 2117, 1690, 1485, 1436, 1408, 1385, 1265, 1217, 1200, 1130, 1115, 1060, 960, 720 645 cm^{-1}; MS m/e = 115.05149 (M^+) (theor. 115.05119).

1,1,4,4-Tetramethyl-2-tetrazene (19).[58] To a solution of 10.0 g (0.17 mol) 1,1-dimethyl hydrazine in 100 mL anhydrous ether was added with stirring under argon 40.0 g (0.185 mol) yellow mercuric oxide in small portions to maintain reflux of the ether. Once addition of the mercuric oxide was complete the mixture was refluxed an additional 20 min and then cooled

on ice. The black precipitate was removed by filtering through celite and sodium sulfate and washed with ether. The light yellow filtrate was dried over sodium sulfate and the ether removed under reduced pressure. The remaining yellow oil was distilled under reduced pressure affording 5.6 g (62%) **19** as a colorless oil; bp 44-45°C (30 mm Hg). Preparative VPC (Carbowax 20M, 135°C, 150°C injector) afforded analytically pure material. NMR ($CDCl_3$) δ 2.83 (s) [lit. ($CDCl_3$) δ 2.83 (s)];[58] IR (film) 3015, 2980, 2875, 2838, 2800, 1475, 1425, 1260, 1245, 1145, 1095, 1042, 1005, 900, 827 cm^{-1}; IR (Ar, 1:700, 10°K) 3022, 3020, 3010, 2980, 2975, 2890, 2880, 2870, 2830, 2795, 2785, 1505, 1475, 1465, 1450, 1438, 1400, 1282, 1245, 1145, 1095, 1040, 1035, 1013, 1005, 900, 828 cm^{-1}; UV (3-methyl pentane) λ_{max} = 278 nm (log ϵ = 4.1).

Photolysis of Tetramethyl-2-tetrazene (19). A mixture of freshly VPC purified tetrazene in argon (1:700) was deposited at 5 mmol/h over 2 h at 20°K. Photolysis with two CS-7-54 UV transmitting visible cut out filters for 15 min. resulted in loss of the IR bands of the tetrazene and formation of new bands consistent with products resulting from combination/disproportionation of two dimethyl amino radicals to form dimethyl amine (ν_{NH}, 3340 cm^{-1}) and N-methyl methylenimine ($\nu_{=CH_2}$, 3030 cm^{-1}) and ($\nu_{N=C}$, 1663 cm^{-1}) lit. (1658 cm^{-1})[129] together with the following product bands: 3340, 3030, 2950, 2910, 2865, 2835, 2795, 1663, 1480, 1475, 1458, 1445, 1400, 1380, 1230, 1225, 1155, 1150, 1055, 1030, 1027, 950, 808, 795, 770, 735 cm^{-1} [lit. N-methylmethylimine IR (Ar, 20 K)[129] 3030, 3005, 2894, 2768, 1658, 1472, 1467, 1439, 1399, 1218, 1098, 1045, 1023, 948, 938

cm^{-1}).

Trans-1,2-dimethyl Diazene (8t).[109] To a suspension of 5.64 g (26 mmol) yellow mercuric oxide in 10 mL distilled water at 0°C was added slowly with stirring a solution of 1.80 g (30 mmol) 1,2-dimethyl hydrazine in 15 mL distilled water. An additional 1.51 g (7 mmol) mercuric oxide was added and the mixture stirred for an additional 2 h at room temperature. The product 1,2-dimethyl diazene was distilled from the reaction mixture under reduced pressure (50 mm Hg) with mild heating to 50°C and collected in a trap at -78°C. The product was further purified by trap (-78°C) to trap (-196°C) distillation through a Drierite column at high vacuum yielding 0.82 g (64%) **8t** as a colorless oil. NMR (d_6-acetone) δ 3.62 (s); lit. NMR (d_6-acetone)[109] δ 3.63 (s) trans (3.51 (s) cis).

Dimethyl Carbamoyl Chloride-d_6 (21-d_6).[47] Hexadeuteriodimethylammonium chloride (KOR Isotopes, 99+% d_6) 3.9 g (45 mmol) was converted to the free amine by stirring with 4.0 g sodium hydroxide in 8.5 mL dd H_2O and 50 mL dichloromethane in an ice bath. After 15 min the dichloromethane layer was separated, dried over potassium hydroxide pellets and added dropwise with stirring over 45 min to 12 g (120 mmol) phosgene (CAUTION: extreme poison!) in 30 mL dichloromethane under argon at -10°C in an ice/salt bath. After 1 h the excess phosgene and 3/4 of the dichloromethane were removed in vacuo and trapped at -78°C over potassium hydroxide pellets. To the concentrated reaction mixture was added 25 mL dry ether to precipitate 1.5 g of hexadeuteriodimethylammonium chloride for filtration. Evaporating the filtrate in vacuo left 2.3 g dimethyl carbamoyl chloride-d_6

(**21-d_6**) which was distilled in vacuo; bp 60-61°C (17 mm Hg) yielding 1.95 g (76%) as a colorless oil. IR (film) 2210, 2140, 2120, 2080, 1740, 1638, 1420, 1370, 1320, 1280, 1220, 1115, 1060, 945, 800, 660, 640 cm^{-1}.

Dimethyl Carbamoyl Azide-d_6 (13-d_6).[47] To a suspension of 1.4 g (22 mmol) sodium azide in 3 mL dry acetonitrile under argon was added with stirring 1.65 g (14.5 mmol) dimethyl carbamoyl chloride-d_6 in 3 mL dry acetonitrile. The mixture was stirred for 24 h at room temperature in the dark or until judged complete by VPC (SE-54 at 60°C). The mixture was filtered and the solvent removed in vacuo. Distillation afforded a colorless oil 1.51 g (87%); bp 55-56°C (8 mm Hg). Preparative VPC (Carbowax 20M, 180°C, 180°C injector) afforded analytically pure **13-d_6**. ^2H NMR ($CDCl_3$, 25°C) δ 2.92 (s, 3H), 2.92 (s, 3H); IR (film) 2240, 2215, 2150, 1685, 1390, 1230, 1115, 1060, 1010, 915, 825, 725, 615 cm^{-1}; MS m/e = 120 (M^+), m/e = 121/120/119 = 6/97/2.

Methylhydrazine-formaldehyde Hydrazone (10). Methyl hydrazine-formaldehyde hydrazone (**10**) was prepared by the method of Muller.[111] To a solution of 14.5 g (101 mmol) methylhydrazine sulfate in 30 mL distilled water was added 40 mL 5 N sodium hydroxide. To this solution was added slowly with stirring 7 mL 37% aqueous formaldehyde. The mixture was stirred 1 h and then saturated with sodium hydroxide. The mixture was extracted with ether (2 x 50 mL) and the ether removed in vacuo. Recrystallization from acetic acid/petroleum ether afforded 2.5 g (46%) colorless needles; mp 121-123°C (lit. 121-123°C).[111] NMR ($CDCl_3$) δ 10.92 (bs, 1H), 6.33, 5.91 (AB quartet, 2H, J = 11.5 Hz), 2.72 (d, 3H, J = 4

Hz).

(Z)-3,3-Dimethyl-1-phenyltriazene-1-oxide (16).[40a] To a solution of 9.36 g (90 mmol) nitrosobenzene in 150 mL 95% ethanol cooled to -5°C in an ice/salt bath was added dropwise with stirring a solution of 1.80 g (30 mmol) 1,1-dimethylhydrazine in 40 mL 95% ethanol. After the addition was completed, the reaction mixture was stirred an additional 45 min at -5°C and then slowly allowed to warm to room temperature. At approximately 0°C the reaction turned from green to bright yellow. The solvent was removed at room temperature in vacuo. The remaining brown oil (5.7 g) was chromatographed on 150 g silica gel eluted with CH_2Cl_2. After approximately 100 mL forerun, a 300 mL fraction containing 5.45 g of bright yellow solid 1,2-diphenyldiazeneoxide was collected. The next 700 mL contained 3.75 g **16** as a light yellow oil. Vacuum distillation bp. 80-81°C (0.5 mm Hz) afforded 3.24 g (65%) **16** as a yellow oil. NMR ($CDCl_3$) δ 8.2-7.9 (m, 2H), 7.6-7.3 (m, 3H), 3.15 (s, 6H) [lit. NMR[40a] ($CDCl_3$) δ 8.2-7.9 (m, 2H), 7.6-7.3 (m, 3H), 3.15 (s, 6H)]; IR (CCl_4) 3080, 3010, 2970, 2900, 2850, 2815, 2785, 2047, 1982, 1795, 1750, 1590, 1470, 1420, 1390, 1295, 1250, 1220, 1165, 1135, 1110, 1063, 1025, 1015, 920, 825, 680, 640 cm^{-1}; UV (EtOH) λ_{max} = 326 nm (log ε = 3.9); λ_{max} = 227 nm (log ε = 3.8).

Diisopropyl Carbamoyl Chloride (22).[83] To a solution of 3.3 mL (45 mmol) phosgene (CAUTION: extreme poison!) in 25 mL dry toluene at -10°C under argon was added dropwise with stirring 10.0 g (99 mmol) dry diisopropyl amine in 20 mL dry toluene. The mixture was stirred for 8 h at -10°C to 0°C and warmed to room temperature. After stirring an additional 4 h at room

temperature the mixture was cooled to 0°C and the precipitated diisopropyl amine hydrochloride was filtered. The filtered solids were washed with dry toluene and the toluene removed in vacuo. The residual solid was recrystallized from dry pentane (hot) yielding 3.15 g (86%) colorless crystals; mp 57°C (lit. 57°C).[83] NMR ($CDCl_3$, 24°C) δ 4.54 (sept, 1H, J = 6.8 Hz), 3.58 (sept, 1H, J = 6.8 Hz), 1.35 (d, 6H, J = 6.8 Hz), 1.22 (d, 6H, J = 6.8 Hz); IR (CCl_4) 3000, 2970, 2920, 2870, 1740, 1465, 1453, 1417, 1380, 1386, 1342, 1315, 1267, 1220, 1197, 1150, 1130, 1103, 1023, 900, 870, 768, 609 cm^{-1}.

Diisopropyl Carbamoyl Azide (17). To 5.0 g (77 mmol) sodium azide in 15 mL dry acetonitrile was added with stirring under argon 3.30 g (20 mmol) diisopropyl carbamoyl chloride (**22**) in 5 mL dry acetonitrile. The mixture was stirred at room temperature in the dark for 24 h or until complete by IR. The mixture was filtered and the acetonitrile removed in vacuo. Vacuum distillation afforded 2.8 g (82%) **17** as a colorless oil; bp. 55-56°C (1.0 mm Hg). Preparative VPC (Carbowax 20M, 180°C, 180°C injector) afforded analytically pure material. NMR ($CDCl_3$, 23°C) δ 3.80 (m, 2H), 1.24 (m, 12H); IR (CCl_4) 2990, 2960, 2920, 2870, 2430, 2140, 1682, 1465, 1450, 1425, 1375, 1365, 1305, 1281, 1220, 1205, 1150, 1130, 1037, 936, 882, 850, 725, 608 cm^{-1}; UV (MeOH) λ_{max} = 230 nm (log ε = 3.5); MS m/e = 170 (M^+), m/e = 171/170 = 8/86; Anal. calcd. for $C_7H_{14}N_4O$: C, 49.40; H, 8.29; N, 32.92. Found: C, 49.38; H, 8.25; N, 32.81.

Diisopropyl Carbamoyl Azide-^{15}N (17-^{15}N). To 0.26 g (4.0 mmol) 1-^{15}N sodium azide in 2 mL dry acetonitrile was added 0.61 g (3.7 mmol) diisopropyl carbamoyl chloride (**22**) in 2 mL dry acetonitrile. After 36 h at

room temperature the mixture was filtered and the solvent removed in vacuo. Bulb-to-bulb distillation at high vacuum (1.0 mm Hg) afforded 0.41 g (79%). Preparative VPC (Cabowax 20M, 180°C, 180°C injector) afforded analytically pure **17-^{15}N**. NMR ($CDCl_3$, 23°C) δ 3.80 (m, 2H), 1.24 (m, 12H); ^{15}N NMR (CH_2Cl_2 vs. $CH_3{}^{15}NO_2$) δ -142.30 (s), -265.70 (s); IR (CCl_4) 2990, 2960, 2920, 2870, 2430, 2140, 2117, 1682, 1465, 1450, 1425, 1375, 1365, 1305, 1281, 1218, 1200, 1150, 1130, 1037, 936, 882, 850, 725, 608 cm^{-1}; MS m/e = 171 (M^+), m/e = 172/171/170 = 8/100/3.

Diisopropyl Nitrosamine (23).[26] (DANGER: Cancer suspect agent!) To a solution of 10.1 g (0.10 mol) diisopropyl amine in 100 mL 6% hydrochloric acid was added with stirring at 70-75°C a solution of 15 g (0.22 mol) sodium nitrite in 80 mL water dropwise. The mixture was heated for 24 h and then cooled in an ice bath. The cooled mixture was saturated with salt and extracted with ether (3 x 50 mL). The combined ether extracts were dried over sodium sulfate and the ether removed in vacuo yielding 11.2 g **23** as a yellow solid. Fractional distillation 87-88°C (18 mm Hg) (lit. 87-88°C, 18 mm)[26] gave a yellow oil which solidified on cooling, 9.9 g (85%). NMR ($CDCl_3$) δ 4.95 (sept, 1H, J = 6.6 Hz), 4.19 (sept, 1H, J = 6.6 Hz), 1.47 (d, 6H, J = 6.6 Hz), 1.16 (d, 6H, J = 6.6 Hz).

1,1-Diisopropyl Hydrazine (24).[114] To a refluxing solution of 5.0 g (43 mmol) diisopropyl nitrosamine (**23**) in 50 mL absolute ethanol under argon was added small chunks was continued in order to maintain a molten globule for 20 min. During this time, the yellow color of the nitrosamine had faded and a white precipitate had formed. The mixture was cooled on ice and 150 mL of

deoxygenated distilled water was slowly added to quench the excess sodium metal and dissolve the sodium ethoxide. The resulting cloudy solution was extracted (2 x 50 mL) with ether and dried over sodium sulfate under argon. The ether was removed in vacuo and the hydrazine distilled 130-132°C (lit. 130-132°C)[26] affording 3.75 g (65%) **24** as a colorless oil.

1,1,4,4-Tetraisopropyl-2-tetrazene (20). 1,1,4,4-Tetraisopropyl-2-tetrazene (20) was prepared by mercuric oxide oxidation of the freshly prepared 1,1-diisopropyl hydrazine by the procedure of Effenberger.[112] NMR ($CDCl_3$) δ 1.14 (d, 24H, J = 7 Hz), 3.92 (sept, 4H, J = 7 Hz) [lit. NMR δ 1.14 (d, J = 7 Hz), 3.92 (sept, J = 7 Hz)];[112] UV (heptane) λ_{max} 291 nm (log ε = 4.05).

Low Temperature Electronic Spectroscopy. The inner cell used for electronic spectroscopy in organic glasses and low temperature solutions was designed by Hinsberg.[50] The cell body is constructed from OFHC copper, with stainless steel tubing soldered to it. The cell body is nickel plated. The cell windows are Suprasil I (Amersil)[117] ground to size. The seals between the windows and the cell body are made with Viton O-rings. The path length of the cell is 10.0 mm and the volume is approximately 4 mL. Two Suprasil (Amersil) outer windows on the rotating optical shroud are employed for electronic spectroscopy and photolysis. Dilute solutions of freshly VPC purified samples are prepared in freshly distilled dry solvents and freeze-pump-thaw-degassed through three cycles. Sample solutions are introduced into the cell through 18 gauge Teflon tubing (Alpha Wire Corp.)[118] which extend to the outside of the optical shroud through two Cajon Ultra-Torr

Table XXXX. Organic Glasses

Solvent	Tg (°K)[a,b]	Finger Dewar	Optical Cell	Comments
2-MTHF	∿90	Yes	Yes	The best overall
3-Methylpentane	∿85	Yes	No	Crystallizes poor solubility
1-Propanol	∿110	Yes	>90°K	Fractures violently
n-Butyronitrile	∿100	Yes	No	Crystallizes
Triacetin	∿210	Yes	No	Fractures
Methylmethacrylate	∿110	Yes	No	--
Poly(methylmethacrylate)	--	Yes	--	--
Freons	--	--	No	Possibly as solvent mixture
Acetonitrile	∿130	Yes	No	Crystallizes
Methylcyclohexane	∿90	Yes	Variable	Crystallizes (undependable)

[a]Taken to be $\eta \geq 10^{12}$ cp.
[b]Ref. 107, 127.

fittings. Sample solutions of the carbamoyl azides in a glass forming solvent are slowly drawn into the cell under positive argon pressure with syringe suction to prevent bubble formation. As the cell is cooled to form a glass, more sample is drawn in due to contraction of the solvent (2-MTHF contracts approximately 22% going to 77 K). Stress fractures in the organic glass often occur unexpectedly during the course of an experiment destroying optical clarity. With most solvents other than 2-MTHF stress fractures occur at or near 77-80°K. This can result in the fracturing of the inner cell windows with devastating effects. Less severe fractures can usually be remedied with annealing to 20-30° above the fracture temperature followed by recooling to a temperature just above the fracture point. Photochemical transformations were carried out with defocused light through an outer Suprasil window and monitored by electronic spectroscopy at appropriate time intervals. Electronic spectra were recorded with the aid of a black cloth to exclude light from the spectrophotometer sample compartment. Temperature control was typically ±0.5°K with the tip of the thermocouple just above the cell taken to be representative of the cell temperature at equilibrium.

FT-IR Spectroscopy. A Mattson Instruments Sirius 100 sample compartment cover was modified to permit access of the Displex optical shroud. In order to maintain an efficient nitrogen purge of the spectrometer and cell compartment as clear vinyl cover was taped to the optical shroud with vinyl tape and affixed to the modified sample compartment cover by means of a detachable Velcro seal cemented around the perimeter of the access hole. A positive dry nitrogen gas pressure was produced from a

regulated high pressure liquid nitrogen dispenser dewar.

For a typical matrix isolation FT-IR experiment, the Displex apparatus, gas handling manifold and flexible connecting line to the matrix gas cylinder regulator are checked to be He leak tight and exhaustively outgassed with frequent warming with a heat gun for 24 h prior to gas admission establishing a vacuum of better than 1×10^{-6} mbar. The carefully purified dry sample vapor is admitted through a greaseless Teflon joint and the desired gas mixture in the desired matrix host gas is prepared by standard manometric techniques. The gas mixture (typically 1:700-1:3000) is allowed to equilibrate for 24 h prior to deposition. If the guest molecule is photoreactive, the glass portion of the gas handling system is wrapped with aluminum foil to exclude light.

The Displex compressor is switched on and the temperature controller adjusted to the desired deposition temperature (20°K for argon and 15°K for nitrogen matrices). Once the inner CsI window temperature has cooled to 77°K, the high vacuum valve isolating the cold head from the diffusion pump is closed to prevent back-streaming of diffusion pump oil to the optical window. The sample window is allowed to equilibrate for approximately 1 h at the deposition temperature prior to deposition. During this period the background interferrogram (empty cell) for the experiment is accumulated after the appropriate nitrogen purge time to achieve a stable baseline.

To start a deposition, the manifold stopcock leading to the Granville-Phillips variable leak valve is opened together with the high vacuum isolation valve (Nupro) to the deposition port on the cold head. The deposition rate is

adjusted with the Granville-Phillips leak valve to the appropriate flow rate and checked periodically. The optical shroud is then rotated and the deposition begun. (For a sublimation or cryopump deposition the sample would have been equilibrated at the bath temperature by this time and the sample isolation valve would be cracked open to allow co-deposition with matrix gas just prior to rotation of the optical shroud.) Deposition progress is monitored by FT-IR at appropriate intervals. Once deposition is complete the window temperature is slowly lowered to $\leq 10^{o}K$ and the spectrum of the matrix isolated material recorded. If deemed necessary, annealing of the matrix can be achieved through several 10-30-10^{o}K temperature cycles followed by cooling to 10^{o}K. (Note that a reproduceable alignment of the sample window is necessary for a constant baseline.)

Photolysis is carried out through an outer Suprasil window through the back of the CsI inner window. The photolysis beam is defocused (incident intensities of approximately 50-100 mW per cm^2) to prevent excessive heating of the sample matrix as evidenced by an increase in the inner window temperature and "boil off" of the matrix. Progress of photochemical transformations is monitored by FT-IR at appropriate time intervals. A reproduceable alignment of the sample window and infrared beam is necessary for a constant baseline.

FT-IR Spectra Workup. Work-up of FT-IR absorbance spectra was achieved using Mattson Instruments FT-IR software. All spectra for a given experiment were ratioed and processed using a background interferrogram of the IR cell (or IR cell and deposited matrix gas) recorded prior to sample

deposition. All absorbance spectra were carefully corrected using interactive subtraction software for interfering residual atmospheric impurities not removed in the nitrogen purge [e.g., H_2O (g), CO_2 (g)]. Ice bands [H_2O (s)] resulting from ice formation on the liquid nitrogen cooled HgCdTe (MCT) detector over the course of an experiment were also judiciously corrected. Baseline inclination or baseline rolls were carefully corrected with appropriate baseline correction software. The narrow half-band widths of matrix isolated species (≤ 2 cm^{-1}) make these corrections straightforward. Difference FT-IR spectra are presented to clearly demonstrate the effects of a given transformation. Subtraction factors (α) refer to the formula $A - \alpha B = C$, where A and B are the absorbance spectra to be subtracted and C is the resulting difference spectrum.

H_2NN Product Analysis. Carbamoyl azide (typically 1.50 mg) was placed in a 5 mm OD quartz tube fitted with a vacuum stopcock. To this was transferred 300 μL 2-MTHF (or appropriate dry solvent) freshly distilled from sodium/benzophenone ketyl. The solution was freeze-pump-thaw-degassed for three cycles. The solution was thoroughly mixed and then immersed in a Suprasil finger dewar filled with liquid nitrogen. Once the solution had glassed it was subjected to photolysis for the requisite time period (typically 5 h photolysis with 2-CS-7-54 filters under carefully reproduced irradiation conditions resulted in $\geq$ 99% decomposition of starting material as determined independently by IR). For thermal product analysis the resulting blue-violet glass of **3** was then allowed to warm slowly to room temperature. Upon removal from the 77°K dewar the glass quickly turned opaque yellow-orange

as it softened (characteristic of 1 λ_{max} = 386 nm and the λ_{max} = 480 nm species) followed by vigorous gas evolution. The solution quickly became colorless and in the -50 to 0°C temperature range there was again vigorous gas evolution together with formation of an insoluble white precipitate ($\overset{+}{N}H_4\bar{N}_3$) from the colorless solution.

Thermal and photochemical products were determined as follows: The gaseous products CO, N_2 and H_2 were identified by VPC coinjection with authentic samples (sieve 5 A column 25°C, He carrier, thermal conductivity detector, injected in 1 atm C_2H_6) by mass spectral analysis or quantitated by Toepler pump analysis. For Toepler pump analysis, the gas mixture was pumped from the sample tube and condensable products trapped at 77°K. The total gas PV was determined and the mixture was then passed through a hot tube of CuO (310°C) to oxidize CO to CO_2 and H_2 to H_2O which were trapped at -78° and the N_2 content determined by PV difference followed by CO_2 PV determination.

Ammonia content was determined for both the volatile (NH_3) and non-volatile ($\overset{+}{N}H_4\overset{-}{N}_3$) components by the indophenol method.[115] The volatile components fo the reaction were vacuum transferred (77°K) to 10 mL saturated boric acid solution (degassed) and allowed to warm to room temperature. This solution was tansferred to a 50 mL volumetric flask. 15 mL saturated boric acid, 5 mL chlorine (Cl_2) saturated distillated water and 5 mL 8% phenol solutions were added with swirling. The mixture was heated on a steam bath for 3.0 min and cooled on ice. After cooling to 5°C, 5.0 mL of a 3.0 M sodium hydroxide solution was added and the mixture diluted to

volume. After 5 min the intense blue color of the indophenol was fully developed. The absorbance at 625 nm was measured relative to a reagent blank containing the appropriate volume of 2-MTHF. The ammonia content was determined from a calibration curve prepared using ammonium chloride as a standard. The non-volatile ammonium azide residue in the sample tube was dissolved in 1.5 mL distilled water and determined as above.

Hydrazine content was determined independent of a volatile NH_3 determination as the bis azine of para-dimethylamino benzaldehyde.[115] The volatile components of the reaction were vacuum transferred (77°K) to a mixture of 5.5 mL 0.1 N H_2SO_4 and 0.5 mL of a solution para-dimethyl amino benzaldehyde (40 mg/mL in 2.0 N H_2SO_4) (degassed). Upon thawing, the orange color of the bis-azine appeared and was fully developed in 15 min at room temperature. The absorbance at 458 nm was measured relative to a reagent blank contining the appropriate volume of 2-MTHF. The hydrazine content was determined from a calibration curve prepared using hydrazine sulfate as a standard (carbamoyl azide does not interfere).

Formaldehyde was determined by the Hantzsch reaction.[113] The reaction mixture was added to 4 mL of reagent (15.0 g ammonium acetate, 300 µL acetic acid, 200 µL freshly purified acetyl acetone in 100 mL distilled water). The mixture was heated in a sealed tube to 37°C for 1 h. The absorbance at 412 nm was measured relative to a reagent blank containing the appropriate volume of 2-MTHF. The formaldehyde content was determined using a molar extinction coefficient of 8000 at 412 nm for the product diacetyl dihydroleutidine (detection limit 2×10^{-8} g H_2CO).

Photochemical products were determined in a similar fashion with visible light irradiation with a CS-1-75 filter (>340 nm) or the combination CS-1-75 and two CS-3-70 filters (>500 nm) until the blue-violet color of the 1,1-diazene was gone (typically 4-5 h) prior to warming the glass for product analysis. Unfiltered photolysis (λ >250 nm) was also carried out for the appropriate time period (typically 5 h) with no color development.

Matrix Isolation of H_2NN (3), H_2NN^{15} (3-^{15}N), D_2NN (3-d_2), D_2NN^{15} (3-d_2-^{15}N). The respective carbamoyl azides **15** (freshly sublimed) were cryopumped from a -10 or -20°C ice/salt bath and co-deposited with matrix gas (UHP argon at 20°K, UHP nitrogen at 15°K) at 5-10 mmol gas per hour over approximately 6-4 h, respectively. The deposition progress was closely monitored by FT-IR. These deposition conditions gave consistently transparent matrices with well resolved bands and minimal atmospheric impurities (CO_2, H_2O). The window temperature was slowly lowered to 10°K (10 min) and the infrared spectrum of the starting carbamoyl azide recorded after the appropriate nitrogen purge time (30-45 min typically). The matirx was photolyzed with defocused light from a 1000 watt xenon source through an outer Suprasil window and through the back of the inner CsI window using 2-CS-7-54 UV transmitting, visible (410-680 nm) cut out filters. Typical photolysis times for 80% conversion of starting carbamoyl azides were 90-120 min. Photolysis of the resulting 1,1-diazenes was carried out with CS-1-75, 2-CS-3-70 filters (>500 nm) for 120-180 min carefully monitored by FT-IR. Photolysis of trans-1,2-diazenes was carried out with either monochromatic light (380 ± 10 nm) from a monochromator or with CS-5-58 and CS-7-51

filters (360-410 nm).

Matrix Isolation of 1,1-Dimethyldiazene (7) and 1,1-Dimethyldiazene-^{15}N (7-^{15}N). A 1:1400 gas mixture of the respective dimethyl carbamoyl azide (freshly purified by preparative VPC) in argon was allowed to equilibrate in the foil wrapped gas manifold of the Displex apparatus. The mixture was deposited (20°K) at 10 mmol/h over approximately 4 h (100 mm gas mixture, 37 mmol). The CsI window temperature was lowered to 10°K and the sample spectrum recorded. Photolysis was carried out through an outer Suprasil window through the back of the inner CsI window with defocused light through 2-CS-7-54 UV transmitting visible cut out filters for 60 to 90 min. Photolysis progress was monitored periodically by FT-IR. Photolysis of the product diazenes was carried out in a similar fashion through CS-1-75, CS-4-96 and CS-3-70 filters (466-610 nm) for approximately 60 min or CS-1-75 and CS-2-61 (> 590 nm). Photolysis of product (IJ) from photolysis 1,1-dimethyldiazene **7** was carried out with CS-5-58 and CS-7-51 filters (360-410 nm) for approximately 60 min.

Matrix Isolation of 1,1-Diisopropyldiazene (18) and 1,1-Diisopropyldiazene-^{15}N (18-^{15}N). The respective carbamoyl azides (freshly purified by preparative VPC) were cryopumped from a -30°C ice/salt bath and co-deposited with argon matrix gas (UHP argon) (20°K) at 15 mmol gas per hour over approximately 4-5 h (150-175 mm gas, 55-65 mmol, respectively). The CSI window was slowly lowered to 10°K and sample spectrum recorded. Photolysis through the back of the CsI inner window with 2-CS-7-54 filters was carried out for 90-150 min and carefully monitored by FT-IR. Photolysis

of the product diazene was effected with defocused visible light from Corning filters CS-1-75 and CS-4-96 (360-610 nm) for 4-6 h and carefully monitored by FT-IR.

Kinetics. 2-MTHF glasses of the respective diazenes were prepared in the low temperature electronic spectroscopy cell as described above. The cell temperature was slowly raised to effect diazene decomposition. Decompositions were monitored using either the repetitive scan program of the Cary 219 spectrophotometer (multiple absorptions) or using a timed delay single wavelength monitor. All data prior to temperature equilibration (~30 min) were discarded. Typically the reactions were monitored through several half-lives and reported rate constants are derived from a conventional linear least squares analysis. First-order decays were checked at two starting concentrations through a minimum of three half-lives and in all cases gave identical rate constants within experimental error.

REFERENCES AND NOTES

(1) (a) Baird, N. C.; Swenson, J. R. Can. J. Chem. **1973**, 51, 3097. (b) Baird, N. C.; Barr, R. F. Ibid. **1973**, 51, 3303. (c) Merenyi, G.; Wettermark, G. Chem. Phys. **1973**, 1, 340. (d) Wagniere, G. Theor. Chim. Acta **1973**, 31, 269. (e) Lathan, W. A.; Curtiss, L. A.; Hehre, W. J.; Lisle, J. B.; Pople, J. A. Prog. Phys. Org. Chem. **1974**, 11, 1975. (f) Winter, N. W.; Pitzer, R. M. J. Chem. Phys. **1975**, 62, 1269. (g) Vasudevan, K.; Peyerimhoff, S. D.; Buenker, R. J.; Kammer, W. E. Chem. Phys. **1975**, 7, 187. (h) Ahlrichs, R.; Staemmler, V. Chem. Phys. Lett. **1976**, 37, 77. (i) Howell, J. M.; Kirschenbaum, L. J. J. Am. Chem. Soc. **1976**, 98, 877. (j) Baird, N. C.; Wernette, D. A. Can. J. Chem. **1977**, 55, 350. (k) Skanke, P. N. Chem. Phys. Lett. **1977**, 47, 259. (l) Baird, N. C.; Kathpal, H. B. Can. J. Chem. **1977**, 55, 863. (m) Cimiraglia, R.; Riera, J. M.; Tomasi, J. Theor. Chim. Acta **1977**, 46, 223. (n) Davis, J. H.; Goddard, III, W. A. J. Am. Chem. Soc. **1977**, 99, 7111. (o) Bigot, B.; Sevin, A.; Devaquet, A. Ibid. **1978**, 100, 2639. (p) Pople, J. A.; Krishnan, R.; Schlegel, H. B.; Binklely, J. S. Int. J. Quantum. Chem. **1978**, 14, 545. (q) Parsons, C. A.; Dykstra, C. E. J. Chem. Phys. **1979**, 71, 3025. (r) Pasto, D. J.; Chipman, D. M. J. Am. Chem. Soc. **979**, 101, 2290. (s) Pasto, D. J. Ibid. **1979**, 101, 6852. (t) Casewit, C.; Goddard, W. A. III. Ibid. **1980**, 102, 4057. (u) Kemper, M. J. H.; Buck, H. M. Can. J. Chem. **1981**, 59, 3044.

(2) (a) Foner, S. N.; Hudson, R. L. J. Chem. Phys. **1958**, 28, 719. (b) Corey, E. J.; Mock, W. L. J. Am. Chem. Soc. **1962**, 84, 685. (c)

Rosengren, K.; Pimentel, G. L. J. Chem. Phys. **1965**, 43, 507. (d) Wiberg, N.; Bachhuber, H.; Fischer, G. Angew. Chem. Int. Ed. **1972**, 11, 829. (e) Willis, C.; Back, R. A. Can. J. Chem. **1973**, 51, 3605. (f) Bondybey, V. E.; Nibler, J. W. J. Chem. Phys. **1973**, 58, 2125. (g) Wiberg, N.; Fischer, G.; Bachhuber, H. Chem. Ber. **1974**, 107, 1456. (h) Back, R. A.; Willis, C.; Ramsay, D. A. Can. J. Chem. **1974**, 52, 1006. (i) Carlotti, M.; Johns, J. W. C.; Trombetti, A. Can. J. Phys. **1974**, 52, 340. (j) Wiberg, N.; Fischer, G.; Bachhuber, H. Angew. Chem. Intl. Ed. **1976**, 15, 385. (k) Frost, D. C.; Lee, S. T.; McDowell, C. A.; Westwood, N. P. C. J. Chem. Phys. **1976**, 64, 4719. (l) Wiberg, N.; Fischer, G.; Bachhuber, H. Angew. Chem. Intl. Ed. **1977**, 16, 780. (m) Foner, S. N.; Hudson, R. L. J. Chem. Phys. **1978**, 68, 3162. (n) Wiberg, N.; Fischer, G.; Bachhuber, H. Z. Naturforsch. **1979**, 34b, 1385. (o) Neudorfl, P. S.; Back, R. A.; Douglas, A. E. Can. J. Chem. **1981**, 59, 506.

(3) For a review of diimide chemistry: Hunig, S.; Muller, H. R.; Thier, W. Angew. Chem. Intl. Ed. **1965**, 4, 271.

(4) Sylwester, A. P.; Dervan, P. B. J. Am. Chem. Soc. **1984**, 106, 4648.

(5) For reviews see: (a) Henderson, R. A.; Leigh, G. J.; Picket, C. J. Adv. in Inorg. Chem. & Rad. **1983**, 27, 197-292 and references therein. (b) Chatt, L. M.; Pina, C.; Richards, R. L., Eds. "New Trends in the Chemistry of Nitrogen Fixation"; Academic Press: London, 1980 and references therein.

(6) For reviews of 1,1-diazenes, see: (a) Lamal, D. M. In "Nitrenes";

Lwowski, W., Ed.; Interscience: New York, 1970, Ch. 10. (b) Ioffe, B. V.; Kuznetsov, M. A. Russ. Chem. Rev. (Engl. Trans.) **1972**, 41, 131. (c) Lwowski, W. In "Reactive Intermediates"; Jones, M.; Moss, R., Eds.; Wiley: New York, 1978, Ch. 6. (d) Lwowski, W. In "Reactive Intermediates"; Jones, M.; Moss, R., Eds.; Wiley, New York, 1981, Vol. 2. (e) Lwowski, W. In "Reactive Intermediates"; Jones, M.; Moss, R., Eds.; Wiley: New York, 1985, Ch. 8.

(7) For a review of 1,2-diazene chemistry see: Engel, P. S. Chem. Rev. **1980**, 80, 99.

(8) (a) Hinsberg, W. D.; Dervan, P. B. J. Am. Chem. Soc. **1978**, 100, 1608. (b) Hinsberg, W. D.; Dervan, P. B. Ibid. **1979**, 101, 6142. (c) Schultz, P. G.; Dervan, P. B. Ibid. **1980**, 102, 878. (d) Dervan, P. B.; Squillacote, M.; Lahti, P.; Sylwester, A. P.; Roberts, J. D. Ibid. **1981**, 103, 1120. (e) Hinsberg, W. D.; Schultz, P. G.; Dervan, P. B. Ibid. **1982**, 104, 766. (f) McIntyre, D. K.; Dervan, P. B. Ibid. **1982**, 104, 6466. (g) Schultz, P. B.; Dervan, P. B. Ibid. **1982**, 6660.

(9) For reviews of low temperature matrix isolation see: (a) Cradock, S.; Hinchcliffe, A. J. "Matrix Isolation"; Cambridge University Press, Cambridge, 1975. (b) Dunkin, I. R. "Matrix Isolation Technique and Its Application to Organic Chemistry." Chem. Soc. Rev. **1980**, 1. (c) Downs, A. J.; Peake, S. C. In "Molecular Spectroscopy"; Barrow, R. F.; Long, D. A.; Millen, D. J., Eds.; The Chemical Society: London, 1973, Vol. 1, 523. (d) Chadwick, D. M. Ibid., 1975, Vol. 3, 281. (e) Barnes, A. J.; Hallam, H. E. Quart. Rev. **1969**, 23, 392. (f) Turner, J.

J. Angew. Chem. Intl. Ed. **1975**, 14, 304. (g) Moskovitz, M.; Ozin, G. A., Eds.; "Cryochemistry"; Wiley-Interscience: New York, 1976. (h) Chapman, O. L. Pure & Appl Chem. **1974**, 40, 511. (i) Barnes, A. J.; Orville-Thomas, W. J.; Müller, A.; Ganfres, R., Eds. "Matrix Isolation Spectroscopy"; D. Reidel: Dodrecht, Holland, 1981.

(10) Swalen, J. D.; Ibers, J. A. J. Chem. Phys. **1962**, 36, 914.

(11) "JANAF Thermochemical Tables"; NSRDS-NBS-37 U.S. Government Printing Office: Washington, D.C., 1970.

(12) (a) Willis, C.; BAck, R. A.; Purdon, J. G. Int. J. Chem. Kinet. **1977**, 9, 787. (b) Willis, C.; Back, R. A.; Parsons, J. M.; Purdon, J. G. J. Am. Chem. Soc. **1977**, 99, 4451.

(13) (a) Benson, S. W. "Thermochemical Kinetics"; 2nd ed.; Wiley: New York, 1976. (b) Benson, S.W.; O'Neal, H. E. "Kinetic Data on Gas Phase Unimolecular Reactions"; NSRDS-NBS **1970**, No. 21, 448.

(14) Benson, S. W.; O'Neal, H. E. NSRDS-NBS **1979**, No. 21, 31.

(15) For example: Baumgarten, H. E.; Whittman, W. F.; Lehmann, G. J. J. Heteroc. Chem. **1969**, 6, 333.

(16) Nakagawa, K.; Konaka, R.; Nakata, T. J. Org. Chem. **1962**, 27, 1597.

(17) For example: Overberger, C. G.; Lombardino, J. G.; Hiskey, R. G. J. Org. Chem. **1957**, 22, 858.

(18) For example: (a) Carpino, L. A. J. Am. Chem. Soc. **1957**, 79, 4427. (b) Lemal, D. M.; Rave, T. W.; McGregor, S. D. Ibid. **1964**, 86, 2395. (c) Dervan, P. B.; Uyehara, T. Ibid. **1979**, 101, 1076.

(19) For example: Bumgardner, C. L.; Freeman, J. P. Tetrahedron Lett.

1966, 5547.

(20) (a) Anderson, D. J.; Gilchrist, T. L.; Horwell, D. C.; Rees, C. W.; Yelland, M. Chem. Commun. 1969, 146. (b) Rees, C. W.; Yelland, M. Ibid. 1969, 377.

(21) Busch, M.; Weiss, B. Chem Ber. 1900, 33, 2701.

(22) (a) For a review of one bond vs. simultaneous two bond scission in 1,2-diazenes, see Ref. 7. (b) Dannenberg, J. J.; Rocklin, D. J. J. Org. Chem. 1982, 47, 4529.

(23) Freeman, J. P.; Graham, W. H. J. Am Chem. Soc. 1967, 89, 1761.

(24) Duan, D. C.; Dervan, P. B. J. Org. Chem. 1983, 48, 970.

(25) Lichter, R. L. Ph.D. Thesis, University of Wisconsin, Madison, 1967, as quoted in Ref. 6.

(26) Lemal, D. M.; Menger, F.; Coats, E. A. J. Am. Chem. Soc. 1964, 86, 2395.

(27) Adams, D. J. C.; Bradbury, S.; Howell, D. C.; Keating, M.; Rees, C. W.; Storr, R. C. Chem. Commun. 1971, 828.

(28) Baldwin, J. E.; Brown, J. E.; Hofle, G. J. Am. Chem. Soc. 1971, 93, 788.

(29) (a) McBride, W.; Kruse, H. W. J. Am. Chem. Soc. 1957, 79, 572. (b) McBride, W.; Bens, E. Ibid. 1959, 81, 5546.

(30) Anderson, D. J.; Gilchrist, T. L.; Rees, C. W. Chem. Commun. 1971, 800.

(31) (a) Atkinson, R. S.; Rees, C. W. Chem. Commun. 1967, 1230. (b) Atkinson, R. S.; Rees, C. W. J. Chem. Soc. (C) 1969, 772. (c)

Atkinson, R. S.; Malpass, J. R.; Skinner, K. L.; Woodthorpe, K. L. Chem. Commun. 1981, 549.

(32) Willis, C.; Back, R. A.; Parsons, J. M. J. Photochem. 1977, 6, 253.

(33) Craig, N. C.; Kliewer, M. A.; Shih, N. C. J. Am. Chem. Soc. 1979, 101, 2480.

(34) Willis, C.; Back, R. A.; Purdon, J. G. Int. J. Chem. Kinet. 1977, 9, 787.

(35) (a) Wiberg, N.; Bayer, H.; Bachhuber, H. Angew. Chem. Intl. Ed., Engl. 1975, 14, 177. (b) Kroner, J.; Wiberg, N.; Bayer, H. Ibid. 1975, 14, 178.

(36) Willis, C.; Back, R. A.; Parsons, J. M.; Purdon, J. G. J. Am. Chem. Soc. 1977, 99, 4451.

(37) Wiberg, N.; Haring, H. W.; Vasisht, S. K. Z. Naturforsch 1979, 34b, 356.

(38) No explanation for the extremely low pre-exponential factors has been offered. From the experimental activation parameters k_H/k_D = 1.97 for gas phase decomposition of 1 at 100°C.

(39) Bock, v. H.; Kompa, K. L. Z. fur Anerg. und Allge. Chem. 1964, 332, 238.

(40) (a) Hoesch, v. L.; Koppell, B. Helv. Chim. Acta 1981, 64, 864. (b) Hoesch, v. L. Ibid. 1981, 64, 890.

(41) (a) Felix, D.; Müller, R. K.; Horn, V.; Soos, R.; Schreiber, J.; Eschenmoser, A. Helv. Chim. Acta 1972, 55, 1276. (b) Annunziata, R.; Fornasier, R.; Montanari, F. J. Org. Chem. 1974, 39, 3195.

(42) Kawasaki, M.; Iwasaki, M.; Ibuki, T.; Takezaki, Y. J. Chem. Phys. **1973**, 59, 6321. Kawasaki, M.; Iwasaki, M.; Tanaka, I. Ibid. **1973**, 59, 6328.

(43) Jacox, M. E.; Milligan, D. E. J. Am. Chem. Soc. **1963**, 85, 278.

(44) (a) Poppinger, D.; Radom, L. J. Am. Chem. Soc. **1978**, 100, 3674. (b) Rauk, A.; Alewood, P. F. Can. J. Chem. **1977**, 55, 1498.

(45) (a) Lieber, E.; Minnis, R. L.; Rao, C. N. Chem. Rev. **1965**, 65, 377. (b) Reichen, W. Ibid. **1978**, 78, 569. (c) Lockley, W. J. S.; Ramakrishnan, V. T.; Lwowski, W. Tetrahedron Lett. **1974** 30, 2621.

(46) Lwowski, W.; deMauriac, R. A.; Murray, R. A.; Lieselotle, L. Tetrahedron Lett. **1971**, 5, 425.

(47) Lwowski, W.; deMauriac, R. A.; Thompson, M.; Wilde, R. E. J. Org. Chem. **1975**, 40, 2608.

(48) Kuck, V. J.; Wasserman, E.; Yager, W. A. J. Phys. Chem. **1972**, 76, 3570.

(49) (a) Thiele, J.; Stange, O. J. Liebigs. Ann. Chem. **1894**, 283, 1. (b) Curtius, T.; Heidenreich, K. J. Prakt. Chem. **1895**, 160, 454.

(50) The low temperature cell was designed by Hinsberg. Hinsberg, W. D. Ph.D. Thesis, California Institute of Technology, Pasadena, CA, 1980.

(51) Quartz optics and 20 cm water (infrared) filter.

(52) (a) We presume this band to be the 0,0 absorption band in the absence of an emission spectrum. (b) Calculated using ratio of force constants from Ref. 1n and the experimental $\nu\,^{14}N{=}^{14}N$ of 1574.16 cm^{-1} for **3**.

(53) For a discussion on the origins of solvent-induced shifts, see: Huberfield, P.; Lux, M. S.; Rosen, D. J. Chem. Soc. **1977**, 99, 6828.

(54) (a) Robinson, G. W.; Frosch, R. P. J. Chem. Phys. **1963**, 38, 1187. Ibid. **1962**, 37, 1962. (b) Dexter, D. L.; Fowlere, W. B. Ibid. **1967**, 47, 1379.

(55) Siebrand, W. J. Chem. Phys. **1967**, 47, 2411.

(56) (a) Ippen, E.P.; Shank, C. V.; Woerner, R. L. Chem. Phys. Lett. **1977**, 46, 20. (b) Heritage, J.P.; Penzkofer, A. Ibid. **1976**, 44, 76.

(57) Miller, R. C.; Lee, E. K. C. Chem. Phys. Lett. **1976**, 41, 52.

(58) Watson, J. S. J. Chem. Soc. **1956**, 3677.

(59) Matrix ratios were estimated by comparison of the asymmetric azide stretches (ν N_3) with a known matrix ratio and known deposition size for gas phase mixture deposited dimethylcarbamoyl azide **13**.

(60) Photolysis of **15** was generally halted at ~80% conversion. Higher conversions gave variable low yields of **3** apparently due to secondary photolysis.

(61) Mattson Instruments FT-IR interactive subtraction software.

(62) (a) Thomas, S. G.; Guillory, W. A. J. Phys. Chem. **1973**, 77, 2469. (b) Khoshkhoo, H.; Nixon, E. R. Spect. Chim. Acta **1973**, 29A, 603.

(63) Prochemical Limited, New Jersey; 97 atom % ($1\text{-}^{15}N\text{-}NaN_3$).

(64) Casewit, C. Ph.D. Thesis, California Institute of Technology, Pasadena, CA, 1982.

(65) In our hands, argon matrix isolation of **3** gave consistently superior and better reproducible matrices than repeated attempts at N_2 matrix

isolation of **3** and its products (1:1000 to 1:3000, N_2, 10-20°K). FT-IR bands for **3** in N_2 matrix (1:2000, 10°K) are found at 2880.98, 2815.89, 1586.45, and 1018.50 cm^{-1}.

(66) Sodeau, J. R.; Lee, E. K. C. Chem. Phys. Lett. **1978**, 57, 71.

(67) Robin, M. B.; Hart, R. R.; Kuebler, N. A. J. Am. Chem. Soc. **1967**, 89, 1564.

(68) Craig, N. C.; Kliewer, M. A.; Shih, N. C. J. Am. Chem. Soc. **1979**, 101, 2480.

(69) These results were sporadic and not readily reproduced suggesting matrix site effects and/or intensity dependent photolysis.

(70) House, H. O. "Modern Synthetic Reactions"; W.A. Benjamin, Inc.: Menlo Park, CA, 1972, p. 254.

(71) Dubost, H.; Abouaf-Marguin, L. Chem. Phys. Lett. **1972**, 17, 269.

(72) Turro, N. J. "Modern Molecular Photochemistry"; Benjamin/Cumings, Inc.: Menlo Park, CA, 1978, Ch. 10.

(73) Andrews, L.; Arlinghaus, R. T.; Johnson, G. L. J. Chem. Phys. **1983**, 78, 6347.

(74) (a) Huo, W. M. J. Chem. Phys. **1965**, 43, 624. (b) Rosen, B. "Spectroscopic Data Relative to Diatomic Molecules"; Pergamon: New York, NY, 1970.

(75) McLean, A. D.; Yoshimine, M. J. Chem. Phys. **1969**, 44, 3467.

(76) Species such as H·,[a] HCO·,[a] NH_2·,[b] H_2NCO·,[c] can be ruled out by comparison with their literature ESR signals. (a) Adrian, F. J.; Cochran, E. L.; Bowers, V. A. J. Chem. Phys. **1962**, 36, 1661. (b)

Foner, S. N.; Cochran, E. L.; Bowers, V. A.; Jen, C. K. Phys. Rev. Lett. **1958**, 1, 91. (c) Bosco, S. R.; Cirillo, A.; Timmons, R. B. J. Am. Chem. Soc. **1969**, 91, 3140.

(77) Smith, D. R.; Pieroni, J. J. Can. J. Chem. **1965**, 43, 876.

(78) Phenyl diazenyl radical has been observed by ESR. Suehiro, T.; Tashiro, T.; Nakausa, R. Chem. Lett. **1980**, 1339.

(79) No new infrared band in the region 2300 to 1600 cm^{-1} showing a ^{15}N multiple was observed. An unidentified band at 1218.83 cm^{-1} grows in with VIS photolysis of **3**.

(80) Ling, A. C.; Willard, J. E. J. Phys. Chem. **1968**, 72, 1918.

(81) Senthilnathan, V. P.; Platz, M. S. J. Am. Chem. Soc. **1980**, 102, 7637 and references therein.

(82) The viscosity of 2-MTHF η is estimated to be greater than 3×10^{20} poise at 77.5°K and approximately 5×10^{11} poise at 90°K.[107] The viscosity decreases approximately an order of magnitude per 0.5°K greater than 92°K. Assuming Fick's law applies, the diffusional rate constant (k_D) can be estimated

$$k_D \simeq \frac{8\ RT}{3\eta} \simeq 4 \times 10^{-6} \pm 10^{2}\ M^{-1}\ sec^{-1} @ 90°K$$

(83) (a) Hasserodt, U. Chem. Ber. **1968**, 101, 113. (b) Gold-Aubert, P.; Gysin, E. Helv. Chim. Acta **1961**, 44, 105.

(84) Hanson, J. E. Unpublished results.

(85) Rao, C. N. R.; Goldman, G. K.; Bala-Subramanian, A. Can. J. Chem.

1960, 38, 2508.

(86) (a) White, D. K.; Greene, F. D. J. Org. Chem. 1978, 43, 4530. (b) Stowell, J. C. J. Org. Chem. 1967, 32, 2360.

(87) Lambert, J. B. "Organic Structural Analysis"; Macmillan, Inc.: New York, NY, 1976.

(88) Preliminary experiments suggest that the major bands of 7 (D_M) are more efficiently photolyzed with long wavelength visible light (> 600 nm) than the minor bands (D_m). This would favor assignment of the bands (D_m) to another species.

(89) Ackerman, M. N.; Craig, N. C.; Isberg, R. R.; Lauter, D. M.; Tacy, E. P. J. Phys. Chem. 1979, 83, 1190.

(90) Milligan, D. E.; Jacox, M. E. J. Chem. Phys. 1967, 47, 5146. Additional weak bands observed for (CH_3·) at 3288 and 736 cm^{-1} not observed here.

(91) Multiple matrix CO stretches resulting from photo-decarbonylation of ketenes have been noted by others. Reference 92.

(92) Sheridan, R. Private communication.

(93) This unpublished result has been communicated by others. Reference 92.

(94) (a) Goddard, J. D.; Schaefer, III, H. F. J. Chem. Phys. 1979, 70, 5117. (b) Gelbart, W. M.; Elert, M. L.; Heller, D. F. Chem. Rev. 1980, 80, 403. (c) Schaefer, III, H. F. Accts. Chem. Res. 1979, 12, 288. (d) Buck, H. M. Rec. Rev. 1982, 6, 193. (e) Buck, H. M. Ibid. 1982, 7, 223.

(95) For recent evidence for sequential photochemical bond cleavage in 1,2-diazenes see: Holt, P. L.; McCurdy, K. E.; Adams, J. S.; Burton, K. A.; Weisman, R. B.; Engel, P. S. J. Am. Chem. Soc. **1985**, 107, 2180.

(96) Singh, B. J. Am. Chem. Soc. **1969**, 91, 3670.

(97) Padwa, A. "1,3-Dipolar Cycloaddition Chemistry"; Wiley-Interscience: New York, NY, 1984, Vols. 1 and 2.

(98) Farina, P. R.; Tieckelmann, H. J. Org. Chem. **1973**, 38, 4259.

(99) McBride, W. R.; Kruse, H. W. J. Am. Chem. Soc. **1957**, 79, 572.

(100) Kuznetsov, M. A. Russ. Chem. Rev. **1979**, 48, 563.

(101) (a) Doba, T.; Ingold, K. U.; Siebrand, W. Chem. Phys. Lett. **1984**, 103, 339. (b) Doba, T.; Ingold, K. U.; Siebrand, W.; Wildman, T. A. J. Phys. Chem. **1984**, 88, 3165.

(102) UV (VIS filtered) photolysis of more concentrated glasses gave proportionately greater absorbances of the red-orange λ_{max} = 464 nm and λ_{max} = 474 nm species. Glass temperatures greater than 85°K gave similar results.

(103) For a review of monosubstituted 1,2-diazenes see: Kosower, E. M. Accts. Chem. Res. **1971**, 4, 193.

(104) Fogel, L. D.; Steel, C. J. Am. Chem. Soc. **1976**, 98, 4859.

(105) Whiteway, S. G.; Masson, C. R. J. Am. Chem. Soc. **1955**, 77, 1508.

(106) (a) Leroi, G. E.; Ewing, G. E.; Pimentel, G. L. J. Chem. Phys. **1964**, 40, 2298. (b) Bentsen, J. G.; Wrighton, M. S. J. Am. Chem. Soc. **1984**, 106, 4041.

(107) Fischer, G.; Fischer, E. Mol. Photochem. **1977**, 8, 279.

(108) Species such as $H_2\dot{N}\cdot$,a, $HN\dot{\cdot}$,b $\cdot N_3$,c H-N=C=O,d, $\cdot$N=C=O,d HO-C≡N,e HOO$\cdot$,g etc., can be ruled out by comparison with literature matrix infrared data. (a) Milligan, D. E.; Jacox, M. E. J. Chem. Phys. **1965**, 43, 4487; (b) McCarty, M.; Robinson, G. W. J. Am. Chem. Soc. **1959**, 81, 4472. (c) Reference 2c.; (d) Milligan, D. E.; Jacox, M. E. J. Chem. Phys. **1967**, 47, 5157. (e) Jacox, M. E.; Milligan, D. E. Ibid. **1964**, 40, 2457. (f) Jacox, M. E.; Milligan, D. E. J. Mol. Spect. **1972**, 42, 495.

(109) (a) Renaud, R.; Leitch, L. C. Can. J. Chem. **1954**, 32, 545. (b) Ackerman, M. N.; Dobmeyer, D. J.; Hurdy, L. C. J. Organomet. Chem. **1979**, 182, 561.

(110) KOR Isotopes, Cambridge, MA; >99% d_6 hexadeuteriodimethylammonium chloride.

(111) Müller, E.; Rundel, W. Chem. Ber. **1957**, 90, 1299.

(112) Effenberger, F.; Fischer, P. Tetrahedron **1970**, 26, 3029.

(113) Nash, T. Biochem. **1953**, 55, 416.

(114) McIntyre, D. K. Ph.D. Thesis, California Institute of Technology, Pasadena, CA, 1983.

(115) Streuli, C. A. "The Analytical Chemistry of Nitrogen and its Compounds"; Wiley-Interscience, New York, NY, 1970, Pt. 1.

(116) Air Products and Chemicals, Inc., Advanced Products Department-Cryogenics, P. O. Box 2802, Allentown, PA 18105.

(117) Amersil, Inc., 685 Ramsey Ave., Hillside, NJ 07205.

(118) Alpha Wire Corp., 711 Lidgerwood Ave., Elizabeth, NJ 07207.

(119) Edwards High Vacuum, Manor Royal, Crawley, West Sussex, RH 102LW, UK.

(120) Oriel Corp., 15 Market St., Stanford, CT 06902.

(121) Pennwalt Corp., Wallace & Tiernan Div., 25 Main St., Belleville, NJ 07109.

(122) Granville-Phillips Co., 5675 E. Arapahoe Ave., Boulder, CO 80803.

(123) Veeco Instruments, Inc., Terminal Dr., Plainview, NY 11803.

(124) International Crystal Labs, 107 Trumball St., P. O. Box 228, Elizabeth, NJ 07206.

(125) Arcadia Valve and Fitting Co., 521 N. First Ave., Arcadia, CA 91106

(126) Ace Glass, Inc., Vineland, NJ 08360.

(127) Angell, C. A.; Sare, J. M.; Sare, E. J. J. Phys. Chem. **1978**, 82, 24.

(128) Frierson, W. J. Inorg. Syn. **1946**, 2, 136.

(129) Hinze, J.; Curl, Jr., R. F. J. Am. Chem. Soc. **1964**, 86, 5068.

APPENDIX

Kinetic Derivations

D = 1,1-Diazene
T = Tautomer (azomethinimine)
P = Product (tetrazene)
H = Hydrocarbons

Mechanism (A)

$$D \underset{k_{-1}}{\overset{k_1}{\rightleftharpoons}} T$$

$$2D \xrightarrow{k_2} P$$

Assuming steady state in (D)

$$\frac{-d(D)}{dt} = k_1(D) - k_{-1}(T) + 2\,k_2(D)^2 = 0$$

$$k_{-1}(T) = (D)(k_1 + 2\,k_2(D))$$

$$(D) = \left(\frac{k_{-1}(T)}{k_1 + 2\,k_2(D)}\right)$$

$$\frac{-d(T)}{dt} = k_{-1}(T) - \frac{k_1 k_{-1}(T)}{k_1 + 2\,k_2(D)}$$

$$= k_{-1}(T)\left(1 - \frac{k_1}{k_1 + 2\,k_2(D)}\right)$$

$$= k_{-1}(T)\left(\frac{k_1 + 2k_2(D) - k_1}{k_1 + 2k_2(D)}\right)$$

$$= k_{-1}(T)\left(\frac{2k_2(D)}{k_1 + 2k_2(D)}\right)$$

if $2k_2(D) >> k_1$

$$\frac{-d(T)}{dt} = k_{-1}(T)$$

Mechanism (B)

$$D \underset{k_{-1}}{\overset{k_1}{\rightleftharpoons}} T$$

$$D + T \xrightarrow{k_2} P$$

Assuming steady state in (D)

$$\frac{d(D)}{dt} = k_{-1}(T) - k_1(D) - k_2(D)(T) = 0$$

$$k_1(D) = k_{-1}(T) - k_2(D)(T)$$

$$(D) = \frac{k_{-1}(T)}{k_1 + k_2(T)}$$

$$\frac{-d(T)}{dt} = k_{-1}(T) - k_1\left(\frac{k_{-1}(T)}{k_1 + k_2(T)}\right) + k_2(T)\left(\frac{k_1(T)}{k_1 + k_2(T)}\right)$$

$$= k_{-1}(T)\left[1 - \left(\frac{k_1 - k_2(T)}{k_1 + k_2(T)}\right)\right]$$

$$\frac{-d(T)}{dt} = k_{-1}(T)\left(\frac{2\,k_2(T)}{k_1 + k_2(T)}\right)$$

if $k_1 \simeq k_2(T)$ then

$$\frac{-d(T)}{dt} = k_{-1}(T)$$

if $k_1 << k_2(T)$ then

$$\frac{-d(T)}{dt} = 2\,k_{-1}(T)$$

if $k_1 >> k_2(T)$ then

$$\frac{-d(T)}{dt} = 2\left(\frac{k_{-1}}{k_1}\right)k_2(T)^2$$

Mechanism (C)

$$D \underset{k_{-1}}{\overset{k_1}{\rightleftharpoons}} T$$

$$D \xrightarrow{k_2} H + N_2$$

Assuming steady state in (D)

$$\frac{d(D)}{dt} = -k_1(D) + k_{-1}(T) - k_2(D) = 0$$

$$[D] = \frac{k_{-1}[T]}{k_1 + k_2}$$

$$\frac{-d[T]}{dt} = k_{-1}[T] - k_1[D]$$

$$= k_{-1}[T] - \left(\frac{k_1 k_{-1}}{k_1 + k_2}\right)[T]$$

$$= k_{-1}\left(1 - \frac{k_1}{k_1 + k_2}\right)[T]$$

$$\frac{-d[T]}{dt} = \frac{k_{-1}k_2}{k_1 + k_2}[T]$$

if $k_1 >> k_2$

$$\frac{-d[T]}{dt} = \left(\frac{k_{-1}}{k_1}\right) k_2[T]$$

CHAPTER 3

^{15}N NMR Spectrum of a 1,1-Diazene

N-(2,2,6,6-Tetramethylpiperidyl)nitrene[1]

^{15}N NMR Spectrum of a 1,1-Diazene. N-(2,2,6,6-Tetramethylpiperidyl)nitrene[1]

Peter B. Dervan,*[2] Michael E. Squillacote,[3]
Paul M. Lahti,[4] Alan P. Sylwester, and John D. Roberts*
Contribution No. 6294 from Gates and Crellin
Laboratories of Chemistry, California Institute
of Technology, Pasadena, California 91125

Abstract: The low-temperature ^{15}N NMR spectrum of the 1,1-diazene, N-(2,2,6,6-tetramethylpiperidyl)nitrene (**1**) is reported. The ^{15}N double- and mono-labeled 1,1-diazenes **1a** and **1b** were synthesized. The nitrene and amino nitrogens of **1** have resonances in dimethyl ether at -90°C at 917.0 and 321.4 ppm, respectively, downfield from anhydrous $^{15}NH_3$, affording a chemical-shift difference of 595 ppm for the directly bonded nitrogen nuclei. The chemical shift of the ring nitrogen is consistent with an amino nitrogen whose lone pair is largely delocalized. The large downfield shift of the nitrene nitrogen is consistent with a large paramagnetic term due to a low-lying n-π* transition.

INTRODUCTION

1,1-Diazenes (aminonitrenes, N-nitrenes) unlike their more stable 1,2-diazene isomers (azo compounds) are usually not isolated or detected by spectroscopic methods, but rather are assumed intermediates based on a substantial body of chemical evidence.[5] Recently, the synthesis and direct

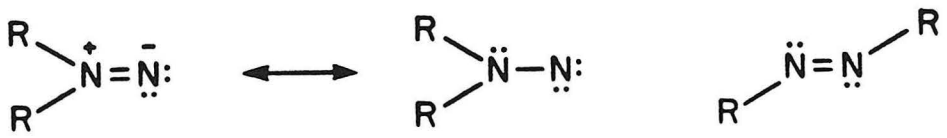

observation of persistent[6] 1,1-diazenes, N-(2,2,6,6-tetramethylpiperidyl)-nitrene (1)[7] and N-(2,2,5,5-tetramethylpyrrolidyl)nitrene[8] were reported. The infrared an electronic spectra, and kinetics of decomposition of these 1,1-diazenes[7,8] allowed the first comparison of experiment with theory on the nature of the bonding and the relative energies of the states of the parent 1,1-diazene (H_2N-N).[9]

^{15}N NMR spectroscopy has proven to be a sensitive probe of the electronic environment of nitrogen nuclei.[10] With the availability of persistent 1,1-diazenes, we have obtained the first ^{15}N magnetic resonance spectrum of a 1,1-diazene. The low-temperature ^{15}N NMR spectrum of N-(2,2,6,6-tetramethylpiperidyl)nitrene 1[7] reveals the different electronic environments of the contiguous nitrogens in the 1,1-diazene. We find the chemical-shift difference for the amino and nitrene nitrogens to be 595 ppm. Their assignments were determined from the spectra of the ^{15}N double- and

mono-labeled 1,1-diazene, **1a** and **1b**. The nitrene nitrogen of the 1,1-diazene has a ^{15}N resonance in dimethyl ether at -90°C 917 ppm downfield form anhydrous $^{15}NH_3$ and represents the most highly deshielded neutral nitrogen-containing organic compound now known.

RESULTS AND DISCUSSION

Successive treatment of phorone **2** with $^{15}NH_4Cl$/sodium hydroxide and hydrazine hydrate/potassium hydroxide afforded ^{15}N-labeled (95+ %) 2,2,6,6-tetramethylpiperidine **3**.[11] Nitrosation ($Na^{15}NO_2$, 95%) and reduction with lithium aluminum hydride gave the double-labeled precursor, N-amino-(2,2,6,6-tetramethylpiperidine) **4**.[7,12] Similarly, nitrosation ($Na^{15}NO_2$) and reduction of unlabeled 2,2,6,6-tetramethylpiperidine **5** afforded the mono-labeled precursor 6 (Scheme I).

Scheme I

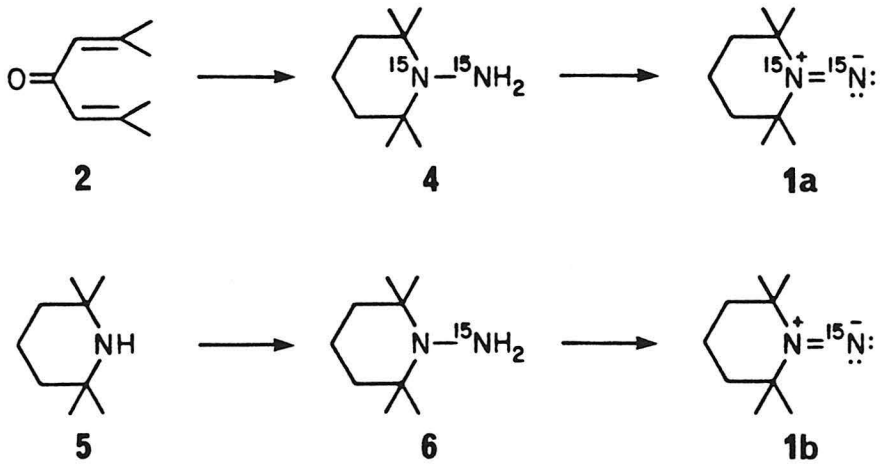

2 **4** **1a**

5 **6** **1b**

Oxidation of **4** with nickel peroxide in dimethyl ether affords upon filtration and concentration (-78°C) a deep purple solution of the persistent 1,1-diazene **1** whose electronic spectrum (λ_{max} = 543 nm $(CH_3)_2O$), infrared spectrum and thermal stability are known.[7] The ^{15}N NMR spectrum of this purple solution (~1 M) at -90°C contains four doublets (Figure 1a). The two doublets, δ 419.5 (J = 6.4 Hz) and 164.6 (J = 6.4 Hz), can be assigned to the tetrazene **7** which has been independently synthesized and characterized.[7] The pair of doublets at 917.0 (J = 15.5 Hz) and 321.4 (J = 15.5 Hz) were shown by ^{15}N-^{15}N decoupling to be directly bonded nitrogen nuclei. Upon warming to 0°C, the purple color disappears and the doublets at 917.0 and 321.4 disappear concomitant with an increase in the resonances of tetrazene **7**, the dimerization product of **1**.[7] These doublets are assigned to the 1,1-diazene **1a**. Oxidation of the mono-labeled precursor **6** in dimethyl ether at -78°C affords singlets at δ 917.0 and 419.5 and no peaks at 165 and 321 (Figure 1b). This fact allows the assignment of the 917 ppm resonance to the nitrene nitrogen of the 1,1-diazene chromophore. The ^{15}N NMR parameters for the 1,1-diazene **1a** and the tetrazene **7** are presented in Table I.

The large NOE for N2 in **1a** suggests almost full nitrogen-proton dipole-dipole relaxation for this nitrogen. The nitrene nitrogen N1 was found to have a smaller NOE than N2 and, as evidenced by the response in a signal intensity to changes in pulse delay, a spin-lattice relaxation time, T_1, which is insensitive to magnetic field strength and much shorter than the T_1 of N2. Thus a spin-rotation relaxation mechanism seemingly predominates for the nitrene nitrogen. This may reflect the different electron distributions

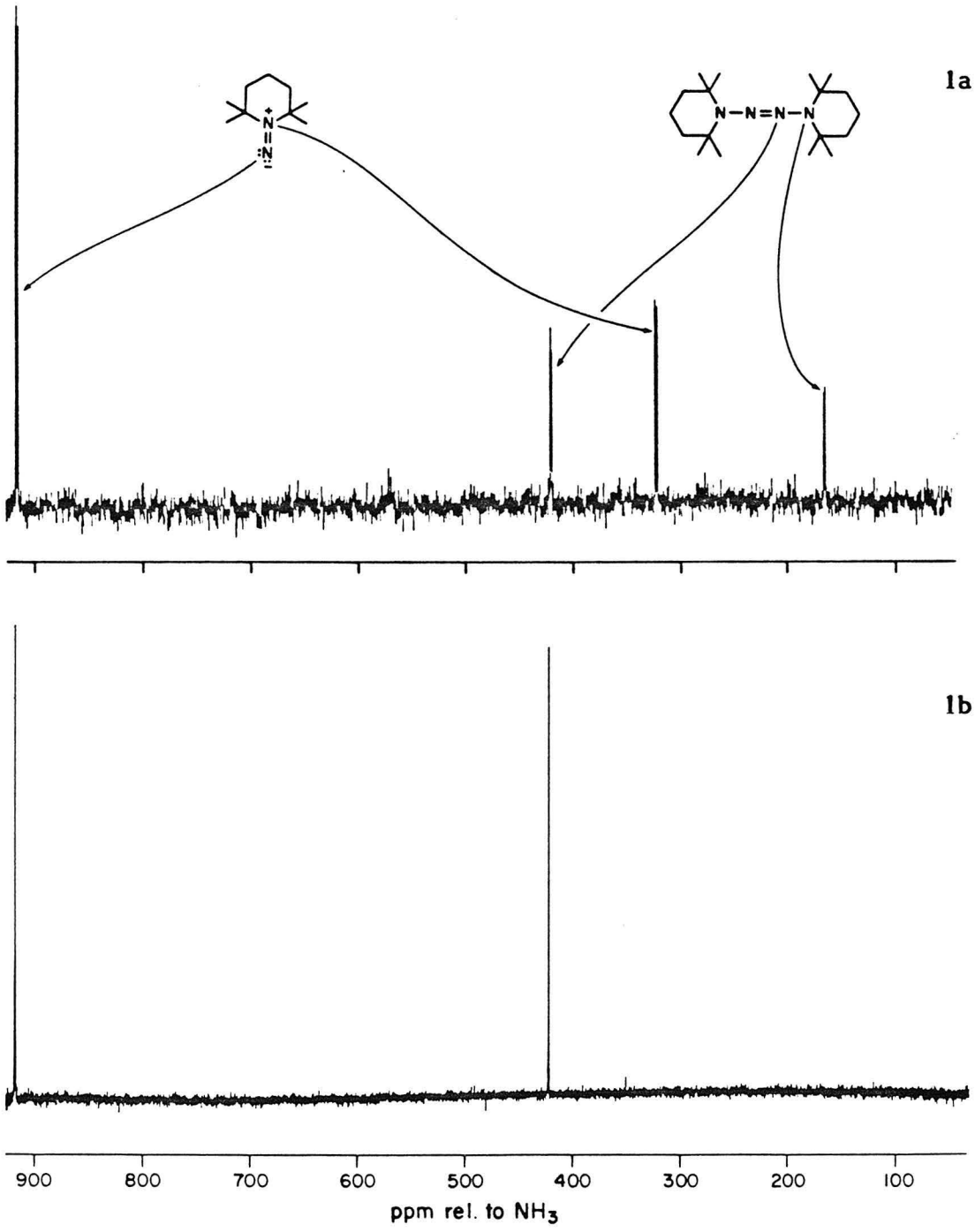

Figure 1. Fourier transform ^{15}N NMR spectra of 1,1-diazene **1** and tetrazene **7** in dimethyl ether at -90°C (30 deg pulse angle, 20 sec repetition time, NOE suppressed). (a) Spectrum of **1a** and **7** from the nickel peroxide oxidation of 200 mg of **4** at 9.04 MHz, 250 transients. (b) Spectrum of **1b** and **7** from the nickel peroxide oxidation of 100 mg of **6** at 50.7 MHz, 190 transients. The assignment of the resonances are described in the text.

Table I

Compound		$^{15}N1$	$^{15}N2$
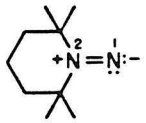	δ[a]	917.0	321.4
	J[b]	15.5	15.5
	NOE	-0.2	-5.0
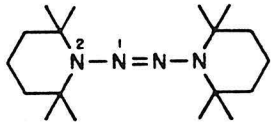 **7**	δ	419.5	164.6
	J	6.4	6.4
	NOE	-2.0	-5.0

[a]Downfield from external anhydrous ammonia, at 25°C using a 1:4 $CH_3{}^{15}NO_2$:CD_2Cl_2 mixture as a secondary standard at 380.7 ppm. [b]Error in coupling constants is ±0.6 Hz. Error in chemical shift is ±0.5 ppm.

between the two nitrogens, since it has been shown that an electron distribution leading to large chemical shifts will lead to large spin-rotation interactions.[13]

The deshielding of the nitrene nitrogen can be attributed to the importance of the paramagnetic term as represented by mixing of the ground state with excited states which results in changes induced by the external field in the electronic wave functions.[14,15] Experimental correlations of ^{15}N chemical shift with the energy of transitions involving low-lying excited states, in particular n-π* transitions, are well documented.[14] The magnitude of the downfield shift of the nitrene nitrogen in **1** is consistent with a very large paramagnetic term due to the low-lying n-π* transition (λ_{max} = 543 nm in $(CH_3)_2O$).[7]

The amino-nitrogen of **1a** N? has a ^{15}N chemical shift of 321 ppm comparable to the shifts of nitrones, nitrates and nitro compounds (280-380) ppm[10] which lack non-bonding electrons on nitrogen. These molecules are formally N-oxides of imines, nitrites, and nitroso compounds (330-900) ppm[10] and are considerably more shielded, even though they are also associated with low-energy n-π^* transitions. Thus, it appears that non-bonding electrons on nitrogen must be involved in the n-π^* absorption of the molecule in order for a large paramagnetic shift to be present for the nitrogen.[14c] The amino nitrogen, N2, is not deshielded and hence its lone pair must be substantially delocalized into the empty p orbital of the nitrene nitrogen, N1. This is consistent with both experiment ($^{14}N=^{14}N$, stretch, 1595 cm^{-1})[7] and theory (GVB-CI)[9] both characterizing the 1,1-diazene as having an N=N π bond.

CONCLUSION

In summary, the low temperature ^{15}N NMR spectrum of the 1,1-diazene, N-(2,2,6,6-tetramethylpiperidyl)nitrene (1) is reported. The nitrene and amino nitrogens of **1** have resonances in dimethyl ether at 917.0 and 321.4 ppm, respectively, downfield from anhydrous $^{15}NH_3$, affording a chemical-shift difference of 595 ppm for the directly bonded nitrogen nuclei. The chemical shift of the ring nitrogen is consistent with an amino nitrogen whose lone pair is largely delocalized. The large downfield shift of the nitrene nitrogen is consistent with a large paramagnetic term due to a low-lying n-π^* transition.

EXPERIMENTAL SECTION

^{15}N nuclear magnetic resonance (^{15}N NMR) data were recorded on a JEOL FX-900 spectrometer at 9.04 MHz (Figure 1a) and a Brucker WM-500 spectrometer at 50.7 MHz (Figure 1b). Chemical shifts are given in parts per million (ppm) downfield from anhydrous $^{15}NH_3$ in δ units and coupling constants in cycles per second (Hz). ^{15}N chemical shifts were obtained using a 1:4 $CH_3{}^{15}NO_2$:CD_2Cl_2 solution as a secondary standard. Proton NMR data were obtained on a Varian EM-390 spectrometer. Chemical shifts are given in ppm downfield from Me_4Si in δ units and coupling constants in Hz. For preparative vapor-phase chromatography (VPC), a Varian Aerograph Model 920 instrument equipped with a thermal conductivity detector and helium carrier gas was used. The VPC column was a 5 ft. x 0.25 in. glass, Pennwalt 223 amine packing (Applied Sciences Laboratories, Inc.). All reactions were run under an argon atmosphere.

4-Oxa-2,2,6,6-tetramethylpiperidine-^{15}N (8). Phorone **2** (10.0 g, 0.072 mmol) and ~100 mg of sodium hydroxide were placed in a 25-mL pyrolysis tube, then frozen under vacuum. An ammonia solution was prepared by neutralizing 5.0 g (0.092 mmol) of $^{15}NH_4Cl$ (Prochemicals Limited, New Jersey; 95.4 atom - %) with 8.0 g (0.20 mol) of sodium hydroxide in 6 mL of water. This solution was distilled under reduced pressure into the pyrolysis tube. The reactants were degassed, sealed under vacuum, and heated in a stainless steel bomb to 135°C for 18 h. The tube was then opened; the contents dissolved in et her, dried (K_2CO_3) and concentrated affording 8.2 g of a yellow oil. Recrystallization from petroleum ether at -78°C gave 7.0 g

(62%) of **8** as white needles, mp 37-38°C (lit. mp 36°C).[17] NMR ($CDCl_3$) δ 1.22 (d, 12, J = 2 Hz), 2.22 (s, 4).

2,2,6,6-Tetramethylpiperidine-^{15}N (9). A total of 7.0 g (0.45 mol) of **8** were stirred with 10 g of potassium hydroxide, 9.3 mL of hydrazine hydrate, and 2.0 mL of water in 67 g of triethylene glycol at reflux for 2 h. The product was distilled (bp 96-112°C), extracted with ether, dried (Na_2SO_4) affording 4.5 g (72%) of a clear liquid **9**, bp 145-147°C (lit. 151-152°C at 750 mm Hg).[11] NMR ($CDCl_3$) δ 1.12 (d, 12, J = 2 Hz), 1.3 (m, 4), 1.6 (m, 2).

1-Nitroso-2,2,6,6-tetramethylpiperidine-$^{15}N_2$ (10). A solution of 1.5 g (0.011 mol) of **9** in 13 mL of a 6.8% solution of aqueous hydrochloric acid was heated to 95°C. To this was added 1.5 g (0.021 mol) of $Na^{15}NO_2$ (Prochemicals Limited, New Jersey; 95.5 atom - %) in 8 mL of water. The solution was stirred at 95°C for 48 h. The reaction mixture was allowed to cool and was extracted with ether, washed with 10% aqueous hydrochloric acid, saturated aqueous sodium bicarbonate, saturated aqueous sodium chloride and dried (Na_2SO_4). The ethereal layer was concentrated affording 1.2 g (64%) of a yellow oil **10.** NMR ($CDCl_3$) δ1.40(d,6,J =2Hz),1.62(d, 6, J = 2 Hz), 1.7 (m, 6).[12]

1-Amino-2,2,6,6-tetramethylpiperidine-$^{15}N_2$ (4). A solution of 1.2 g (7.0 mmol) of **10** in 4 mL of dry ether was added dropwise to 580 mg (15.3 mmol) of lithium aluminum hydride in 17 mL of 1:1 di-n-butyl ether:diethyl ether. The temperature was slowly raised to 95°C with distillation of solvent; the temperature was then maintained at 95°C for 3 h. The slurry was cooled to 0°C, excess lithium aluminum hydride was quenched with water, and 25 mL of

ether was added. The layers were separated and the aqueous layer was washed with ether. The combined ether layers were extracted with 10% aqueous hydrochloric acid. The aqueous layer was made basic with 20% aqueous sodium hydroxide. This was extracted with ether, dried (Na_2SO_4), and concentrated affording 1.1 g of a clear oil. This was further purified by preparative VPC (Pennwalt, 180°C) affording a 70% yield of pure 1-amino-2,2,6,6-tetramethylpiperidine-$^{15}N_2$ **4**. NMR ($CDCl_3$) δ 1.05 (d, J = 2 Hz, 12), 1.5 (s, 6), 2.8 (broad s, 2).[12]

N-(2,2,6,6-tetramethylpiperidyl)nitrene-$^{15}N_2$ (1a). To 20 mL of anhydrous dimethyl ether, cooled to -78°C, was added 191 mg (1.9 mmol) triethylamine and 300 mg (1.9 mmol) 1-amino-2,2,6,6-tetramethylpiperidine-$^{15}N_2$ (**4**) with the aid of a syringe. To this was added 3.4 g (19 mmol) nickel peroxide[18] through a solid addition funnel with stirring over 5 min. The reaction mixture was stirred at -78°C for 2 h, then transferred through a Teflon tube to a cooled (-78°C) jacketed filter funnel, and filtered into a three-necked flask cooled to -78°C. The clear purple filtrate was concentrated ($\sim$1 M) and transferred into a 10-mm NMR tube for low-temperature (-90°C) ^{15}N NMR studies.

REFERENCES AND NOTES

(1) The authors are grateful to the National Science Foundation for generous support.

(2) Camille and Henry Dreyfus Teacher Scholar 1978-1983.

(3) National Science Foundation Postdoctoral Fellow.

(4) National Science Foundation Predoctoral Fellow.

(5) For reviews of 1,1-diazene behavior, see: (a) Lemal, D. M. In "Nitrenes"; Lwowski, W., ed.; Interscience: New York, 1970, Ch. 10. (b) Ioffe, B. V.; Kuznetsov, M. H. Russ. Chem. Rev. (Engl. Transl.) **1972**, 41, 131.

(6) Griller, D.; Ingold, K. U. Accts. Chem. Res. **1976**, 9, 13 and references cited therein.

(7) (a) Hinsberg, III, W. D.; Dervan, P. B. J. Am. Chem. Soc. **1978**, 100, 1608. (b) Hinsberg, III, W. D.; Dervan, P. B. Ibid. **1979**, 101, 6142.

(8) Schultz, P. G.; Dervan, P. B. J. Am. Chem. Soc. **1980**, 102, 878.

(9) (a) Hayes, L. J.; Billingsley, F. P.; Trindle, C. J. Org. Chem. **1972**, 37, 3924. (b) Baird, N. C.; Barr, R. F. Can. J. Chem. **1973**, 51, 3303. (c) Lathon, W. A.; Curtiss, L. A.; Hehre, W. J.; Lisle, J. B.; Pople, J. A. Prog. Phys. Org. Chem. **1974**, 1, 175. (d) Ahlrichs, R.; Staemmler, V. Chem. Phys. Lett. **1976**, 37, 77. (e) Baird, N. C.; Wernette, D. A. Can. J. Chem. **1977**, 55, 350. (f) Davis, J. H.; Goddard, III, W. A. J. Am. Chem. Soc. **1977**, 99, 711. (g) Casewit, C. J.; Goddard, III, W. A. Ibid. **1980**, 102, 4057.

(10) (a) Levy, G. C.; Lichter, R. L. "Nitrogen-15 Nuclear Magnetic

Resonance Spectroscopy"; John Wiley & Sons: New York, 1979. (b) Witanowski, M.; Webb, G. A. "Nitrogen NMR"; Plenum Press: New York, 1973. (c) Witanowski, M.; Stefaniak, L.; Webb, G. A. Ann. Rep. NMR Spectrosc. **1977**, 7, 117.

(11) Leonard, N. J.; Nommensen, E. W. J. Am. Chem. Soc. **1949**, 71, 2808.

(12) Roberts, J. R.; Ingold, K. U. J. Am. Chem. Soc. **1973**, 95, 3228.

(13) (a) Ramsey, N. F. "Molecular Beams"; Oxford University Press: 1956, p. 164. (b) Deverell, C. Mol. Phys. **1970**, 54, 64.

(14) (a) Herbison-Evans, D.; Richards, R. E. Mol. Phys. **1964**, 8, 19. (b) Baldeschwieler, J. D.; Randall, E. W. Proc. Chem. Soc. **1961**, 303. Gil, V. M. S.; Murrell, J. N. Trans. Faraday Soc. **1964**, 60, 248. (c) Lambert, J. B.; Roberts,J. D. J. Am. Chem. Soc. **1965**, 87, 4087. (d) Anderson, L. O.; Mason, J.; van Bronswijh, W. J. Chem. Soc. (A) **1970**, 296. (e) Mason, J.; van Bronswijh, W.; Vinter, J. G. J. Chem. Soc., Perkins II **1977**.

(15) The paramagnetic shielding term, σ_p, of the Pople chemical shift theory[16] can be approximated as being inversely proportional to ΔE, the mean excitation energy for all excited states. Low-lying n-π^* excited states will dominate this term affording the largest deshielding contribution to σ_p.

(16) (a) Karplus, M.; Pople, J. A. J. Chem. Phys. **1963**, 38, 2803. (b) Pople, J. A. Dicuss Faraday Soc. **1962**, 34, 7.

(17) Francis, F. J. J. Chem. Soc. **1927**, 2897.

(18) Nickel peroxide was prepared and the oxygen content determined by

the method of Nakagawa.[19] Activation of nickel peroxide prepared in this manner with 6% sodium hypochlorite solution yielded a dark solid with an activity of 3.9 to 4.5 x 10^{-3} g atom oxygen/g nickel peroxide.

(19) Nakagawa, K.; Konaka, R.; Nakata, T. J. Org. Chem. **1962**, 27, 1597.